AD-A258 572

1. AGENCY USE ONLY (Leave blank)	2. REPORT DATE 1992	3. REPORT TYPE AND DATES COVERED THESIS/~~DISSERTATION~~

4. TITLE AND SUBTITLE	5. FUNDING NUMBERS
Equatorial F-Region Electron Densities Over a Solar Cycle: Comparisons Between Observations and Numerical Models	

6. AUTHOR(S)

Amanda Preble Creamer, Captain

7. PERFORMING ORGANIZATION NAME(S) AND ADDRESS(ES)	8. PERFORMING ORGANIZATION REPORT NUMBER
AFIT Student Attending: Utah State University	AFIT/CI/CIA- 92-079

9. SPONSORING/MONITORING AGENCY NAME(S) AND ADDRESS(ES)	10. SPONSORING/MONITORING AGENCY REPORT NUMBER
AFIT/CI Wright-Patterson AFB OH 45433-6583	

DTIC ELECTE DEC 8 1992 S C D

11. SUPPLEMENTARY NOTES

12a. DISTRIBUTION/AVAILABILITY STATEMENT	12b. DISTRIBUTION CODE
Approved for Public Release IAW 190-1 Distributed Unlimited ERNEST A. HAYGOOD, Captain, USAF Executive Officer	

13. ABSTRACT (Maximum 200 words)

92-31013

14. SUBJECT TERMS	15. NUMBER OF PAGES 201
	16. PRICE CODE

17. SECURITY CLASSIFICATION OF REPORT	18. SECURITY CLASSIFICATION OF THIS PAGE	19. SECURITY CLASSIFICATION OF ABSTRACT	20. LIMITATION OF ABSTRACT

EQUATORIAL F-REGION ELECTRON DENSITIES

OVER A SOLAR CYCLE: COMPARISONS

BETWEEN OBSERVATIONS AND

NUMERICAL MODELS

by

Amanda Preble Creamer

A thesis submitted in partial fulfillment
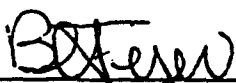of the requirements for the degree
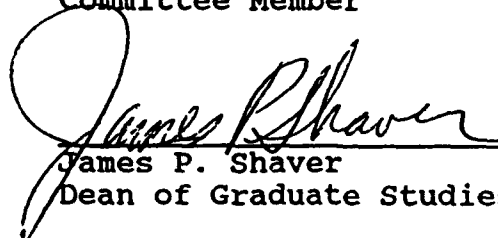
of

MASTER OF SCIENCE

in

Physics
(Upper Atmospheric Option)

Approved:

_____
Bela G. Fejer
Major Professor

_____
Joe R. Doupnik
Committee Member

_____
Kent L. Miller
Committee Member

_____
James P. Shaver
Dean of Graduate Studies

UTAH STATE UNIVERSITY
Logan, Utah

1992

ACKNOWLEDGEMENTS

TABLE OF CONTENTS

LIST OF TABLES

LIST OF FIGURES

ABSTRACT

Equatorial F-Region Electron Densities

Over a Solar Cycle: Comparisons

Between Observations and

Numerical Models

by

Amanda Preble Creamer, Master of Science

Utah State University, 1992

Major Professor: Dr. Bela G. Fejer
Department: Physics

Incoherent scatter radar observations at Jicamarca, Peru, from 1964 to the present, have been used to study the seasonal and solar cycle variations in the daily equatorial ionospheric plasma density profiles for select hours. The peak density, peak layer height, and layer thickness are dependent on solar activity which is determined by F10.7 cm flux. There are large variations in the daily plasma density profiles for each season and solar flux. The peak plasma densities are largest for December solstice (southern hemisphere summer), and smallest for June Solstice (southern hemisphere winter). The changes in the peak height, bottomside density, and topside density are dependent on seasonal and on temporal variations in the equatorial F-

region vertical plasma drifts at Jicamarca. Geomagnetic disturbance affects primarily the topside F-region density layer.

The average quiet-time seasonal profiles were compared with the International Reference Ionosphere (IRI), the Fully Analytic Ionospheric Model (FAIM), and the Parameterized Real-time Ionospheric Specification Model (PRISM) for similar time, season, and solar activity. The IRI is particularly good at representing the peak density for all seasons and all levels of solar activity; however, the model does not reproduce well the observed variations of the peak heights and layer thickness with season and solar flux. FAIM gives a good estimate of the peak density during winter and equinox, and a rate of increase in peak layer height with flux comparable to the data for all seasons. The FAIM layer thickness fits to the data are better than those of the IRI. However, they do not reproduce the data for high solar activity. PRISM gives a good fit to the data for all parameters except day and evening topside profiles. The layer thickness calculated from this model also gives the best representation of the experimental results.

(220 pages)

CHAPTER I

INTRODUCTION

The Earth is surrounded by a partially ionized gas which forms the ionosphere, an interface between the atmosphere and space which separates two very different and dynamic regions [Kelley, 1989]. The ionosphere is located between approximately 70 and 800 kilometers. This is an electrically neutral plasma where molecular nitrogen and atomic oxygen are the most abundant neutral and ion, respectively. The ionosphere can be divided into regions based on electron/ion density with various chemical reactions and transport regimes governing the density of each layer. The D-region (70-90 km) is characterized by complex ions, and dynamics are determined by the neutral atmosphere. The E-region, extending from 90 to 150 km, is composed of the molecular ions. Tidal oscillations in the E-region generate winds which in turn generate dynamo electric fields and currents. The electric fields map to the F-region along the magnetic field lines. The F-region extends between about 150 and 800 km and can be divided into the F1 and F2 regions where the F1-region is the transition between the E and F2 regions. The general characteristics of the ionosphere regions are described in detail in a number of textbooks [e.g., Rishbeth and Garriott, 1969; Kelley, 1989].

There are significant latitudinal effects on the ionospheric density distribution and dynamics. At high

latitudes the magnetosphere has a strong effect on the ionospheric dynamics, and factors such as auroral particle precipitation must be taken into account when considering the plasma densities. The middle latitudes are somewhat less complex. In this case, the plasma corotates with the Earth and the height of the density peak is raised or lowered by the neutral wind and by electric fields which also affect the peak densities. At very low latitudes one must consider the transport effects associated with vertical drifts which result from the equatorial zonal electric fields, nearly horizontal geomagnetic field lines, and interhemispheric plasma flows.

The equatorial ionosphere has been probed extensively with ground-based radio and radar systems and with in situ rocket and satellite probes [e.g., Kelley, 1989]. Most of the ground-based observations of the equatorial ionosphere have been made at the Jicamarca Incoherent Scatter (IS) Radar Observatory (11.95° S, 76.87° W, 1° N magnetic) in Peru. A description of the Jicamarca observatory is contained in Chapter III. Observations of F-region ionospheric temperature, plasma density and composition have been made there since 1961 [e.g.,Farley, 1991], and measurements of plasma drifts have been made since 1968 [e.g., Fejer, 1981, 1991]. The Jicamarca IS Radar Observatory is operated by the Geophysical Institute of Peru, Ministry of Education, with partial support from the National Science Foundation as contracted through Cornell University.

The focus of this thesis will be on the equatorial F2-region which is a complex and dynamical region of the ionosphere where a variety of processes affect the plasma concentration. In this region, the predominant neutral constituent is atomic oxygen which is ionized by solar radiation of wavelength less than 911 Å [e.g., Anderson, 1981]. However, as altitude increases in the F2-region the plasma density distribution is determined more by transport processes such as ambipolar diffusion, neutral wind drag and electrodynamic drift than by local ionization. Plasma is transported along the magnetic field lines by diffusion and the neutral wind effects, and across the magnetic field due to electromagnetic forces. There is a strong variability in the F2 layer peak and topside plasma density profile. This variability, and the occurrence of plasma instabilities, makes the predictability of the F-region density distribution and its effect on communications systems particularly difficult. The understanding of the ambient ionosphere is essential for the optimization of communications systems as well as for testing empirical and numerical ionospheric models.

Over the past 30 years numerous empirical and numerical models have been developed specifically for computing the electron density profiles either regionally, such as the Fully Analytic Ionospheric Model (FAIM) [Anderson et al., 1989] or globally, such as the International Reference Ionosphere (IRI) [Bilitza, 1989], the Parameterized Real-time

Ionospheric Specification Model [Anderson et al., 1991], the Utah State University (USU) Model [Sojka et al., 1985], and the Bailey/Sheffield Model [Bailey and Sellek, 1990]. There are also models that calculate the electron densities and apply these calculations to find other parameters, such as the Field Line Interhemispheric (FLIP) Model [Richards and Torr, 1988; Torr et al., 1990; Richards, 1991], which computes the peak electron concentration of the F2 layer (hmF2) in order to establish a relationship between hmF2 and the meridional winds. We will not discuss this model because it has no application at the equator.

The goal of most ionospheric modeling is an accurate representation of the electron density height profile with minimum computational time [Schunk and Szuszcewicz, 1988]. The models considered here are based on numerical/statistical descriptions of the ionosphere in terms of geographic or geomagnetic location, season, solar activity, and time. Data compiled from incoherent scatter radars, ionosondes, topside sounders, and in situ satellite and rocket profiles provide information on electron density profiles, and in particular on critical frequencies and peak electron density altitudes. From this melange of data emerges an "intelligent mix of empiricism, physics, extrapolation, and intuition" [Schunk and Szuszczewicz, 1988, page 19] which becomes the ionospheric plasma density profile.

The theoretical/numerical model profiles require solutions to the coupled continuity, momentum, and energy

equations for ions and electrons with respect to altitude or along geomagnetic flux tubes. The solutions give a spatial distribution for ionospheric densities, plasma drifts, thermospheric winds, and temperatures. However, since this results in a complex, time- and computer-time consuming problem, most modeling efforts thus far have been divided into regional models, covering the equatorial and low latitude ionosphere, mid-latitude ionosphere, or the high latitude ionosphere. Or they are parameterized versions based on solutions to the coupled equations with specific input parameters. Often the problem is further complicated by the lack of statistically meaningful baseline plasma density profiles for the regions considered.

In this thesis research I will examine Jicamarca incoherent scatter radar observations from 1964 to the present and compile a series of hourly baseline electron density profiles for each season for periods of minimum, moderate, and high solar cycle activity during magnetically quiet and disturbed times. Solar activity is determined by the F10.7 cm (2800 Mhz) solar radio noise flux units (10^{-22} W m^{-2} Hz^{-1}) (Φ) for the day of the observation. Magnetic activity is determined by the Kp index for the given observation. The examined data will be compared with the IRI, FAIM, and PRISM. This will determine the agreement between the numerical models and the experimental data, and also will indicate what changes need to be made to improve their predictive capability. The parameters of interest for

these comparisons are the peak density, peak height, topside and bottomside fit, and layer thickness. Finally, the main weaknesses of each model will be explored and suggestions made for their improvement and for future work.

CHAPTER II

THE EQUATORIAL IONOSPHERE

2.1. DESCRIPTION OF THE EQUATORIAL IONOSPHERE

The dynamics of the equatorial ionosphere is characterized by the unique geographic and geomagnetic features of the equatorial region of the Earth. The Coriolis force disappears at the equator, causing the winds to blow away from sunward side of the Earth. The Earth's geomagnetic field can be considered as a dipole field tilted approximately 11° from the geographic axis. The geomagnetic equator, as a result of this tilt, tends to deviate from the geographic equator northward in the Asian sector and southward in the American sector as illustrated in Figure 1. Intensity of the geomagnetic field at the equator also varies with longitude; it's highest in the Asian sector and lowest in the American sector. The horizontal configuration of the magnetic field lines over the equator is especially critical in the upper F2-region of the equatorial ionosphere, where diffusion along field lines is an important dynamic factor in determining the plasma distribution. Energy in the low latitude ionosphere comes primarily from solar heating.

The equatorial ionosphere is horizontally stratified due to gravity, and the regions can be specified by the plasma density. The approximate breakdown of the ionospheric region
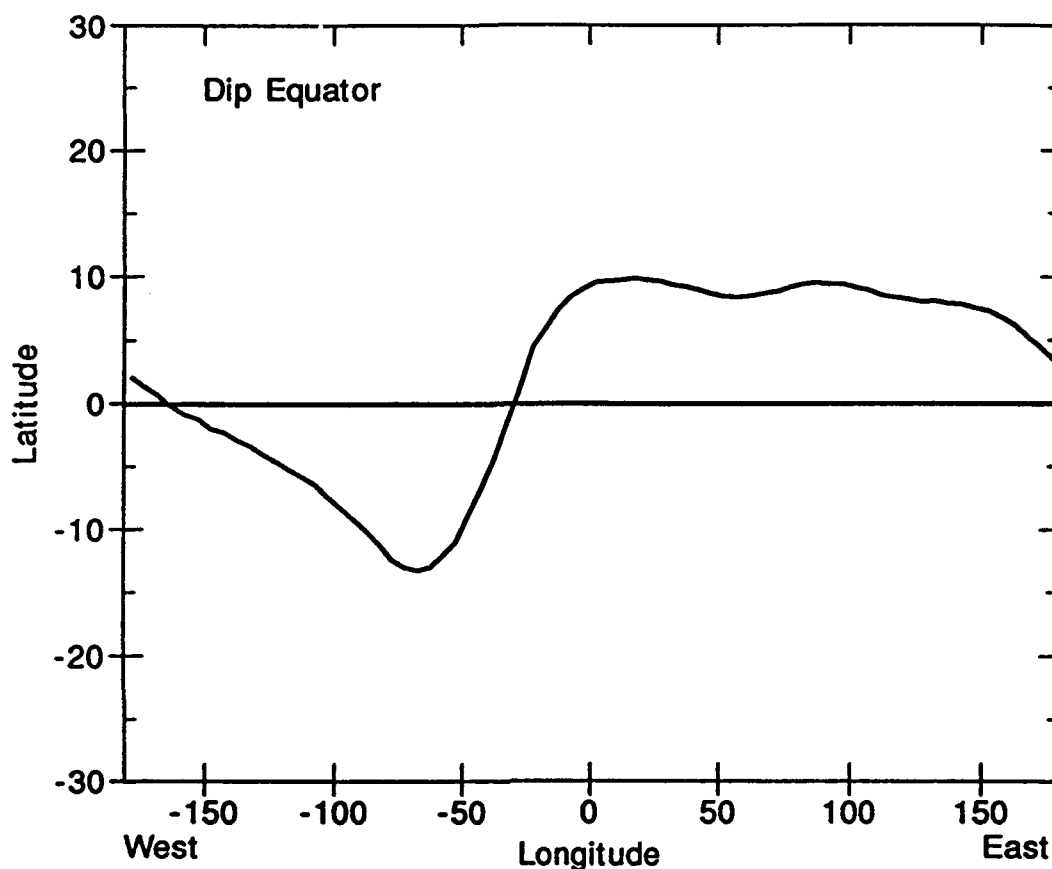
Fig. 1. Location of the magnetic dip equator world-wide.

by height and daytime plasma densities is given in Table 1.

The ionospheric plasma density distribution is the result of the complex processes of production, loss, and transport in the ionosphere. It also depends on the type of ionic species, which dictates the region's solar radiation absorption capacity and affinity for aeronomic reactions [e.g., Rishbeth and Garriott, 1969; Rajaram, 1977; Anderson, 1981; Kelley, 1989]. Figure 2 depicts the general structure

TABLE 1. Ionospheric regions by height and daytime density.

REGION	ALTITUDE RANGE	TYPICAL DENSITIES
D	60-90 km	$10^2 - 10^4$ cm^{-3}
E	90-150 km	$10^4 - 10^5$ cm^{-3}
F1	150-200 km	$10^5 - 10^6$ cm^{-3}
F2	200-800 km	$1.0 \times 10^6 - 3.0 \times 10^6$ cm^{-3}

of the ionosphere with respect to plasma density and chemical constituents. In the following sections we describe the main ionization production, loss, and transport processes.

2.2. PHYSICAL PROCESSES

2.2.1. Production

In the ionospheric regions below the height of the peak density (hmF2) production through solar ionization and loss through chemical reactions are frequent enough that transport is not as important in maintaining the plasma density. Molecular ions and neutrals are abundant in this region, providing ample opportunity for photoionization. As one moves higher in the ionosphere, atomic oxygen becomes the dominant ion until well into the topside ionosphere where helium and hydrogen prevail. Ionization reactions are determined by the chemical composition of each region. In the E- and F- regions the most important reactions are:
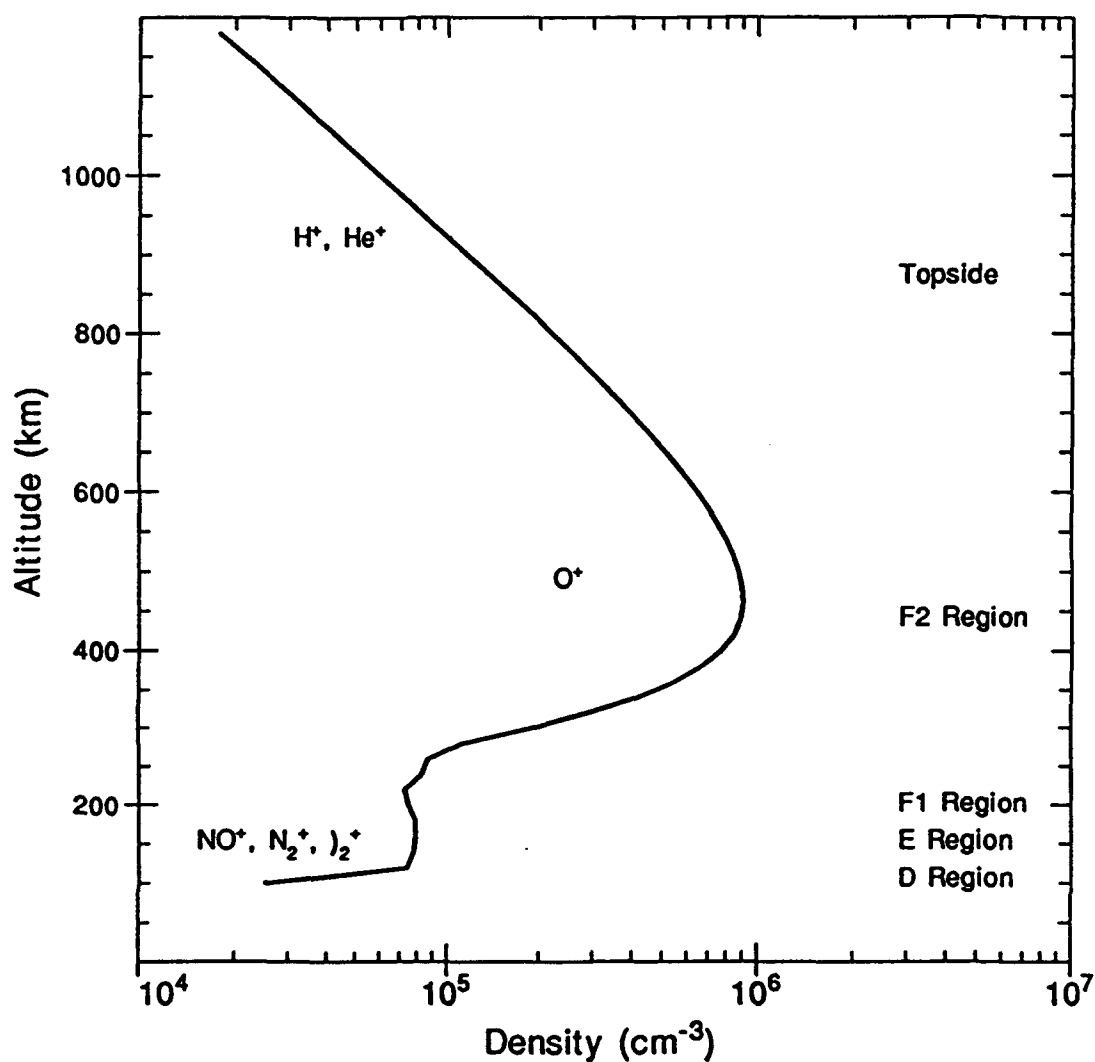
Fig. 2. Typical location of the D-, E-, F1-, and F2-regions of the atmosphere based on plasma density. The heavier molecular ions are dominant in the lower ionosphere where chemical reactions determine the ion concentration. The plasma density profile is similar to one under June solstice conditions for moderate F10.7 cm flux (Φ = 150 units) at 1800 LT.

$$N_2 + h\nu \rightarrow N_2 + e \rightarrow N^+ + N + e \tag{1}$$

$$O_2 + h\nu \rightarrow O_2^+ + e \tag{2}$$

$$O + h\nu \rightarrow O^+ + e \tag{3}$$

and

$$N + h\nu \rightarrow N^+ + e \tag{4}$$

where $h\nu$ is the energy from incoming solar radiation. The details of these reactions have been discussed by several authors [e.g., Rishbeth and Garriott, 1969; Schunk, 1983; Kelley, 1989]. Ionization production in the F2-region requires a minimum of 13.6 eV. Solar extreme ultraviolet (XUV) radiation of wavelength less than 911 Å provides enough energy for ionization of atomic oxygen.

2.2.2. Loss

At night, the plasma density decreases with the absence of solar ionization and the loss processes such as recombination or charge exchange. Recombination through ion-ion interaction occurs primarily in the lower ionosphere where the negative ions are more abundant for recombination with positive ions. Recombination through electron-ion interaction occurs throughout the ionosphere and involves electrons and molecular or atomic ions. In the lower altitudes the high concentration of molecular ions leads to

rapid recombination and the density at night can drop dramatically. The most common recombination reactions are:

$$NO^+ + e^- \rightarrow N + O \tag{5}$$

and

$$O^+ + e^- \rightarrow O + h\nu \tag{6}$$

In the first reaction (5), dissociative recombination, the molecule bonds with the electron and breaks apart into neutral ions. The reaction rate is approximately 1000 times faster [Kelley, 1989] than the second one (6), radiative recombination, which requires a photon emission to conserve energy and momentum. Because of the difference in reaction rates, the atomic ions have a much longer lifetime than the molecular ions. Molecular and atomic ions may also charge exchange, a two-step reaction in which the atomic ion exchanges its charge with a molecule, forming a molecular ion. The two most important charge exchange reactions are:

$$O^+ + O_2 \rightarrow O_2^+ + O \tag{7}$$

and

$$O^+ + N_2 \rightarrow NO^+ + N \tag{8}$$

The molecular ion will then dissociatively recombine (5). The rate coefficients for these reactions are dependent on the neutral gas temperature, and the rate at which O_2^+ and NO^+ are produced determines the loss rate of the electrons [e.g.,

Anderson, 1971; Anderson, 1973b]. Because the loss rate is proportional to the ion and neutral molecular density, it decreases with altitude.

The recombination reactions described above, as well as particle bombardment, produce optical emissions known as Airglow. At equatorial latitudes, above 160 km, the 6300 Å oxygen red line corresponds to enhanced F2 electron concentrations [e.g., Rishbeth and Garriott, 1969] and is an important mechanism for tracking the equatorial anomaly [Rajaram, 1977].

At higher altitudes in the F2 region, where the concentration of ions is reduced and the recombination rate is slower, transport becomes the key ingredient for maintaining the O^+ density. There are several mechanisms by which ions are transported: ExB drift, diffusion, and neutral thermospheric winds, for example.

2.2.3. Transport

The ionospheric electric field is generated by the low latitude thermospheric winds. The thermospheric winds above approximately 120 km are driven by pressure gradients due the daily temperature variations in the ionosphere which are caused by the daytime expansion of the atmosphere. The winds are generally westward during the day and eastward during the postsunset period, decaying from 150 m/s to 50 m/s between sunset and midnight at the equator; the winds are smaller elsewhere. At night, the winds arise from the thermospheric

bulge -- the sun heats the day side of the atmosphere, causing a temperature bulge which in turn causes winds which blow across the sunset terminator to the night side. The thermospheric neutral winds contribute to the transport of ionization by moving ions and electrons along the magnetic field lines. Daytime winds are poleward, forcing the ions down the field lines and resulting in lower peak heights. At night the winds blow towards the equator, forcing the ions up and increasing the altitude of peak plasma concentration. To within 3-5° of the magnetic equator the magnetic field lines are nearly horizontal and the thermospheric winds generate an interhemispheric flow. On a smaller scale the winds separate positive and negative charges in the ionosphere, which generates a charge density and an electric field which attempts to oppose the charge separation. This dynamo electric field associated with the thermospheric winds induces ionospheric currents in regions of large conductivities.

In the ionosphere, where the electric field (E) is essentially perpendicular to the magnetic field (b), the electrons and ions will drift with velocity ExB/B^2. An eastward electric field causes upward/poleward plasma drifts and an upward electric field drives a westward plasma motion. The general pattern of ionospheric plasma drifts was described by several authors [e.g., Richmond et al., 1980]. In the equatorial region, the vertical plasma drifts are upward during the day and downward at night with typical

values of 20-30 m/s. In the Peruvian equatorial region an upward drift velocity of 40 m/s corresponds to an eastward electric field of 1mV/m [Fejer, 1981, 1991]. The patterns of equatorial vertical (positive upward) ExB drift over Jicamarca for each season and for the three indicated levels of solar activity are presented in Figure 3. The average zonal drifts for three seasons and three levels of solar activity are illustrated in Figure 4. A comparison of Figure 3 and Figure 4 shows that seasonal and solar cycle variations have greater effects on the vertical drifts than on the zonal drifts. The equatorial vertical drifts move ionization up and down; the zonal drifts affect the density distribution only in longitudinal sectors with large magnetic declination.

The evening upward drifts show significant prereversal and post sunset enhancements near dusk during equinox and December solstice solar maximum conditions, as seen in Figure 3. The prereversal enhancement raises the F2 layer to regions of decreased neutral concentrations where the recombination rates are significantly reduced and the ion lifetime is extended [e.g., Anderson, 1971; Anderson, 1973a,b; Fejer, 1991]. This effect is essential in the establishment of the nighttime distribution of ionization in the equatorial and low latitude ionosphere. A large prereversal enhancement can cause a rapid post-sunset rise in the F2 layer, which often contributes to the occurrence of instabilities such as equatorial spread F [e.g., Fejer and Kelley, 1980; Anderson, 1981; Fejer et al., 1991]. A steep
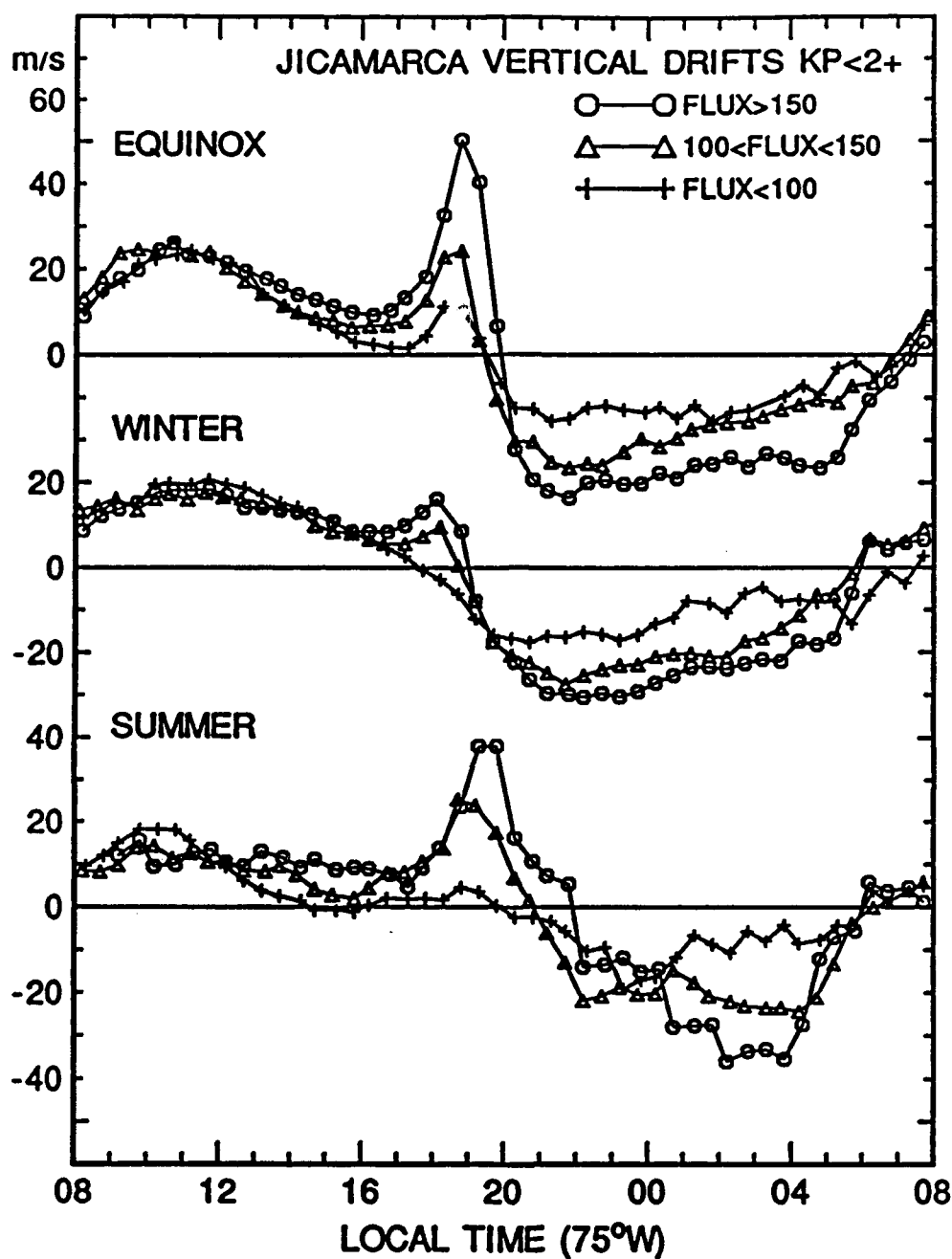
Fig. 3. Average vertical plasma drifts for equinox, winter, and summer for three flux levels, measured at Jicamarca (after Fejer et al., [1991]).
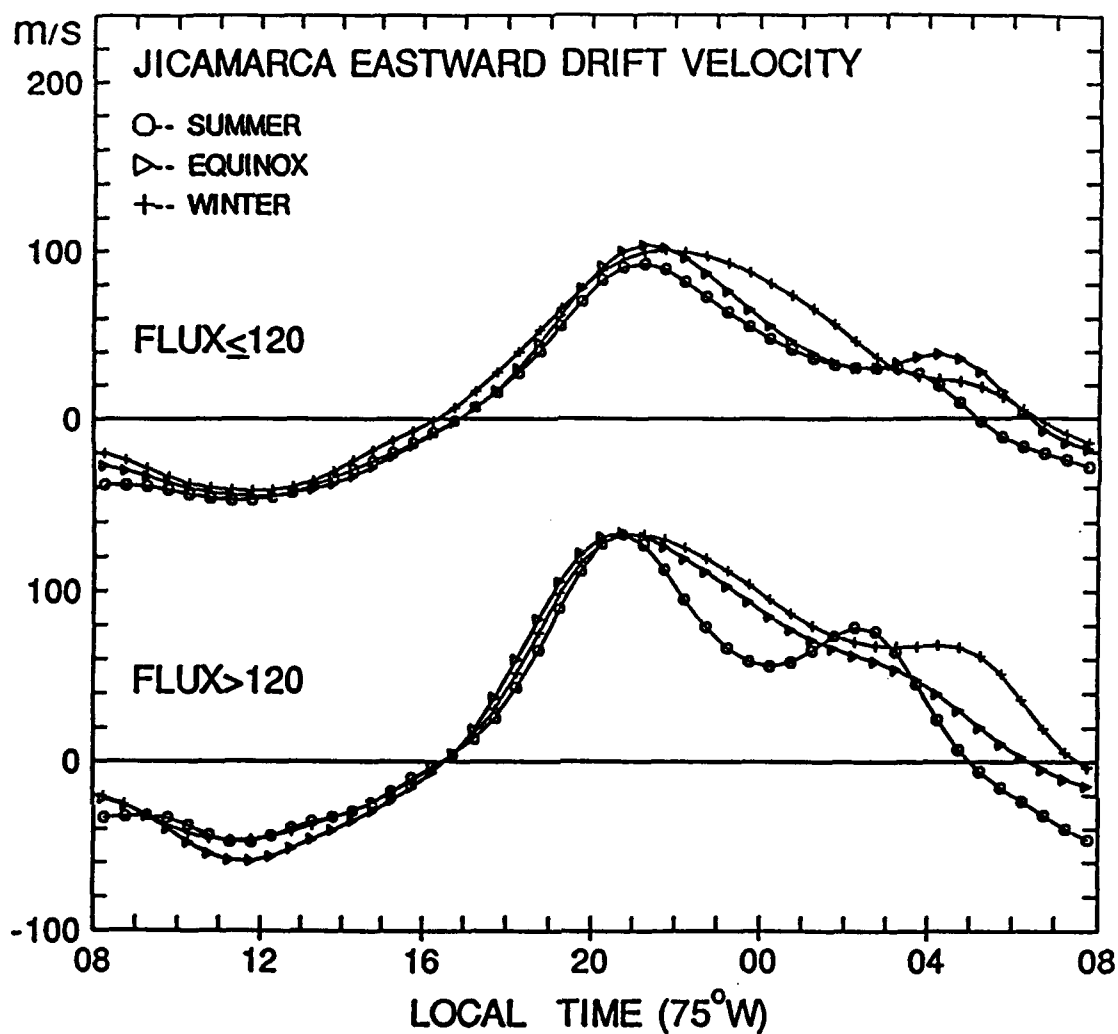
Fig. 4. Seasonal variations of the zonal plasma drifts over Jicamarca for low and high solar activity. The drifts are positive eastward. The daytime westward drift velocities do not change appreciably with flux, the nighttime eastward drift velocities increase with flux for all seasons (after Fejer et al., [1991]).

upward density gradient in the bottomside of the F2 region at night results from the molecular recombination with no solar ionization to offset the loss.

The vertical drifts at the equator are the primary force determining the height of the plasma layer. Daytime drifts raise the layer, causing the peak to become broader and the topside denser as ionization is moved into regions where transport effects apply (above 300 km). The evening prereversal enhancement moves the layer out of the chemical loss region to a region where the ionization is transported in from the sunlit side. This maintains the nighttime F2 layer. Under the influence of the nighttime downward drift, the layer moves to lower altitudes (approximately 200-300 km) just prior to sunrise. At sunrise solar radiation causes production to begin and the daytime electric field moves the layer up.

The electromagnetic force from the electrostatic field will transport ionization across magnetic field lines. The nonelectromagnetic forces in the ionosphere -- gravitation, pressure gradients, and collisions -- are not strong enough to move the ionization perpendicular to the magnetic field lines [Anderson, 1971]. These forces will, however, move the ions and electrons parallel to the magnetic field at similar rates because the two are held together by electrical forces. In the F2 region collisions are less frequent and ions and electrons tend to diffuse together unless a strong force is present to separate the charge. Under the influence of the

daytime upward vertical drift, the plasma will move to higher altitudes and diffuse along the field lines to higher latitudes, leaving what is termed the "noon bite-out" at the equator. This process is fundamental in creating the equatorial ionization anomaly [Appleton, 1946; Lyon and Thomas, 1963; Thomas, 1968; Sharma and Hewens, 1976; Anderson, 1971; Anderson, 1973a,b; Rajaram, 1977; Rajaram and Rastogi, 1977; Anderson, 1981; Raghavarao et al., 1988]. In addition to the vertical drift and diffusion effects on the equatorial anomaly, the interhemispheric plasma flow during solstices results in higher electron densities in the winter hemisphere than in the summer hemisphere by the transport of ionization.

CHAPTER III

PRESENTATION AND ANALYSIS OF JICAMARCA DATA

3.1. INTRODUCTION

F-region plasma density data have been obtained from the Jicamarca Incoherent Scatter Radar, Peru, from 1964 to the present, covering more than two solar cycles. The location of the Jicamarca radar -- the American sector incoherent scatter radar closest to the magnetic equator -- makes it ideal for equatorial ionospheric studies. There is an extensive database of plasma density observations from 1961 to the present from Jicamarca, facilitating a comprehensive study of density variation over a solar cycle. The data sets are compiled from isodensity contour plots reported by McClure et al. [1970] from 1964 to 1966, from unpublished contour plots covering 1965-1974, from Faraday rotation data for select days in 1895, 1989, 1990, and 1991, and profiles from 1966 to 1969 were obtained from the Coupling, Energetics, and Dynamics of Atmospheric Regions (CEDAR) database at the National Center for Atmospheric Research. The isodensity plots were digitized to determine the height profile of the plasma density at selected times. Figure 5 shows an example of a typical isodensity profile.

The Jicamarca radar operates at a frequency of 49.92 MHz with a 290x290 m^2 antenna array consisting of 9216 pairs of
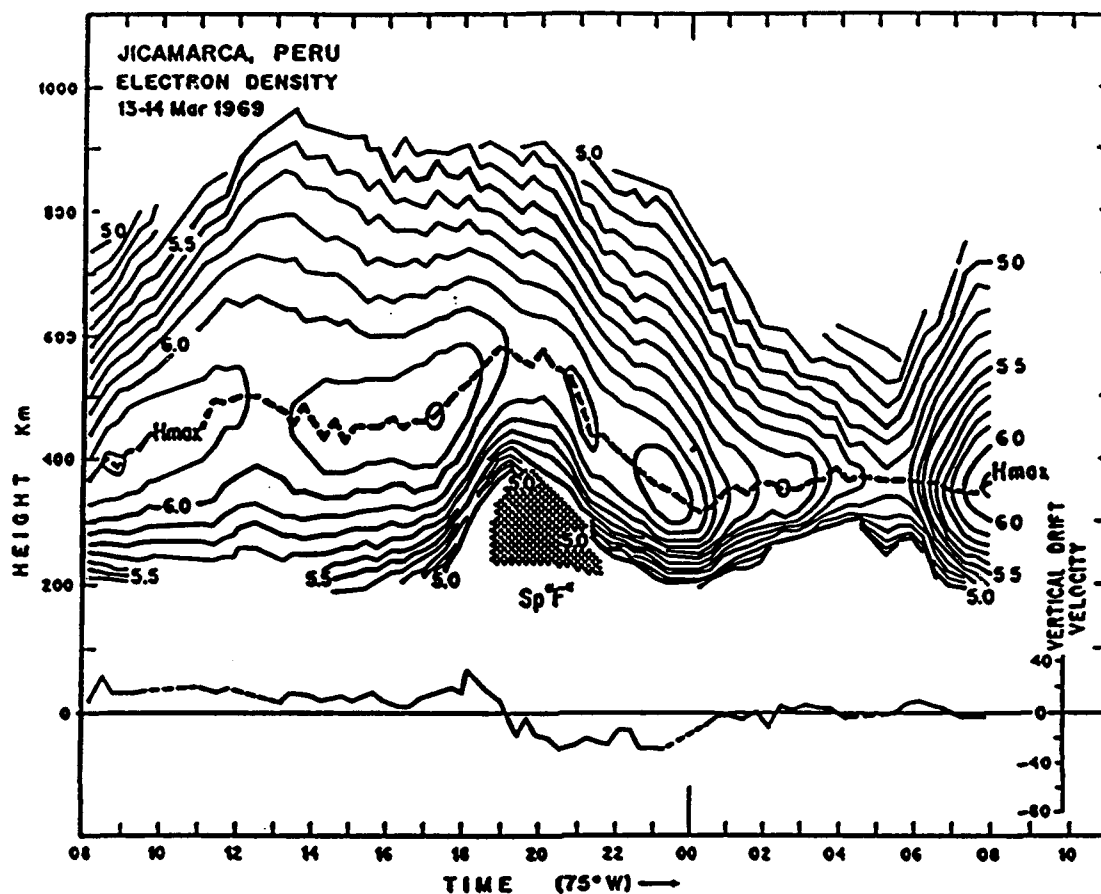
Fig. 5. Isodensity contour plot for Jicamarca, Peru, 13-14 March 1969. The contours are logarithmic (5.0 corresponds to 10^5 electrons/cm^3). The heavy dashed line corresponds to the peak density and height. The vertical drift velocity is presented at the bottom of the figure. The presence of coherent echoes (caused by F-region irregularities) is indicated by the small dotted portion seen between 1800 and 2100 LT.

crossed half-wave dipoles arranged in 64 modules of 12x12 pairs each. The antennae within each module are all in phase, but the phase of each module relative to each other may be changed. The beam can be steered approximately 3-4° in any direction off axis, to include directions parallel and perpendicular to the magnetic field. The radar can be used

to calculate ion and electron temperature, plasma density, and ion drifts as functions of altitude from backscatter due to thermal fluctuations. The plasma density is determined from the Faraday rotation of the scattered signal, a process that is good from 150 to 800 km using a single power profile [McClure et al., 1970]. Higher altitudes may be reached using additional power measurements, and coverage of the lower altitudes is obtained from ionosonde measurements. The power profiles are fit to the profiles from Faraday rotation where independent Jicamarca data indicate that the ion and electron temperatures are equal. The accuracy of the measurement near the peak is usually better than 5% [McClure et al., 1970] for densities greater than 10^4 cm^{-3}. Above 500 km the random errors in the measurements increase because of decreasing radar sensitivity, decreasing electron concentration, and increasing Faraday dispersion.

In our study density profiles were smoothed using a three-point running average. Data as close to the hour on either side were used and these were averaged to create a single profile for that hour. As an example, a 1945 and 2015 local time (LT) observation were averaged to create a profile at 2000 LT. When available, observations from consecutive days were used to eliminate any transient effects in the data.

The data were binned according to F10.7 cm flux less than 100 units for low solar activity; flux between 100 and 150 units for moderate activity; and flux above 150 units for

high solar activity. The bins were chosen based on the solar cycle distribution of the Jicamarca observations we used. The hourly data were divided into observations for each season per flux bin. The seasons are December solstice (November - February), June solstice (May - August), and equinox (March, April, September, and October). This seasonal organization is typical of that used in the most models. Data sets were also grouped bimonthly, i.e., November and December, and in smaller flux bins, i.e., 100 to 125 units, where there are adequate profiles available.

In order to establish a single averaged profile for the specified parameters (flux, season, and hour) each data point (height versus density) was binned into 40 km bins, and each profile for the flux bins was averaged together to establish a single profile and standard deviation in the resulting data file. However, we have used the unbinned raw data for determining the variation of the peak electron density and layer height as a function of solar activity. The layer thickness is determined using average profiles from 10 unit flux bins.

The emphasis of the following analysis is on peak density (NmF2) and corresponding peak height (hmF2), on bottomside and topside profiles, and on the overall layer thickness (ΔH). The layer thickness is directly related to the total electron content (TEC) of the layer. The layer thickness used in these evaluations is based on the

calculations incorporated into PRISM by <u>Anderson et al.</u> [1991] and is defined as:

$$\Delta H = TEC/NmF2 \qquad (9)$$

where ΔH is the thickness of the layer (km) and TEC (m^{-3} km) is the integrated electron content evaluated by:

$$TEC = \sum_{i=1}^{n} \frac{DEN(i)\,HGT(i)}{1000}$$

$$(10)$$

where:

$$DEN(i) = \sum_{j=1}^{i} \frac{den(j) + den(j+1)}{2}$$

$$(11)$$

and

$$HGT(i) = \sum_{j=1}^{i} hgt(j+1) - hgt(j)$$

$$(12)$$

where den(i) and hgt(i) refer to the individual density and corresponding height of the plasma profile and 1000 represents a scaling factor. We examine the daily and seasonal variations during low, moderate, and high solar flux

conditions. Unless indicated, all data are from magnetically quiet (Kp < 4.0) days.

3.2. SOLAR MINIMUM CONDITIONS

The observations from solar minimum are examined for the hours 1200 LT, 1800 LT, 2000 LT, 0000 LT, and 0400 LT for each of the three seasons to illustrate the behavior of the equatorial ionospheric plasma density. There is little variation in the peak density and height during daytime hours, so the 1200 LT observations were chosen to represent typical daytime conditions. We have examined 1700 LT observations, but only the significant deviations from the 1200 LT data will be described. Two hours were chosen around sunset to examine the evening variability of the plasma. Midnight was selected to represent the nighttime conditions, and 0400 LT to represent the state of the ionosphere just prior to sunrise.

Figure 6 provides an example of the variability of the 1200 LT daily electron density profiles for December solstice solar minimum conditions. The measurements were made in 1964, 1965, 1966, 1972, and 1974. The top curve is an average of those profiles with horizontal bars representing the standard deviations from the averages. The observations in Figure 6 were made during periods with Kp < 4.0.

The midday quiet-time solar minimum ionosphere is characterized by plasma densities of generally less than 1.00×10^6 cm^{-3}. A summary of layer parameters is given in
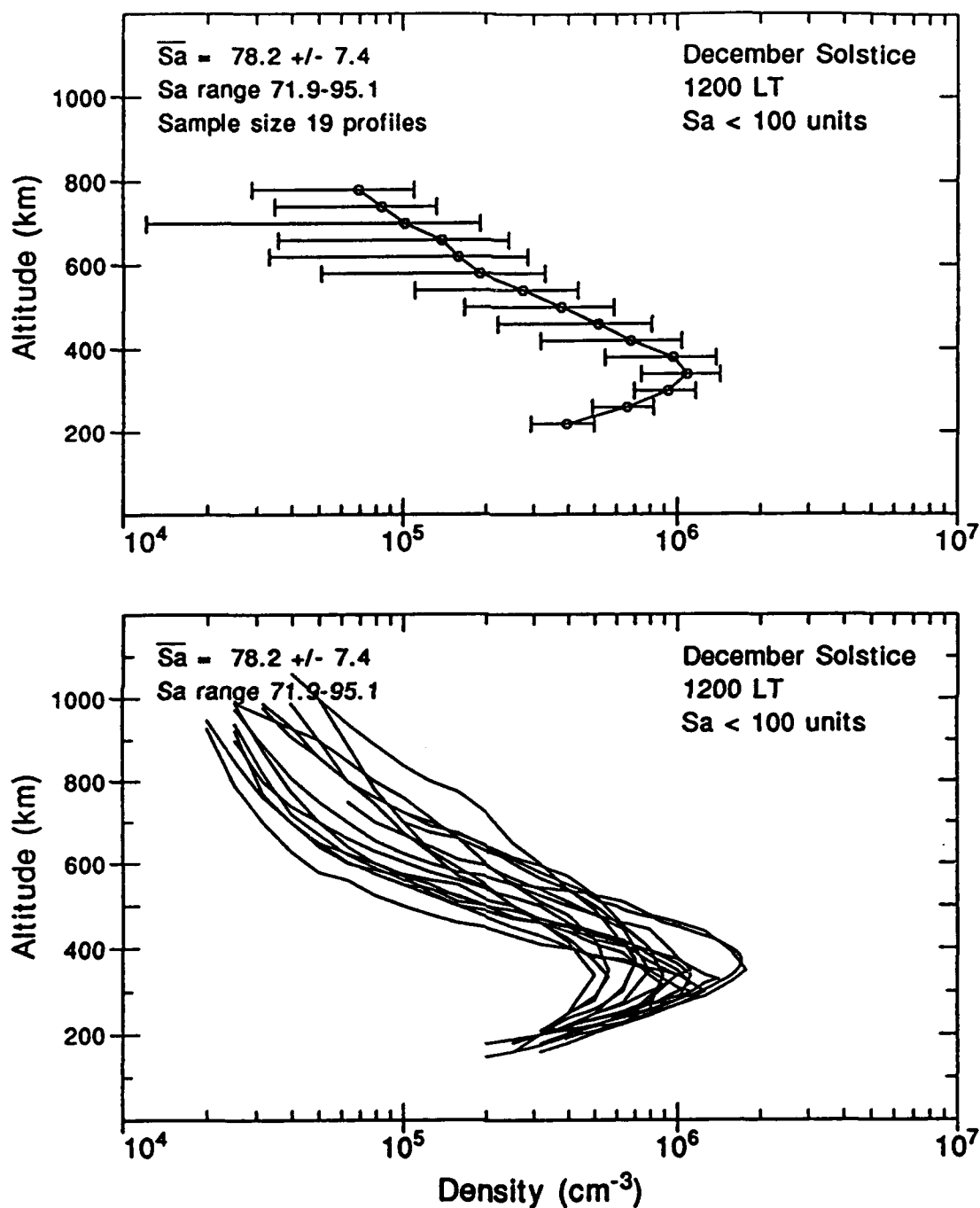
Fig. 6. Scatter plot (bottom panel) and average profile (top panel) for 1200 LT, December solstice, solar minimum conditions. The average flux of the data is given in the upper left corner of each panel along with the range of the flux of the samples. The number of samples is provided in the upper left corner of the top panel.

Table 2. Notice that the number of days of observations, given in the upper right corner of each box, is smallest during June solstice. The day to day variability of the data is evident for all seasons. The layers are between 230 and 270 km wide and the peaks center around 340 km. The results at midday are:

1) The average peak density is largest in summer (November - February), least in winter (May - August). This result may be biased by the number of summer observations (19) versus equinox observations (7) and winter observations (7).

2) The layer height is highest at equinox, lowest at June solstice. These results were obtained without binning the density measurements into 40 km height ranges.

3) The bottomside gradient is steeper for winter than for summer or equinox. The bottomside densities for each season have smaller scatter below 300 km.

4) The topside density gradients show no seasonal variation. All seasons exhibit larger variations in the topside than bottomside electron densities.

5) The F2 layer is broadest during winter and thinnest observed at summer at noon. The 1700 LT equinoctial profiles are the thickest. The equinoctial profiles for 1200 and 1700 LT display both the low density characteristic of winter months and the high density features typical of summer months. We will come back to this point later.

TABLE 2. Averaged peak electron density (cm^{-3}), peak height (km) and layer thickness (km) for each season at solar minimum. Standard deviations of the density average are given in parentheses below the average density, the number of samples contributing to the average are to the right of the density.

Season	Summer		Equinox		Winter	
1200 LT	9.16×10^5	19	9.00×10^5	7	4.36×10^5	7
(σ)	(2.7×10^5)		(4.5×10^5)		(8.5×10^4)	
hmF2	342		352		333	
ΔH	235		265		278	
1700 LT	1.04×10^6	9	7.44×10^5	6	5.68×10^5	5
(σ)	(1.5×10^5)		(3.9×10^5)		(9.3×10^4)	
hmF2	330		359		327	
ΔH	255		262		254	
1800 LT	1.03×10^6	17	8.27×10^5	8	5.44×10^5	6
(σ)	(1.8×10^5)		(3.3×10^5)		(1.3×10^5)	
hmF2	342		347		333	
ΔH	242		245		235	
2000 LT	7.80×10^5	18	5.34×10^5	3	4.45×10^5	6
(σ)	$(2.8 \times 10^5$		(1.5×10^5)		(1.2×10^5)	
hmF2	354		362		311	
ΔH	239		217		194	
0000 LT	3.43×10^5	9	5.32×10^5	5	N/A	
(σ)	(1.4×10^5)		(2.9×10^5)			
hmF2	341		306			
ΔH	256		213			
0400 LT	6.90×10^4	6	1.50×10^5	3	N/A	
(σ)	(5.5×10^4)		(1.0×10^5)			
hmF2	265		276			
ΔH	224		209			

At 1800 LT the summer and equinoctial plasma layers typically undergo a small increase in vertical drift as a result of the prereversal enhancement, the density layers show a slight increase in peak height consistent with the vertical drift observations from Jicamarca, illustrated in Figure 3 from Chapter II. An example of the 1800 LT December solstice data is given in Figure 7. The results of the

$\overline{Sa}$ = 77.8 +/- 6.4
Sa range 73.1-95.1
Sample size 17 profiles

December Solstice
1800 LT
Sa < 100 units

$\overline{Sa}$ = 77.8 +/- 6.4
Sa range 73.1-95.1

December Solstice
1800 LT
Sa < 100 units

Density (cm^{-3})
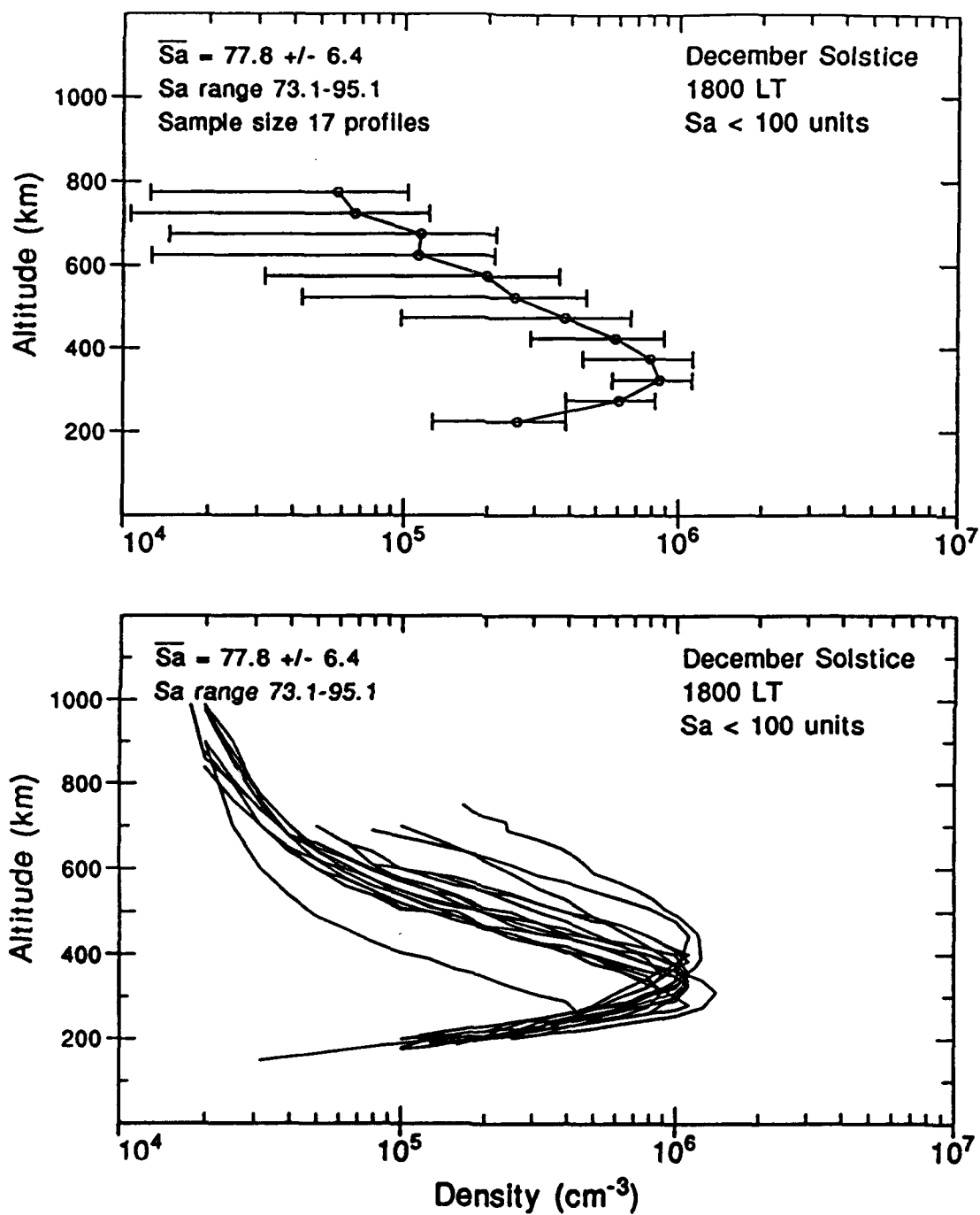
Fig. 7. Scatter plot (bottom panel) and average profile (top panel) for 1800 LT, December solstice, solar minimum conditions.

plasma density observations at 1800 LT, solar minimum conditions, are:

1) The peak density is still greater in summer than in equinox or winter.   In this case the winter NmF2 is almost half that of the summer NmF2 (see Table 2).

2)   The peak height is greatest for equinox and smallest for winter.

3) The bottomside densities show little variability for all seasons up to 300 km.   The density gradients for all seasons are comparable.

4)   The topside density distribution shows smallest scatter at June solstice although there is only a small number of observations, and is most variable at December solstice (Figure 7).   The topside gradients are comparable for each season whereas the topside densities are the lowest in winter and highest in equinox.

5) The layer is broadest at equinox, but the difference between widest and most narrow layer is only 30 km.

The observations at 2000 LT reflect the condition of the ionosphere immediately after sunset for each season.   There is a decrease in both layer electron density and peak height. The results for equinox are speculative based on the lack of enough data for this hour under these solar flux conditions. The December solstitial data exhibit large variability for a range of ϕ between 71 and 96 units, as seen in Figure 8.   The following summarizes these postsunset observations:

Fig. 8. Scatter plot (bottom panel) and average profile (top panel) for 2000 LT, December solstice, solar minimum conditions.

1)   The NmF2 during summer is greater than winter or equinox, corresponding to the longer period of sunlight available during this season. At this time, the winter NmF2 is almost half that of summer.

2)   The summer and equinox hmF2's are greater than winter. The summer layer at 350 km is almost 40 km higher than it was at 1800 LT. The heights of the equinoctial and winter layers are decreasing.

3)   The bottomside density distribution at December solstice is broader than seen in earlier observations. There is not enough bottomside data for either winter or equinox to make a conclusive statement. The bottomside electron density gradients during the solstices are comparable and larger than the equinoctial average gradient.

4)   The topside densities show large variability for summer. The density gradients are all comparable, but the densities are significantly less during winter.

5)   The width of the post sunset layer is greatest during summer (240 km) and least in winter (195 km).

At local midnight there was one observation available for June solstice, so the analysis will concentrate on December solstice and equinox. The layers for each season are situated at lower heights and the densities have decreased from their daytime and evening counterparts. The day to day variability of the profiles is evident in the equinoctial profiles shown in Figure 9. At midnight, the main results are:
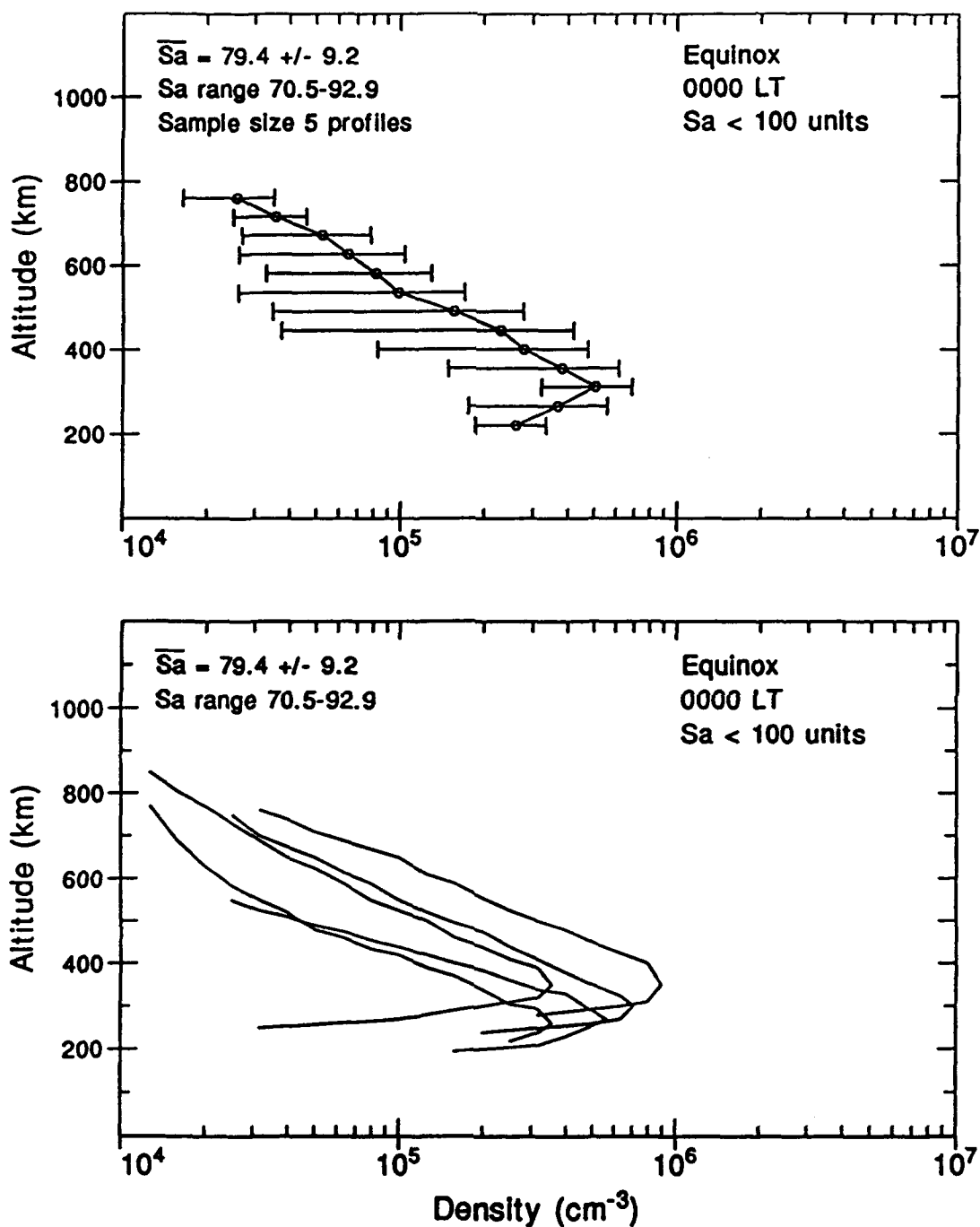
Fig. 9. Scatter plot (bottom panel) and average profile (top panel) for 0000 LT, equinox, solar minimum conditions.

1) The peak density at equinox is greater than during summer. There are large density variations for both seasons.

2) The equinoctial layer is over 100 km lower than the summer layer, reflecting the stronger post-sunset downward drifts during this season (see Figure 3).

3) The bottomside density layers are highly variable, in contrast to the daytime and evening observations.

4) There is also large variability in the topside layers. The averaged profiles indicate comparable topside density gradients for both seasons.

5) The layer average thickness is greatest for December solstice (302 km). However, these results may be questionable as a result of the small number of samples. The layer is 213 km thick at equinox.

There was a similar lack of data at 0400 LT during June solstice. The very limited data at equinox (Figure 10) are more similarly shaped and placed than the profiles that contribute to the summer average. We present this figure and these results for completeness. Both seasons show the layer has moved to lower heights (around 270 km) and that the densities are smaller by almost a factor of two than seen in the daytime observations. These results are consistent with the nighttime downward vertical drift moving the layer away from a region of transport which helps to maintain the density into a region of faster loss rates through recombination with neutral molecules. The characteristics of the pre-sunrise ionosphere at solar minimum are:
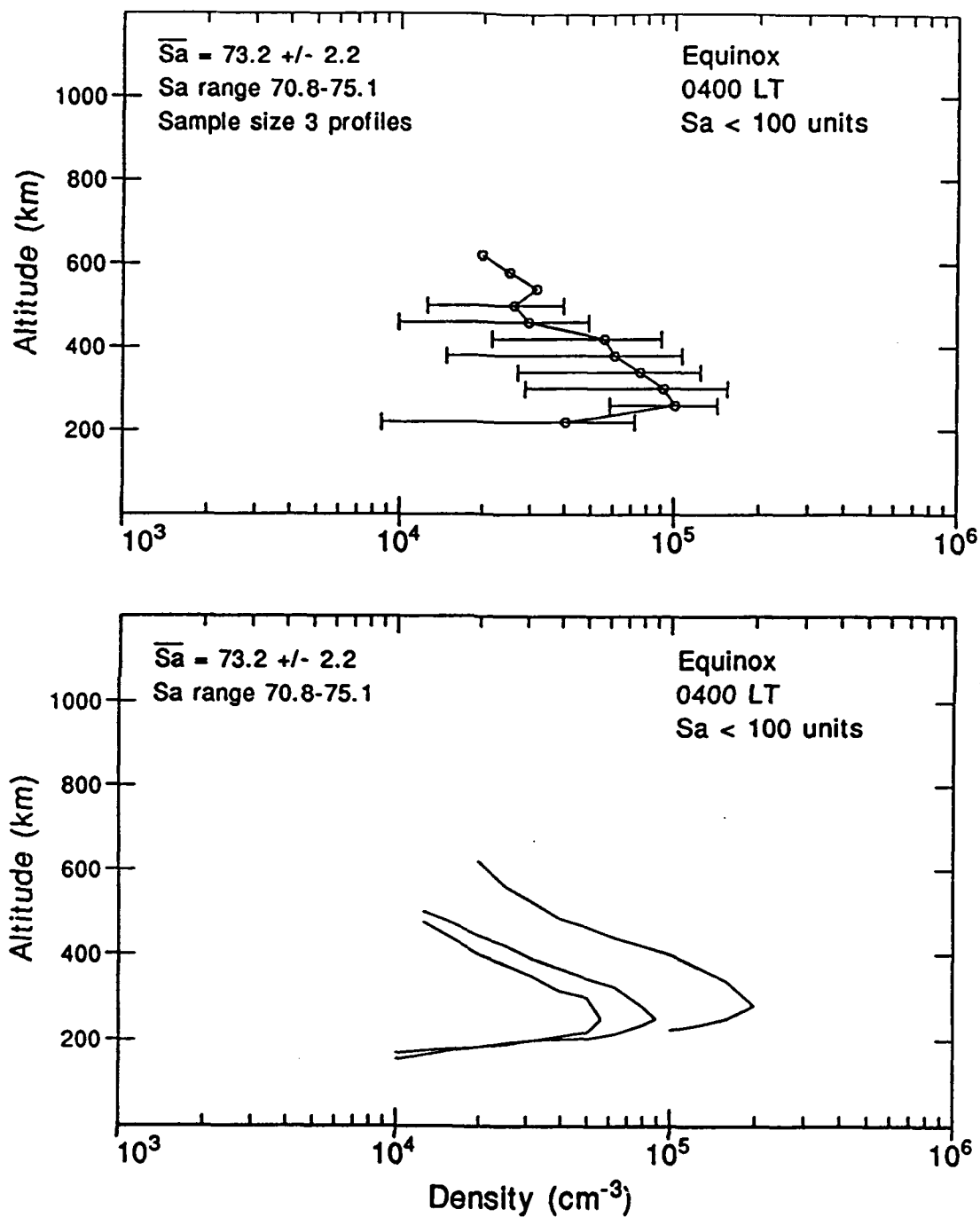
Fig. 10.   Scatter plot (bottom panel) and average profile
(top panel) for 0400 LT, equinox, solar minimum conditions.
We include this figure for completeness.

1)   The peak densities are greater in equinox.   A comparison of December solstice and equirox scatter plots shows that the two seasons have similar profiles with the exception of the largest one on each, but the statistics are very weak for this time frame so not much can be concluded accurately.

2)   The peak height is centered around 270 km for each season.

3)   The topside density decreases less with height during December solstice than during equinox.   There was not enough data available to make a bottomside comparison.

4)   The calculated layer thickness for December solstice was 369 km as a result of the unreliable density available for this period.   The thickness of 208 km for equinox seems more reasonable.

Figure 11 presents a summary of the hourly profiles for each season and selected times.   No profiles are presented when the number of measurements is smaller than five.   The main results can be summarized as:

1)   The noontime summer electron densities are significantly larger than evening or nighttime periods, as one would expect with the presence of daytime solar ionization.   This result is less dramatic for equinox and winter.

2)   There is little difference in the 1800 and 2000 LT profiles during summer.   The 2000 LT layers are clearly less dense in equinox and winter.   The layer height increases from

Fig. 11. Hourly variations in the electron density profiles for (a) December solstice, (b) equinox, and (c) June solstice, solar minimum conditions. The average flux of each profile is given in the legend.

1700 LT to 2000 LT in summer, from 1800 to 2000 LT in equinox, and decreases from 1800 LT to 2000 LT in winter.

3) The comparisons with midnight data are meaningless and the 0400 LT data have not been used in this figure because of the poor statistics.

3.3. MODERATE SOLAR CONDITIONS

The flux bin of 100 to 150 units used for moderate solar activity enables a much more meaningful comparison of the profile parameters for each season. Under increased solar activity the plasma concentration and peak layer height increase. There is no significant increase in daytime vertical drift (see Figure 3), but there is an increase in prereversal enhancement and nighttime downward vertical drift. Because the range of solar activity is so large, the data appear quite variable in some instances. In these cases the data were divided into smaller flux bins to determine if the variability was due to solar ionization effects and into bimonthly profiles to determine if the variability was due to seasonal effects. These results will be discussed below. Again, the comparisons begin with the noon profiles.

The midday layers are similar in shape and altitude placement for each season. There are no outstanding features present in the noontime or 1700 LT profiles. Refer to Figure 12 for an example of the 1200 LT summer profiles. A comparison of the three seasons shows:
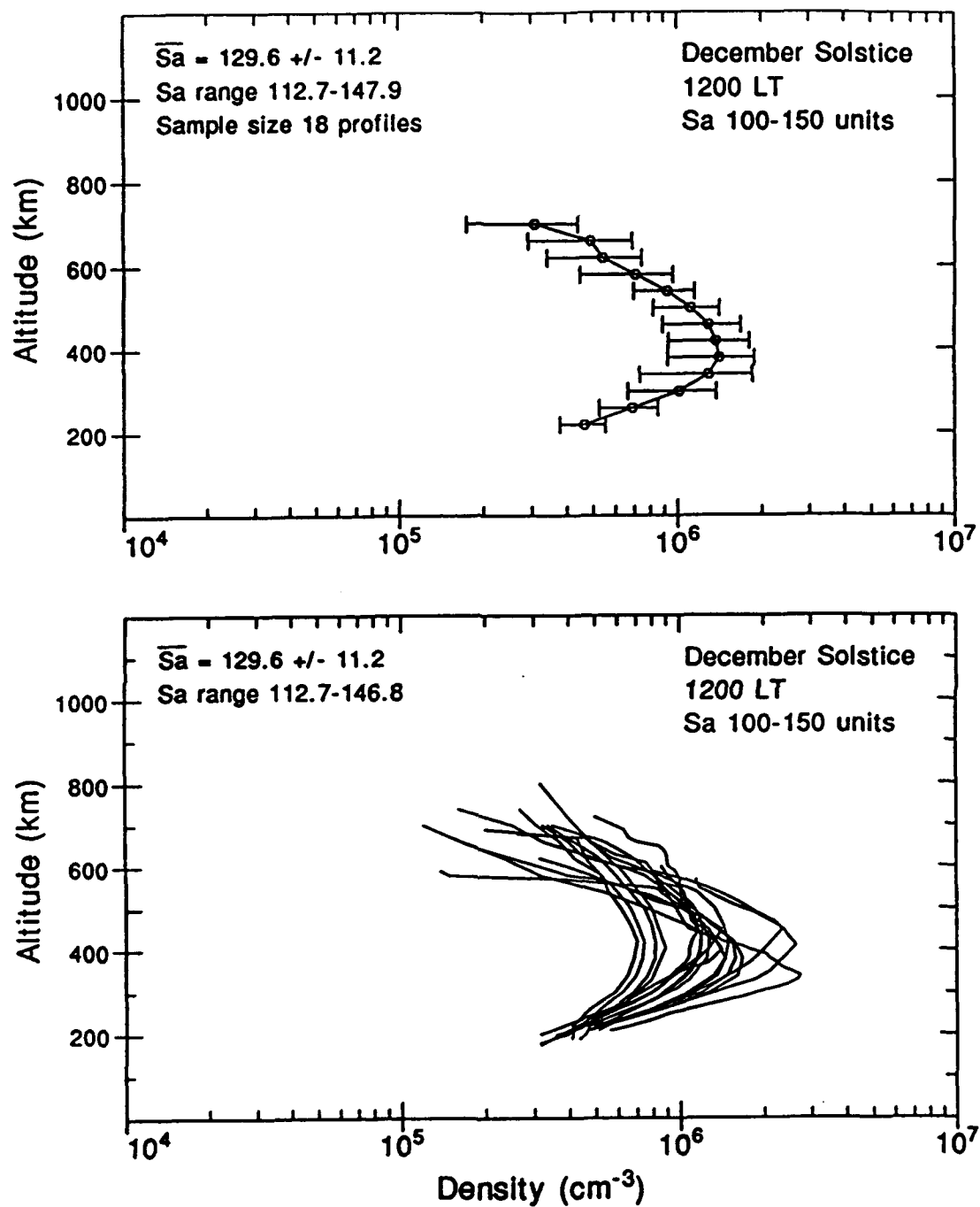
Fig. 12. Scatter plot (bottom panel) and average profile (top panel) for 1200 LT, December solstice, moderate solar conditions.

1)   The peak density in summer and equinox are not significantly different (see Table 3). Both peaks are almost twice the magnitude of the winter peak.

2)   There is a difference of about 40 km between the lowest peak at June solstice and the highest peak at equinox.

3)   The bottomside layer is less dense in winter, but the density gradient is identical for each season. The bottomside in summer has the broadest density distribution.

4)   The topside density distribution is also greatest for December solstice. The topside density gradient is comparable for all seasons.

5)   The F2 layer is the broadest at equinox (around 375 km) and most narrow during the December solstice (around 320 km).

At 1700 LT the topside gradient is largest in equinox and decreases the most rapidly in summer. The bottomside layers for all seasons are higher at 1700 LT. All other parameters follow those seen at 1200 LT.

The vertical drift during equinox causes the 1800 LT layer to be higher than at solstice, increasing the bottomside gradient and moving the layer above the region of peak production which lowers the peak density and broadens the layer immediately around the peak. It also places the layer in a region of increased transport, which causes the topside to be denser and the layer to be wider. At 1800 LT the main characteristics of the ionosphere over Jicamarca are:

TABLE 3. Averaged peak electron density (cm^{-3}) and height (km), and layer thickness (ΔH) for each season during moderate solar flux. Standard deviations to the peak density are given in parentheses below the average density, the number of samples contributing to the average are to the right of the density.

Season	Summer		Equinox		Winter	
1200 LT	1.52×10^6	18	1.35×10^6	11	9.18×10^5	20
(σ)	(5.9×10^5)		(4.3×10^5)		(1.9×10^5)	
hmF2	411		432		395	
ΔH	319		375		353	
1700 LT	1.70×10^6	27	1.48×10^6	28	8.63×10^5	17
(σ)	(3.6×10^5)		(4.7×10^5)		(1.7×10^5)	
hmF2	410		435		398	
ΔH	287		360		351	
1800 LT	1.65×10^6	32	1.45×10^6	30	8.22×10^5	19
(σ)	(3.9×10^5)		(4.6×10^5)		(2.3×10^5)	
hmF2	427		461		405	
ΔH	331		347		329	
2000 LT	1.31×10^6	21	1.00×10^6	26	6.80×10^5	14
(σ)	(4.1×10^5)		(3.0×10^5)		(1.3×10^5)	
hmF2	498		490		414	
ΔH	326		367		297	
0000 LT	5.71×10^5	19	8.17×10^5	29	5.27×10^5	15
(σ)	(3.6×10^5)		(2.9×10^5)		(1.5×10^5)	
hmF2	437		327		311	
ΔH	299		255		246	
0400 LT	3.18×10^5	5	2.73×10^5	20	2.75×10^5	9
(σ)	(9.1×10^4)		(6.5×10^4)		(1.00×10^5)	
hmF2	293		302		321	
ΔH	190		275		219	

1) The peak density in summer and equinox is almost twice as great as in winter. Figures 13, 14, and 15 illustrate the seasonal profiles.

2) The peak height is highest during equinox and lowest in winter.

3) The bottomside density is steepest during equinox.

$\overline{Sa}$ = 131.6 +/- 13.2
Sa range 105.5-149.3
Sample size 32 profiles

December Solstice
1800 LT
Sa 100-150 units

$\overline{Sa}$ = 131.6 +/- 13.2
Sa range 105.5-149.3

December Solstice
1800 LT
Sa 100-150 units

Altitude (km)

Density (cm^{-3})
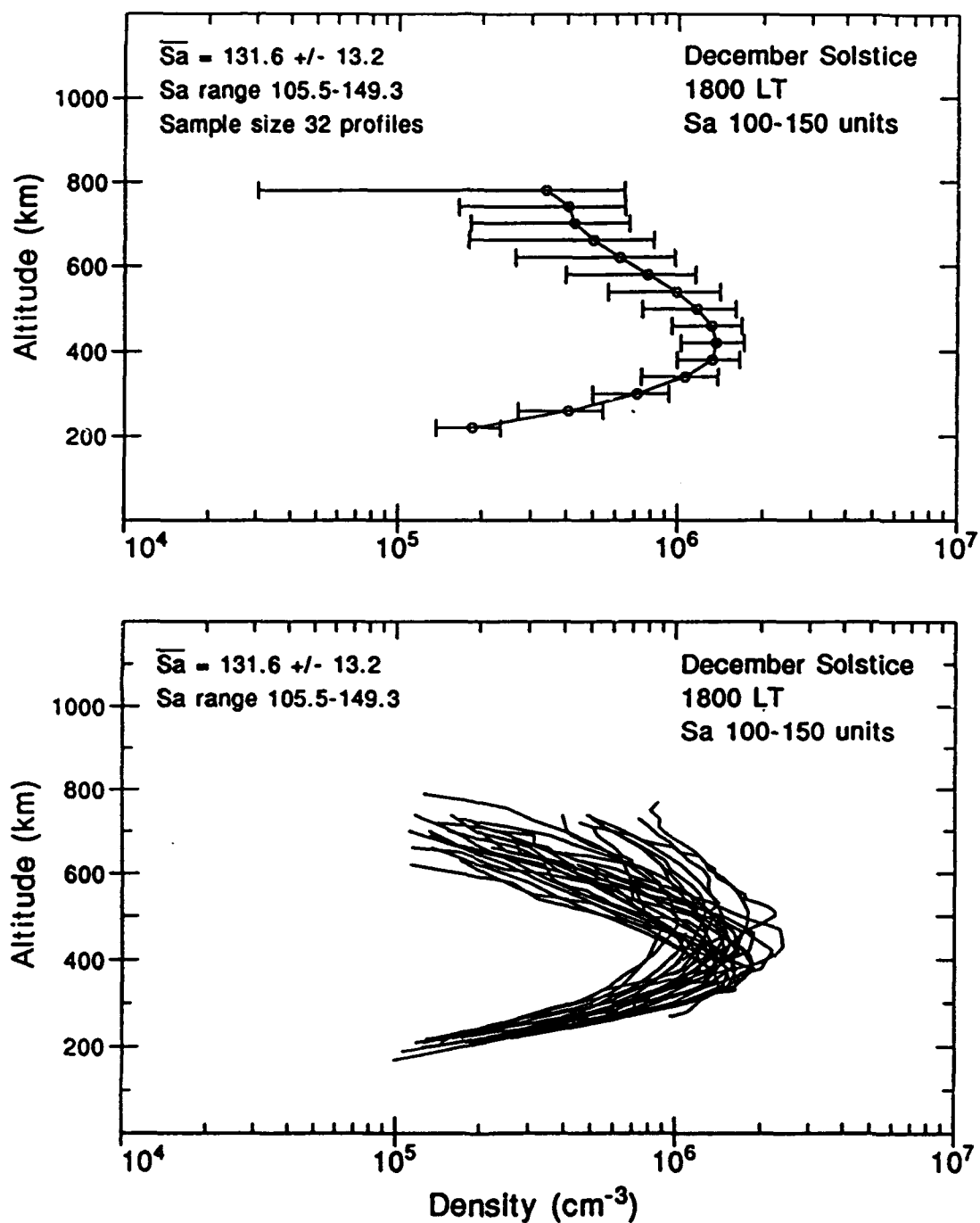
Fig. 13. Scatter plot (bottom panel) and average profile (top panel) for 1800 LT, December solstice, moderate solar conditions.
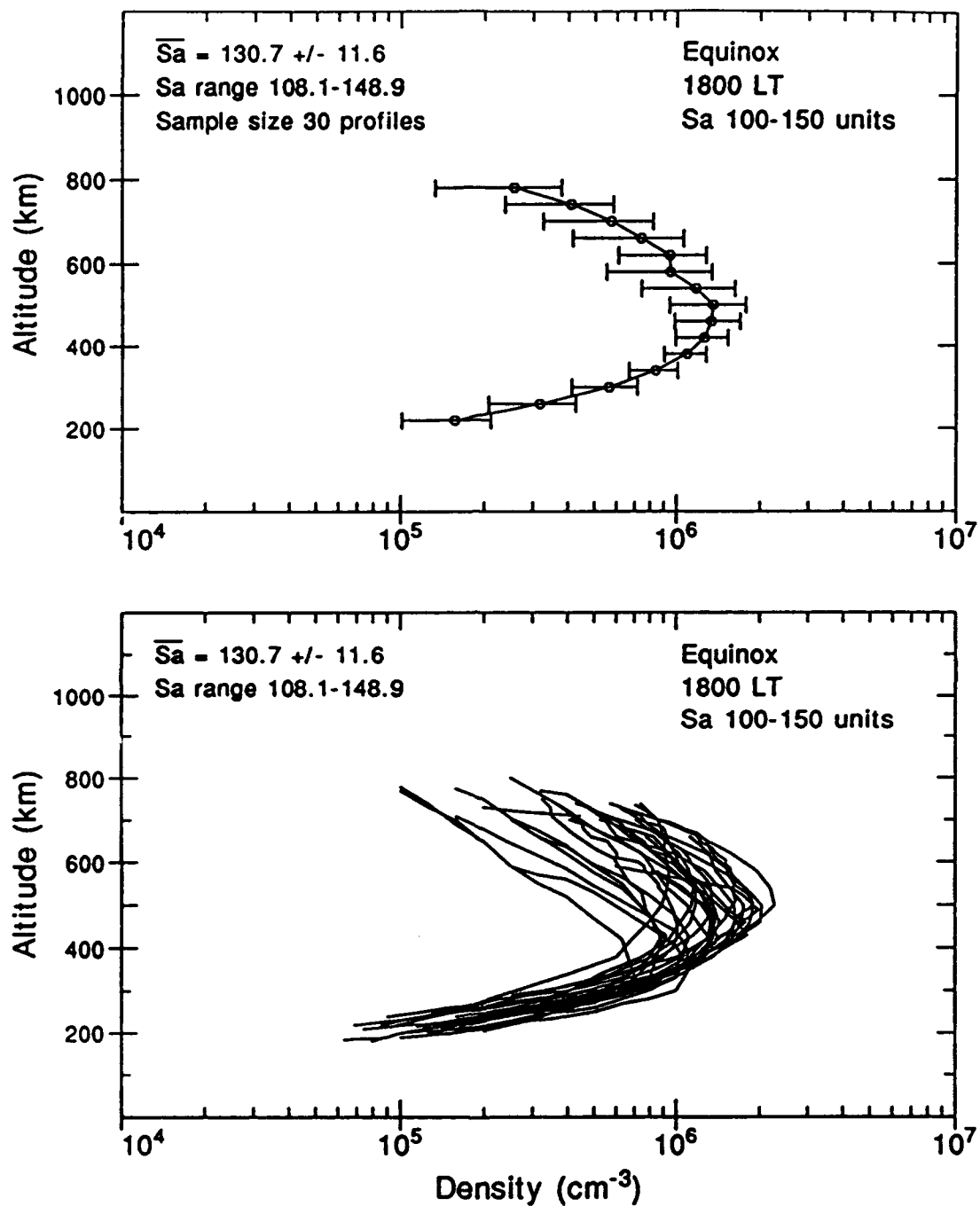
Fig. 14. Scatter plot (bottom panel) and average profile (top panel) for 1800 LT, equinox, moderate solar conditions.

$\overline{Sa}$ = 128.5 +/- 11.9
Sa range 104.8-148.0
Sample size 19 profiles

June Solstice
1800 LT
Sa 100-150 units

$\overline{Sa}$ = 128.5 +/- 11.9
Sa range 104.8-148.0

June Solstice
1800 LT
Sa 100-150 units

Altitude (km)

Density (cm^{-3})

Fig. 15. Scatter plot (bottom panel) and average profile (top panel) for 1800 LT, June solstice, moderate solar conditions.

The density shows little variation below 300 km for all seasons.

4) Based on an examination of the scatter plots, the general trend is for the summer topside density gradient to decrease more rapidly than winter or equinox. The variability of the topside density profiles in summer and equinox is large, however, and the averaged topside profiles have similar height dependence.

5) The layer thickness is greatest during equinox at 347 km and almost identical for the solstices, 329 and 331 km for June and December solstice, respectively.

There appear to be two distributions emerging in the December solstice observations at 1800 LT. The scatter plot in Figure 13 shows a well organized series of layers in which the topside densities decrease more rapidly. There are profiles with higher topside densities, which resemble the equinoctial profiles, shown in Figure 14, which are broader than the more predominant summer pattern. There are also several profiles which clearly resemble the winter data. The winter profiles, Figure 15, show the smallest variability in density over the entire four-month period.

Figure 16 presents an illustration of this seasonal mixture. The top panel illustrates the winter profiles superimposed on the equinox average. The equinoctial data in this figure are from September only. The bottom panel shows the equinox average superimposed on the broader December
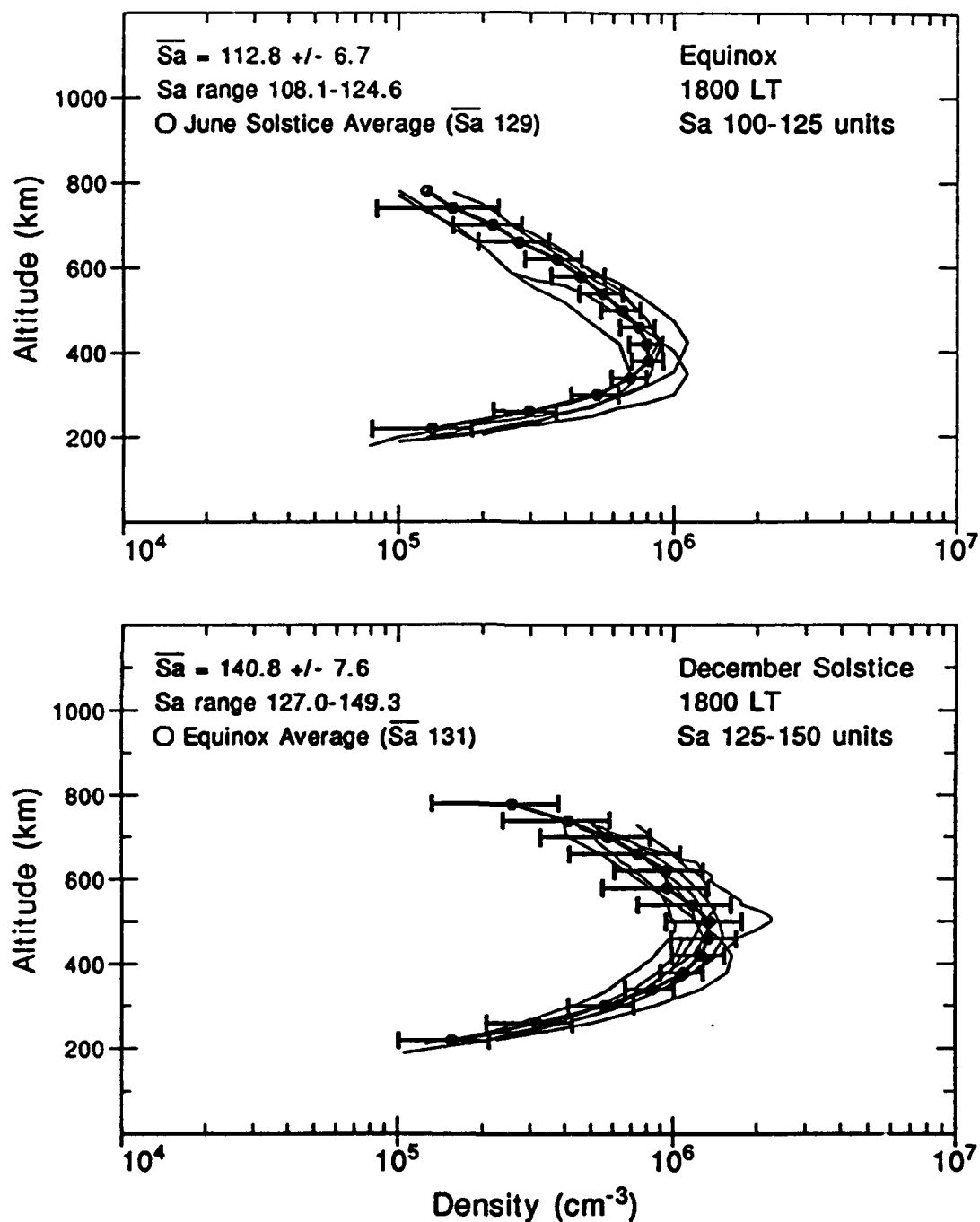
Fig. 16. Comparison of the summer profiles with the equinoctial average profile at 1800 LT (bottom panel) and of the equinoctial profiles with the winter average profile at 1800 LT (top panel). The range of flux for the summer-equinoctial comparison is 125-150 units, the range for the equinoctial-winter comparison is 100-125 units.

solstice profiles. The summer profiles correspond to observations from the end of January and February during periods of higher fluxes. The profiles were also divided into spring and fall equinoctial bins and are shown in Figure 17. The March-April profiles show smaller variation than the September-October profiles. Further, the March-April profiles have higher densities than the September-October profiles. This makes sense given that the March-April equinox follows the high density period of summer and the September-October equinox follows the low density period of winter. This also suggests a difference in the two equinoctial seasons, and with support from the observations that several equinoctial profiles resemble the solstitial profiles they are closest to, we conclude that the time frame allotted to equinox is far too long at Jicamarca.

The equinoctial profiles were also divided into smaller flux bins, shown in Figure 18. With the exception of the two anomalous profiles in the top panel, it is clear that the higher flux profiles are more dense and that the range of 100 to 150 units can be further subdivided.

The plasma density layers at 2000 LT in summer should be higher than the other seasons because the prereversal enhancement is in effect. During equinox and winter the enhancement is earlier and the layers will be under the influence of the downward drift. The summer layer will also experience more solar effects than the other two based on local sunset at Jicamarca. The summer layers are presented
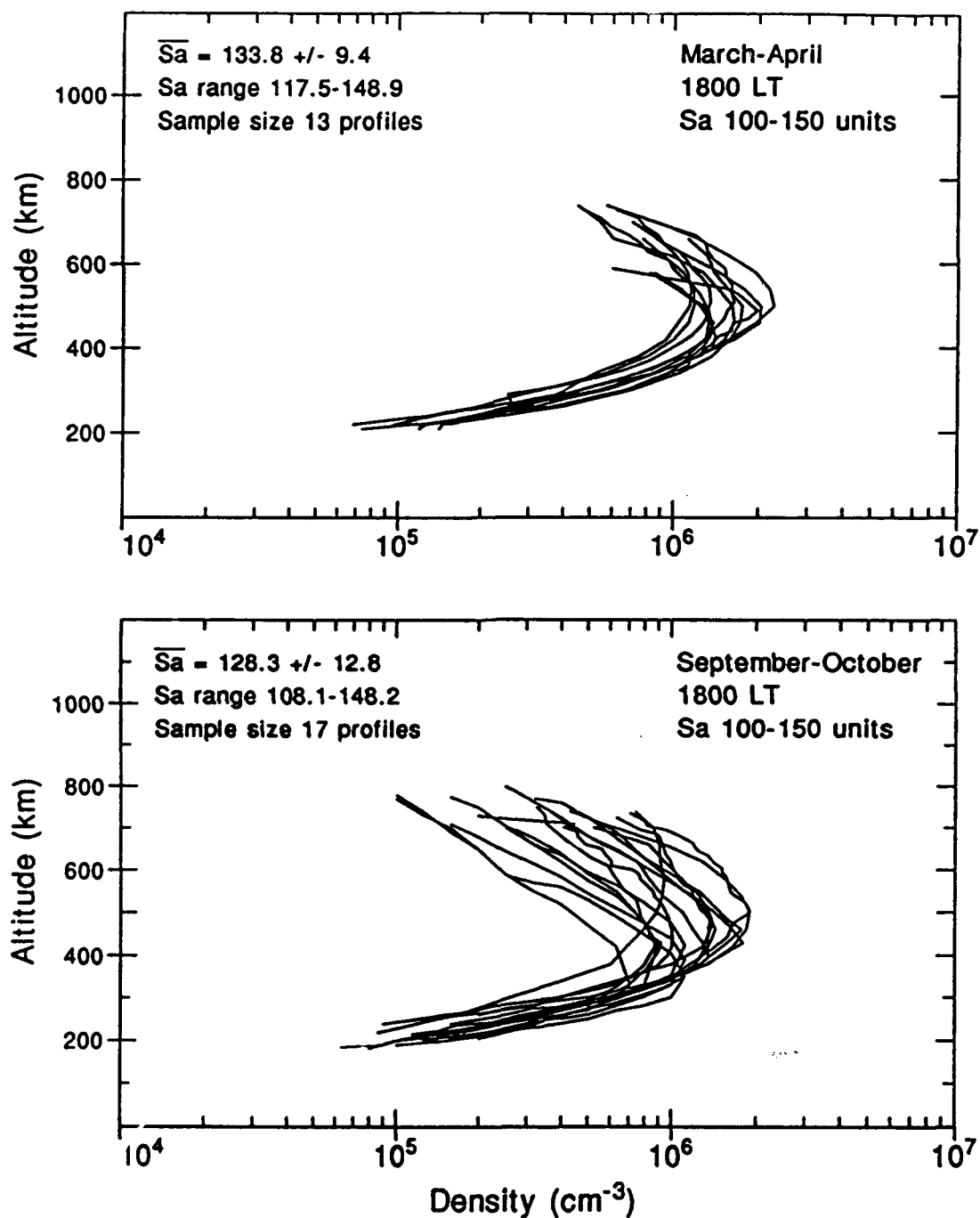
Fig. 17. Comparison of the March-April (fall) and September-October (spring) equinoctial data at 1800 LT.

$\overline{Sa} = 115.4 +/- 6.3$
Sa range 108.1-124.6
Sample size 8 profiles

Equinox
1800 LT
Sa 100-125 units

$\overline{Sa} = 136.2 +/- 7.2$
Sa range 125.4-148.9
Sample size 22 profiles

Equinox
1800 LT
Sa 125-150 units

Altitude (km)

Density (cm^{-3})
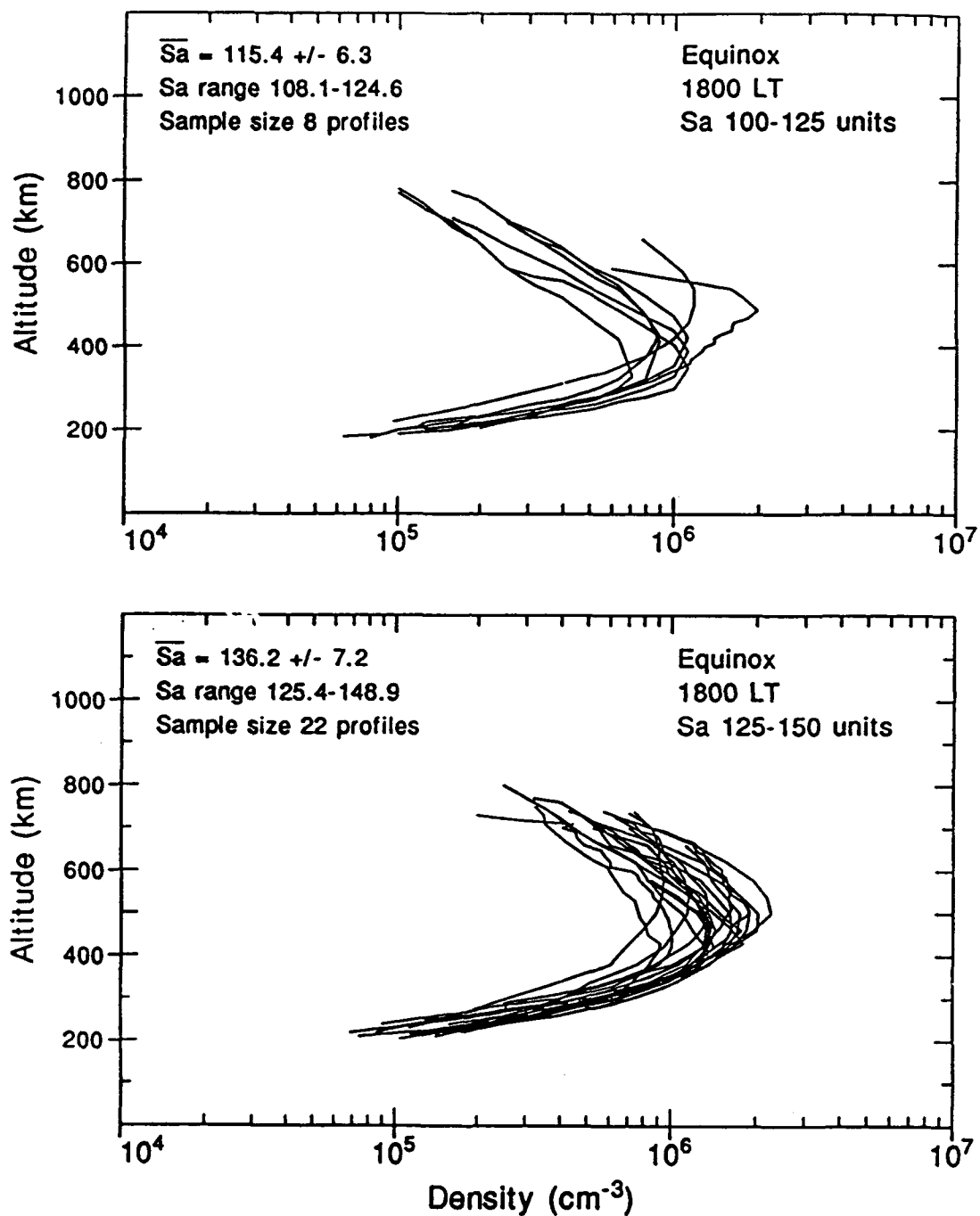
Fig. 18. Equinoctial 1800 LT profiles for two smaller flux bins. The bottom panel shows profiles for Φ between 125 and 150 units, the top for Φ between 100 and 125 units.

in Figure 19. The peak densities typically decrease from their midday values, but the topside densities under the influence of transport will be as high as their daytime values. The main results of the 2000 LT comparisons are:

1) The peak density is greatest in summer, smallest in winter.

2) The peak height is higher in equinox and summer. The winter layer is almost 80 km lower.

3) The bottomside density for all seasons is more variable than seen in the daytime observations. There is a steeper increase in density during equinox; the solstitial bottomside profiles are nearly identical.

4) The topside density is the least variable for June solstice, but all three seasons show a wide variation in the topside densities. The layer decreases the most rapidly for winter and the least rapidly for equinox.

5) The equinoctial layer is the widest and the winter layer the most narrow.

The effects of the vertical drift around sunset have a greater influence on the plasma density distribution seasonally than any other ionization source. As seen in the summary above, the vertical drift creates a steeper bottomside gradient during equinox, moving the layer up and increasing its width.

At midnight the density distribution is determined solely by transport effects which are evident in the organization of the daily profiles. The smallest variability
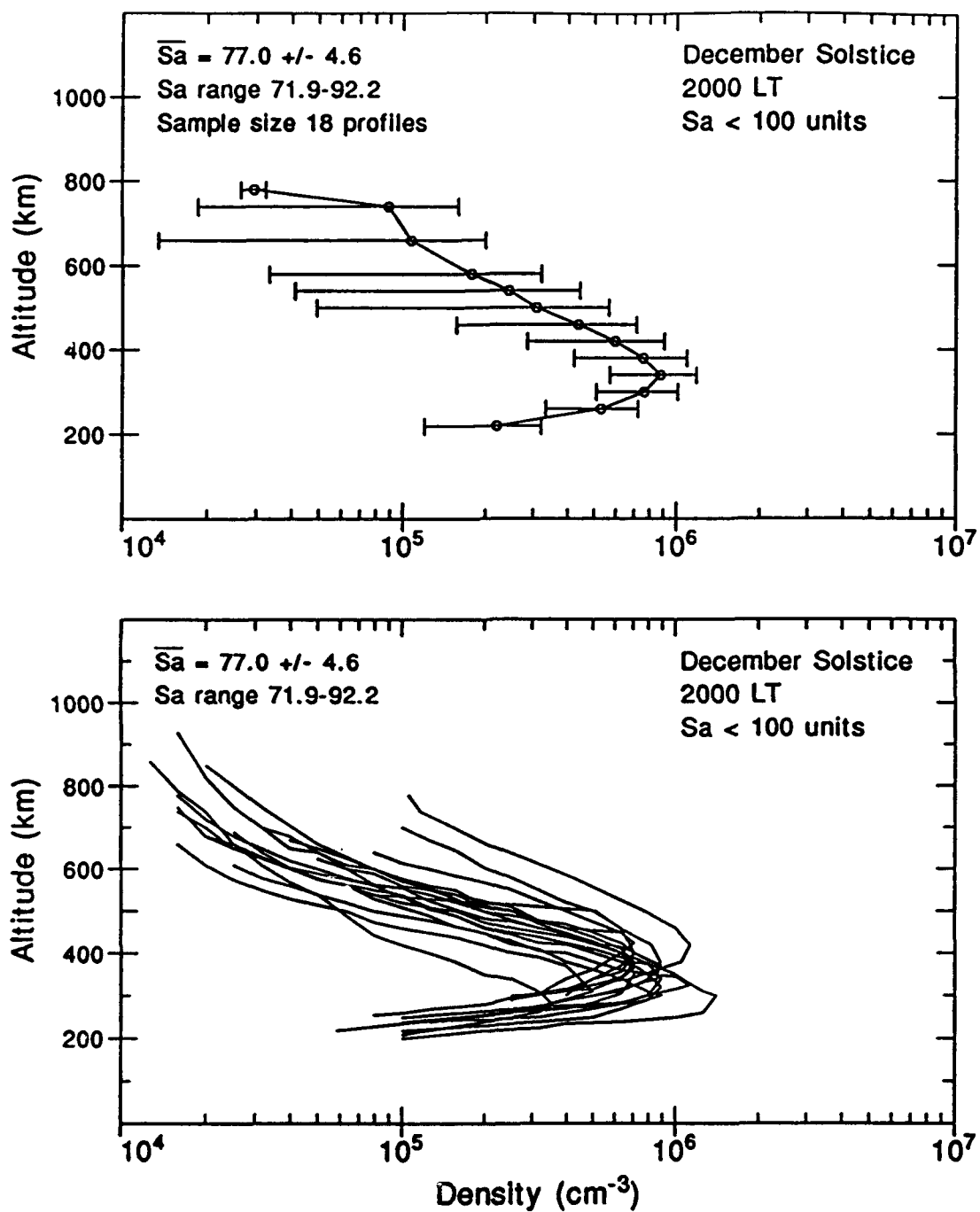
Fig. 19. Scatter plot (bottom panel) and average profile (top panel) for 2000 LT, December solstice, moderate solar conditions.

is observed in the 15 winter profiles, shown in Figure 20. At this time, the layers are moving down in altitude during all seasons. The results at midnight are:

1) The peak density is greatest during equinox. The peak densities during solstice are similar.

2) The layer peak is highest during summer and lowest during winter.

3) The bottomside profiles during equinox and winter are less variable than during summer. The differences in bottomside gradients are small.

4) There is no difference in topside gradient. The summer layer has highest topside densities.

5) The layer is the broadest in summer (almost 300 km) and the most narrow in winter (around 245 km).

These conclusions show that the winter and equinox layers have moved lower in altitude than the summer layer, which is consistent with the Jicamarca vertical drift observations reported by Fejer et al. [1991]. The midnight profiles are more organized during equinox than they appear during the day.

As was the problem with the solar minimum period, the statistics at 0400 LT are rather weak. The summer and winter profiles show small scatter on the downward vertical drift than the equinox profiles (see Fejer et al. [1991]). All three seasonal profiles have similar narrow shapes and it is the few wider profiles that make the equinoctial and winter
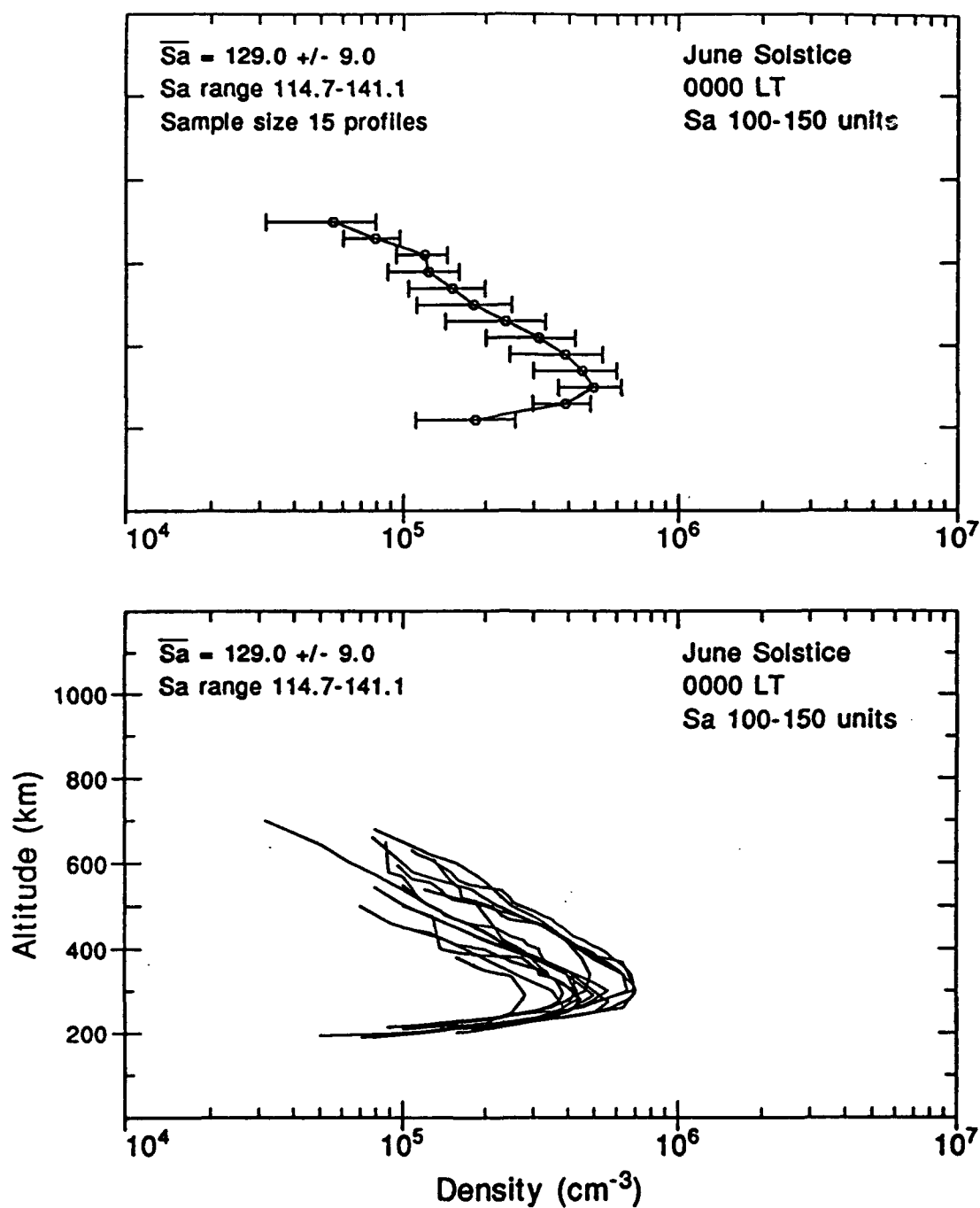
Fig. 20. Scatter plot (bottom panel) and average profile (top panel) for 0000 LT, June solstice, moderate solar conditions.

averaged profiles more broad than the summer profile, which is presented in Figure 21. The results at 0400 LT are:

1) NmF2 is the largest in summer and the smallest during equinox.

2) The peak height is highest in winter, lowest in summer.

3) The bottomside is least variable in summer. The winter bottomside layer is the most steep while the summer bottomside density gradient is more gradual.

4) The topside gradients are parallel during both solstices. The gradient is more vertical during equinox.

5) The layer shape appears more broad during equinox and more narrow during summer.

From these results the winter layer does not move down as rapidly as during the other two seasons. The increased variability of the equinoctial data shows evidence of summer-type and winter-type profiles, supporting earlier observations that equinox may not cover the two months in fall and spring that it has been divided into.

The hourly variation of moderate solar activity data is provided in Figure 22. The 0400 LT observations were included on this figure. The main difference between the midday (1200 LT) and evening (1800 LT) observations is the increase in altitude of the bottomside layer at all seasons. The equinox 2000 LT layer is the highest due to the vertical drift effects discussed earlier. The downward motion of the layers during nighttime is more evident in the equinox and
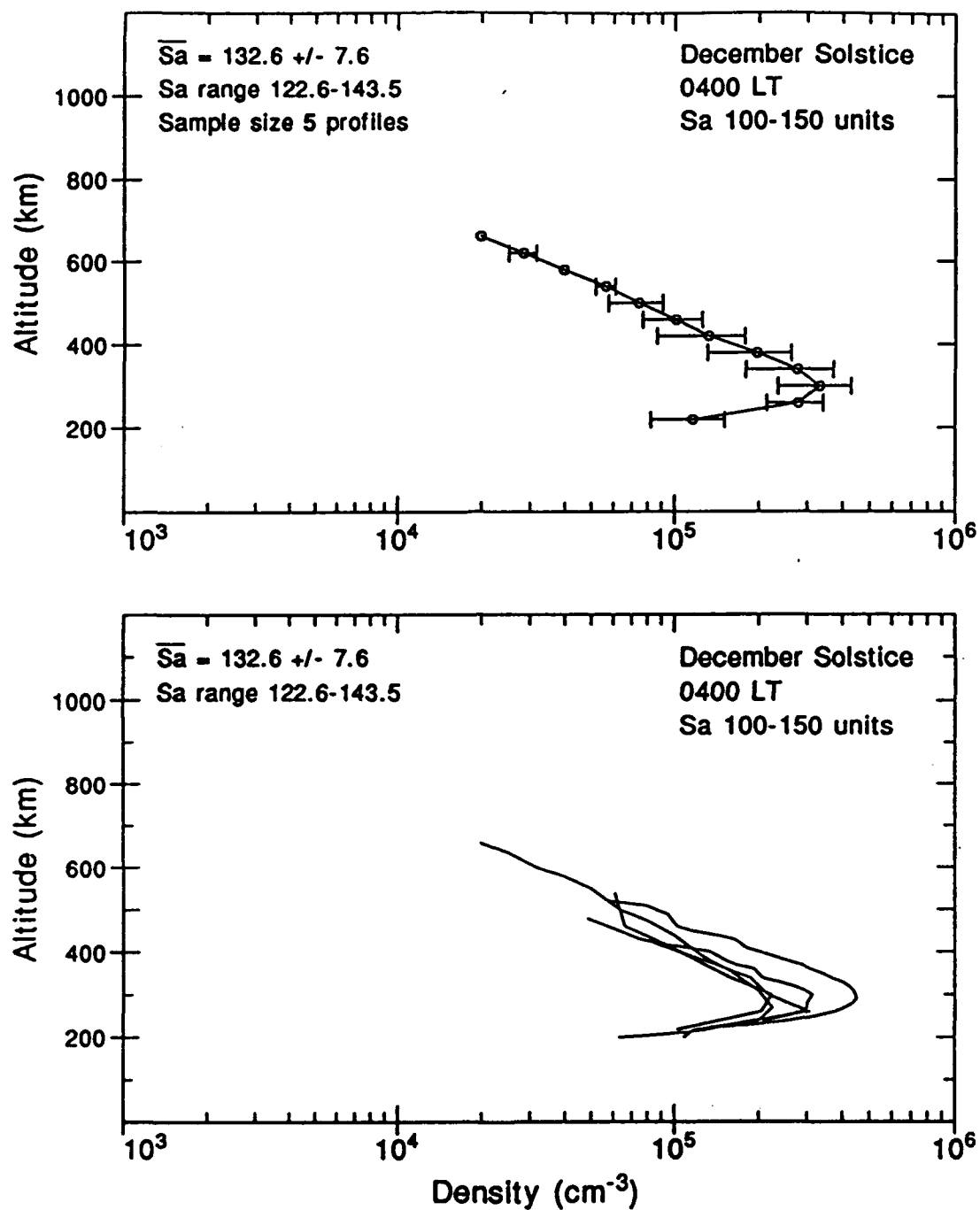
Fig. 21.   Scatter plot (bottom panel) and average profile (top panel) for 0400 LT, December solstice, moderate solar conditions.

(a) December solstice

O 1200 LT, $\overline{Sa}$ 126.6 +/- 9.7
△ 1800 LT, $\overline{Sa}$ 126.2 +/- 11.7
+ 2000 LT, $\overline{Sa}$ 125.9 +/- 10.4
◇ 0000 LT, $\overline{Sa}$ 126.6 +/- 10.3
✳ 0400 LT, $\overline{Sa}$ 132.6 +/- 7.6

(b) Equinox

O 1200 LT, $\overline{Sa}$ 137.4 +/- 4.5
△ 1800 LT, $\overline{Sa}$ 127.6 +/- 10.2
+ 2000 LT, $\overline{Sa}$ 126.8 +/- 11.2
◇ 0000 LT, $\overline{Sa}$ 126.7 +/- 11.6
✳ 0400 LT, $\overline{Sa}$ 130.2 +/- 10.9

(c) June solstice

O 1200 LT, $\overline{Sa}$ 122.6 +/- 9.4
△ 1800 LT, $\overline{Sa}$ 125.4 +/- 10.1
+ 2000 LT, $\overline{Sa}$ 125.2 +/- 7.9
◇ 0000 LT, $\overline{Sa}$ 129.0 +/- 9.0
✳ 0400 LT, $\overline{Sa}$ 124.3 +/- 10.9
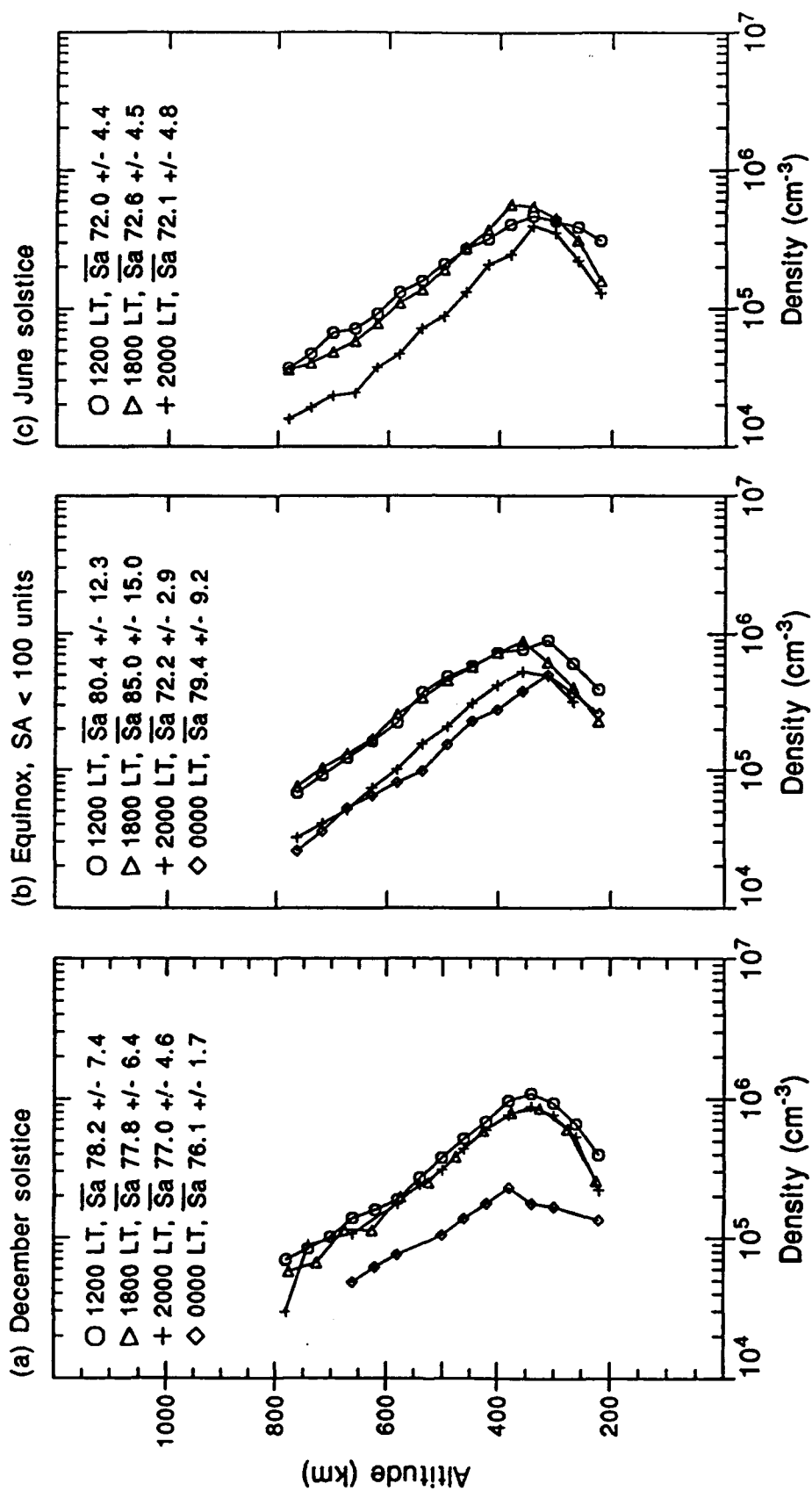
Density (cm^{-3})

Altitude (km)

Fig. 22. Hourly variations in the electron density profiles for (a) December solstice, (b) equinox, and (c) June solstice, moderate solar conditions. The average flux of each profile is given in the legend.

winter than in the summer. Conversely, the 0400 LT layers are significantly lower with respect to the other hours for December solstice. These results are consistent with what is already known about the ionosphere in general. The peak production occurs during the day and those layers will be the most dense. The peak height depends on the vertical drift at Jicamarca, and presumably other locations along the magnetic equator, which dictates when and how much the layer will rise or fall.

3.4. SOLAR MAXIMUM CONDITIONS

The range of flux for the solar maximum observations was generally as broad as that used for moderate solar activity; days with ✦ greater than 150 units were used. There were fewer observations available, however, so the statistics are not as good. Under higher levels of solar flux there will be an increase in layer density for all seasons and all hours. A comparison of the December solstice and equinox scatter plots shows very little difference in these two seasons (see Figures 23 and 24). The main results of the effects from the midday observations are:

1) The peak density at equinox is equal to NmF2 at summer. The winter NmF2 is smaller than both by about a factor of two, as seen in Table 4.

2) The peak layer height during local summer is close to 20 and 30 km higher than during equinox and during winter,
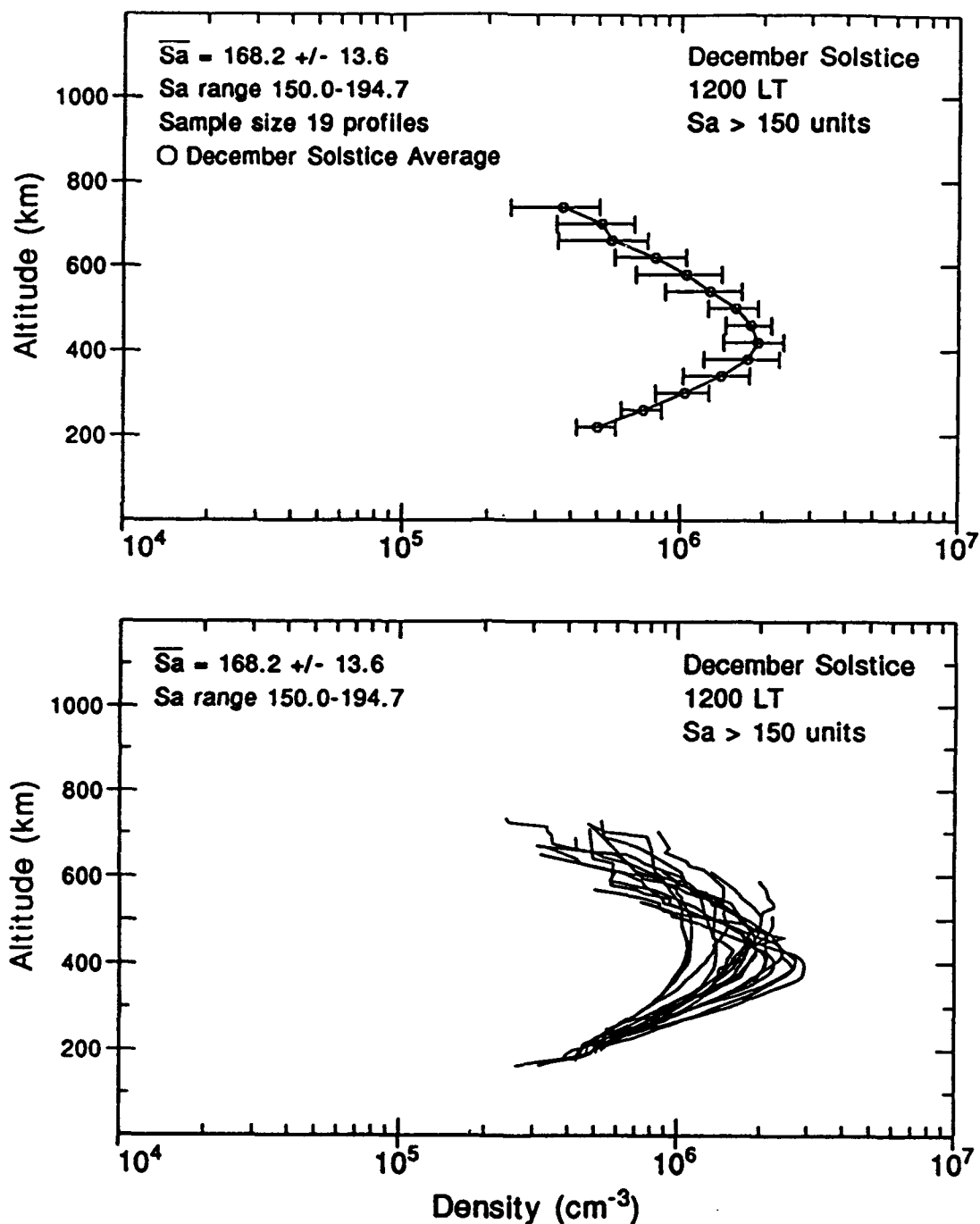
Fig. 23. Scatter plot (bottom panel) and average profile (top panel) for 1200 LT, December solstice, solar maximum conditions.
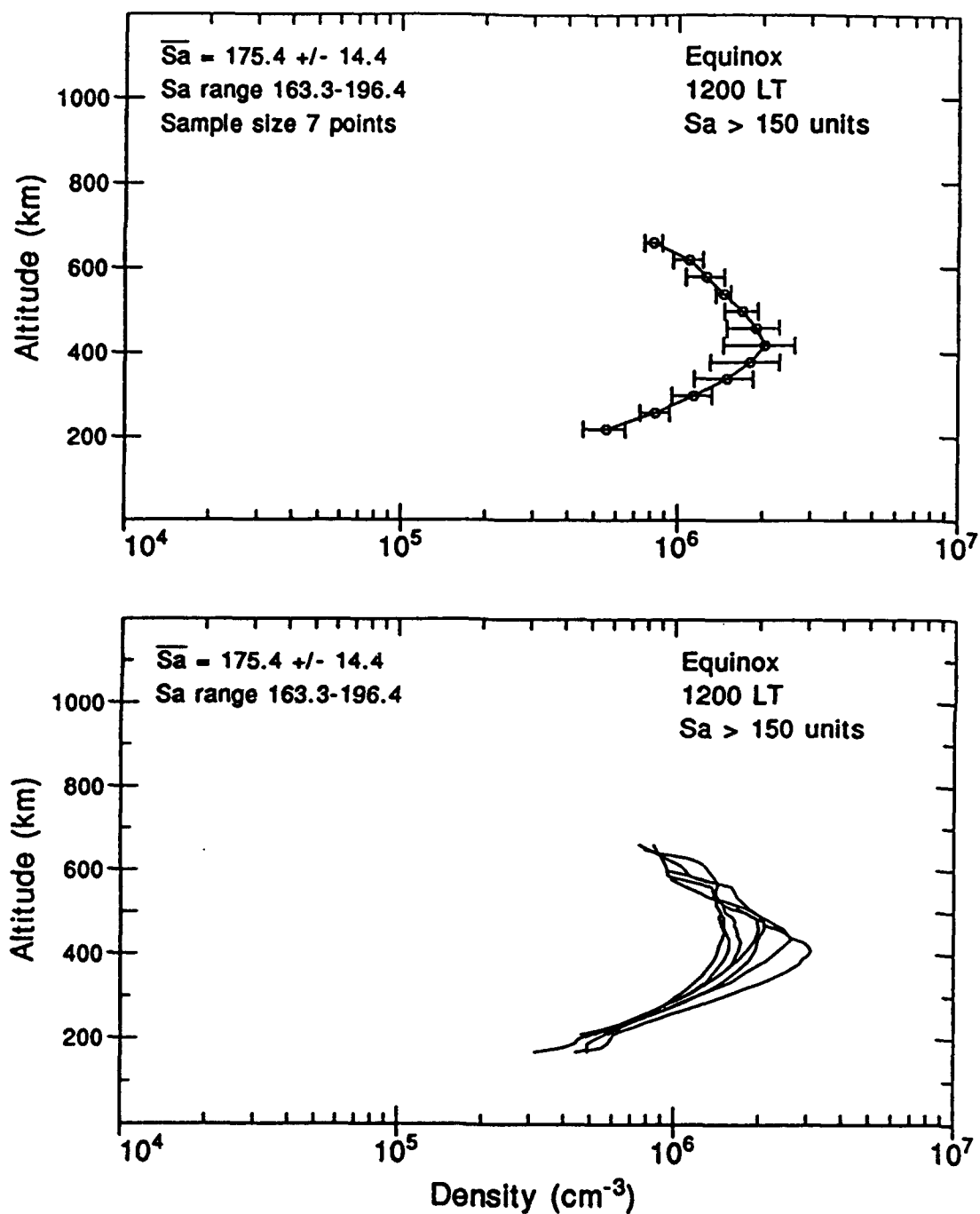
Fig. 24. Scatter plot (bottom panel) and average profile (top panel) for 1200 LT, equinox, solar maximum conditions.

TABLE 4. Averaged peak electron density (cm^{-3}) and height (km), and layer thickness (ΔH) for each season at solar maximum. Standard deviations to the peak density are given in parentheses below the average density, the number of samples contributing to the average are to the right of the density.

Season	Summer		Equinox		Winter	
1200 LT (σ) hmF2 ΔH	2.03×10^6 (5.5×10^5) 461 312	19	2.03×10^6 (6.1×10^5) 444 303	7	1.08×10^6 (9.1×10^4) 442 398	10
1700 LT (σ) hmF2 ΔH	1.82×10^6 (4.6×10^5) 453 328	14	1.90×10^6 (3.2×10^6) 476 367	11	1.05×10^6 (1.6×10^5) 423 375	14
1800 LT (σ) hmF2 ΔH	1.86×10^6 (4.6×10^5) 468 321	18	1.64×10^6 (3.2×10^5) 513 378	8	1.07×10^6 (2.2×10^5) 423 345	13
2000 LT (σ) hmF2 ΔH	1.35×10^6 (5.2×10^5) 545 330	14	1.20×10^6 (4.0×10^5) 531 315	4	8.24×10^5 (1.8×10^5) 449 294	9
0000 LT (σ) hmF2 ΔH	1.05×10^6 (5.9×10^5) 433 287	11	8.71×10^5 (3.4×10^5) 338 310	8	7.92×10^5 (1.9×10^5) 307 294	11
0400 LT (σ) hmF2 ΔH	3.43×10^5 (7.1×10^4) 330 279	6	3.80×10^5 (2.7×10^4) 343 194	4	3.20×10^5 (1.2×10^5) 316 303	6

respectively. The peak heights of all three seasons range from 420 to 470 km.

3) The bottomside density is steeper in winter. The bottomsides are more dense in summer and during equinox. The bottomside density gradients at 1700 LT are similar for all seasons.

4) The topside density gradients for equinox and summer are identical. The topside gradient for winter is more steep and the overall topside density is less than that of the other two seasons. There is a rapid decrease in the topside density of the summer layer at 1700 LT.

5) The equinoctial layer is broader than the summer layer, but part of this effect may be due to the lower densities present in several summer observations since the equinoctial profiles are identical to the higher summer profiles. The winter layer is the widest. The summer layer at 1700 LT is over 20 km more narrow than the equinoctial layer.

These results indicate that the winter layer may be under a stronger vertical drift than the other two seasons for these particular observations, though vertical drift measurements from Fejer et al. [1991] indicate that there should be no difference in the winter and equinox drifts at noon, that both are approximately 20 m/s while the summer drifts are closer to 10 m/s. These results are further supported by the observation that the equinoctial profiles are identical to the higher density profiles for December solstice as shown in Figure 25. The data used for December solstice range from mid November to the end of February, while the equinox profiles are almost exclusively from early March and late October -- there is one observation from the end of March -- so it is highly likely that the equinoctial
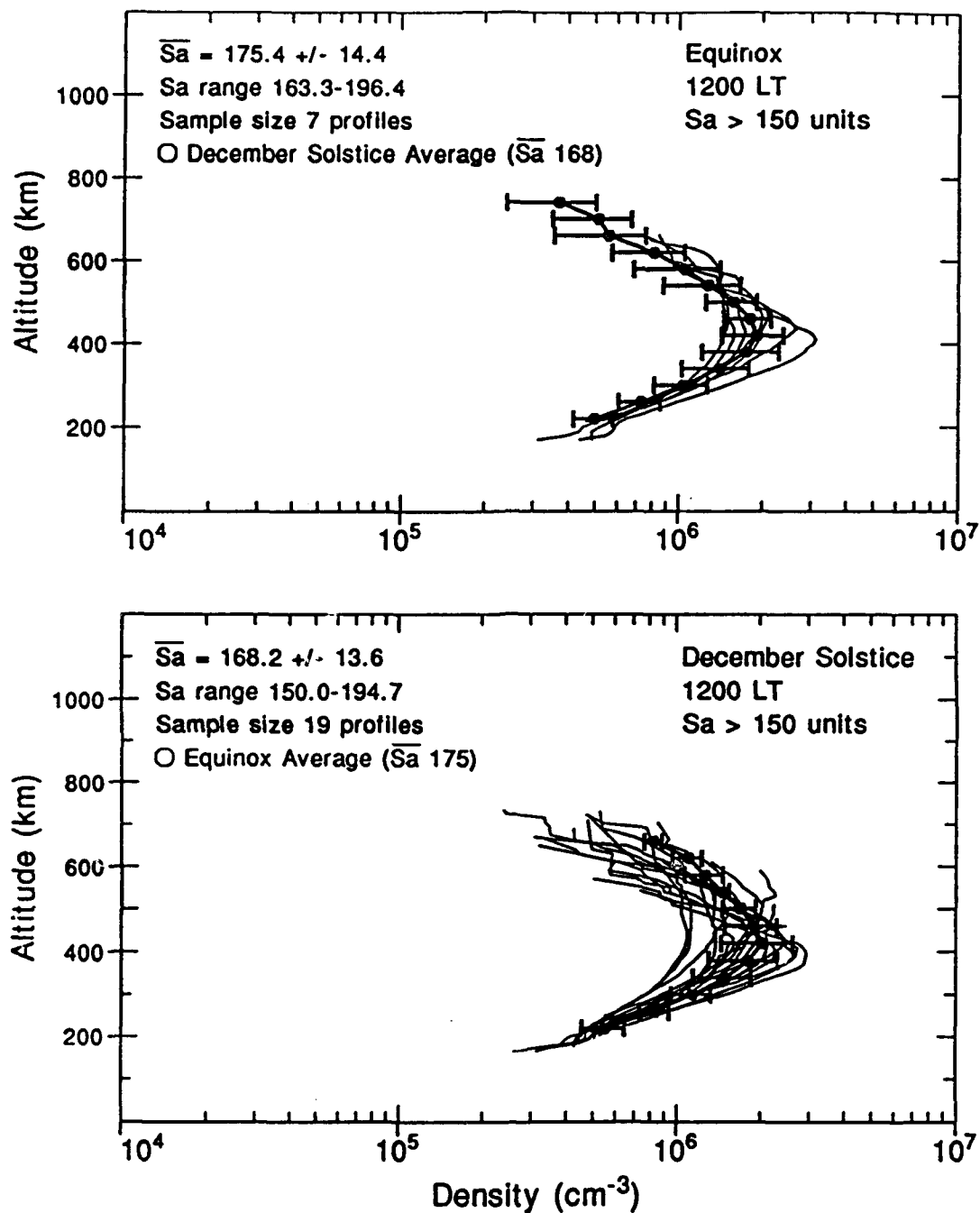
Fig. 25. Comparison of the 1200 LT summer profiles with the equinoctial average (bottom panel) and the equinoctial profiles with the summer average (top panel) for solar maximum conditions.

days in question were under the ionospheric summer conditions and that this comparison is actually between June and December solstices.

The vertical drift effects are somewhat harder to detect under these conditions. Typically the upward vertical drift is around 10 m/s at 1700 LT during the summer and the changes in the density profile for December solstice days support this observation. However, the winter profiles are on the ascending edge of the prereversal enhancement and exhibit the effects of the drift in the increased broadness of the layer. Refer to Table 4 for a comparison of NmF2, hmF2, and ΔH for solar maximum.

The smaller sample size of equinoctial profiles at 1800 LT contributes to the apparent similarity with the December solstice observations, as shown in Figures 26. The equinoctial and winter layers are presented in Figures 27 and 28, respectively. The equinoctial layer is broader than the solstitial layers. The main results of the 1800 LT data observations are:

1) The peak layer density results are similar to the results at 1800 LT during minimum and moderate solar activity.

2) The peak layer height results mirror the results at moderate and minimum solar flux.

3) The bottomside profiles are comparable to the results seen at solar minimum.
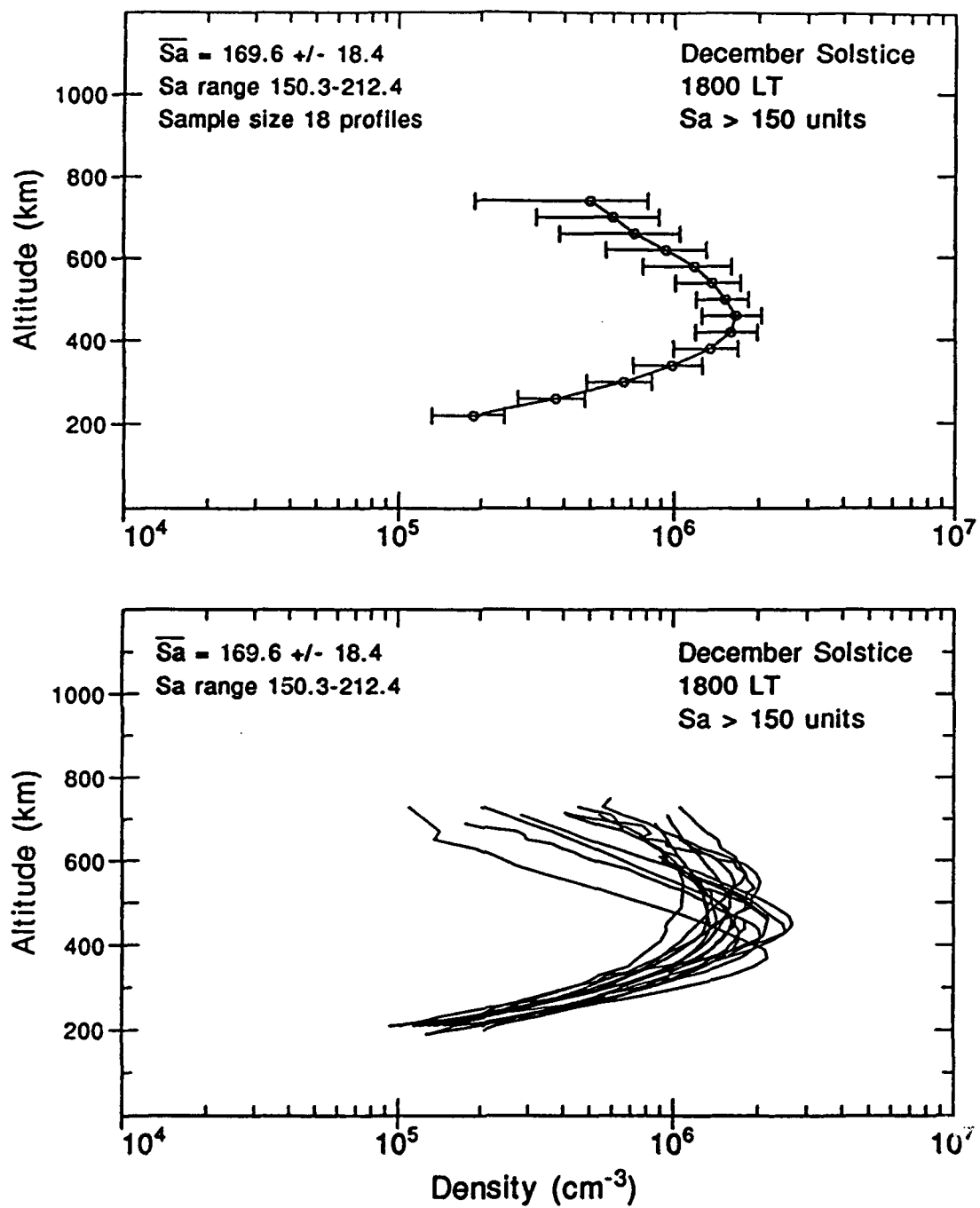
Fig. 26. Scatter plot (bottom panel) and average profile (top panel) for 1800 LT, December solstice, solar maximum conditions.
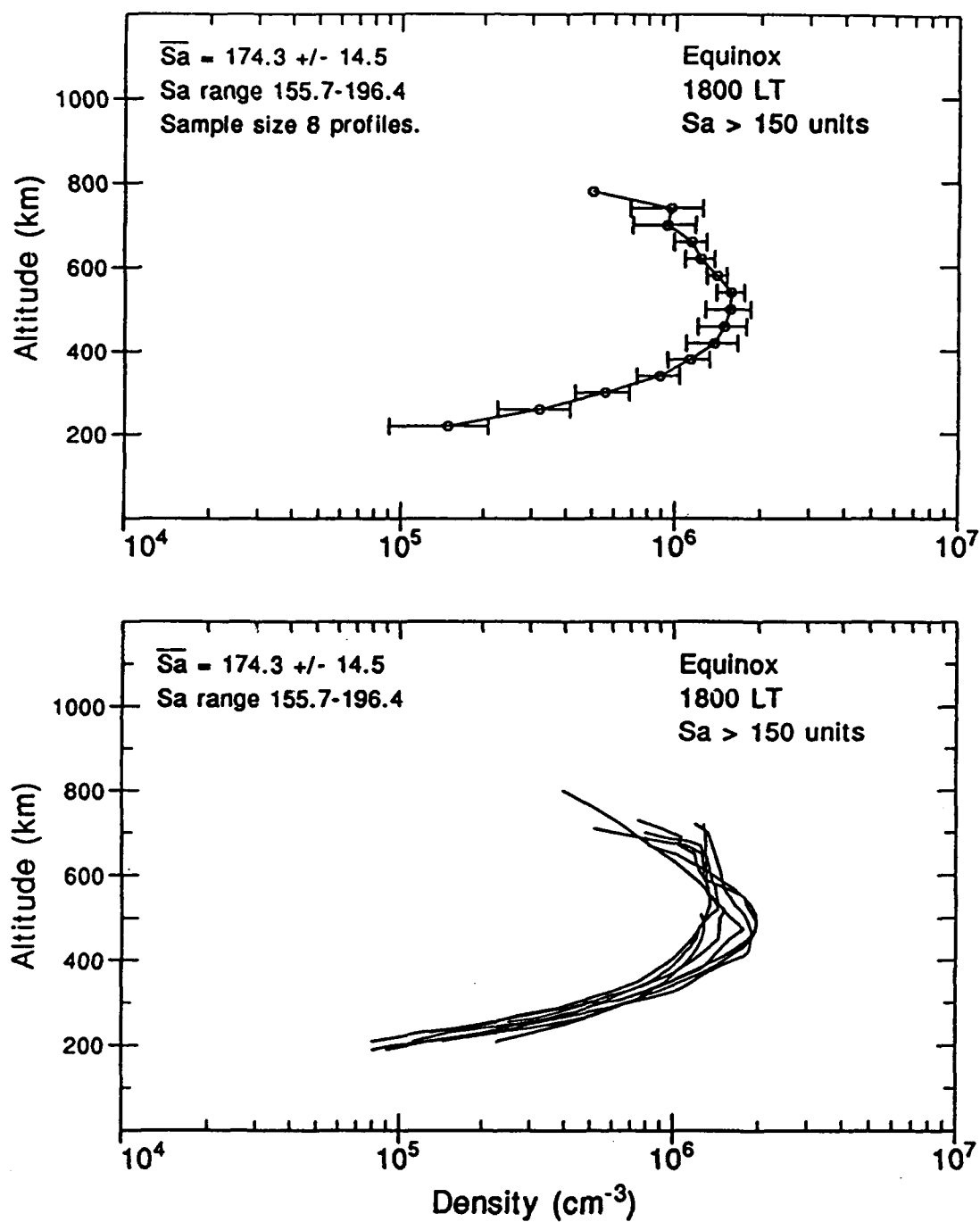
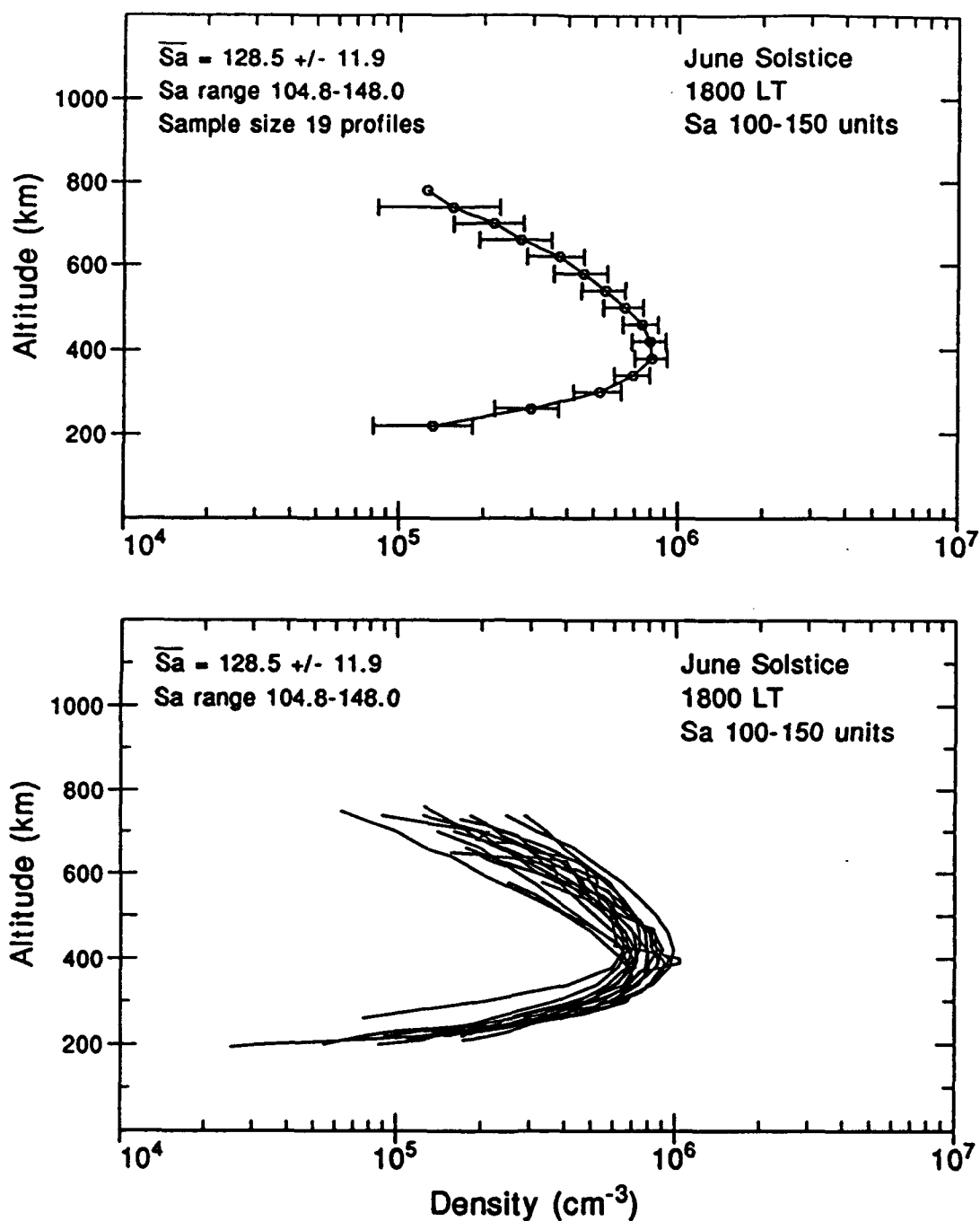Fig. 27. Scatter plot (bottom panel) and average profile (top panel) for 1800 LT, equinox, solar maximum conditions.
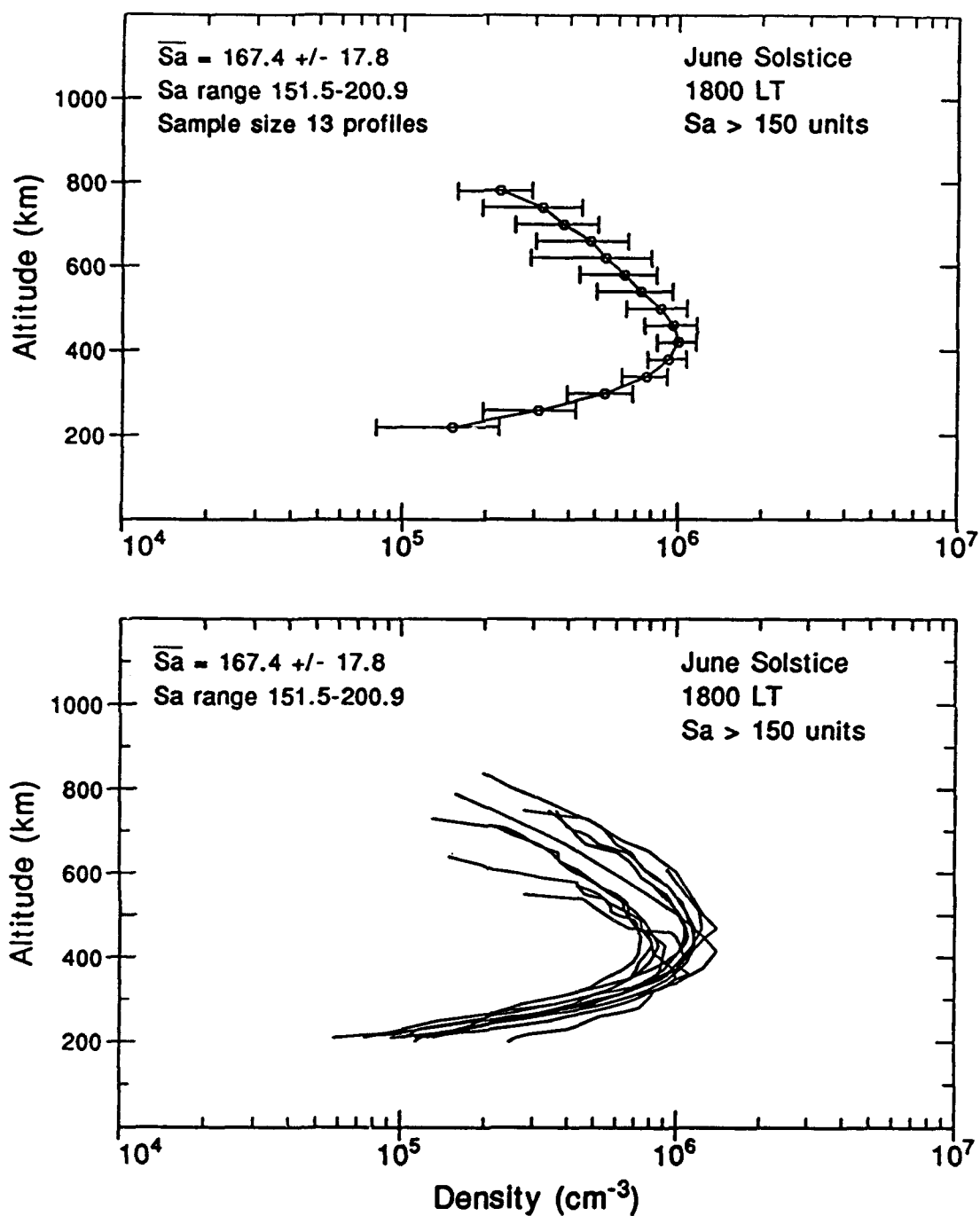
Fig. 28. Scatter plot (bottom panel) and average profile (top panel) for 1800 LT, June solstice, solar maximum conditions.

4) The topside density comparisons are similar to the results for moderate solar activity at 1800 LT.

5) The plasma layer is widest during equinox, following the trend reported for solar minimum and moderate solar activity.

The higher and broader layer at June solstice reflects the peak of the prereversal enhancement centered at 1800 LT during winter. Both the summer and equinoctial profiles are on the ascending edge of the enhancement and will continue to rise. The NmF2 for each season is the highest for all flux levels, commensurate with the increase in density expected with an increase in solar activity.

The data at 2000 LT show a marked amount of variability for each season. The limited data for equinox make those results less reliable. The winter profiles show less variability than the summer profiles, which show an unusually large variability in the bottomside. All three seasons are on the descending side of the prereversal enhancement, which is typically the latest for summer. The winter profiles are shown in Figure 29. The profiles will also be less dense since this period is after local sunset. The post-sunset and high solar activity effects on the ionosphere at Jicamarca are:

1) The seasonal difference in peak density duplicates that of moderate and minimum solar activity.

2) The trend in peak layer height is similar to that seen for moderate and minimum solar activity.
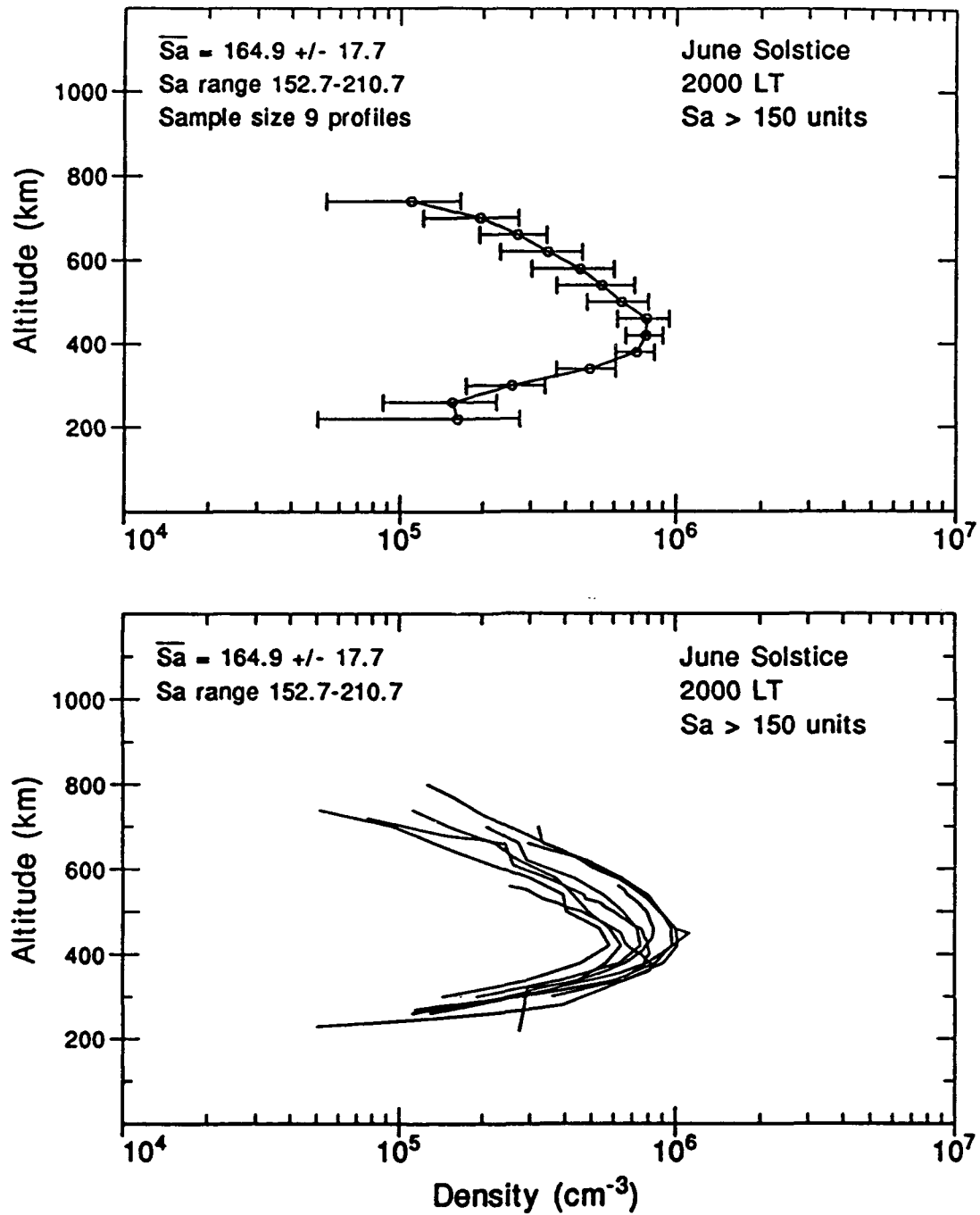
Fig. 29. Scatter plot (bottom panel) and average profile
(top panel) for 2000 LT, June solstice, solar maximum
conditions.

3)　The bottomside gradient is smaller during winter than during summer.

4) The topside profiles show greater density variations during summer than during winter as well as a higher density and a steeper density gradient.

5)　The summer layer is more broad than the winter layer.

Because there were so few equinoctial observations and because they resembled the December solstice profiles, the only meaningful comparison for this hour is made between the solstices.　The summer layer is placed higher than the winter layer because of the stronger and slightly later prereversal enhancement.　The topside transport along magnetic fieldlines is reflected in the variability in the topside data and the higher topside density in summer than in the lower winter layer.

At midnight all the layers appear lower and more compressed than the layers during and immediately after daytime production.　The sample size for summer and winter are identical (11 profiles), but the summer profiles are much more variable than the winter profiles.　The winter profiles are presented in Figure 30.　The main results at midnight are:

1)　Contrary to the results for minimum and moderate flux conditions, the peak density during summer is greater than the peak during winter or equinox.
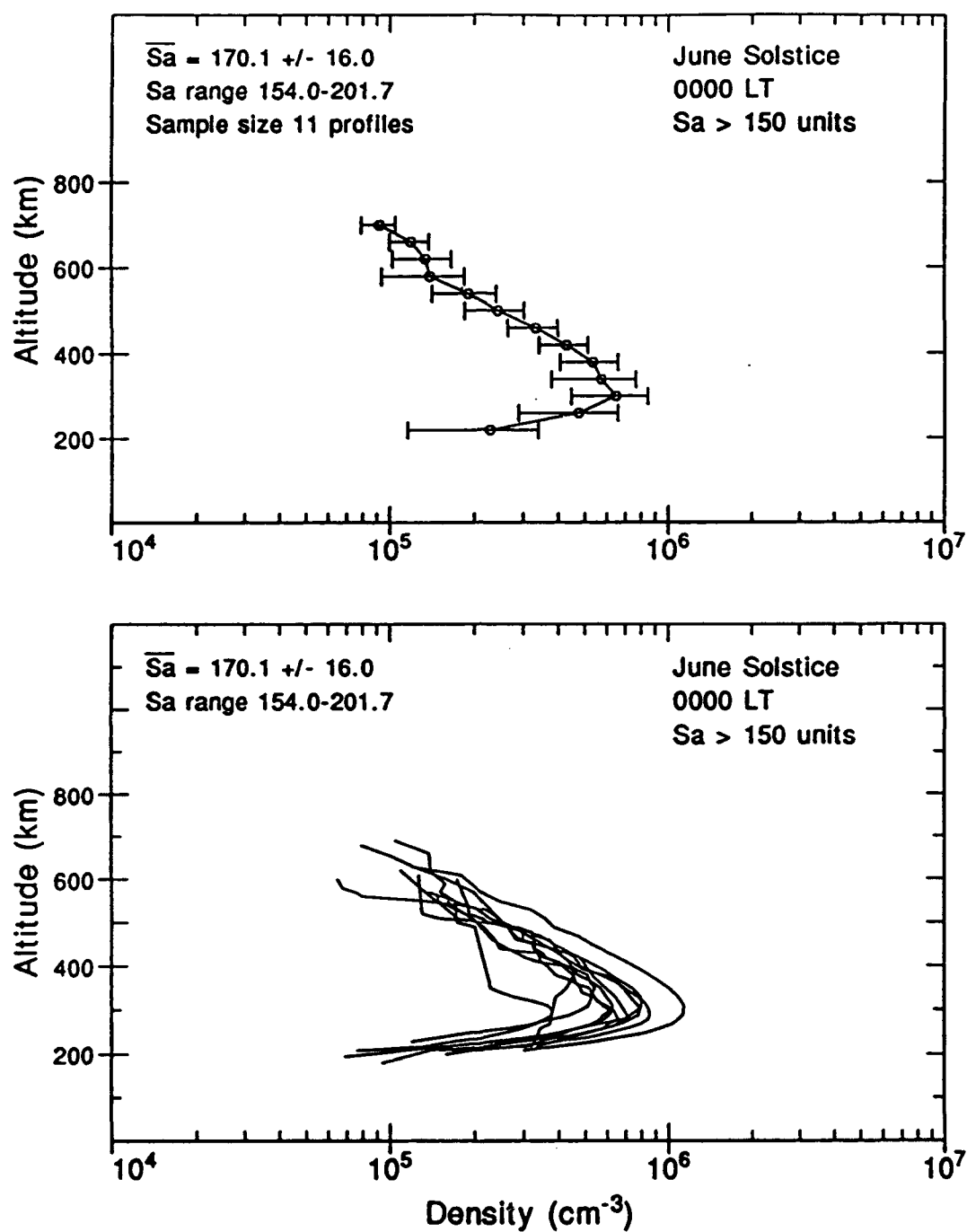
Fig. 30. Scatter plot (bottom panel) and average profile (top panel) for 0000 LT, June solstice, solar maximum conditions.

2) The peak height variation follows that of moderate and minimum solar activity variations.

3) The bottomside densities show less variability during winter and equinox. The bottomside is higher in summer and there is no significant seasonal difference in density gradient.

4) The topside is more dense in summer and the gradient more steep. The winter and equinox gradients are parallel, with the winter topside being the least dense of the seasons.

5) The variability of the data during summer makes the layer appear to be the widest. The winter layer is the most narrow.

The F-region plasma layers at midnight are almost 100 km lower than at 2000 LT. The corresponding density has decreased, but it is still higher than at lower flux levels. An increase in the number of observations is necessary to determine better the nature of the night-time F-region ionosphere.

These layers are the lowest and have smaller densities at 0400 LT following the almost eight hours of downward plasma drift. The number of samples for this period ranges only from four to six, but the data available have smaller variability than at midnight. The summer profiles are presented in Figure 31. The main characteristics under these flux conditions at this hour are:

1) NmF2 is largest for summer and smallest for winter, but with little seasonal variation between the three seasons.

$\overline{Sa}$ = 172.0 +/- 18.7
Sa range 150.0-197.1
Sample size 6 profiles

December Solstice
0400 LT
Sa > 150 units

$\overline{Sa}$ = 172.0 +/- 18.7
Sa range 150.0-197.1

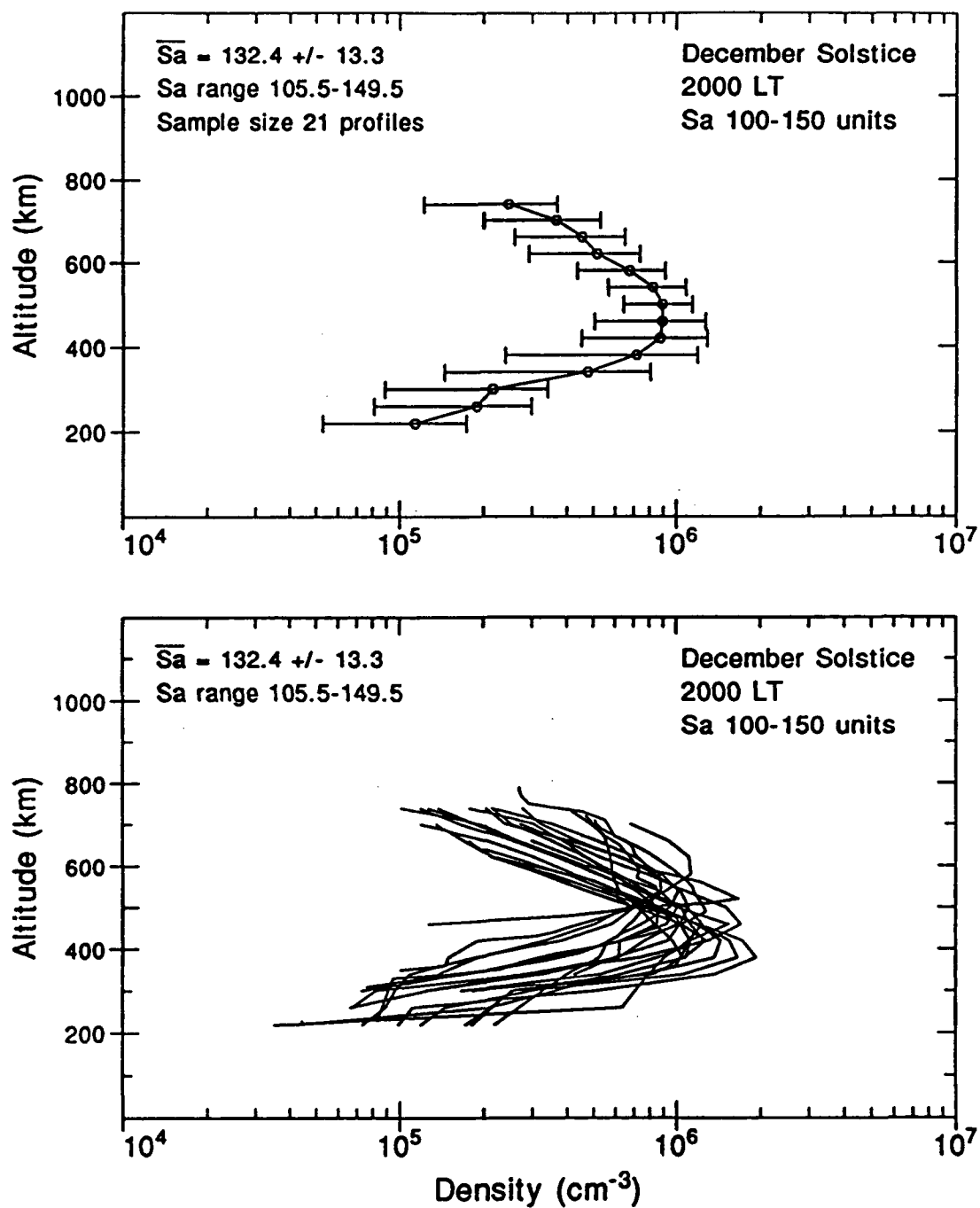December Solstice
0400 LT
Sa > 150 units

Altitude (km)

Density (cm^{-3})
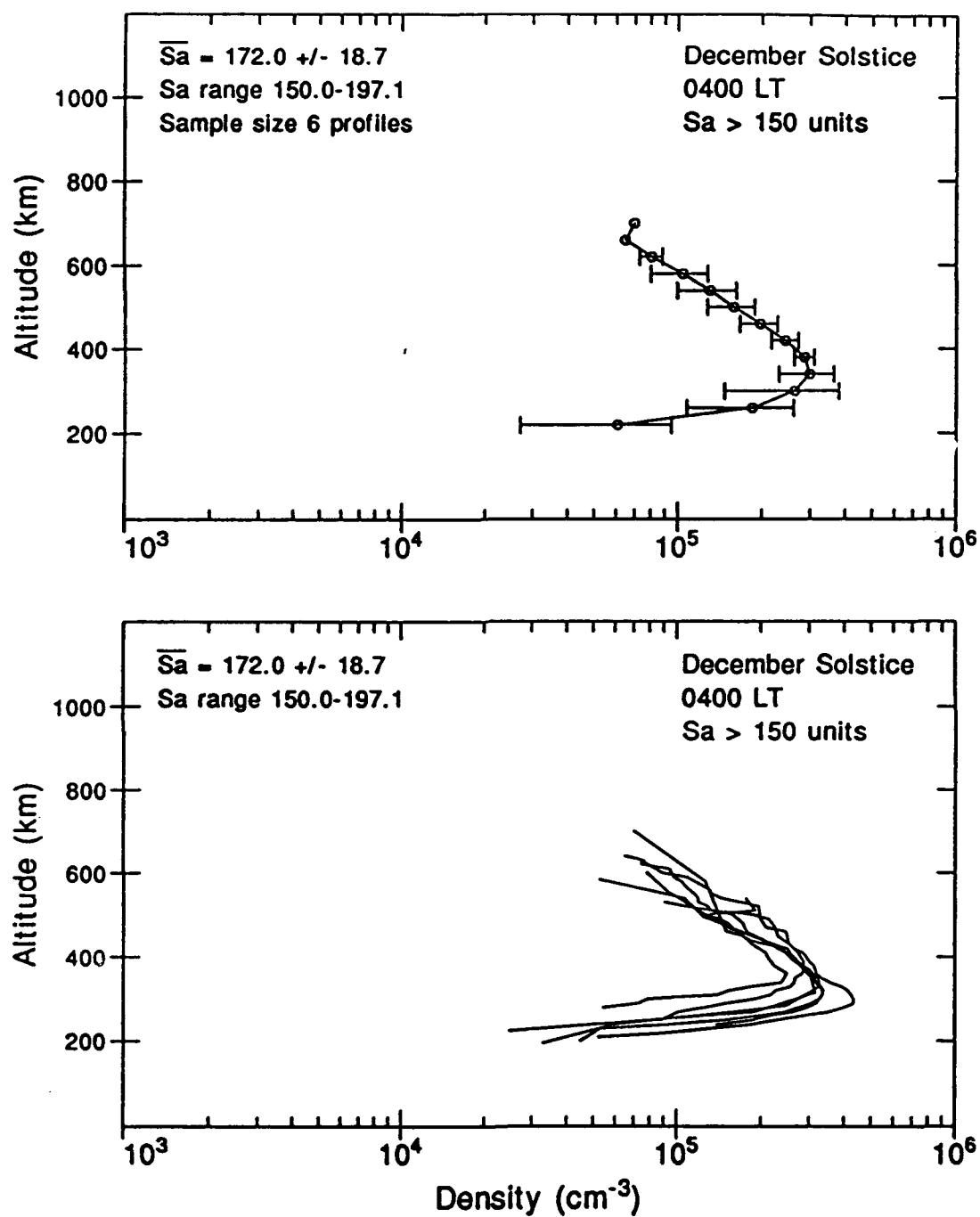
Fig. 31. Scatter plot (bottom panel) and average profile (top panel) for 0400 LT, December solstice, solar maximum conditions.

2) The difference in peak layer heights resembles those at solar minimum.

3) The bottomside density profiles are steeper in winter than in summer. There is not enough data at equinox to compare this parameter.

4) The topside densities decrease more rapidly during equinox. There is no difference in topside density or density gradients for the solstices.

5) The equinoctial layer appears to be the most narrow, but the conclusion is not as reliable as the solstitial comparison. The layer around the peak is broader during winter than summer, but the overall layer shapes are similar.

From these results it is fair to say that there is little difference in the plasma density layers during the solstices. More data are clearly necessary to characterize the equinoctial layer.

Figure 32 presents the hourly average moderate flux profiles by season. The noontime densities are highest due to the daytime production rates. The topsides of the noon and early evening profiles are very similar for all seasons. The bottomside layers of the daytime and evening layers are quite different, though. The prereversal effects during solar maximum can be quite dramatic and the effect of the enhancement on the plasma layers by season is evident in this comparison, especially for equinox. The nighttime decrease in density is also apparent. There is little difference in

(a) December solstice

O 1200 LT, Sa 168.2 +/- 13.6
△ 1800 LT, Sa 169.6 +/- 18.4
+ 2000 LT, Sa 165.1 +/- 17.3
◇ 0000 LT, Sa 167.5 +/- 17.0
✳ 0400 LT, Sa 172.0 +/- 18.7

(b) Equinox

O 1200 LT, Sa 175.4 +/- 14.4
△ 1800 LT, Sa 174.3 +/- 14.5
+ 2000 LT, Sa 162.6 +/- 8.6
◇ 0000 LT, Sa 172.2 +/- 15.8
✳ 0400 LT, Sa 177.5 +/- 12.2

(c) June solstice

O 1200 LT, Sa 167.2 +/- 14.1
△ 1800 LT, Sa 167.4 +/- 17.8
+ 2000 LT, Sa 164.9 +/- 17.7
◇ 0000 LT, Sa 170.1 +/- 16.0
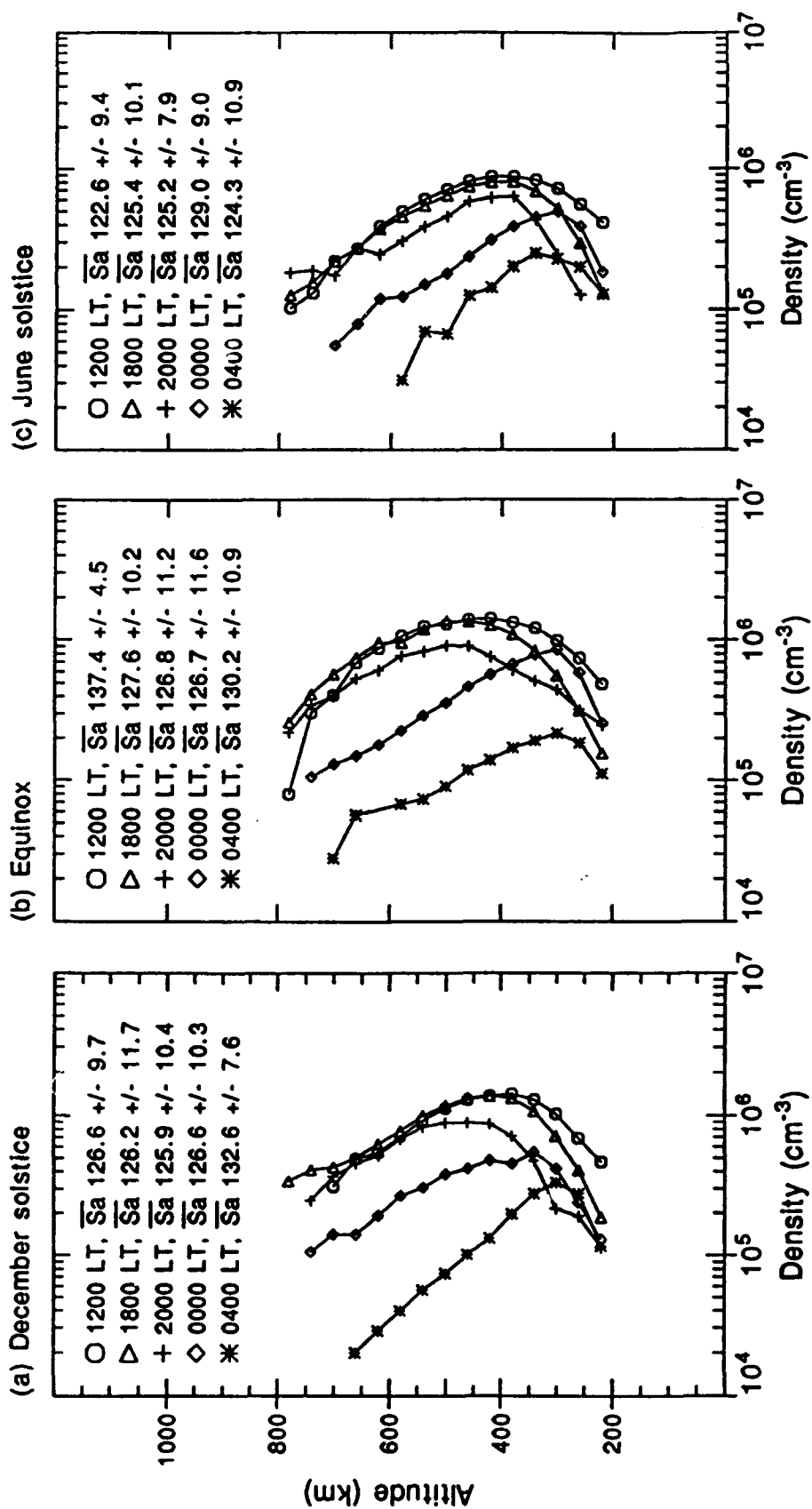✳ 0400 LT, Sa 179.9 +/- 15.8

Altitude (km)

Density (cm^{-3})
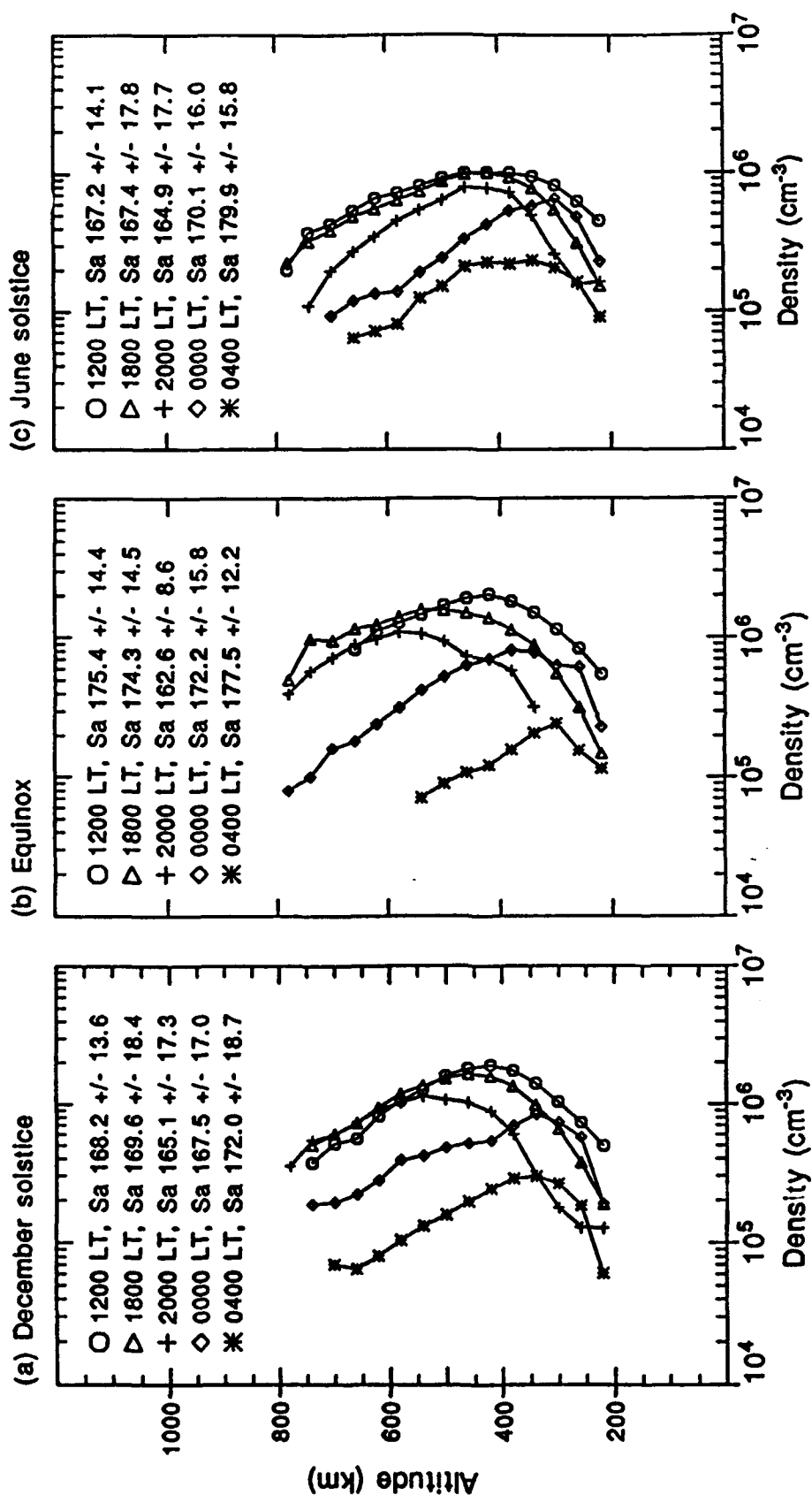
Fig. 32. Hourly variations in the electron density profiles for (a) December solstice, (b) equinox, and (c) June solstice, solar maximum conditions. The average flux of each profile is given in the legend.

the layer heights of the midnight and 0400 LT layers in summer.

3.4. SOLAR CYCLE VARIATIONS

Figures 33, 34, and 35 show the scatter plots of the peak densities, heights, and layer thickness, respectively, as a function of flux for each season at 1200 LT. The open circles correspond to the quiet-time data (Kp < 4.0) and the stars correspond to the disturbed data (Kp > 4.0). The line through each data set is a least squares fit to the quiet-time data and the formula in the top left corner of each plot corresponds to that line. The plots show extensive variation in the peak density, height, and layer thickness over a solar cycle for the local times considered. The data are less scattered at June solstice, but this may be an effect of fewer samples for that season. At noon the increase in NmF2 is similar for December solstice and equinox. The June solstice NmF2 increases half as rapidly. The slope of the lines to hmF2 versus flux comparisons are almost identical for all seasons. The seasonal layer thickness comparison indicates that thickness should increase the most for June solstice and remain almost constant during equinox.

The correlation between flux and density at 1800 LT (Figure 36) is almost identical to the noontime correlation. There is less density variability in summer and equinox; the winter results are similar to the noon results. The changes
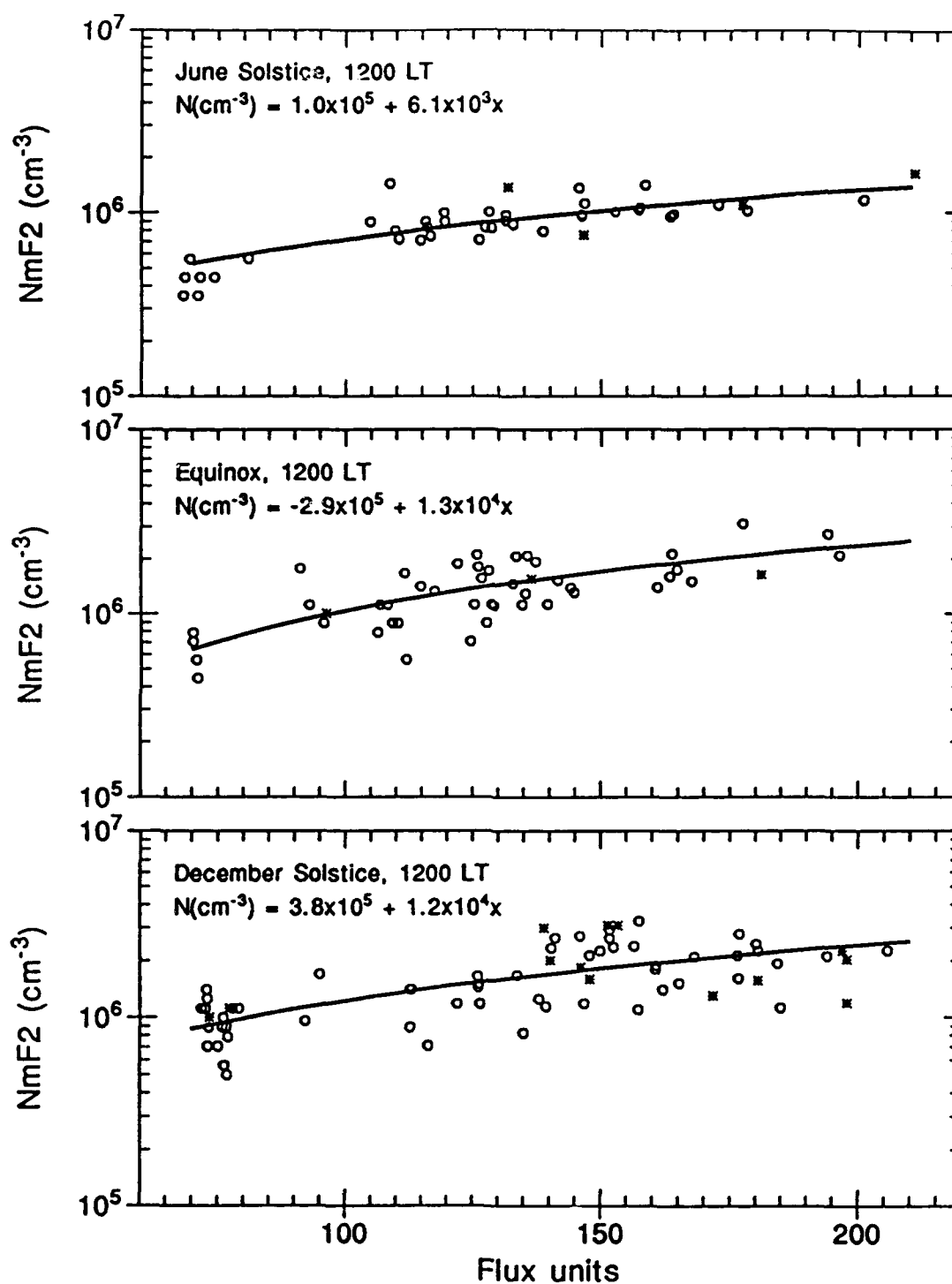
Fig. 33. Seasonal variation of peak density (NmF2) with flux for 1200 LT. The heavy line is a least squares fit to the scattered qiiet-time data (open circles). The formula in the upper left corner corresponds to the least squares fit. The stars denote data obtained under disturbed conditions.
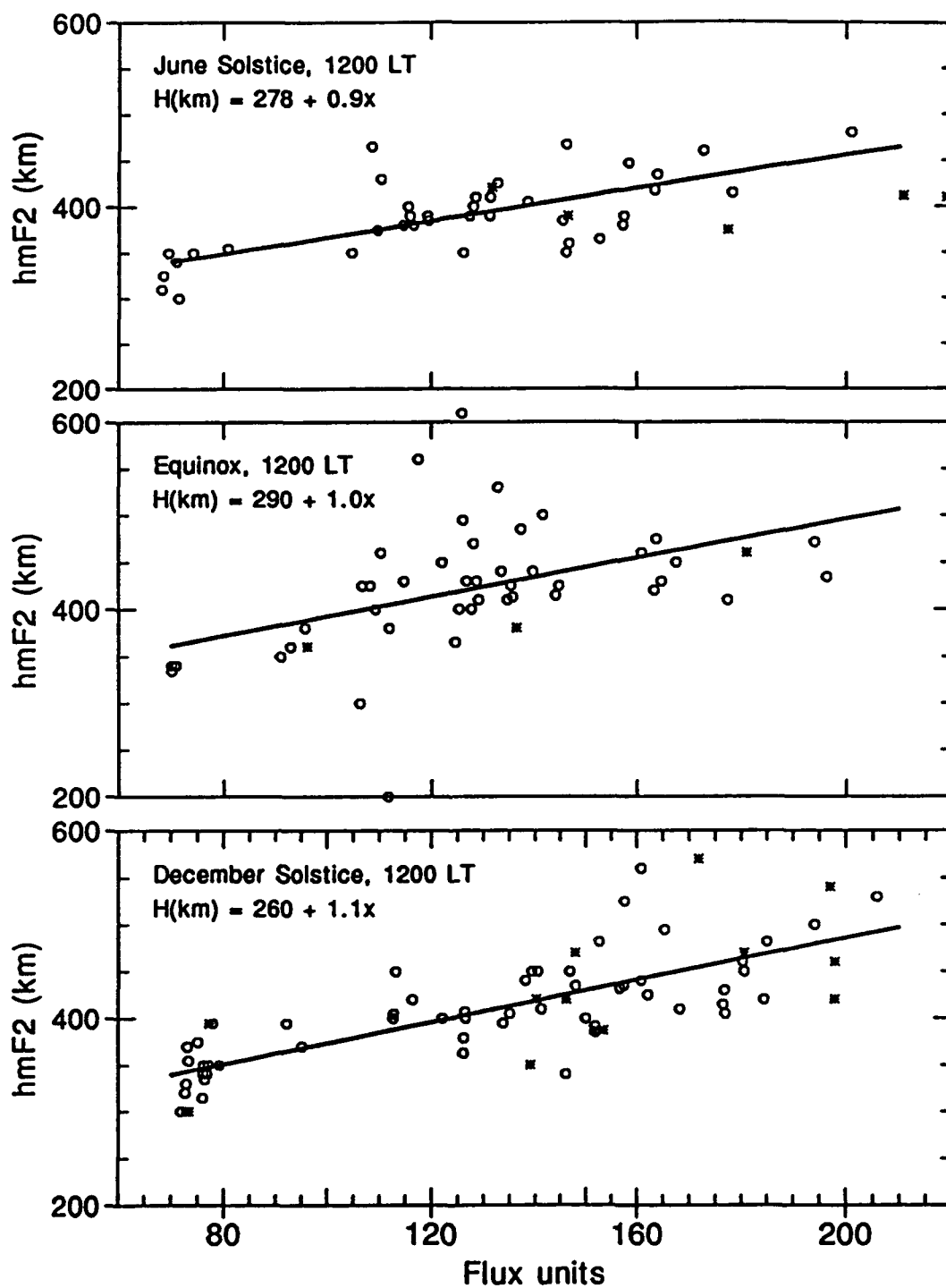
Fig. 34. Seasonal variation of peak height (hmF2) with flux at 1200 LT. The heavy line is a least squares fit to the scattered quiet-time data (open circles). The formula in the upper left corner corresponds to the least squares fit. The stars denote data obtained under disturbed conditions.
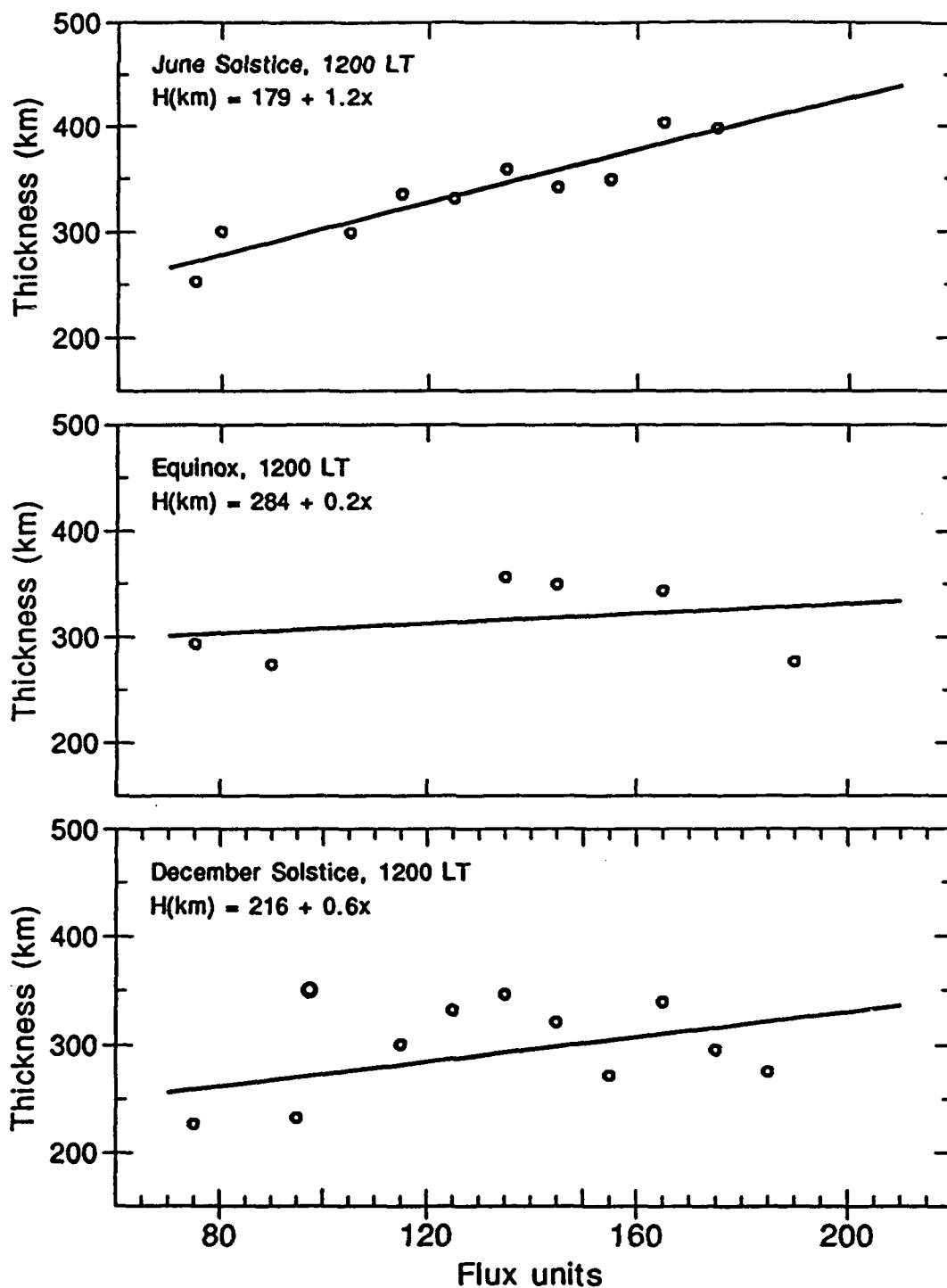
Fig. 35. Seasonal variation of the layer thickness (ΔH) with flux at 1200 LT. The heavy line is a least squares fit to the quiet-time data. Results obtained under disturbed conditions were not used in this comparison.
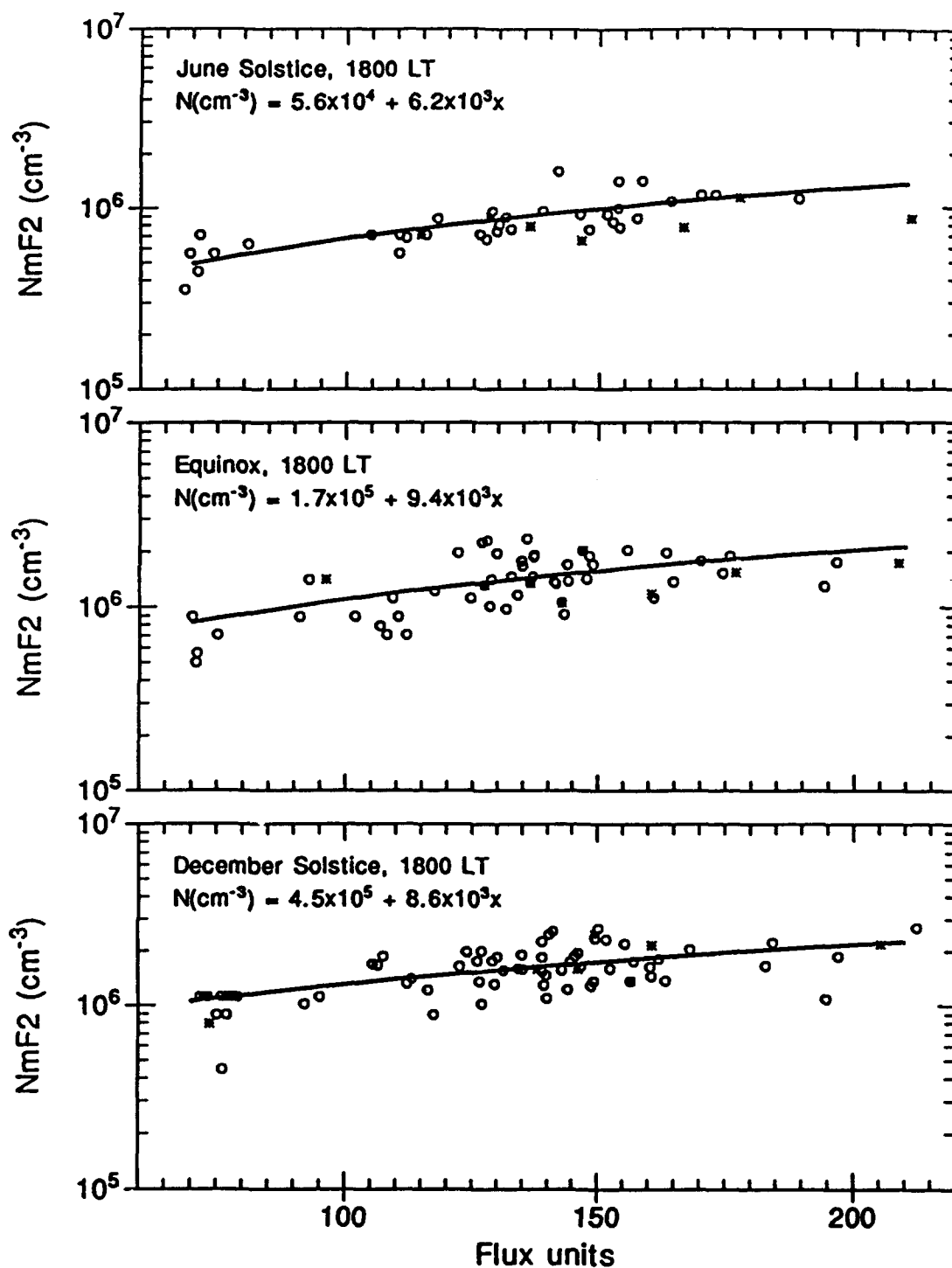
Fig. 36. Seasonal variation of the peak density (NmF2) with flux at 1800 LT. The heavy line is a least squares fit to the scattered quiet-time data (open circles). The formula in the upper left corner corresponds to the least squares fit. The stars denote data obtained under disturbed conditions.

in hmF2 with flux show greater variability at 1800 LT than at noon, and the increase in hmF2 is most dramatic at equinox (see Figure 37). The solstitial thickness at 1800 LT is comparable. The equinoctial layer begins narrower than the solstitial layers, but shows a greater increase with flux, as illustrated in Figure 38.

The peak density, peak height, and layer thickness are all highly correlated with flux for the daytime and evening observations.

The effects of increased magnetic activity on the plasma density profiles are also considered. The disturbed data are not significantly different from the quiet-time data for any season, time, or flux level, indicating that magnetic disturbance does not have a clear effect on the peak height or density at Jicamarca, as shown with the starred disturbed data points in Figures 33 through 38. A report by Rishbeth [1991] indicates that the geomagnetic influence on hmF2 is important, but may be masked by high solar activity during the day. The effects are especially diminished at the magnetic equator where the electric field is the primary factor in controlling the height of the F2 layer.

There are disturbance effects on the overall profile as illustrated for the 1200 LT profiles for moderate solar activity, seen in Figure 39, and for the 1800 LT moderate activity profiles in Figure 40. The average quiet-time profiles generated for the figures earlier in this chapter are compared with the superimposed disturbed profiles. The
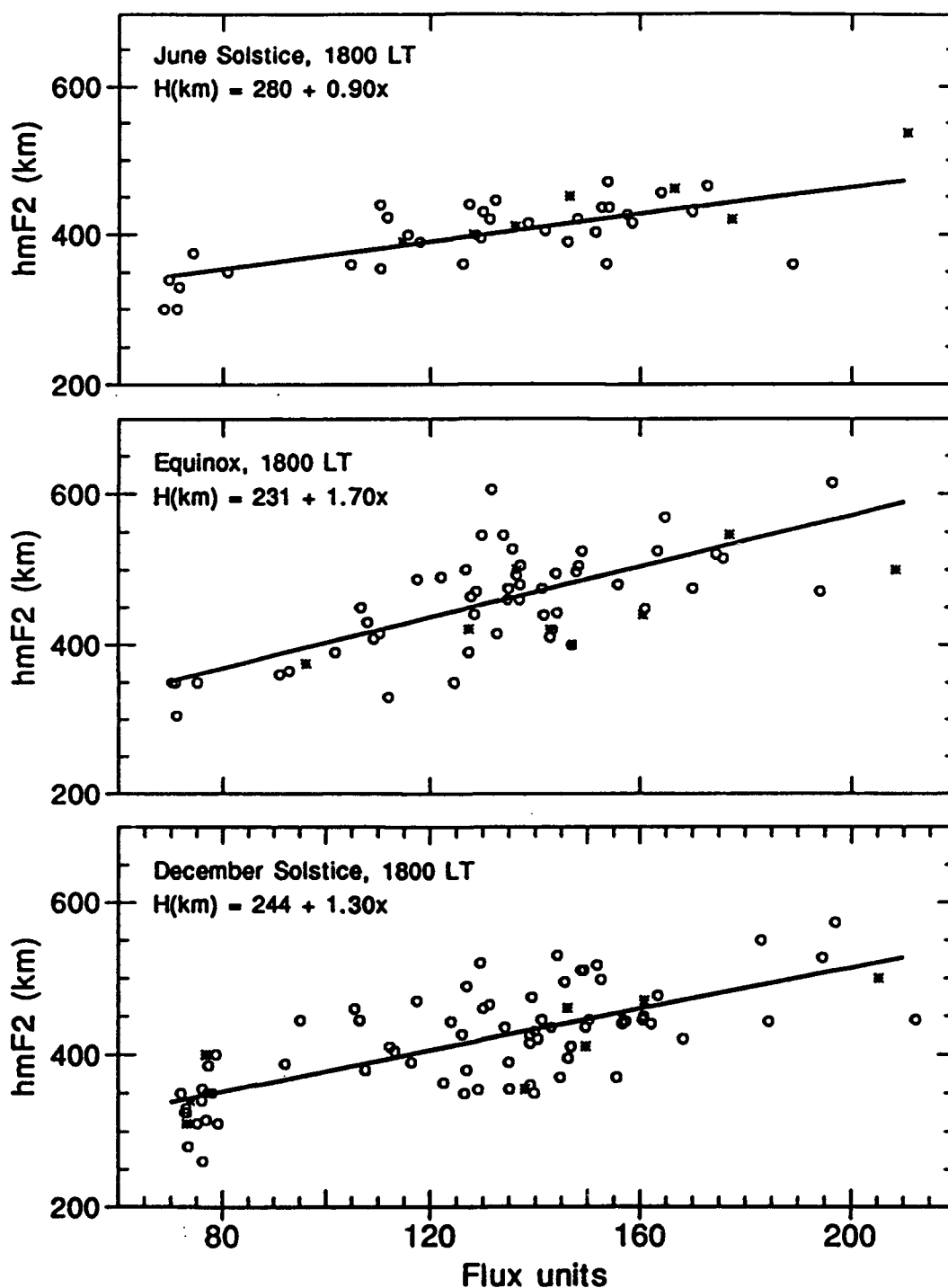
Fig. 37. Seasonal variation of the peak height (hmF2) with flux for 1800 LT. The heavy line is a least squares fit to the scattered quiet-time data (open circles). The formula in the upper left corner corresponds to the least squares fit. The stars denote data obtained under disturbed conditions.
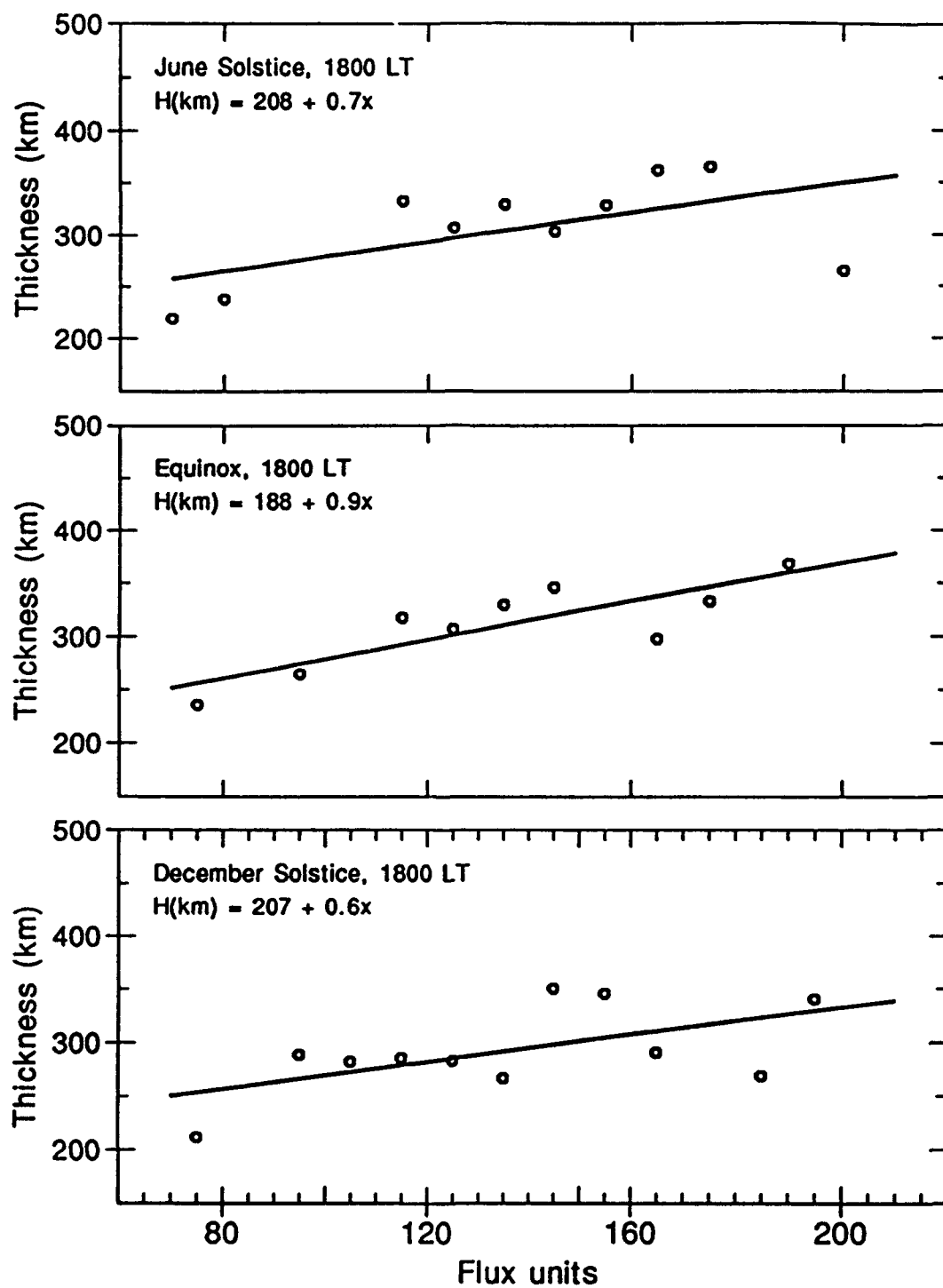
Fig. 38. Seasonal variation of the layer thickness (ΔH) with flux for 1800 LT. Results obtained under disturbed conditions were not used.
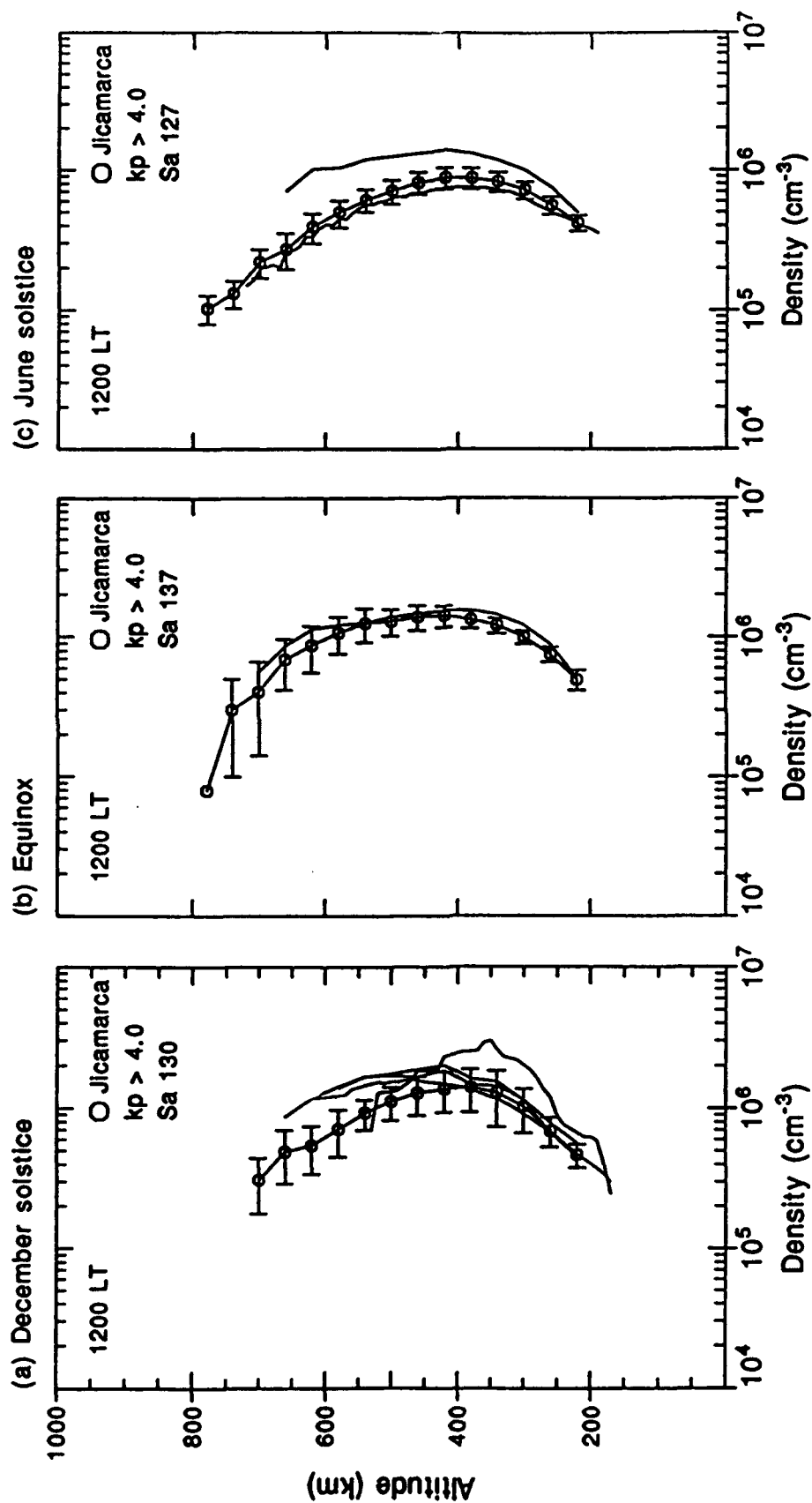
Fig. 39. Seasonal comparison of 1200 LT averaged profiles and disturbed data. The quiet-time (Kp < 4.0) average profiles are presented with standard deviation bars. The disturbed profiles (Kp > 4.0) are superimposed to illustrate their variability.
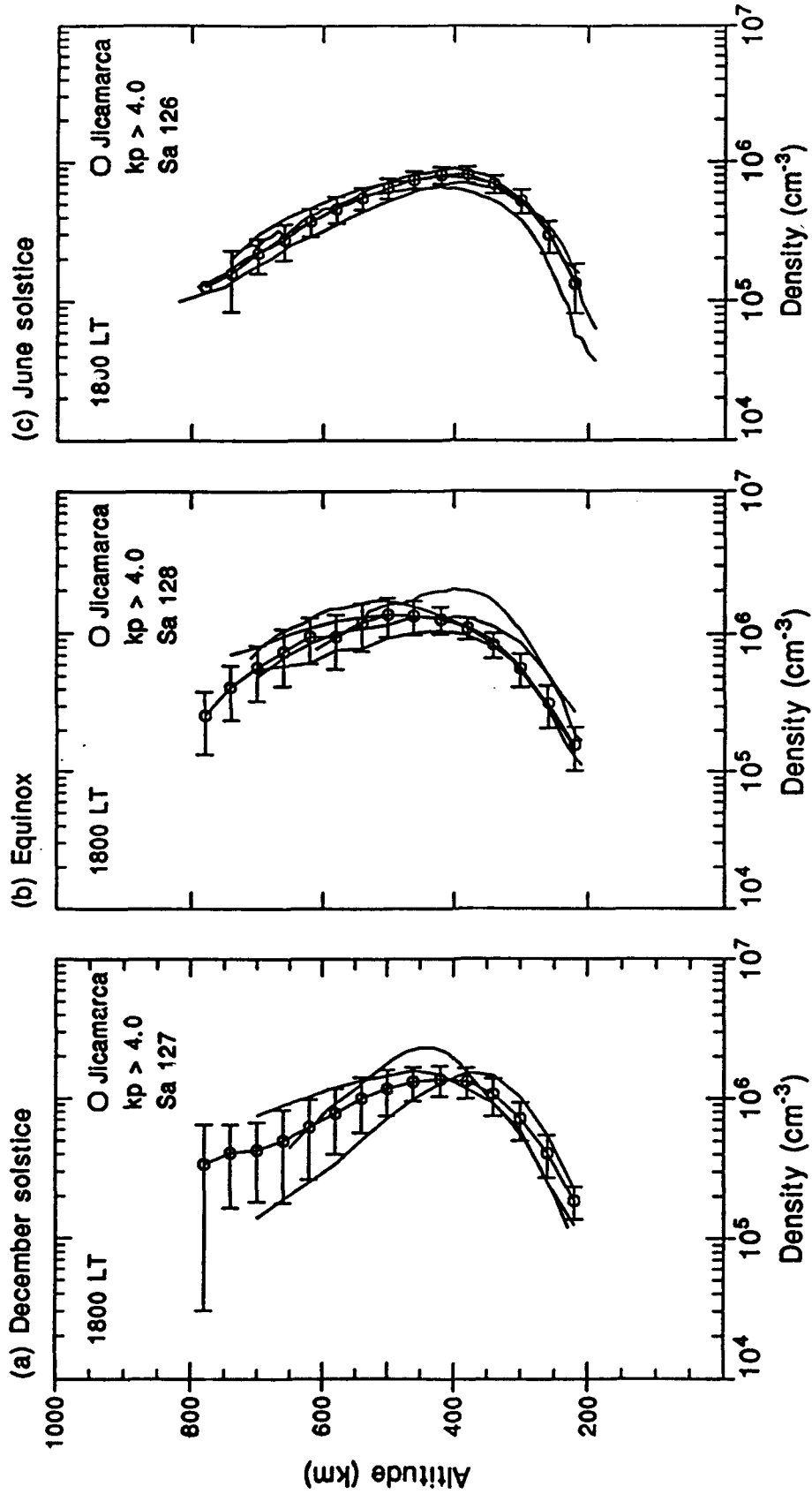
Fig. 40. Seasonal comparison of 1800 LT averaged profiles and disturbed data. The quiet-time (Kp < 4.0) average profiles are presented with standard deviation bars. The disturbed profiles (Kp > 4.0) are superimposed to illustrate their variability.

flux is given for the quiet-time profile and the flux of each disturbed profile is similar to that of the quiet-time data.

The results indicate that the topside profile is affected the most with magnetic disturbance for the noon time, moderate solar activity observations. This result is not consistent throughout the day, nor is it consistent throughout the solar cycle. The statistics for the comparison are limited not only by the lack of a significant number of profiles during disturbed days, but also by the relatively small disturbance levels in our data. The disturbed profiles used generally have Kp values of 4.0 to 5.0, so the effects may not be as dramatic as would be seen with higher magnetic activity.

CHAPTER IV

IONOSPHERIC MODELS

In this chapter descriptions of a number of ionospheric models used for the comparisons with the Jicamarca data in Chapter V are presented. These models include the International Reference Ionosphere (IRI) and two theoretical models, the Fully Analytic Ionospheric Model (FAIM), and the Parameterized Real-time Ionospheric Specification Model (PRISM), which will be described in detail. We present more brief descriptions of the Chiu model, Semi-Empirical Low Latitude model (SLIM), USU model, and Sheffield models which will not be used for the comparisons in the following chapter. The models to be compared with the data are fast running computer models that require little storage space.

4.1. INTERNATIONAL REFERENCE IONOSPHERE

The IRI is a global empirical reference model based on the thirteen standard CCIR parameters obtained from ionosondes, incoherent scatter radars, satellites, and rocket observations or URSI parameters scaled from ionosondes to provide an average ionospheric density height profile [Rawer, 1984; Bilitza, 1989]. The IRI provides global-scale information about electron density, ion and electron temperatures, and ion composition using either the CCIR-67 or

URSI-89 set of coefficients for a given location, time of day, day of year, and F10.7 cm flux. The profiles are generated by a synthesis of functions identified with six different mathematically and/or geophysically unique altitude regions: D/E region, E valley, Intermediate region, F1, F2 and topside ionosphere. We have obtained the 1990 version of IRI which employs the URSI-89 coefficients that are scaled from ionosonde data. Because the Huancayo ionosonde (Huancayo, Peru, -12° S, 284° E, +2° dip) contributes to this database [Rush et al., 1984], we expect very good agreement with the peak electron density and corresponding peak layer height measured with the Jicamarca radar.

The IRI calculates the plasma density profiles from 50 to 2000 km for every hour. The shape is specified by a combination of geometric functions which provide an analytic description of the profile. The model produces plasma density profiles, electron and ion temperature profiles, and percentages of ion compositions for O^+, O_2^+, NO^+, H^+, and He^+ for a given latitude and longitude (either geographic or geomagnetic) for specified solar activity (either sunspot number or F10.7 cm flux). Month, day, and local or universal time are also inputs to the model.

An example of profiles generated by the IRI model is given in Figure 41. In this case, the model was run for 1200 LT for three F10.7 cm flux levels -- 70, 130, and 210 -- and for the three seasons at Jicamarca, Peru (11.95° S, 76.87° W,
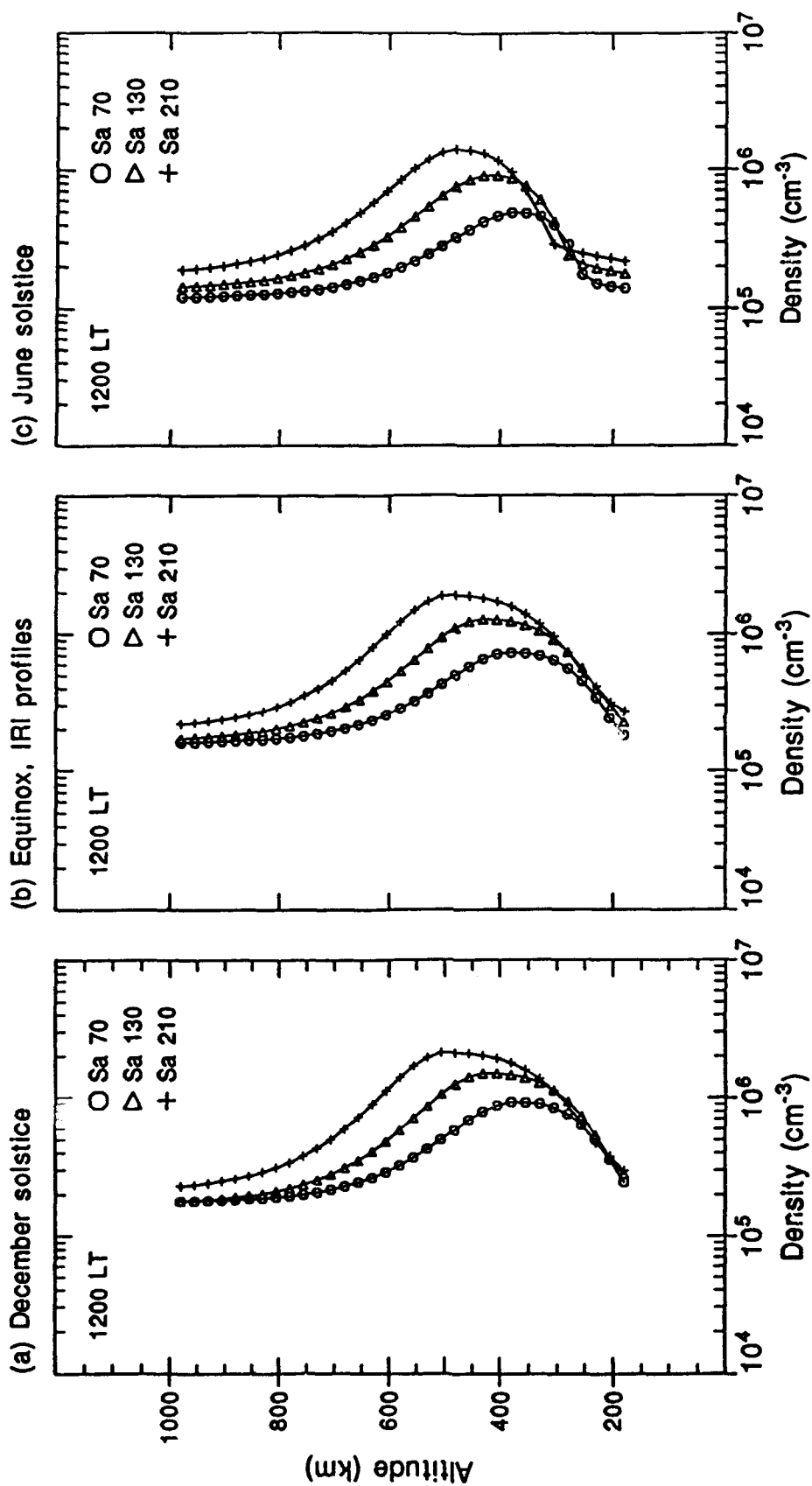
Fig. 41. Seasonal variations of the noontime IRI profiles for three flux levels -- 70 units for solar minimum conditions, 130 units for moderate solar conditions, and 210 units for solar maximum conditions.

dip 2° N). These are fairly typical IRI profile in that there is a "bowing" in the topside from approximately 600 to 800 km which tends to make the layer width too narrow. The IRI also has an asymptotic profile above 600 km which is entirely unrealistic, as will be seen in the comparisons with Jicamarca data in the next chapter.

Workshops are held every two years to update IRI with current observations from the sources listed above. The latest version, IRI 90, allows the user a choice between various input models and coefficient databases. The electron density options for the calculations are the CCIR-67 model or the URSI-89 model to specify NmF2/foF2. The analytical Lay-representation for the E-F region, the Gulyaeva-1987 model for F2 bottomside thickness, and the Danilov-Yaichnikov-1985 model for ion composition were also included in IRI-90. The user may input hmf2 or use the CCIR-M3000 based model. The neutral temperature is obtained with the updated CIRA-86 model.

The IRI makes no claims to prediction capabilities, but merely attempts to provide global ion/electron density profiles and associated information listed above. Its low computer costs, global-scale representation, worldwide availability and continuous updating make it a convenient tool for model comparisons as well as a readily available source of temperature, composition, and density inputs to other models.

4.2. THE CHIU IONOSPHERIC MODEL

The Chiu model was developed out of a need to have a self-contained global model of ionospheric electron densities for global thermospheric and ionospheric dynamical calculations [Ching and Chiu, 1973]. The incorporation of production and loss of ions with the three-dimensional time-dependent dynamical calculations of the thermosphere ionosphere interactions (such as ion drag, Joule heating, and atmospheric dynamo action) gave a complex model which required more computer time than could be justified by the output of only electron densities to be used in further calculations [Ching and Chiu, 1973]. The original model [Ching and Chiu, 1973] was constructed by organizing vertical incidence sounding of 50 stations from 1957 to 1970 (provided by the World Data Center (A), Boulder, Colorado) into empirical formulas. The formulas involve elementary functions of local time, annual time, altitude, geographic latitude, geomagnetic latitude, and Zurich-smoothed sunspot number. The model required little storage space and yielded electron density at any space-time point, though it was limited to large-scale phenomena. Ching and Chiu began with the basic premise that the average electron density at any given space and time point and solar condition is the sum of contributions from the E, F1 and F2 layers whose electron density is in turn the product of a global amplitude constant, a vertical profile function, and a layer peak

density function, the profile functions being standard Chapman profiles. The layer peak density functions contain the greater part of the space time variation of the ionospheric layers. For the E- and F1-regions, they considered the solar zenith angle to be the primary source of ionization and used this to organize the daytime peak electron density data, so functions whose major variations depend only of the zenith angle and sun spot number were used.

For the F2-region, the modeling was more difficult. Phenomena such as the equatorial anomaly have a greater effect on the variations in NmF2 and HmF2 on a daily and seasonal basis, which entails more complex calculations. Shortly after the development of this model, Chiu modified it to include the magnetic dip angle, magnetic longitude, and north-south asymmetry effects to improve the modeling of the F2 region [Chiu, 1975]. The database was also expanded to include critical frequencies from 18 stations. This gave a database of 58 stations, 18 of which include complete chronologies from 1957-1970 [Chiu, 1975]. The outcome of these efforts is an empirical model that describes the F2 layer critical frequencies at any space-time point -- the Chiu Ionospheric model.

Acknowledged shortcomings of the model are the coverage of polar and subpolar regions and the required simplicity of the model which placed restrictions on the number of independent variables. These restrictions primarily

precluded the use of longitudinal variation within the model, although a measure of longitudinal variation is contained by use of the geomagnetic latitude for F2-region calculations and geographic latitude for E- and F1-calculations [Chiu, 1975]. The Chiu model is not able to accurately reproduce the hmF2's observed at middle and low latitudes and, in spite of improvements cited above, it still cannot reproduce the equatorial anomaly [Anderson et al., 1989]. The model representation of the equatorial anomaly is presented in the section describing FAIM.

In summary, this model is designed to be simple and comprehensive in its coverage of large annual and solar cycle variations which affect the electron density in the ionosphere. It is designed to be used in the dynamical calculations of the thermospheric-ionospheric interactions, electrostatic field mapping in the atmosphere, ion drag in thermospheric modelling, and applications in radio propagation studies and space communications [Chiu, 1975]. The results from this model will not be compared with our radar data.

4.3. THE SEMI-EMPIRICAL LOW-LATITUDE
IONOSPHERIC MODEL

Over the years, improvements were made in low latitude modeling. In response to a need to better model the peak density and height in the plasma, the Semi-Empirical Low-latitude Ionospheric Model (SLIM) was developed [Anderson et

al., 1987]. In keeping with conservation of computer time and space, SLIM was designed to theoretically calculate electron density profiles as a function of latitude and local time from the parameters NmF2, hmF2, and the modified Chapman expression below

$$N_e(Z) = NmF2 \exp (C[1 - Z - \exp(-Z)]) \qquad (13)$$

where NmF2 is the peak plasma density, hmF2 is the height where the peak plasma density occurs, $Z = (h - hmF2)/H$, and C is the coefficient c_{lo} or c_{up} referring to the regions above and below hmF2 respectively [*Anderson et al.*, 1989]. There are separate sets of coefficients that reproduce these profiles for each 2° interval in latitude and every half hour.

The coefficients are stored in tabular format and are easily retrievable. They reproduce electron density profiles every hour over a 24-hour period, every two degrees from 24° S to 24° N for the June/December solstices and equinox, for solar cycle maximum and minimum periods. The profiles are normalized to the peak electron density, NmF2. The profiles are F-region profiles, ranging from 180 to 1800 km. The density profiles can be regenerated by specifying N internally or externally via an empirical model. The topside and bottomside ionosphere are not well represented by SLIM because the modeling takes into account only the chemistry associated with atomic oxygen reactions. A further limitation of the model is the lack of longitudinal variation, which gives average condition profiles rather than

truly representing the ion/electron density for a particular region. In order to calculate the coefficients for SLIM, the time-dependent ion continuity equation below is solved:

$$\frac{\partial N}{\partial t} + \nabla \cdot (N \underline{V}) = P - L \qquad (14)$$

where N is the ion density, P is the ion production rate, L is the loss rate, and $\nabla(N\underline{V})$ is the ion transport term derived from the ion momentum equation. Plasma transport is along geomagnetic field lines by diffusion and neutral winds. Vertical transport is through ExB drift. The coefficients for the continuity equation come from models of the neutral composition, ion and electron temperatures, production, loss and diffusion rates, ExB drift, and neutral wind models [Anderson et al., 1987]. The following models were used to solve the above equation for ion concentration:

1) The MSIS neutral atmospheric model [Hedin, 1983] is used to calculate the atomic oxygen densities and neutral temperature as a function of altitude, latitude, and local time. Values for the average F10.7 cm flux for solar cycle maximum and minimum are 180 and 70 units respectively. To represent average geomagnetic conditions, Ap is set to 15 in the MSIS model.

2) Production rates are defined as $P_{\bullet} = 5.5 \times 10^{-7}$ sec^{-1} for solar maximum and 2.3×10^{-7} sec^{-1} for solar minimum.

Loss rates are 2×10^{-11} $(t_g/200)^{-\frac{1}{2}}$ cm^3/sec (t_g is the temperature of the neutral gas) for the reaction

$$O^+ + O_2 \rightarrow O_2^+ + O \tag{15}$$
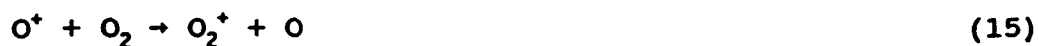
and 7×10^{-3} cm^3/sec for the reaction

$$O^+ + N_2 \rightarrow NO^+ + N \tag{16}$$

3) Plasma temperatures as a function of local time, altitude and season are derived from the IRI as ratios of Te/Tn and Ti/Tn and are applied to the neutral temperature (Tn) results from MSIS.

4) The geomagnetic field is represented by an Earth axis aligned dipole model.

5) Observed mean (DC), diurnal, semidiurnal, and terdiurnal harmonics from Arecibo (30° N, 2.4° W, geomagnetic), Millstone Hill (54.1° N, 356.9° E, geomagnetic), and St. Santin (46.8° N, 82.4° E, geomagnetic) are used to construct a simple analytic formulation of the meridional neutral wind field [Anderson et al., 1987]. The latitude variations of phase and amplitude are derived from theoretical simulations [Forbes, 1982a,b]. The general latitudinal pattern is assumed to be guided by the tidal calculations of Forbes [1982a,b] and zonal mean velocities from Roble et al. [1977]. The current wind model parameterization is assumed to be independent of solar activity [Anderson et al., 1987].

6) SLIM uses six vertical drift models obtained from Fejer et al. [1981] to represent the three seasons under solar cycle maximum and solar cycle minimum conditions. The model assumes the vertical drift velocity is independent of altitude and the east-west component of the ExB drift is neglected in these calculations because of its negligible effect on the electron density profiles. Because these are Jicamarca drifts, they may be inappropriate for longitudes other than the American sector.

With these inputs, six internal databases are produced from the theoretical calculations. Three are the solar minimum runs for the June and December solstices and equinox (spring and fall equinox are taken to be equal), and three are similar runs for solar cycle maximum. The databases each contain profile parameters for a fixed geographic/geomagnetic point and a fixed time. The results of the SLIM calculations are available in tabular format, with the total electron content (TEC) and the 6300 Å Airglow specified for each latitude, season, and solar cycle. The model has no longitudinal variation and its seasonal calculations are based on four-month averages which may be inappropriate for representing variations in the peak density and heights of the equatorial ionospheric layers. In addition, there is no variation in flux outside the solar minimum and solar maximum levels. This model will not be used in our comparisons with the experimental data.

4.4. THE FULLY ANALYTIC IONOSPHERIC MODEL

The Fully Analytic Ionospheric Model (FAIM), developed by Anderson et al. [1989], is based on theoretically calculated profiles which are parameterized to be reproduced quickly. It used the Chiu model as a starting base and added analytic corrections to make them fit the SLIM profiles.

Corrections were made to two of the Chiu calculations to improve the calculation of hmF2 at low and middle latitudes and to improve the representation of the equatorial anomaly [Anderson et al., 1989]. New analytic functions were derived for foF2, hmF2, H_{up}, and H_{LO} in the Chiu model and the C in equation (13) is given a value of one.

FAIM improves the peak density/frequency and peak height representation as well as extending the model out to +/- 40 degrees latitude. FAIM takes into consideration the dynamics at the equator in calculating the electron density profiles. A vertical ExB drift based on Jicamarca observations reported by Fejer et al. [1985] is incorporated into the model as well as general physical mechanisms which act on the ionospheric plasma at the equator.

The model generates electron/ion density profiles for a twenty-four hour period for the three seasons -- December solstice (mid-October to mid-February, June solstice (mid-April to mid-August), and equinox (mid-February to mid-April and Mid-August to mid-October) -- for height ranges from 90 to 1000 km at 10 km intervals. Figure 42 illustrates the
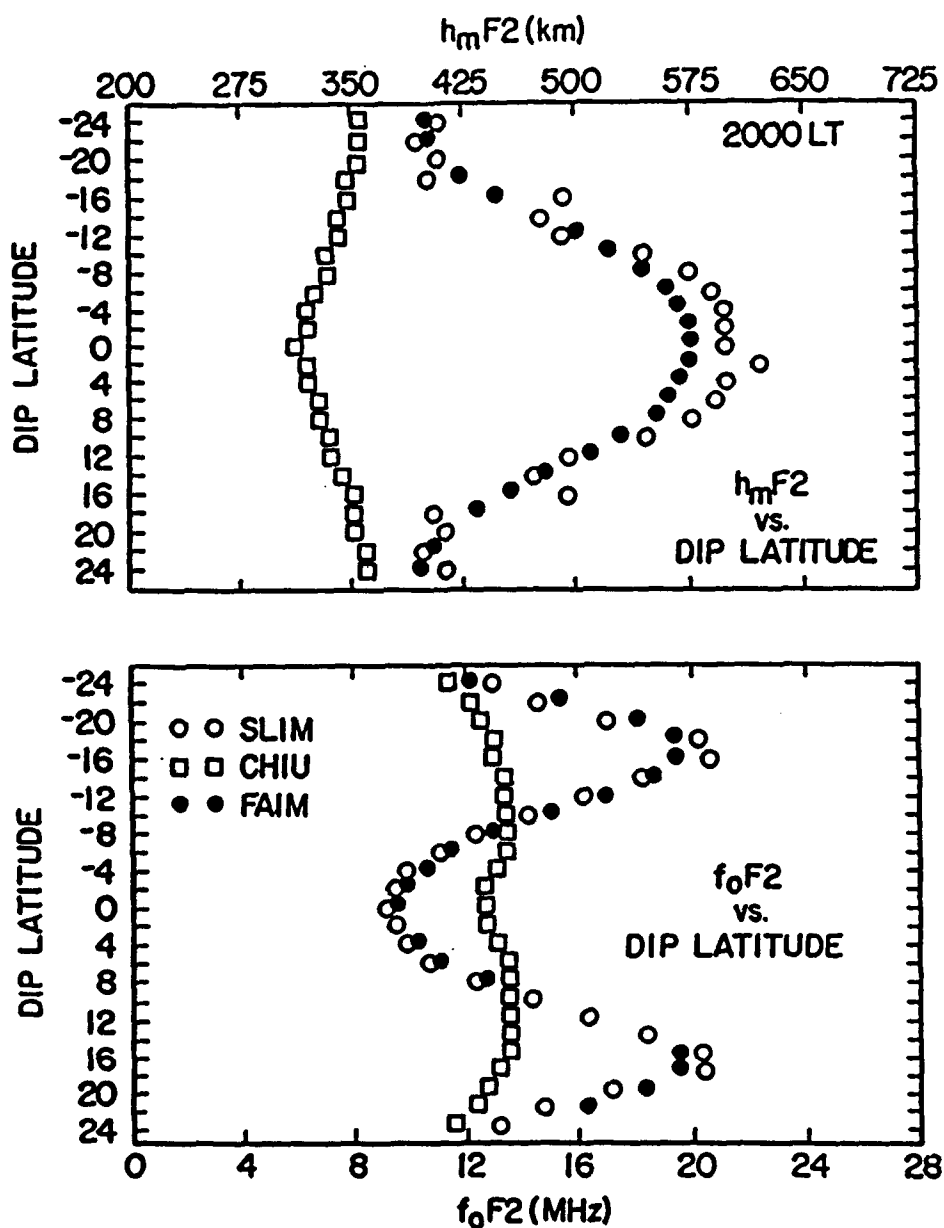
Fig. 42.   Latitudinal variation of the F2-layer critical
frequency foF2 (MHz) (bottom panel) and peak layer height
(top panel) at 2000 LT, for solar minimum equinoctial
conditions as predicted by the Chiu model, SLIM, and FAIM
(after Anderson et al. [1989]).

improvement of FAIM over both SLIM and the Chiu model in depicting the equatorial anomaly at 2000 LT for solar minimum equinoctial conditions.

Sunspot number is the required input for indicating solar inputs to the ionosphere. A running program is used to specify month, flux, latitude, and time. The program can be modified to calculate profiles for multiple latitudes for a single hour or multiple hours for a single latitude.

The model was run for the same conditions as the IRI runs earlier (see Figure 41 for IRI profiles, Figure 43 for FAIM profiles). The profiles for FAIM under Equinox conditions are much broader than those of the IRI, but the peak layer densities are almost twice as small as the IRI peak layer densities, especially for the southern hemisphere summer, December solstice. The topside decreases rapidly with height because the model incorporates only chemistry associated with atomic oxygen. The neutral wind is specified by the sinusoidal functions used in SLIM. The electric field in FAIM is based on electric field data from _Fejer et al._ [1979] and _Fejer et al._ [1985] and reflects the increased vertical drift prior to sunset that is especially dramatic during equinox and high solar activity. The model also reproduces the increasing layer width that occurs with increasing solar activity. FAIM is similar to SLIM with respect to limitations in longitudinal variation, but FAIM calculates profiles for flux between 70 and 185 units.
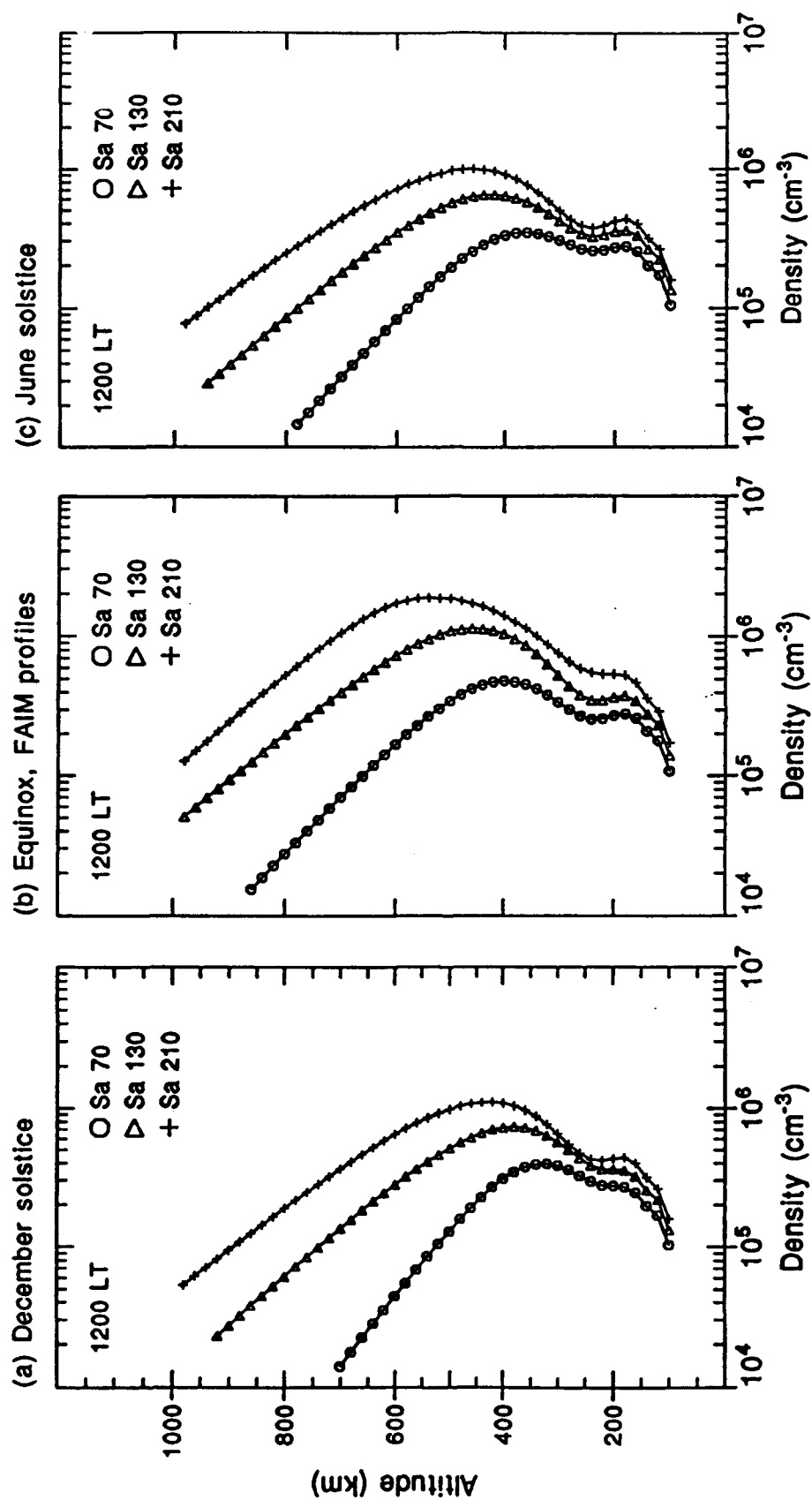
Fig. 43. Seasonal variations of the noontime FAIM profiles for three flux levels -- 70 units for solar minimum conditions, 130 units for moderate solar conditions, and 210 units for solar maximum conditions.

4.5. THE PARAMETERIZED REAL-TIME IONOSPHERIC

SPECIFICATION MODEL

The Parameterized Real-time Ionospheric Specification Model (PRISM) was developed by Anderson and co-workers out of the need for accurate forecasting of ionospheric conditions as they apply to operational space and communications systems parameters and the optimization of these systems based on real-time global ionospheric conditions [Anderson et al., 1991]. Accurate specification of the current state of the ionosphere is imperative in the development of an ionospheric forecast model and may be calculated through either a climatological model or a physical model. The first approach averages ionospheric observations over a period of time and thus presents an average picture of the ionosphere in which temporal structures, such as equatorial spread F (ESF) and plasma bubbles, will be smoothed out. The physical model approach solves the coupled plasma continuity, momentum, and energy equations to provide a more instantaneous representation of the ionosphere. The physical model approach was chosen for PRISM based on this ability to provide a more realistic specification of the ionosphere. With precise initial conditions and correct energy and momentum calculations, the time-dependent phenomena of the ionosphere can be accurately modeled. When run over a period of time, the initial conditions are expected to damp out and the model would be dependent solely on the recent history of

energy and momentum input -- solar EUV, high latitude thermospheric heating and convection, and low latitude dynamo electric fields [Anderson et al., 1991]. Unfortunately, this takes considerable computer time and power, which is not practical for daily applications. Therefore, the physical model results are parameterized and the parameterized model is adjusted with near real-time data to give a more viable model for use in ionospheric forecasting. A two-step process is involved in parameterizing the physical models for PRISM. The models are run for selected values of solar and geophysical parameters to produce the databases of ion density profiles covering specified latitude and longitude ranges for 24 hours. A series of linear combinations of Empirical Orthonormal Functions (EOF's) are produced from each database. The EOF coefficients that vary longitudinally are represented by a truncated Fourier series, the coefficients that vary latitudinally are given by a linear combination of orthogonal polynomials. The EOF calculation procedure is described in detail by Anderson et al. [1991]. This representation is semi-analytic because of the tabulated format of the EOF's, which allows the physical model run results to be quickly and accurately reconstructed.

There are four separate physical models that contribute to PRISM: a low latitude F-region model, a low and middle latitude E region model, a midlatitude F-region model, and a high latitude E- and F-region model. With the focus of our work on Jicamarca, we will concentrate on the low latitude F-

region model with the understanding that hereafter "PRISM" refers strictly to the low latitude model contributing to PRISM.

The low latitude theoretical model is based on the initial work by <u>Anderson</u> [1973<u>a,b</u>]. It too solves the time dependent ion continuity equation, equation 14, numerically to find ion and electron densities as a function of altitude, latitude and local time [<u>Anderson</u>, 1973<u>a,b</u>; <u>Klobuchar et al.</u>, 1991]. The ion velocity <u>V</u> includes plasma diffusion and collisions with neutrals along geomagnetic fieldlines as well as **ExB** drift perpendicular to the field lines. The model uses a tilted dipole magnetic field and a transformation is used to transfer the independent coordinates <u>r</u>, <u>θ</u>, and <u>φ</u> to a coordinate system parallel and perpendicular to <u>B</u> (see <u>Anderson</u>, [1973<u>a</u>]) to solve the continuity equation:

$$\partial N_i / \partial t + V_{i\perp} \cdot \nabla N_i = P_i - L_i - \nabla \cdot N_i V_{i\parallel} - N_i \nabla \cdot V_{i\perp} \qquad (17)$$

The right-hand side of (17) contains the terms which are second order in the coordinate parallel to <u>B</u>, and the left-hand side gives the time rate of change of the ion density in a frame of reference that drifts with the **ExB** velocity [<u>Klobuchar et al.</u>, 1991].

Coefficients leading to solutions to the continuity equation are obtained through models of the neutral atmosphere, ion and electron temperature, production, loss,

and diffusion rates, and models of the neutral wind and vertical ExB drift pattern.

The mass spectrometer/incoherent scatter (MSIS-86) neutral atmosphere [Hedin, 1987] was adapted for use to derive the neutral temperature. Ion and electron temperatures are derived from the model of Brace and Theis [1981]. Thermospheric winds are derived from the Horizontal Wind Model (HWM) [Hedin, 1988].

Production and loss rates are similar to those in Anderson [1973b]. The production rates are based on atomic oxygen production by solar EUV radiation only, excluding corpuscular radiation ionization. The photoionization rate used for solar minimum -- 3.0×10^{-7} s^{-1} -- differs slightly from that used in the SLIM calculations. The rate for solar maximum remains the same. The following formula is used to generate the photoionization rate (P_∞) based on Zurich sunspot number (R):

$$P_\infty(R) = P_{\infty 0}(1 + 0.0124R) \qquad (18)$$

which gives a value of 5.5×10^{-7} s^{-1} at the top of the atmosphere for solar maximum conditions ($R = 110$) and the value above for solar minimum conditions ($R = 0$). Loss rates were obtained from Torr and Torr [1979] for the dissociative recombination reactions:

$$O^+ + O_2 \rightarrow O_2^+ + O \qquad (19)$$

and

$$O^+ + N_2 \rightarrow NO^+ + N \tag{20}$$

which were presented as the primary loss reactions in the Equatorial F2-region. The loss rate for equation (19) is:

$$\kappa_1 = 2.82 \times 10^{-11} - 7.74 \times 10^{-12}(T_{eff}/300) +$$
$$1.073 \times 10^{-12}(T_{eff}/300)^2 - 5.17 \times 10^{-14}(T_{eff}/300)^2$$
$$+ 9.65 \times 10^{-16}(T_{eff}/300)^4 \tag{21}$$

for $300 \leq T_{eff} \leq 6000°$ K. The loss rate for equation (20) depends on the vibrational temperature of N_2 as well as the gas temperature and has the form:

$$\kappa_2 = 1.533 \times 10^{-12} - 5.92 \times 10^{-13}(T_{eff}/300) +$$
$$8.6 \times 10^{-14}(T_{eff}/300)^2 \tag{22}$$

for $300 \leq T_{eff} \leq 1700°$ K and

$$\kappa_2 = 2.73 \times 10^{-12} - 1.155 \times 10^{-12}(T_{eff}/300) +$$
$$1.483 \times 10^{-13}(T_{eff}/300)^2 \tag{23}$$

for $1700 < T_{eff} \leq 6000°$K. The effective temperature (T_{eff}) is defined by Torr and Torr [1979] to be:

$$T_{eff} = \frac{2}{k} \left(\frac{m_n}{m_i + m_n} + \frac{m_{iu}^2}{2} + \frac{3kT_i}{2} - \frac{3kT_n}{2} \right) + \frac{3kT_n}{2} \tag{24}$$

where m_i and m_n are the mass of the ion species and neutrals, respectively. The diffusion rate is given by:

$$D = 1/n(o) [6.9 \times 10^{18}(T_g/1000)^k] \; cm^2/sec \tag{25}$$

which is the diffusion coefficient for O^+ ions diffusion through a neutral gas [Anderson, 1973b].

Vertical drifts for the American sector were obtained from Fejer [1981] and Fejer et al. [1989] using the Jicamarca ISR. The drifts were modified to simulate longitudinal variation.

PRISM calculates the low latitude electron density for altitudes from 160 to 1600 km over dip latitudes from -32° to +32° in two degree increments, in half hour time increments from 0030 to 2400 LT, and for longitudes of 0°, 30°, 139°, and 237°, locations where drift measurements are available [Anderson et al., 1991]. Additional regional coverage is listed in Anderson et al. [1991]. The initial physical model runs were made with F10.7 cm flux levels of 70, 150, and 210 units. In addition to the density results, it will also enumerate NmF2, hmF2, total electron content, and slab (layer) thickness in the header for the data files. The results of each calculation are presented in a single large file covering the input region for given flux over the twenty-four hour time period.

The low latitude profiles from PRISM were kindly supplied by Dr. David N. Anderson of the Ionospheric Modeling Branch, Phillips Laboratory. Figure 44 follows the previous figures from IRI and FAIM regarding input parameters. The modeled profiles exhibit a secondary peak around 500 km for December and June solstice, and 600 km for equinox. The peak
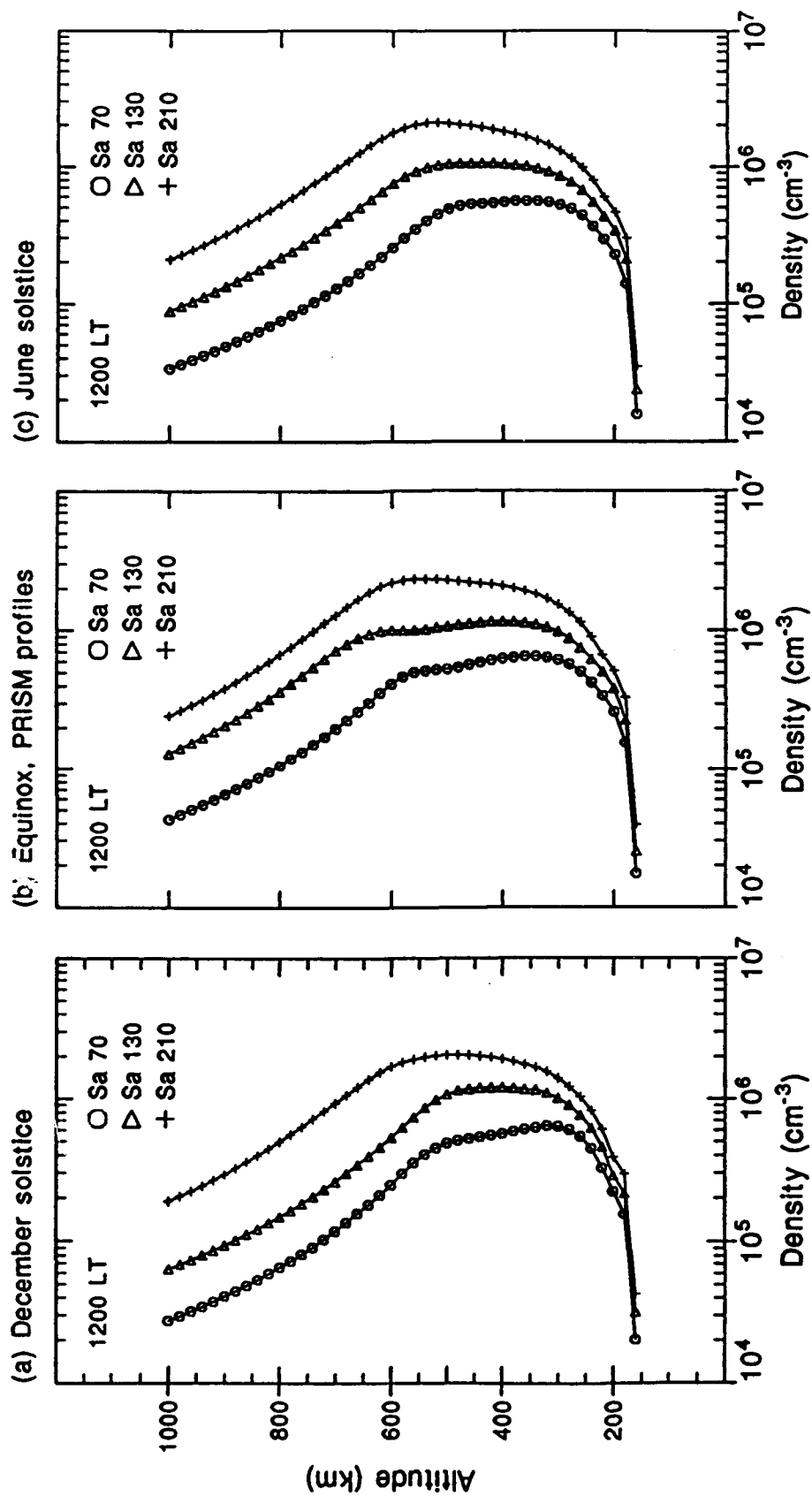
Fig. 44. Seasonal variations of the noontime PRISM profiles for three flux levels --
70 units for solar minimum conditions, 130 units for moderate solar conditions, and 210
units for solar maximum conditions.

of ionization occurs around 200 km near sunrise and rises during daylight hours as a result of the upward drift velocities. At noon the maximum ionization occurs around 300 km. The secondary peak shown in the PRISM profiles is the morning peak under the effects of the upward plasma drift. The PRISM layers have a tendency to be very broad as a result of this peak and the ensuing topside densities are frequently too large.

It is the parameterized model instead of the physical model that is adjusted based in input from Digital Ionospheric Sounding System (DISS) and Defense Meteorological Satellite Program (DMSP) satellite observations. There are 20 operational DISS sites, primarily northern hemisphere sites, that provide information about the critical F2 layer frequency (foF2), the critical E layer frequency (foE), the peak F2 layer height (hmF2), and the peak E layer height (hmE). Additional information is expected to be provided by the Transionospheric Sensing System (TISS), which will provide Total Electron Content (TEC) between the site and the GPS satellites when the satellites are operational. TISS data are not incorporated into the version of PRISM used in this study. The DISS and TISS sites are listed in Anderson et al. [1991]. The DMSP satellites carry the Special Sensor Ionospheric Electron Density Scintillation (SSIES) instrument which provides ion and electron densities and temperatures, and ion drift velocities. The DMSP electron/ion energy spectrometer (SSJ/4) measures and provides precipitating

differential ion and electron fluxes between 20 eV and 20 keV [Anderson et al., 1991]. Towards the latter half of this decade the DMSP satellites are expected to carry two more imagers, the Special Sensor Ultraviolet Spectrographic Imager (SSUSI) and the Special Sensor Ultraviolet Limb Imager (SSULI). The SSUSI will look down and the SSULI will look at the limb, measuring Airglow and auroral optical intensities to determine the electron and neutral density profiles. Once operational, all four instruments will provide complementary information about the plasma profiles which will be used to modify the following eight adjustment parameters.

The corrections are made to the electron density profiles by adjusting foF2, foE, hmF2, and hmE, topside electron density and scale height at DMSP altitude (N_{top} and H_{top}), and to the electron density 8 and 16 km below the E layer peak (N1 and N2) [Anderson et al., 1991]. The O^+ profiles are adjusted for foF2, hmF2, N_{top}, and H_{top}, the remaining parameters are used to adjust the molecular ion profiles. Currently, it is near real-time input from the 20 DISS sites and the DMSP data which are used to modify PRISM. The order of adjustment is foF2/NmF2, followed by a layer height adjustment, followed by the topside adjustment and bottomside adjustment as needed. The nominal value of the adjustment parameters -- ΔfoF2, ΔhmF2, ΔN_{top}, and ΔH_{top} -- is zero. A positive value indicates the model should be increased, a negative value indicates the model should be decreased. The modification procedure is outlined in

Anderson et al. [1991]. The flexibility to adjust the model with near real-time data will facilitate the continuous improvement in performance of PRISM.

4.6. ADDITIONAL MODELS

4.6.1. The Utah State University Model

The Utah State University (USU) Model was developed by Schunk and colleagues [Sojka and Schunk, 1985] to be a three-dimensional, multi-ion, time-dependent numerical model of the global F-region ionosphere between 120 and 800 km [Sojka and Schunk, 1985]. The global model contains a mid-high latitude and an equatorial F-region model and employs processes such as field-aligned diffusion, cross-field electrodynamic drifts (equatorial and high latitude), interhemispheric flow, thermospheric winds, energy-dependent chemical reactions, neutral composition changes, ion production, thermal conduction, diffusion-thermal heat flow, and local heating and cooling [Sojka and Schunk, 1985] to calculate the ion density distribution for NO^+, O_2^+, N_2^+, N^+, O^+, and He^+ as a function of time. The global model inputs are neutral temperature and composition (MSIS) and wind (simple analytic function); electric field distribution by Richmond et al. [1980]; auroral precipitation pattern (empirical model by Spiro et al. [1982]); solar EUV spectrum; and a magnetic field model [Mead, 1970] as detailed by Sojka and Schunk [1985].

The mid-high latitude model has its origins in the mid-latitude F-region model developed by Schunk and Walker [1973]. It was expanded to include the high latitudes [Schunk and Sojka, 1975; Schunk et al., 1976] and N^+ chemistry and improved photochemistry [Schunk and Raitt, 1980]. The entire high latitude region coverage came with the addition of the plasma convection model, described by Sojka et al. [1979, 1980]. And finally, thermal conduction and diffusion-thermal heat flow were included [Schunk and Sojka, 1982] to provide more accurate ion temperature calculations between 120 and 800 km. In this model plasma flux tubes are followed as they convect through the moving neutral atmosphere [Sojka and Schunk, 1985]. The coupled continuity, momentum, and energy equations are solved to generate density profiles of the previously specified ions from 120 to 800 km. At 120 km the boundary conditions are given by chemical equilibrium and at 800 km they are designated by a specific plasma escape flux. The model calculations assume that the magnetic field lines are straight and inclined and the plasma flux through 800 km is specified in order to solve the coupled equations.

The equatorial component of the model also computes the time-dependent ion densities along plasma flux tubes, in this case from equatorial flux tubes at 120 km in one hemisphere to 120 km in the conjugate hemisphere. The flux tubes are followed as they corotate with the earth and ExB drift. Sojka and Schunk [1985] detail the sources for the equatorial

model calculations which include transforming them into a coordinate system similar to the calculations used by Anderson [1973a]. The partial differential coefficients from Sterling et al. [1969] were modified to match those in the mid-high model and allow for a global scale definition of the input variabl·s. The photochemical reactions in the equatorial model are adapted from Schunk and Raitt [1980].

These two models were combined to create the global Time Dependent Ionospheric Model (TDIM), which we refer to as the USU Model. The mid-high transport equations are solved as a function of altitude, while the equatorial transport equations are solved as a function of altitude and latitude to accommodate the effects of the earth's tilted magnetic field. The mid- and high-latitude flux tubes are followed as they corotate with the earth, and the low latitude flux tubes are followed as they corotate and convect due to the electric fields.

Extensive studies using the USU Model have been conducted in conjunction with the SUNDIAL campaign [Szuszczewicz et al., 1988, 1990, 1992]. Abdu et al. [1988] reports that while the USU Model does well in the higher latitudes, improvements in the neutral wind and electric field specification and, particularly at solar maximum conditions, higher upper altitude boundaries are necessary for realistic simulations at low latitudes. The results from this model will not be compared to our data.

4.6.2. The Sheffield Model

The Sheffield Model is a plasmasphere model developed at the University of Sheffield, Sheffield England [Bailey and Sellek, 1989; Bailey, 1983]. The model solves the time-dependent continuity, momentum, and energy equations for atomic ion (O^+, H^+ and He^+) concentrations, molecular ion (N_2^+, O_2^+, and NO^+) concentrations, and electron concentrations. The equations are solved along the fieldlines of a centered dipole magnetic field from a base altitude in one hemisphere to the corresponding base altitude in the conjugate hemisphere. The MSIS-86 model provides the neutral constituent concentrations and temperatures; the zonal component of the ExB drift velocity, based on Jicamarca observations [Woodman, 1970; Woodman et al., 1977; Fejer et al., 1979] is included. The model inputs are F10.7 cm flux, magnetic activity (Ap), season, specified flux tube, and geographic location. Geographic location is specified by geographic longitude and L value. In addition, the input parameters required by MSIS-86 are varied within the model calculations. Details of the model calculations are presented by Bailey and Sellek [1989]. The model calculations provide the ion and electron concentrations, field-aligned fluxes, field-aligned velocities, and temperatures at a discrete set of points along the magnetic field line [Bailey and Sellek, 1989]. The model's strength lies in its depiction of the H^+ and He^+ concentrations and O^+-

H^* transition height. The results from this model will not be discussed.

CHAPTER V

MODEL RESULTS AND DATA COMPARISONS

This chapter will present results from comparisons of the Jicamarca data from Chapter III with IRI, FAIM, and PRISM. The inputs to each model were: F10.7 cm flux indices of 70, 130, and 210, time (1200, 1700, 1800, 2000, 0000, and 0400 LT), geographic/geomagnetic location (-12° S, -76° W, 2° dip for Jicamarca), and season (mid December, mid June, and mid March to represent the solstices and equinoxes). The comparisons are based on NmF2 and hmF2, bottomside and topside fit, and layer thickness. The layer thickness is determined in the same manner as described in Chapter III. In this instance the altitudes of the modeled profiles were modified to cover the same height as the data to avoid biasing the total electron content (TEC) of the modeled layers. We consider that a parameter is "in range of the variability of the data" when it falls within one standard deviation to either side of the average value of the profile. Of course, this criterion is only meaningful if there are enough experimental observations for reliable calculations of averages and standard deviations. We consider only geomagnetically quiet conditions.

The following figures consist of the modeled profiles compared with the quiet-time Jicamarca data. The profiles are divided by season, time, and solar activity.

5.1. SOLAR MINIMUM COMPARISONS

5.1.1. Midday Solar Minimum Comparisons

The midday observations for December solstice, equinox, and June Solstice at solar minimum are compared with the IRI, FAIM, and PRISM in Figure 45. The experimental profile was determined using observations when Kp was less than 4.0. The standard deviation from the Jicamarca peak density is about 7.6×10^4 to 3.0×10^5 cm^{-3}. The variability of the peak heights is approximately 20 km. The NmF2, hmF2, and layer thickness of the data and each model for all seasons are presented in Table 5. The main results of the daytime solar minimum comparisons for each model follow.

1. There is good agreement between the peak density of the IRI and the data for all seasons. The IRI does not vary the peak height of the layer at noon and this height is higher than the data peak height for all seasons. The bottomside fit of the IRI to the data is good in summer and equinox, but the IRI layer is higher and more gradual in winter. The topside layer of the IRI is more dense than the layer during solstices and above 650 km it deviates significantly from the data. The IRI layers are at least 30 km broader than the data layers.

2. The peak density predicted by FAIM is lower than the data NmF2 for all seasons. The modeled peak layer height is higher than the data in equinox and winter, and is lower in summer. The bottomside fit to the data is better in winter,

Fig. 45. Seasonal comparison of IRI, FAIM, and PRISM with the Jicamarca average profile for 1200 LT, quite-time solar minimum conditions. The average flux for the data is given in the upper right corner of each panel. The models were run with a flux of 70 units.

TABLE 5. Comparison of Jicamarca (JRO) NmF2 (cm^{-3}), hmF2 (km), and layer thickness (km) with IRI, FAIM, and PRISM calculations at 1200 LT, solar minimum.

		Summer	Equinox	Winter
JRO	NmF2	$9.16x10^5$	$6.28x10^5$	$4.36x10^5$
	hmF2	342	344	329
	ΔH	235	265	278
IRI	NmF2	$9.23x10^5$	$7.33x10^5$	$4.84x10^5$
	hmF2	380	380	380
	ΔH	312	321	310
FAIM	NmF2	$3.95x10^5$	$4.84x10^5$	$3.44x10^5$
	hmF2	320	400	360
	ΔH	240	309	240
PRISM	NmF2	$6.38x10^5$	$6.59x10^5$	$5.60x10^5$
	hmF2	317	348	358
	ΔH	341	387	366

where FAIM is able to depict the steep bottomside density gradient of the layer. The FAIM topside fit is good in equinox and winter. The FAIM layer is broader than the data at equinox and narrower in winter. The December solstice layer predicted by FAIM gives a poor fit to all parameters, except layer thickness.

3. The PRISM calculations give a good fit to the Jicamarca peak density for all seasons. There is good agreement with the layer height at equinox, but the PRISM summer layer is too low and the winter layer is too high. The modeled bottomside layer agreement is good for summer and equinox. The PRISM bottomside increases too gradually in winter. The presence of a secondary peak around 600 km in

the modeled profile results in increased topside densities and layer widths for all seasons.

5.1.2. Evening Solar Minimum Comparisons

The model comparisons at 1800 LT were similar to those at 1700 LT, so we present the 1800 LT comparisons and cite the differences at 1700 LT as necessary. Figure 46 shows the models compared with each averaged 1800 LT profile. The secondary peak in PRISM has almost disappeared in the summer profile and has shifted to 800 km in the equinoctial and winter profiles. The peak densities have a standard deviation of 1.8×10^5 cm^{-3} and the peak heights have a standard deviation of 30 km. Values for NmF2, hmF2, and ΔH are provided in Table 6 for 1700 LT and Table 7 for 1800 LT. The results at 1800 LT indicate that:

1. There is good agreement of the IRI peak density with the data for all seasons. The peak layer height is within range of the variability of the data for all seasons. The bottomside fit to the data is better in winter. The IRI bottomside density gradient is too gradual in equinox and the layer is too low in summer. The topside fit shows improvement over the IRI noontime topside layers in summer and winter. The equinoctial topside layer is higher than the data. The IRI topside fit is poor above 650 km. The IRI continues to overestimate the layer thickness, though there is better agreement in summer.

Fig. 46. Seasonal comparison of IRI, FAIM, and PRISM with the Jicamarca average profile for 1800 LT, quite-time solar minimum conditions. The average flux for the data is given in the upper right corner of each panel. The models were run with a flux of 70 units.

TABLE 6. Comparison of Jicamarca (JRO) NmF2 (cm^{-3}), hmF2 (km), and layer thickness (km) with IRI, FAIM, and PRISM calculations at 1700 LT, solar minimum conditions.

		Summer	Equinox	Winter
JRO	NmF2 hmF2 ΔH	1.04×10^6 330 226	4.85×10^5 338 262	5.33×10^5 324 254
IRI	NmF2 hmF2 ΔH	1.14×10^6 305 252	9.86×10^5 355 273	6.45×10^5 330 282
FAIM	NmF2 hmF2 ΔH	3.95×10^5 340 241	6.11×10^5 360 265	4.43×10^5 340 259
PRISM	NmF2 hmF2 ΔH	8.93×10^5 317 252	9.17×10^5 329 305	6.37×10^5 333 347

TABLE 7. Comparison of Jicamarca (JRO) NmF2 (cm^{-3}), hmF2 (km), and layer thickness (km) with IRI, FAIM, and PRISM calculations at 1800 LT, solar minimum conditions.

		Summer	Equinox	Winter
JRO	NmF2 hmF2 ΔH	1.03×10^6 332 242	7.11×10^5 339 245	5.27×10^5 329 235
IRI	NmF2 hmF2 ΔH	1.09×10^6 305 260	9.44×10^5 355 272	5.73×10^5 330 276
FAIM	NmF2 hmF2 ΔH	3.95×10^5 340 231	6.31×10^5 380 253	4.67×10^5 340 239
PRISM	NmF2 hmF2 ΔH	8.95×10^5 324 246	9.37×10^5 336 284	6.66×10^5 320 309

2. The FAIM profiles give a good fit to the peak density at equinox and winter. The summer density is less

than the data by more than a factor of two. The layer heights fit the data well during the solstices, the equinoctial hmF2 is approximately 40 km too high at 1800 LT. The hmF2 fit at 1700 LT is good for all seasons. FAIM gives an excellent fit to the Jicamarca bottomside in winter. The equinoctial and summer layers are less dense and higher. The summer bottomside density gradient is similar to that of the data. The topside fit to the data is excellent in winter and equinox, and the summer topside layer is within range of the variability of the Jicamarca data. The FAIM layer thickness is comparable to the data for all seasons.

3. PRISM gives a good fit to the data peak density in summer and winter. The peak layer heights are good for all seasons at 1800 LT. The PRISM hmF2 is too high at equinox, 1700 LT. The bottomside fit is good in summer, but the equinoctial and winter bottomside density gradients are more gradual than the data bottomside gradient. The 1700 LT PRISM bottomside fits are outstanding in the solstices and compare well at equinox. The topside fit in summer is good to 500 km. Above that, and in winter and equinox, the topside layer is too dense. The modeled layer thickness is in excellent agreement in summer, but continues to be too thick in both equinox and winter.

The agreement of layer heights indicates the models' ability to simulate the vertical drift enhancement at 1700 LT. There is a broad enough altitude range of Jicamarca data to provide a reliable estimate of layer thickness, so the

greater widths given by IRI and PRISM can be attributed to their respective topside profiles. There is an improvement in the density calculations of FAIM. Both IRI and PRISM continue to overestimate the topside density, but there is improvement in PRISM's topside performance during summer. The secondary peak in PRISM has moved higher in altitude, a feature especially evident in the June solstice panel of Figure 46. There is good agreement by PRISM and IRI around the peak of the 1800 LT layer, but the topside agreement is poor for both models. FAIM continues to underestimate the summer profile, but performs well for equinox and winter. The models give good agreement with the data for peak height and layer thickness. However, only FAIM is able to reproduce the steep bottomside density gradient during June solstice.

5.1.3. Post-sunset Solar Minimum Comparisons

Figure 47 illustrates the model-data comparisons at 2000 LT. The models are in good agreement with the layers at equinox, except in the topside. The PRISM secondary peak in the topside has almost completely dissipated. The values for NmF2, hmF2, and layer thickness are presented in Table 8. The standard deviation to the peak density is approximately 1.8×10^5 cm^{-3} and to the peak height is approximately 45 km. The results of the comparisons are:

1. The IRI fit to the data NmF2 is better during the solstices. The equinoctial peak is overestimated. The IRI hmF2 fits the data quite well in equinox and in winter. The
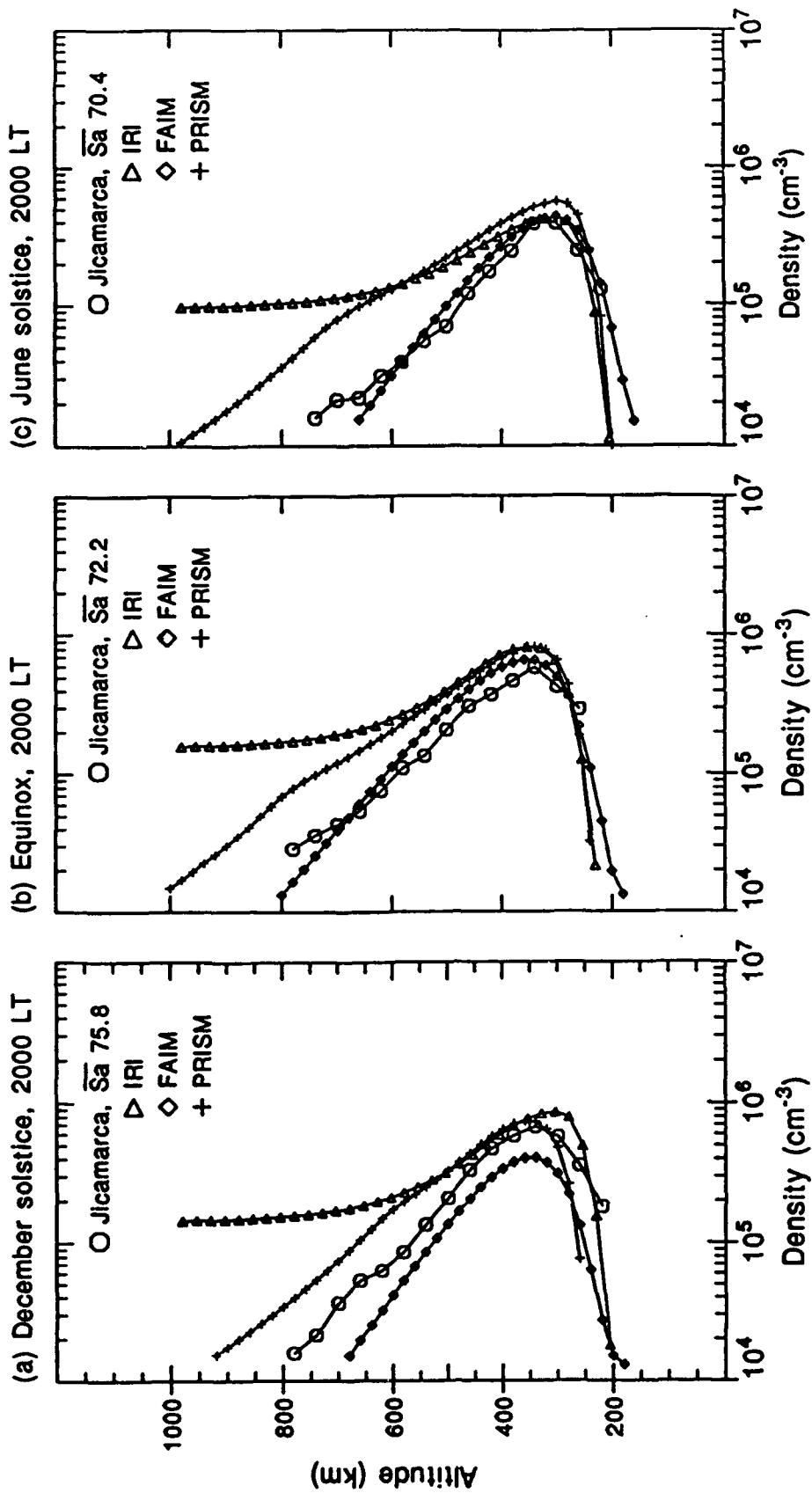
Fig. 47. Seasonal comparison of IRI, FAIM, and PRISM with the Jicamarca average profile for 2000 LT, quite-time solar minimum conditions. The average flux for the data is given in the upper right corner of each panel. The models were run with a flux of 70 units.

TABLE 8. Comparison of Jicamarca (JRO) NmF2 (cm^{-3}), hmF2 (km), and layer thickness (km) with IRI, FAIM, and PRISM calculations at 2000 LT, solar minimum conditions.

		Summer	Equinox	Winter
JRO	NmF2	$7.45x10^5$	$5.34x10^5$	$4.44x10^5$
	hmF2	354	362	303
	ΔH	239	217	195
IRI	NmF2	$8.67x10^5$	$8.30x10^5$	$4.24x10^5$
	hmF2	305	355	305
	ΔH	257	262	285
FAIM	NmF2	$4.06x10^5$	$6.68x10^5$	$4.29x10^5$
	hmF2	340	360	300
	ΔH	204	223	200
PRISM	NmF2	$7.46x10^5$	$8.25x10^5$	$5.56x10^5$
	hmF2	355	341	298
	ΔH	224	240	252

bottomside fit is good in winter, but the data layer is more steep in summer and equinox, a feature the IRI cannot match under these conditions. The topside fit to the data is good through 500 km in summer and winter, but the layer is substantially higher than the data in equinox. The IRI layer thickness is still greater than that of the experimental data, but there continues to be improvement in the model's handling of this parameter.

2. FAIM gives a good estimate of peak density for equinox and winter. The summer NmF2 is still almost half that of the data. The peak layer heights are in excellent agreement with the data for all seasons. The bottomside density gradient is well represented for all seasons. The gradient for summer is good, but the bottomside density is

again almost half that of the data. FAIM gives a good fit to the data topside for all seasons. The layer thickness calculations compare well with the experimental data in winter and equinox.

3. The PRISM peak density is in good agreement with the data for all seasons. The modeled layer heights are better for summer and winter, but within range of the data variability. The PRISM bottomside density gradients are more gradual than the data. The topside layer fit is good in summer, but only to around 500 km. The winter and equinoctial PRISM topsides are significantly more dense than the data topside layer. The higher bottomside in PRISM contributes to its lower estimate of layer thickness in summer and equinox.

The wider IRI layer is attributed to the asymptotic decrease of the topside layer above 600 km for all seasons at 2000 LT, which significantly impacts the TEC calculations. There is excellent agreement between the modeled hmF2's and the data hmF2's, which indicates a good representation of the solar minimum vertical drift which is the least complex drift of the solar cycle.

5.1.4. Midnight Solar Minimum Comparisons

At midnight the comparisons in Figure 48 are made only with December solstice and equinox because of the limited June solstice solar minimum data. The models give a better layer shape for equinox than for summer. The comparison is
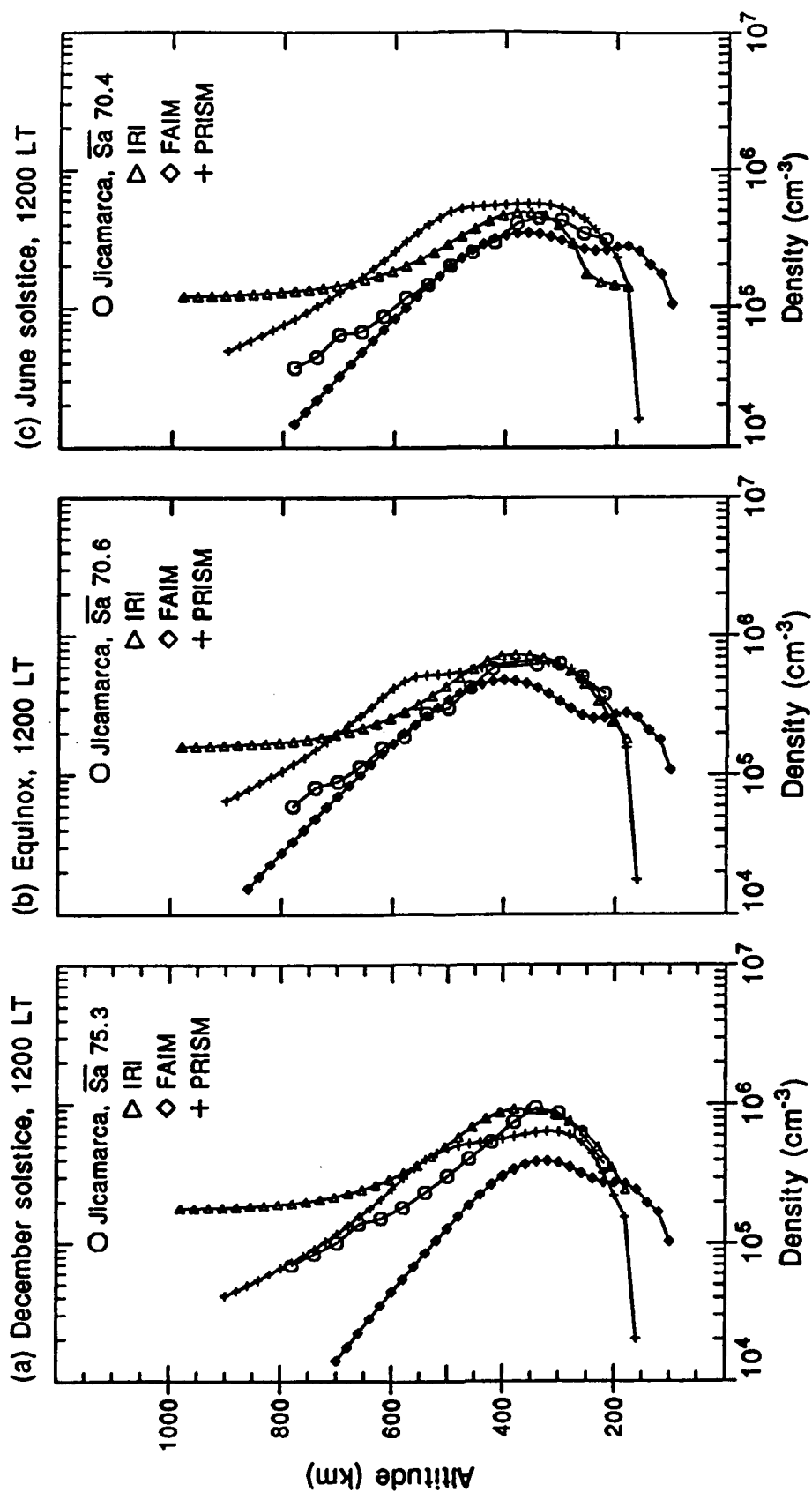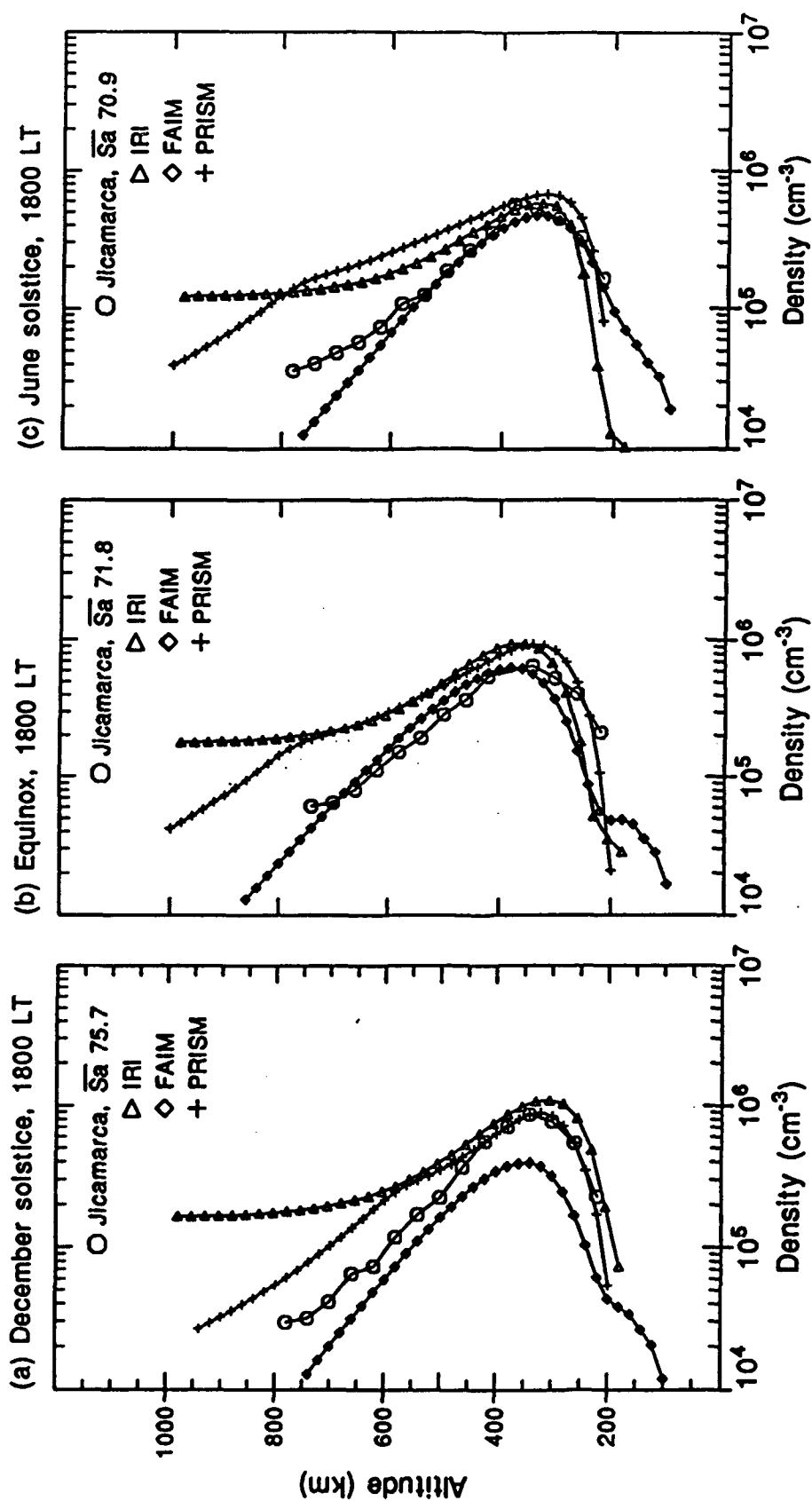
Fig. 48. Seasonal comparison of IRI, FAIM, and PRISM with the Jicamarca average profile for 0000 LT, quite-time solar minimum conditions. The average flux for the data is given in the upper right corner of each panel. The models were run with a flux of 70 units.

further limited by the small number of samples contributing to the averaged data profile and the wide variability of these samples as seen in Chapter III. Table 9 gives the respective seasonal peak densities, heights, and layer thickness. The peak density varies by about 1.4×10^5 cm^{-3} in summer and 1.9×10^5 cm^{-3} in equinox. The peak heights vary by 49 km in equinox and 69 km in winter. The results at midnight are:

1. The IRI fit to the peak density is better in summer than at equinox, but both peaks are within range of the data. The layer height is also within the broad variability of the data. The bottomside fit cannot be determined from the limited data. The topside fit is good to 500 km in summer and too dense above that and in equinox. The layer thickness comparable to the data layer in summer, but higher than the data in equinox.

2. FAIM overestimates the peak density for both seasons, but is within the variability of the data. The layer heights are underestimated by the model for both seasons. The topside fit is poor for both seasons. FAIM underestimates the topside in summer and overestimates it during equinox. The layer thickness does not compare well with the data.

3. The PRISM peak density compares well with the data for both seasons. The layer height is within the variability of the data, though the PRISM equinoctial peak height is the lowest of the three modeled hmF2's. The topside fit follows

TABLE 9. Comparison of Jicamarca (JRO) NmF2 (cm^{-3}), hmF2 (km), and layer thickness (km) with IRI, FAIM, and PRISM calculations at 0000 LT, solar minimum conditions.

		Summer	Equinox
JRO	NmF2	3.43×10^5	3.53×10^5
	hmF2	340	293
	ΔH	256	213
IRI	NmF2	2.65×10^5	5.84×10^5
	hmF2	305	280
	ΔH	265	263
FAIM	NmF2	3.57×10^5	5.02×10^5
	hmF2	280	280
	ΔH	168	197
PRISM	NmF2	3.55×10^5	4.57×10^5
	hmF2	312	260
	ΔH	193	224

that described for FAIM. The modeled layer thickness is less than the thickness for the experimental layer for both seasons.

The limited and varied data give a surprisingly good comparison of most parameters with the models at midnight.

5.1.5. Pre-sunrise Solar Minimum Comparisons

There was also not enough data available at 0400 LT for a June solstice comparison. The statistics at 0400 LT for the data are very weak and the resulting profiles are irregular, as illustrated in Figure 49. The comparisons are therefore less reliable. The standard deviation to the density is 2.3×10^4 and 5.2×10^4 cm^{-3} for summer and equinox, respectively. The variation in peak heights now (only 15 km) is less than that seen at midnight. Table 10 summarizes the
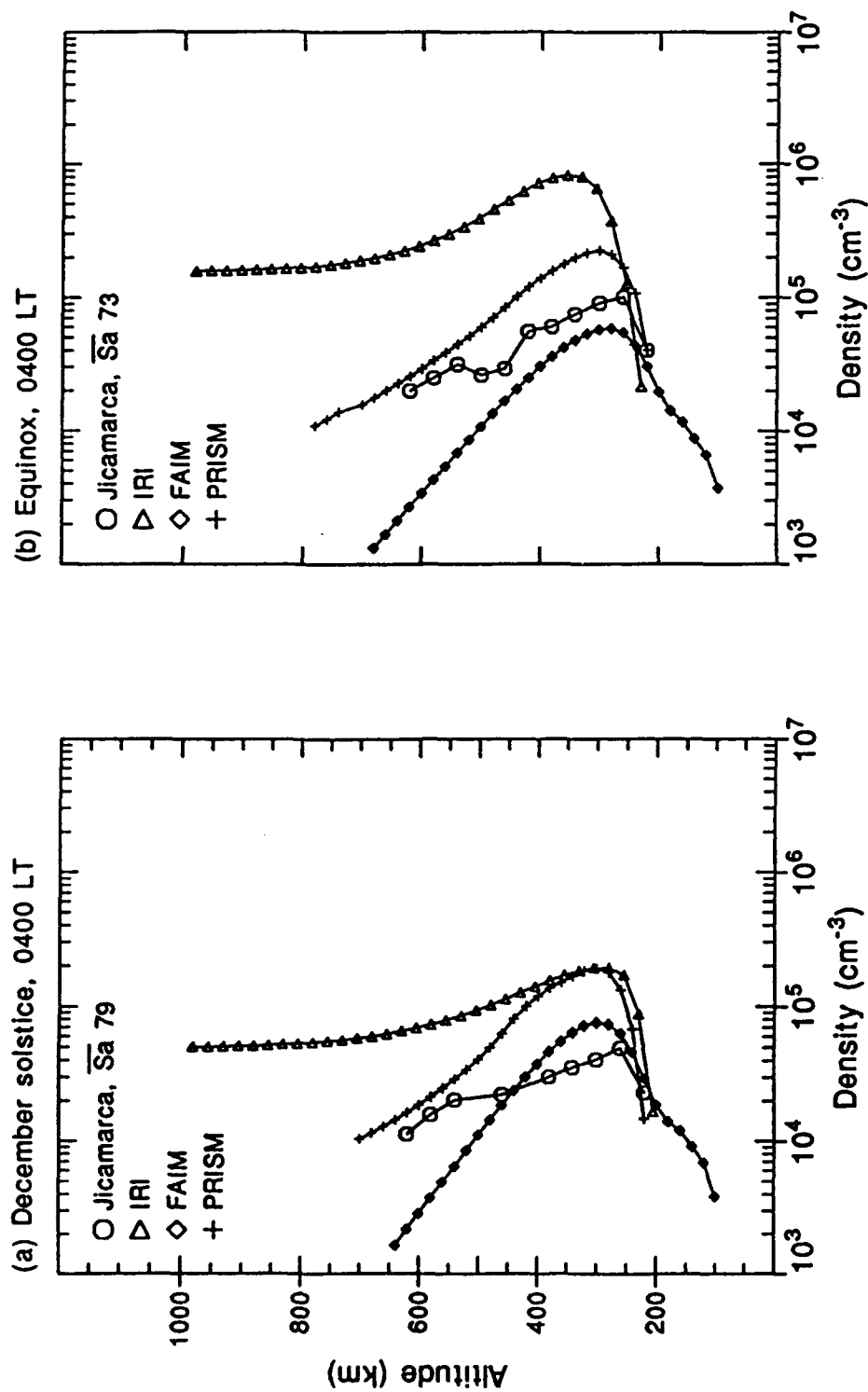
Fig. 49. Seasonal comparison of IRI, FAIM, and PRISM with the Jicamarca average profile for 0400 LT, quite-time solar minimum conditions. The average flux for the data is given in the upper right corner of each panel. The models were run with a flux of 70 units.

TABLE 10.   Comparison of Jicamarca (JRO) NmF2 (cm^{-3}), hmF2 (km), and layer thickness (km) with IRI, FAIM, and PRISM calculations at 0400 LT, solar minimum conditions.

		Summer	Equinox
JRO	NmF2	4.82x10^4	1.01x10^5
	hmF2	250	260
	ΔH	226	209
IRI	NmF2	1.93x10^5	8.30x10^5
	hmF2	380	280
	ΔH	265	263
FAIM	NmF2	1.52x10^5	1.87x10^5
	hmF2	280	300
	ΔH	177	187
PRISM	NmF2	3.06x10^5	3.81x10^5
	hmF2	300	330
	ΔH	224	244

results of the NmF2, hmF2, and layer thickness comparisons. At 0400 LT, the model and data comparisons are:

1.   The IRI gives the highest estimate of peak density for both seasons.   In summer the IRI peak is almost five times greater than the data peak.   The IRI hmF2 is over 100 km higher than the data in summer.   The IRI bottomside density gradient is more gradual than the data gradient.   The topside IRI layer is substantially more dense and higher than the data and the layer is wider than the data layer.

2.   The peak density predicted by FAIM comes the closest of the three models to the data for both seasons.   It is greater than the data in summer and less in winter.   The bottomside density gradients are comparable for both seasons. The bottomside layer fit is excellent in summer.   The topside

fit is poor for both seasons. The FAIM layer is not as broad as the Jicamarca layer.

3. The PRISM comparison is similar to the IRI comparison. The peak density and height are significantly higher than the data. The bottomside fit is poor in summer, slightly better in equinox. The topside layer is more dense than the data, though not as dense as the IRI layer. Of the three models, PRISM comes closest to matching the layer thickness of the data in summer.

During solar minimum FAIM provides better estimates to the peak density, peak height, and layer thickness of the data. FAIM does substantially better at depicting the bottomside and topside layers at each hour and for each season. Based on the numeric comparisons, FAIM gives better peak density estimates in equinox and winter, good peak height estimates in summer, and the better layer thickness estimates in equinox and winter. PRISM gives a better peak density estimate in summer. Of the models, it gives the better equinoctial peak height representation and the better summer layer thickness calculations. The IRI outperforms FAIM and PRISM in the winter layer height calculations. Generally, PRISM provides a good fit to the data afte⁻ sunset in summer, and in midday and early evening in equinox and winter. The IRI gives a good daytime peak density fit in summer and winter and an excellent peak height fit in winter. An improvement in the topside calculations of PRISM and IRI would substantially improve the calculation of layer

thickness and the placement of the topside layer. A summary of the model performances of peak density, peak height, and layer thickness over a solar cycle for each season will be discussed at the end of this chapter.

5.2. MODERATE SOLAR COMPARISONS

The statistics for moderate solar activity are the strongest of the three flux levels and with few exceptions the averaged profile is a combination of more than 15 daily profiles. However, this also means that there is a larger standard deviation to the peak densities and heights.

5.2.1. Midday Solar Moderate Comparisons

Figure 50 shows the comparison of the experimental and model data for noontime, moderate solar flux conditions. The standard deviation of the data NmF2 ranges from 1.9×10^5 (winter) to 4.2×10^5 (equinox) to 6.7×10^5 (summer) cm^{-3}. The solstitial hmF2's vary by 30 km, the equinoctial hmF2's vary by over 70 km. The layers are more dense, higher, and broader than the solar minimum profiles, corresponding to increased production from the higher solar activity, and the increase in layer thickness is reflected in the models. These parameters are compared numerically in Table 11. The results of the midday comparison of the models and data are:

1. There is good agreement between the IRI and data peak densities for all seasons. The layer heights are well represented for summer and equinox, the winter IRI layer is

(a) December solstice, 1200 LT

(b) Equinox, 1200 LT
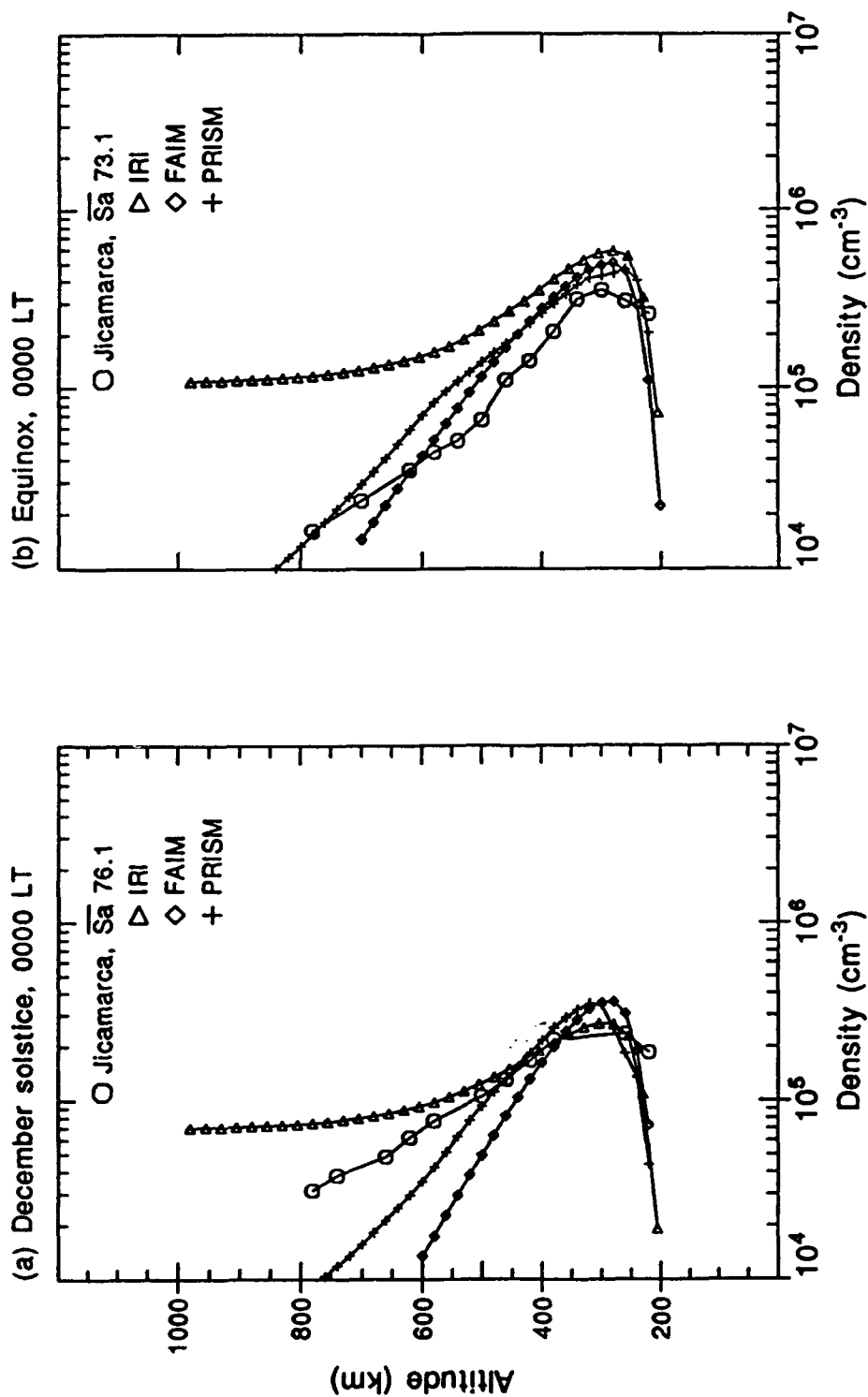
(c) June solstice, 1200 LT
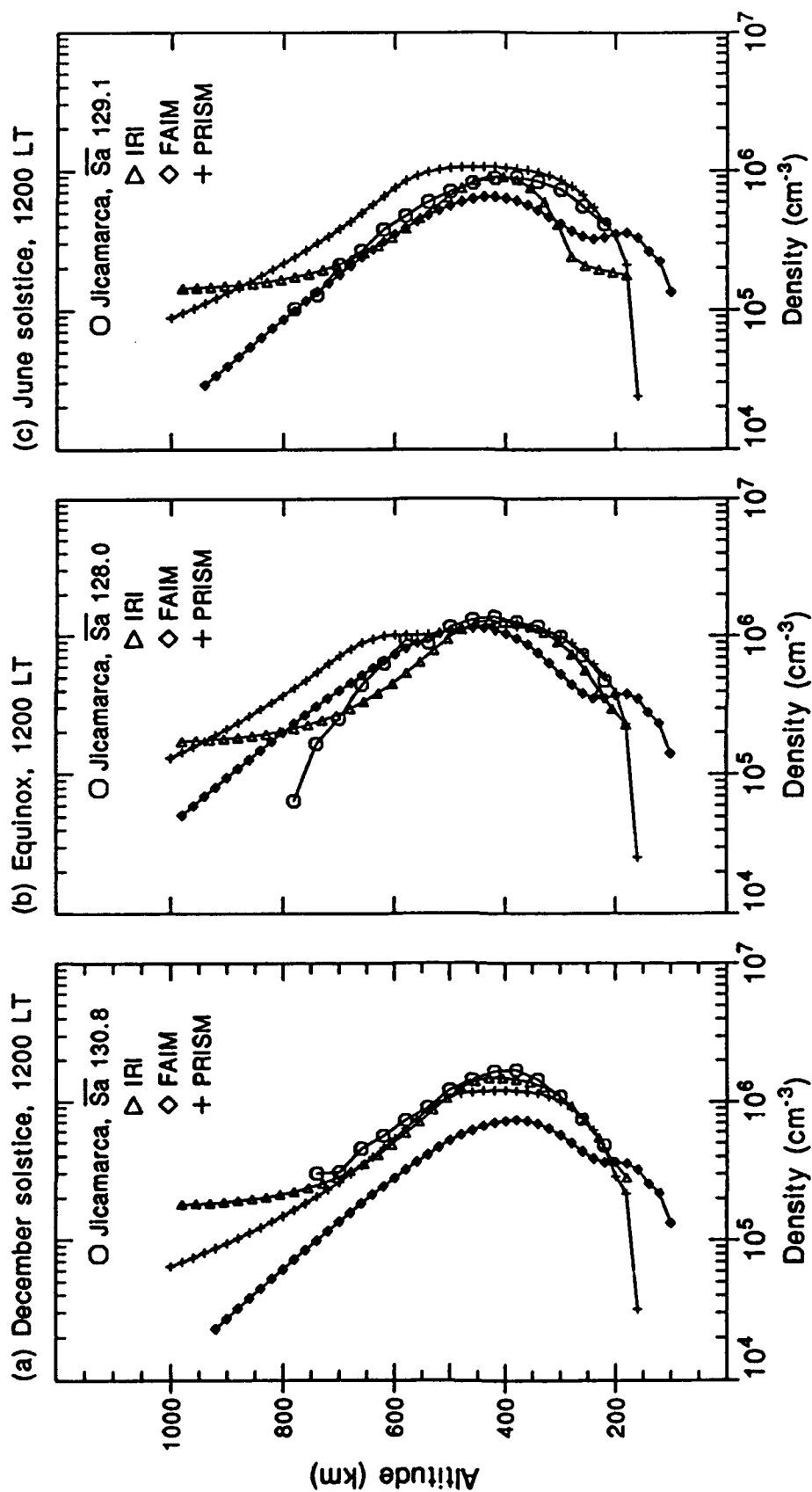
Fig. 50. Seasonal comparison of IRI, FAIM, and PRISM with the Jicamarca average profile for 1200 LT, quite-time moderate solar conditions. The average flux for the data is given in the upper right corner of each panel. The models were run with a flux of 130 units.

TABLE 11. Comparison of Jicamarca (JRO) NmF2 (cm^{-3}), hmF2 (km), and layer thickness (km) with IRI, FAIM, and PRISM calculations at 1200 LT, moderate solar conditions.

		Summer	Equinox	Winter
JRO	NmF2	$1.65x10^6$	$1.34x10^6$	$9.07x10^5$
	hmF2	406	425	392
	ΔH	319	360	351
IRI	NmF2	$1.49x10^6$	$1.28x10^6$	$8.96x10^5$
	hmF2	405	430	430
	ΔH	297	312	289
FAIM	NmF2	$6.73x10^5$	$1.14x10^6$	$6.46x10^5$
	hmF2	380	460	420
	ΔH	316	348	351
PRISM	NmF2	$1.21x10^6$	$1.16x10^6$	$1.06x10^6$
	hmF2	419	394	456
	ΔH	340	448	404

more than 30 km higher than the data. *The bottomside fit is excellent in summer and equinox.* The winter bottomside is more than 50 km higher than the data and the IRI density gradient is not as steep as the data density gradient. The modeled topside fit is better in summer, and it fits the data well to 700 km in winter, and to 600 km in equinox. The layer thickness is less than that of the data for all seasons.

2. The FAIM peak density fit is closest to the data at equinox. Both solstices are underestimated; the summer NmF2 is less than half that of the data. The bottomside gradients compare well with the data for all seasons, but the bottomside densities are significantly less than the data. The FAIM topside fit is excellent for equinox and winter and

within range of the summer topside variability. FAIM is in good agreement with the data for layer thickness and gives an outstanding fit in winter, as shown in Table 11.

3. The PRISM calculations for NmF2 are good for all seasons. The peak height compares well in summer, but the winter hmF2 is more than 50 km higher. The wide variability of the layer heights at equinox enables the model to come within a standard deviation of the data. The PRISM bottomsides give the better fit to the data for all seasons. There is marked improvement in the summer and equinoctial PRISM topsides. The winter topside remains too dense. The layer thickness calculated by PRISM is higher than the data thickness for all seasons. The large difference at equinox (88 km) is a reflection of the secondary peak in the PRISM topside.

At noon the peak height and density appear to be well represented by the models, the FAIM profile in summer being the exception. There is also an improvement in the topside representation of IRI and PRISM. The PRISM profiles at noon retain the secondary peak at 600 km in equinox and winter. The IRI is not able to reproduce the data layer thickness at noon under higher flux conditions. The equinoctial IRI layer shows a topside bow around 600 km and the June solstice bottomside is significantly less dense. Both features contribute to the poorer layer thickness calculations. There is improvement in the PRISM layer shapes and the elimination of the secondary peak in the topside of the equinox and

winter PRISM layers would improve these layer shapes even more. FAIM continues to give a marginal performance for December solstice.

5.2.2. Evening Solar Moderate Comparisons

The 1700 LT and 1800 LT comparisons of the experimental data with the models are quite similar. The 1800 LT comparison is presented in Figure 51. There is large variability in the data, the standard deviations to the peak density being 2.2×10^5 cm^{-3}, 4.4×10^5 cm^{-3}, and 4.7×10^5 cm^{-3} for winter, summer, and equinox, respectively. The peak heights show the least variability in winter (30 km) and are similar for summer and equinox (51 and 59 km). The comparisons between NmF2, hmF2, and ΔH at 1700 LT and 1800 LT are given in Table 12 and 13, respectively. The results of the comparisons are:

1. The IRI fit to peak density is good for all seasons. The peak layer height calculation is closer to the data peak during equinox at 1800 LT. The model comes within the range of the wide variability of the data hmF2 for all seasons. The bottomside fit is good during summer. The winter and equinoctial layers are too high and the density gradients are too gradual. The IRI topside layers are less dense than the data for all seasons. The topside layer fits the data better in winter. The summer and equinoctial topsides are especially poor above 400 km. The thickness of the IRI layer is over 60 km narrower than the data layer.

Fig. 51. Seasonal comparison of IRI, FAIM, and PRISM with the Jicamarca average profile for 1800 LT, quite-time moderate solar conditions. The average flux for the data is given in the upper right corner of each panel. The models were run with a flux of 130 units.

TABLE 12. Comparison of Jicamarca (JRO) NmF2 (cm^{-3}), hmF2 (km), and layer thickness (km), with IRI, FAIM, and PRISM calculations for 1700 LT, moderate solar conditions.

		Summer	Equinox	Winter
JRO	NmF2	1.73×10^6	1.50×10^6	8.60×10^5
	hmF2	410	435	394
	ΔH	287	360	351
IRI	NmF2	1.51×10^6	1.37×10^6	8.96×10^5
	hmF2	380	405	430
	ΔH	259	259	262
FAIM	NmF2	8.45×10^5	1.25×10^6	7.84×10^5
	hmF2	380	440	400
	ΔH	280	318	296
PRISM	NmF2	1.32×10^6	1.48×10^6	1.10×10^6
	hmF2	397	398	389
	ΔH	345	367	393

TABLE 13. Comparison of Jicamarca (JRO) NmF2 (cm^{-3}), hmF2 (km), and layer thickness (km) with IRI, FAIM, and PRISM calculations for 1800 LT, moderate solar conditions.

		Summer	Equinox	Winter
JRO	NmF2	1.67×10^6	1.45×10^6	8.18×10^5
	hmF2	429	456	404
	ΔH	331	347	329
IRI	NmF2	1.42×10^6	1.28×10^6	8.65×10^5
	hmF2	380	430	380
	ΔH	254	255	257
FAIM	NmF2	8.53×10^5	1.18×10^6	7.87×10^5
	hmF2	420	460	400
	ΔH	269	292	276
PRISM	NmF2	1.28×10^6	1.46×10^6	1.10×10^6
	hmF2	409	415	396
	ΔH	353	350	360

2. There is little difference between the FAIM comparisons at 1700 LT and 1800 LT. The peak density fit to

the data is good in winter and equinox. The summer density is less than half that of the data. The peak layer heights are comparable to the data layer heights for all seasons. The bottomside density gradient is comparable in summer, but all FAIM bottomside layers are over 50 km higher than those of the data. The topside layers obtained from the FAIM calculations fit the data well for equinox and winter. The FAIM layers are narrower than the data layers for all seasons. The model gives a better fit to the data ΔH at 1700 LT, summer.

3. The PRISM fit to peak density is outstanding during equinox at 1800 LT. The solstices are well within the variability of the data NmF2's. The solstitial layers show better agreement than the equinoctial layer to the data peak height. The PRISM bottomside fit is closer to the data in summer than the other models. The bottomside densities are comparable in winter and equinox, but the data bottomside density gradient is steeper than the modeled gradients. There is excellent agreement between the PRISM topside layers and the data in summer and equinox. The winter layer continues to be more dense than the data. The layer thickness is in good agreement with the data in summer and equinox.

Here is more evidence that the IRI is not able to depict the increasing broadness of the Jicamarca layer under higher flux conditions. The problem rests in the bottomside calculations in winter and equinox as well as the topside

bow, seen in Figure 51. In the IRI calculations it is also clear that the layers do not move substantially higher in altitude and never broaden under the influence of the upward motion to a region of increased transport. The vertical drift in FAIM raises the layer an adequate amount, but it also raises the bottomside layer, reducing that density and subsequently the TEC of the layer. The well-defined secondary peak in the winter and equinoctial profiles of PRISM contributes to the model's poor layer thickness agreement with the data, but this is not as dramatic as it was for solar minimum conditions. The PRISM profiles have improved in their topside representation of the summer and equinox layers, but remain too broad in winter.

5.2.3. Post-sunset Moderate Solar Comparisons

Figure 52 illustrates the models' ability to depict the post-sunset ionosphere at Jicamarca under moderate solar conditions. The peak density is the least variable in winter (σ = 1.4×10^5 cm^{-3}) and the most variable in summer (σ = 4.0×10^5 cm^{-3}). The standard deviation to the equinoctial data is 3.0×10^5 cm^{-3}. The peak height of the data varies from 52 km in winter to 59 km at equinox to 80 km in summer. The peak densities, heights, and layer thickness are given in Table 14. The main results of these comparisons are:

1. The IRI calculations give a good fit to the peak density of the data. The peak heights from IRI are as much as 122 km lower than the data in summer. The IRI is not able
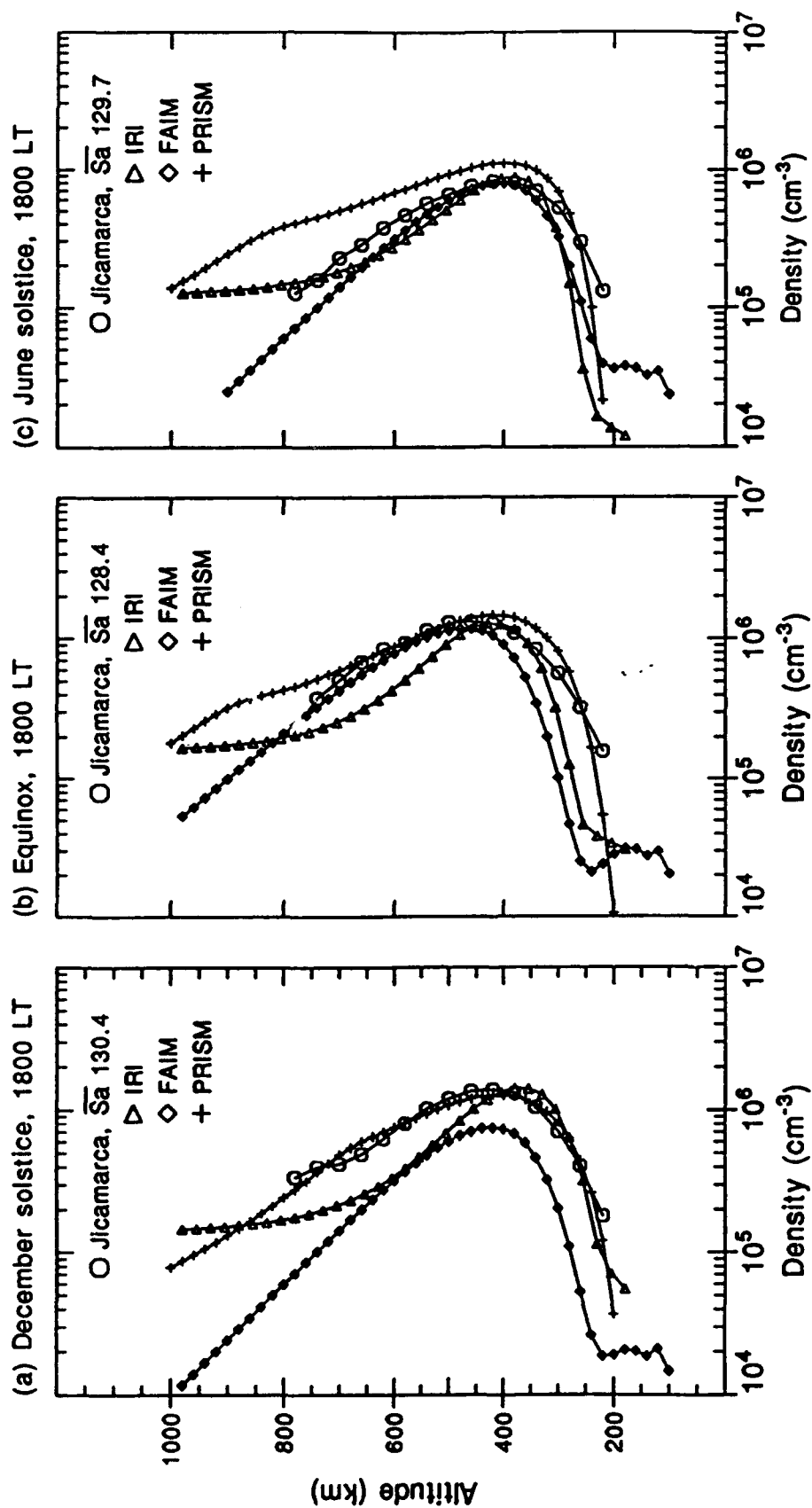
Fig. 52. Seasonal comparison of IRI, FAIM, and PRISM with the Jicamarca average profile for 2000 LT, quite-time moderate solar conditions. The average flux for the data is given in the upper right corner of each panel. The models were run with a flux of 130 units.

TABLE 14. Comparison of Jicamarca (JRO) NmF2 (cm^{-3}), hmF2 (km), and layer thickness (km) with IRI, FAIM, and PRISM calculations for 2000 LT, moderate solar conditions.

		Summer	Equinox	Winter
JRO	NmF2	1.26×10^6	1.00×10^6	6.75×10^5
	hmF2	502	490	410
	ΔH	326	363	297
IRI	NmF2	1.14×10^6	1.13×10^6	7.07×10^5
	hmF2	380	405	355
	ΔH	241	249	259
FAIM	NmF2	7.57×10^5	1.03×10^6	7.85×10^5
	hmF2	440	480	380
	ΔH	247	259	250
PRISM	NmF2	8.97×10^5	1.12×10^6	9.47×10^5
	hmF2	517	481	378
	ΔH	285	292	303

to accurately represent the bottomside profile. The topside fit of the IRI to the data is good in winter. The layer thickness is less than the data layer thickness for all seasons.

2. The FAIM profiles show good agreement with the peak density of the data for all seasons. The modeled peak layer heights are better at equinox. The bottomside density gradient in FAIM gives a good representation of the summer bottomside layer. FAIM is in good agreement with the winter and equinoctial topside layers. The modeled layer thickness is less than the data thickness for all seasons.

3. The PRISM fit to the peak density is good for all seasons, even with the trend towards overestimating the winter peak density. The peak layer height is in good

agreement with the data in summer and equinox. PRISM is the only model to reproduce the high layer height in summer for this time period. The bottomside agreement is poor for all seasons. The topside agreement is excellent for summer and equinox. The winter topside of PRISM continues to be more dense than the data. The PRISM winter ΔH has a good fit to the data layer, but summer and equinox are too low.

The comparisons between the models and the data at 2000 LT illustrate the effectiveness of the electric field used within each model. There is an increase in layer height in summer and equinox that is well represented by the increased layers of PRISM and FAIM, especially PRISM in summer. An improvement in the vertical drift calculations in the models for this time period would substantially improve the model agreement with the data. PRISM gives the better estimate of layer thickness, IRI gives the better estimate of NmF2, and there is no significant trend for peak height.

5.2.4. Midnight Solar Moderate Comparisons

At 0000 LT the ionosphere has moved back into the lower region of the ionosphere where recombination with neutral molecules depletes the plasma density. The model agreements with the data are illustrated in Figure 53. The peak density typically varies by 1.4×10^5 cm^{-3} for each season. The peak height varies by 65, 53, and 44 km for summer, equinox, and winter, respectively. Table 15 illustrates the model-data

Fig. 53. Seasonal comparison of IRI, FAIM, and PRISM with the Jicamarca average profile for 0000 LT, quite-time moderate solar conditions. The average flux for the data is given in the upper right corner of each panel. The models were run with a flux of 130 units.

TABLE 15. Comparison of Jicamarca (JRO) NmF2 (cm^{-3}), hmF2 (km), and layer thickness (km) with IRI, FAIM, and PRISM calculations for 0000 LT, moderate solar conditions.

		Summer	Equinox	Winter
JRO	NmF2	$4.18x10^5$	$8.71x10^5$	$5.27x10^5$
	hmF2	435	338	311
	ΔH	311	255	245
IRI	NmF2	$5.67x10^5$	$9.43x10^5$	$4.95x10^5$
	hmF2	330	305	305
	ΔH	269	228	255
FAIM	NmF2	$7.84x10^5$	$1.02x10^6$	$4.95x10^5$
	hmF2	340	320	300
	ΔH	245	246	229
PRISM	NmF2	$4.98x10^5$	$7.04x10^5$	$4.59x10^5$
	hmF2	389	275	290
	ΔH	282	274	232

comparisons of NmF2, hmF2, and layer thickness. The main results are:

1. The IRI is in excellent agreement with the data for peak density and peak height for all seasons, with the exception of the summer hmF2. The bottomside fit to the data is good for all seasons. The topside fit shows marked improvement for all seasons. The IRI layer thickness calculation is better in winter, than in equinox or summer.

2. In contrast to the previous comparisons, FAIM overestimates the peak density of the summer layer at 0000 LT for moderate solar conditions. The fits at equinox and June solstice are good. FAIM has no trouble with the bottomside or the topside fit to the data. The FAIM layer thickness is better at equinox.

3. PRISM gives a good fit to the peak density of the data for all seasons. The peak heights from PRISM are lower than the data peak heights for all seasons, but within the variability of the data for the solstices. The bottomside agreement is good for equinox and winter. PRISM has the worst bottomside agreement of the models in summer, but it is not out of range of the data. The PRISM topside agreement is good for all seasons. The model compares well with the data in equinox and winter for layer thickness.

The midnight model-data comparisons are some of the best seen yet. There is almost no difference between the calculated profiles and the data below 500 km in winter. The differences in NmF2 and hmF2 are well within the variability of the data.

5.2.5. Pre-sunrise Solar Moderate Comparisons

The statistics are not as good at 0400 LT as at other local times, so the model comparisons are not as reliable. The models do well in representing the lower layer height at this hour. The layer agreement between the parameters in summer and equinox is better than in winter, as shown in Figure 54. The standard deviation of the peak density is less than 1.0×10^5 cm^{-3} for each season. The peak layer heights vary by as much as 35 km for each season. The comparison of peak density, peak height, and layer thickness is shown in Table 16. The results of the pre-sunrise comparison are:
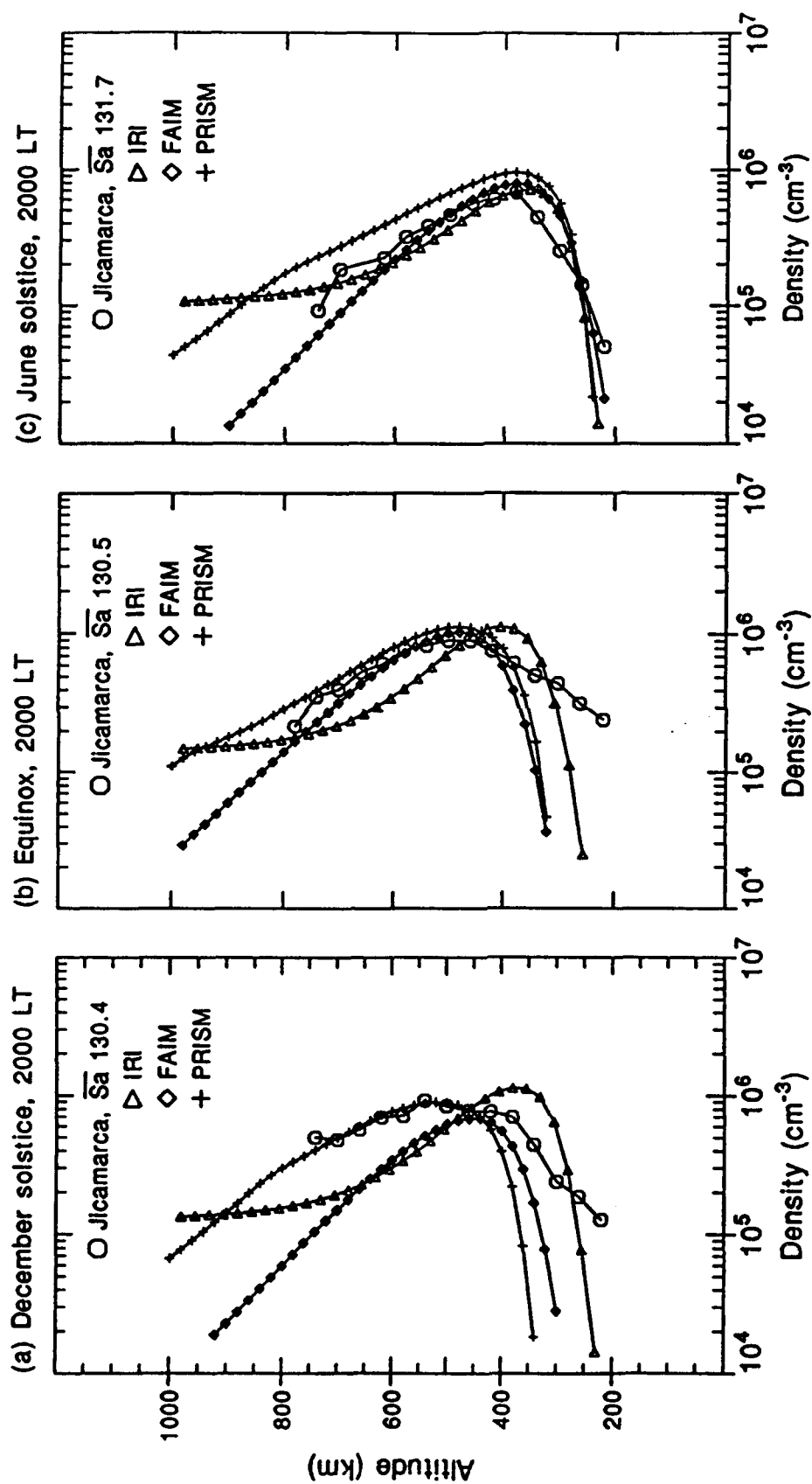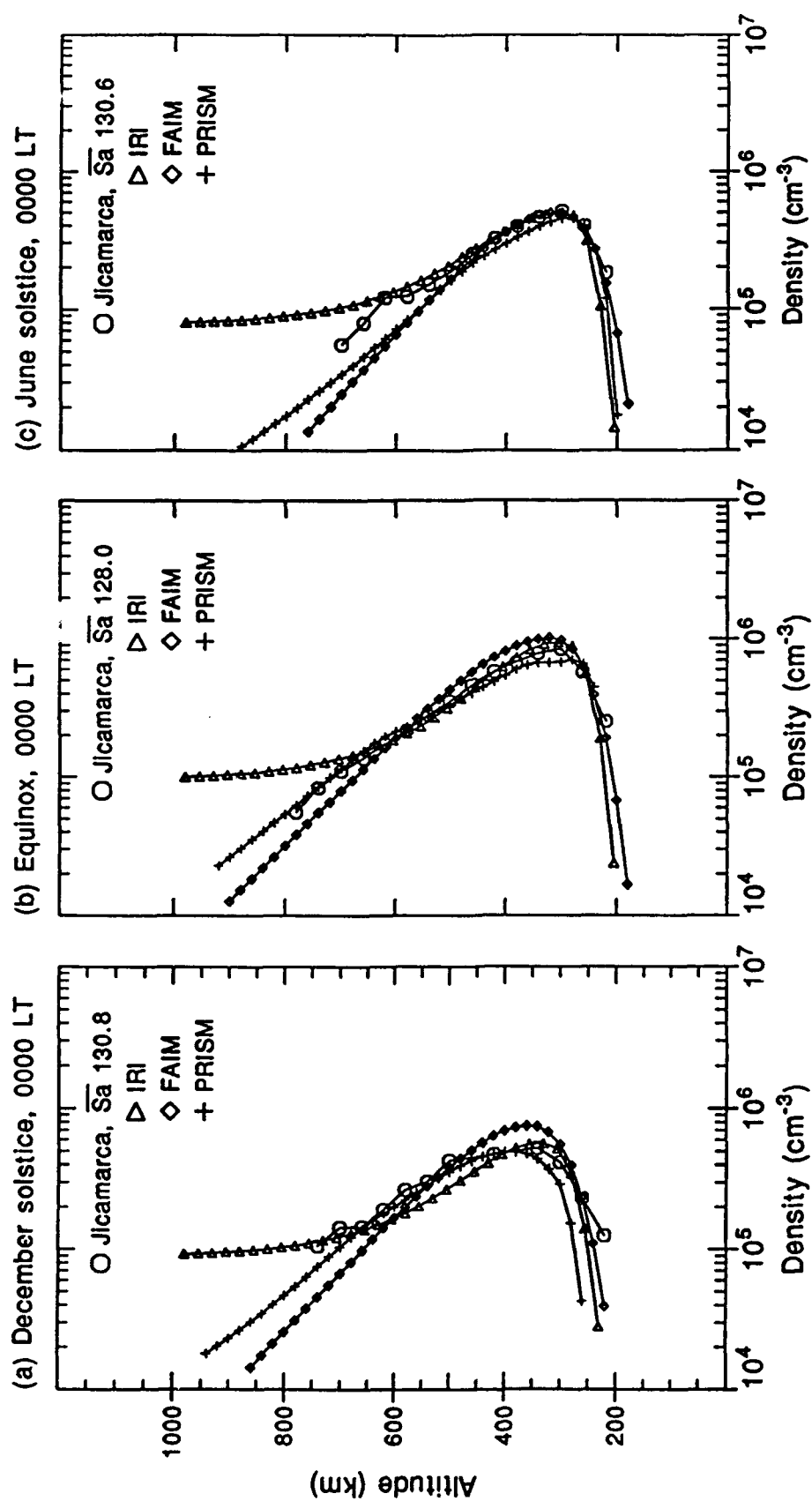
Fig. 54. Seasonal comparison of IRI, FAIM, and PRISM with the Jicamarca average profile for 0400 LT, quiet-time moderate solar conditions. The average flux for the data is given in the upper right corner of each panel. The models were run with a flux of 130 units.

TABLE 16. Comparison of Jicamarca (JRO) NmF2 (cm^{-3}), hmF2 (km), and layer thickness (km) with IRI, FAIM, and PRISM calculations for 0400 LT, moderate solar conditions.

		Summer	Equinox	Winter
JRO	NmF2	$3.18x10^5$	$2.73x10^5$	$2.75x10^5$
	hmF2	293	304	321
	ΔH	190	275	219
IRI	NmF2	$2.74x10^5$	$2.29x10^5$	$2.12x10^5$
	hmF2	280	305	305
	ΔH	271	286	246
FAIM	NmF2	$1.65x10^5$	$2.26x10^5$	$1.25x10^5$
	hmF2	300	320	320
	ΔH	208	222	206
PRISM	NmF2	$1.92x10^5$	$2.25x10^5$	$1.49x10^5$
	hmF2	300	302	293
	ΔH	230	258	220

1. The IRI fit to the data peak density and height is good for all seasons. The bottomside layer fit is comparable to the data layer in summer and equinox. The topside fit is better at equinox. The modeled layer thickness is greater than the data layer thickness for all seasons.

2. FAIM underestimates the peak density for all seasons, providing an especially poor comparison in winter. The peak layer height is comparable for all seasons. The modeled bottomside fit is good in equinox and summer. The FAIM bottomside density gradient is comparable to the data for all seasons. The layer thickness calculated from the FAIM profile is good during solstices, but over 50 km lower than the data at equinox.

3.   The PRISM fit to peak density is better at equinox than at the solstices. The layer heights fit the data well in summer and equinox. The bottomside fit of PRISM to the data is good in summer and equinox. The PRISM topsides are less dense than the data topsides for all seasons. PRISM gives the better winter representation of layer thickness.

The models give a better fit to the data during equinox at 0400 LT. Generally there is little difference in the peak density calculations, but the winter densities are vastly different for each model. We suggest that more data are needed to make a better comparison with the models.

Under moderate solar conditions the IRI gives the better estimates of peak density for all seasons. FAIM gives the better peak heights for winter and equinox, PRISM for summer. PRISM gives good layer thickness calculations in winter and equinox, while FAIM has a better summer representation of this parameter. PRISM is consistently second in the peak density and peak height representations.   Of the three modeled profiles for each season and hour, PRISM gives the most realistic shape and layer placement.

5.3. SOLAR MAXIMUM COMPARISONS

The models were run with a flux of 210 at solar maximum because we have solar maximum PRISM results only for this flux level. This flux was initialized to 185 in the running program for FAIM. In all instances the flux averages of the data are substantially lower than 210 units.

5.3.1. Midday Solar Maximum Comparisons

At noon the models and data all show a broad, high, dense layer consistent with the increase in NmF2, hmF2, and layer thickness associated with an increase in solar activity and its effects on the dynamics that determine these parameters, as seen in Figure 55. The peak density variation is approximately 9.0×10^4 cm^{-3} in winter, 5.0×10^5 cm^{-3} in summer, and 6.0×10^5 cm^{-3} at equinox. The data peak height varies by 25, 26, and 41 km for June solstice, equinox, and December solstice, respectively. The peak densities, peak heights, and layer thickness of the data and the models are summarized in Table 17. The main results of the model performances at midday are:

1. The IRI gives a good fit to the data for peak density and height at 1200 LT. The bottomside fit for IRI is good in summer and equinox. The winter bottomside IRI layer is over 100 km higher than the data layer. The topside fit to the data is comparable for all seasons. The modeled layer thickness compares well with the data for summer and equinox.

2. The FAIM fit to peak density is better in equinox and winter than summer. The solstitial layers are more representative of the peak height. The equinoctial layer is too high. The bottomside fit is good during equinox. The topside of the FAIM layer compares well with the data for all seasons. The layer thickness calculated by the model gives a good fit to the data for all seasons.
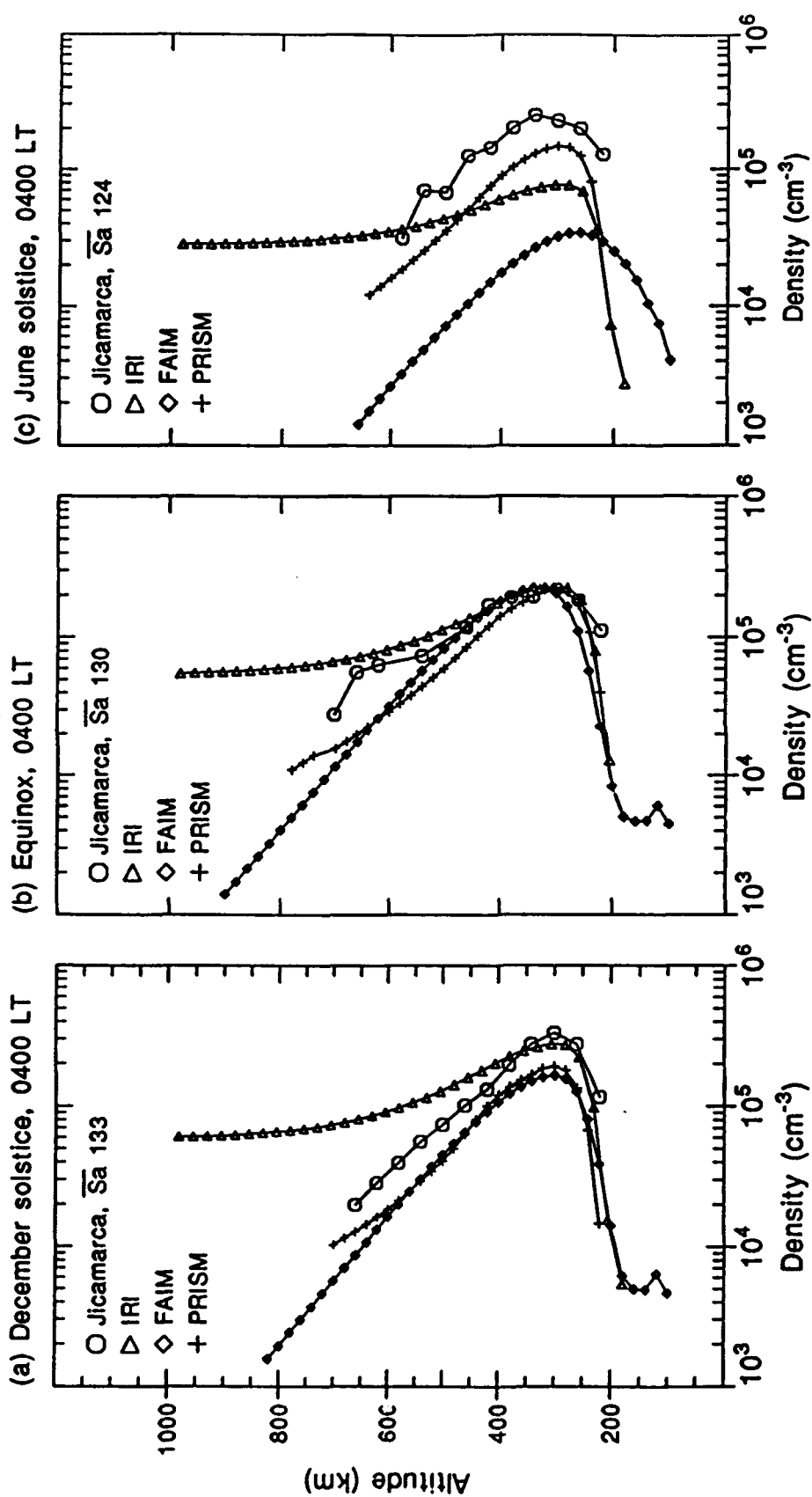
Fig. 55. Seasonal comparison of IRI, FAIM, and PRISM with the Jicamarca average profile for 1200 LT, quite-time solar maximum conditions. The average flux for the data is given in the upper right corner of each panel. The models were run with a flux of 210 units.

TABLE 17. Comparison of Jicamarca (JRO) NmF2 (cm^{-3}), hmF2 (km), and layer thickness (km) with IRI, FAIM, and PRISM calculations at 1200 LT, solar maximum conditions.

		Summer	Equinox	Winter
JRO	NmF2	$1.98x10^6$	$2.21x10^6$	$1.04x10^6$
	hmF2	452	445	442
	ΔH	312	303	398
IRI	NmF2	$2.12x10^6$	$1.91x10^6$	$1.39x10^6$
	hmF2	480	480	480
	ΔH	322	293	286
FAIM	NmF2	$1.11x10^6$	$1.88x10^6$	$9.96x10^5$
	hmF2	420	540	460
	ΔH	343	318	373
PRISM	NmF2	$2.07x10^6$	$2.36x10^6$	$1.06x10^6$
	hmF2	485	547	456
	ΔH	390	359	397

3. The peak densities calculated by PRISM give an excellent fit to the data for all seasons. The peak height comparisons are similar to those for FAIM. The bottomside density gradient of the data is steeper than that from PRISM; the bottomside densities are comparable for all seasons. The topside layer fit is better in summer. The winter topside from PRISM is denser than the data topside. PRISM overestimates the layer thickness for all seasons.

The three models give a good representation of the broadening of the midday layer under higher flux conditions. They also perform well with the peak density and height calculations. The IRI shows a now-familiar exceptional narrowness in winter, the result of the higher bottomside layer. The PRISM layers continue to depict a secondary peak

around 600 km and hence a higher topside density than the data. There is little change in the FAIM comparisons from previous solar cycle comparisons for this hour.

5.3.2. Evening Solar Maximum Comparisons

The model fits at 1800 LT are similar to the comparisons at 1700 LT. Each model is successful in raising the plasma layer in agreement with the evening prereversal enhancement. Figure 56 shows this comparison. The standard deviation to the peak density is 1.7×10^5 cm^{-3} for June solstice, 3.0×10^5 cm^{-3} for equinox, and 5.6×10^5 cm^{-3} for December solstice. The peak heights have standard deviations of 40 km, 50 km, and 60 km for June solstice, equinox, and December solstice. NmF2, hmF2, and ΔH are compared for 1700 LT in Table 18 and 1800 LT in Table 19. The main results at 1800 LT are:

1. There is good agreement between the peak density predicted by the IRI and the data peak density. The IRI peak layer heights are less than those of the data for summer and equinox, at 1800 LT. The peak height is well represented for summer and equinox at 1700 LT. The IRI bottomside is placed higher than the Jicamarca bottomside for all seasons. The topside fit is comparable to the data during solstices, and is less dense than the data during equinox. The width of the IRI layers is less than that of the data for all seasons.

2. FAIM continues to underestimate the summer peak density, but the peak height calculation is good in summer. The FAIM fits to NmF2 in winter and in equinox are good. The
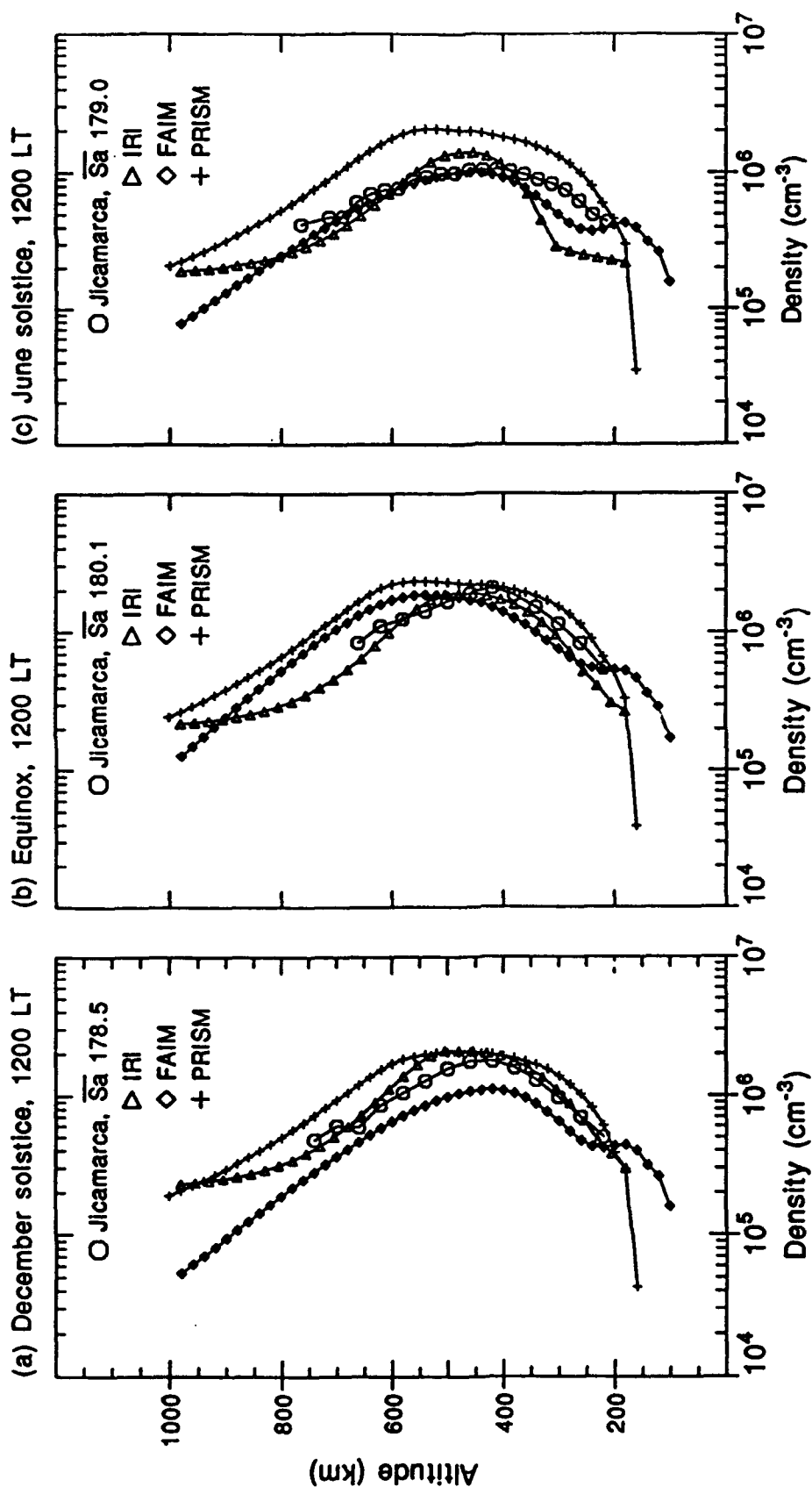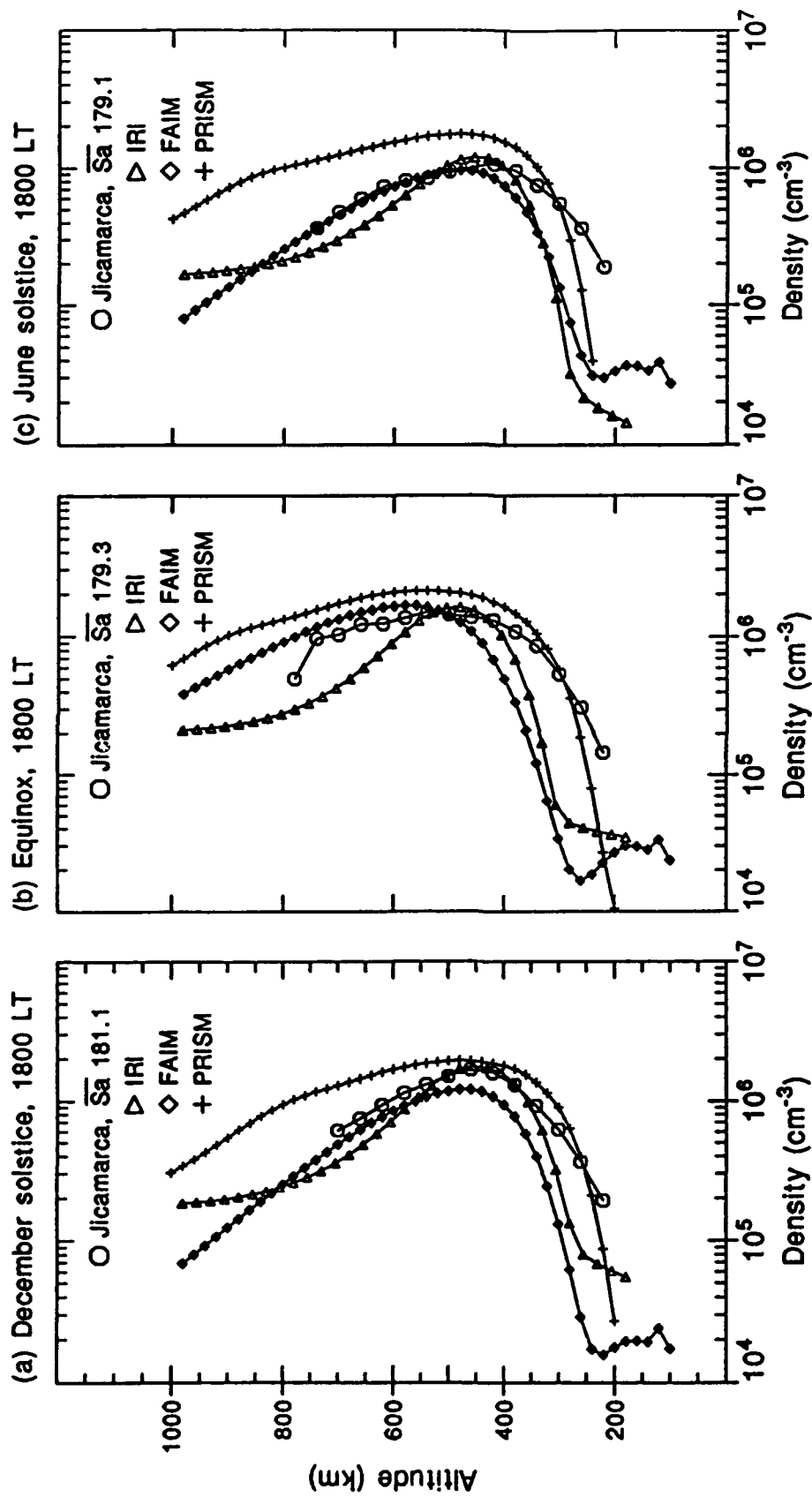
Fig. 56. Seasonal comparison of IRI, FAIM, and PRISM with the Jicamarca average profile for 1800 LT, quite-time solar maximum conditions. The average flux for the data is given in the upper right corner of each panel. The models were run with a flux of 210 units.

TABLE 18.   Comparison of Jicamarca (JRO) NmF2 (cm^{-3}), hmF2 (km) and layer thickness (km) with IRI, FAIM, and PRISM calculations at 1700 LT, solar maximum conditions.

		Summer	Equinox	Winter
JRO	NmF2	1.86×10^6	1.82×10^6	1.13×10^6
	hmF2	462	485	408
	ΔH	328	367	375
IRI	NmF2	1.89×10^6	1.76×10^6	1.27×10^6
	hmF2	455	480	455
	ΔH	268	259	261
FAIM	NmF2	1.20×10^6	1.84×10^6	9.93×10^5
	hmF2	420	500	480
	ΔH	316	365	351
PRISM	NmF2	1.97×10^6	2.28×10^6	1.79×10^6
	hmF2	486	505	471
	ΔH	398	420	429

TABLE 19.   Comparison of Jicamarca (JRO) NmF2 (cm^{-3}), hmF2 (km), and layer thickness (km) with IRI, FAIM, and PRISM calculations at 1800 LT, solar maximum conditions.

		Summer	Equinox	Winter
JRO	NmF2	1.90×10^6	1.59×10^6	1.14×10^6
	hmF2	484	517	425
	ΔH	321	378	345
IRI	NmF2	1.77×10^6	1.62×10^6	1.19×10^6
	hmF2	455	480	455
	ΔH	255	254	259
FAIM	NmF2	1.21×10^6	1.66×10^6	9.61×10^5
	hmF2	460	560	480
	ΔH	293	315	322
PRISM	NmF2	1.94×10^6	2.12×10^6	1.76×10^6
	hmF2	477	543	484
	ΔH	384	399	430

winter and equinoctial hmF2's are higher than the data.   The

FAIM bottomside layer is also higher than the data bottomside

layer for all seasons. The topside fit to the data is excellent for all seasons. The FAIM calculations give a good estimate of the layer thickness for all seasons at 1700 LT. The widths of the FAIM layers are an improvement over the IRI, but they remain less than the data.

3. The peak density fit of PRISM to the data is good in summer. The equinoctial and winter NmF2's are larger than the data peak densities, but the modeled layers are within the variability of the equinoctial and winter data. The peak layer height is also better for December solstice than June solstice or equinox. The bottomside fit to the data is good in summer and equinox. The topside at equinox for PRISM fits the data the well at 1800 LT. The summer PRISM topside layer is within the variability of the data, but the winter layer is too dense. The PRISM layers are all broader than the data layers.

The models continue to have difficulty in depicting the steep bottomside gradients in the Jicamarca profiles. The IRI layers do not exhibit a significant broadening with flux and the seasonal peak height variation is not comparable with that of the data layers. The FAIM layers are consistent in their representation of the data. The PRISM layers are much broader than the data layers under these conditions. The secondary peak has moved to higher altitudes, approximately 800 km, providing less influence on the topside density than seen at earlier hours. The peak density comparisons indicate that if the Jicamarca data were at a higher flux and

subsequently had higher densities, neither FAIM or IRI could reproduce the density profiles. The bow in the IRI topside and the high bottomside contributes to the model's poor representation of the layer. The vertical drift in FAIM did an impressive job of raising the equinoctial layer, but unfortunately it did not quite match the drift of the data.

5.3.3. Post-sunset Solar Maximum Comparisons

At 2000 LT there is a wide range of profile displays for each season, as shown in Figure 57. The standard deviations to the peak density are: 2.0×10^5 cm^{-3} (winter), 4.0×10^5 cm^{-3} (equinox), and 6.0×10^5 cm^{-3} (summer). The peak heights of the data layers have large variability: 33 km for winter, 67 km for summer, and 77 km for equinox. Table 20 gives a comparison of the peak densities, peak heights, and layer thicknesses for the data and the models. The main conclusions at 2000 LT are:

1. The IRI gives a good fit to the peak density and height in winter. The bottomside fit to the data is improved in the solstices. The topside fit to the data is better in winter than the other seasons. The model underestimates the width of the layer for all seasons.

2. FAIM gives a good fit to the peak density in equinox and winter. The layer height is well represented in winter. The summer and equinoctial heights are within range of the variability of the data. The bottomside fit is good in winter. The bottomside density gradient in summer is similar

Fig. 57. Seasonal comparison of IRI, FAIM, and PRISM with the Jicamarca average profile for 2000 LT, quite-time solar maximum conditions. The average flux for the data is given in the upper right corner of each panel. The models were run with a flux of 210 units.

TABLE 20. Comparison of Jicamarca (JRO) NmF2 (cm^{-3}), hmF2 (km), and layer thickness (km) with IRI, FAIM, and PRISM calculations at 2000 LT, solar maximum conditions.

		Summer	Equinox	Winter
JRO	NmF2	$1.77x10^6$	$1.20x10^6$	$9.43x10^5$
	hmF2	522	533	440
	ΔH	330	315	294
IRI	NmF2	$1.43x10^6$	$1.42x10^6$	$1.02x10^6$
	hmF2	455	455	430
	ΔH	252	244	257
FAIM	NmF2	$1.07x10^6$	$1.21x10^6$	$9.49x10^5$
	hmF2	540	580	460
	ΔH	260	278	274
PRISM	NmF2	$1.47x10^6$	$1.22x10^6$	$1.51x10^6$
	hmF2	612	679	468
	ΔH	279	253	330

to that of the data. The topside fit to the data is good for all seasons. The thickness of the layer is more representative in winter. The data layer is wider in summer and equinox.

3. PRISM gives the better fit of the models in summer and provides a good fit at equinox. The winter peak density is higher than the data. The layer heights are significantly overestimated at equinox and December solstice. The bottomside fit is good in winter. The model has a poor topside fit to the data for all seasons. The PRISM layer is wider than the data layer in winter, narrower in summer and equinox.

PRISM uses a very large electric field at solar maximum, and the results are evident in the summer and equinoctial

layer heights. There is not a significant difference in the layer heights predicted by the IRI, and the layers are lower than the data in summer and winter. FAIM gives a good estimate of the winter and equinoctial heights. The models give better profile calculations under the southern hemisphere winter conditions.

5.3.4. Midnight Solar Maximum Comparisons

The June solstice and equinoctial comparisons at midnight are quite good for all the models, as shown in Figure 58. The standard deviations to the peak density are 2.0×10^5 cm^{-3} (winter) and 3.5×10^5 cm^{-3} for summer and equinox. The peak heights show a large variation in summer (105 km), and vary by 20 and 40 km for winter and equinox, respectively. A summary of the peak densities, peak heights, and layer thicknesses is presented in Table 21. The main results at midnight are:

1. The IRI gives a good fit to the peak density of the data during the solstices. The peak height of the IRI layers has good agreement with the data in winter and equinox. The bottomside fit of the model to the data is good in equinox and winter. The topside profile fits the data well for all seasons. The model layer thickness is consistently lower than the data layer thickness.

2. Similar results are found for the FAIM peak density comparisons. The peak heights of the FAIM layer are within range of the wide data variability. The bottomside fits of
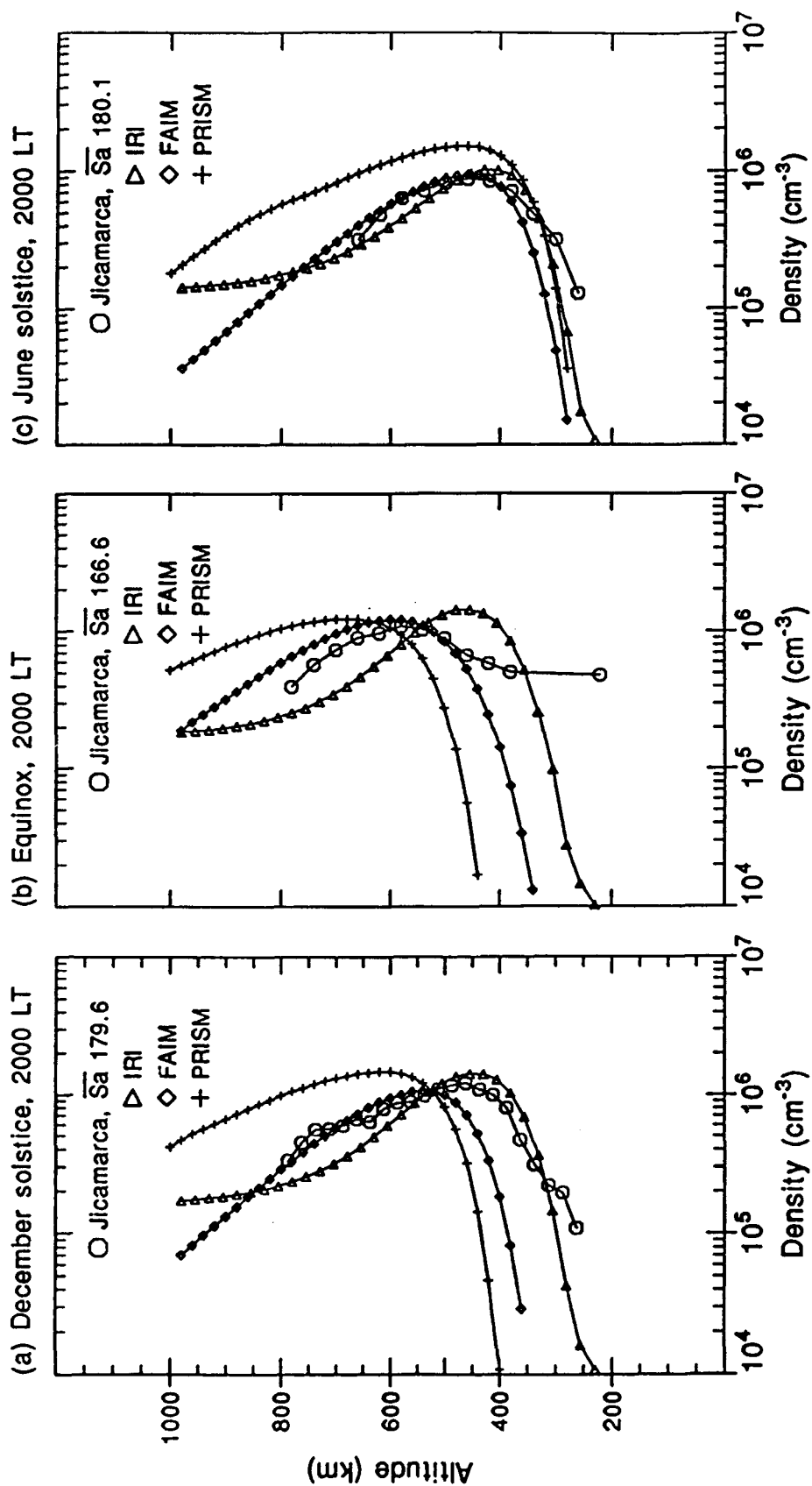
Fig. 58. Seasonal comparison of IRI, FAIM, and PRISM with the Jicamarca average profile for 0000 LT, quite-time solar maximum conditions. The average flux for the data is given in the upper right corner of each panel. The models were run with a flux of 210 units.

TABLE 21. Comparison of Jicamarca (JRO) NmF2 (cm^{-3}), hmF2 (km), and layer thickness (km) with IRI, FAIM, and PRISM calculations at 0000 LT, solar maximum conditions.

		Summer	Equinox	Winter
JRO	NmF2	$8.72x10^5$	$8.71x10^5$	$7.92x10^5$
	hmF2	429	338	307
	ΔH	286	310	245
IRI	NmF2	$9.34x10^5$	$1.34x10^6$	$8.87x10^5$
	hmF2	380	330	330
	ΔH	258	237	245
FAIM	NmF2	$8.99x10^5$	$1.34x10^6$	$8.11x10^5$
	hmF2	460	360	340
	ΔH	264	306	250
PRISM	NmF2	$4.59x10^5$	$1.33x10^6$	$1.01x10^6$
	hmF2	611	370	322
	ΔH	234	321	261

FAIM to the data are good in winter and equinox. The modeled layer thickness compares quite well with the data for all seasons.

3. The peak density of the summer PRISM layer is almost half that of the data. The winter and equinoctial peak densities are similar to the Jicamarca peak densities. The layer height in summer is exceptionally high with respect to the data. The bottomside agreement of PRISM with the data follows that of the FAIM and IRI agreements. The PRISM topside gives the better fit in winter. The modeled layer thickness gives a good fit to the data in winter and equinox.

The variability of the model calculations for midnight, December solstice, is much greater than seen in the previous flux level comparisons for this hour. We have come to expect

that the equinoctial and winter layers will be well represented.

5.3.5. Pre-sunrise Solar Maximum Comparisons

The models are all able to depict the descending layer at 0400 LT. The comparison is presented in Figure 59. There is caution in giving too much weight to these comparisons, based on the limited Jicamarca data available. The comparisons of peak density, peak height, and layer thickness at 0400 LT are presented in Table 22. The standard deviations to the peak density are typically 7.0×10^4 to 2.0×10^5 cm^{-3} for summer and equinox, respectively. The winter peak varies by 1.0×10^5 cm^{-3}. The peak heights of the Jicamarca layer have standard deviations of 27, 37, and 58 km for summer, winter, and equinox. The main results are:

1. The IRI overestimates the peak density for all seasons. The placement of the peak height shows no seasonal variation for the IRI and comes closest to the data peak in winter. The IRI bottomside fit to the layer is good during the solstices. The topside layer fit is within the variability of the solstitial data. The layer thickness is comparable for summer.

2. The peak density in summer is well represented by the FAIM calculations. The modeled layer heights are comparable in summer and winter. There is good agreement between FAIM and the data in the solstitial bottomside layers. There is likewise good agreement in the solstitial
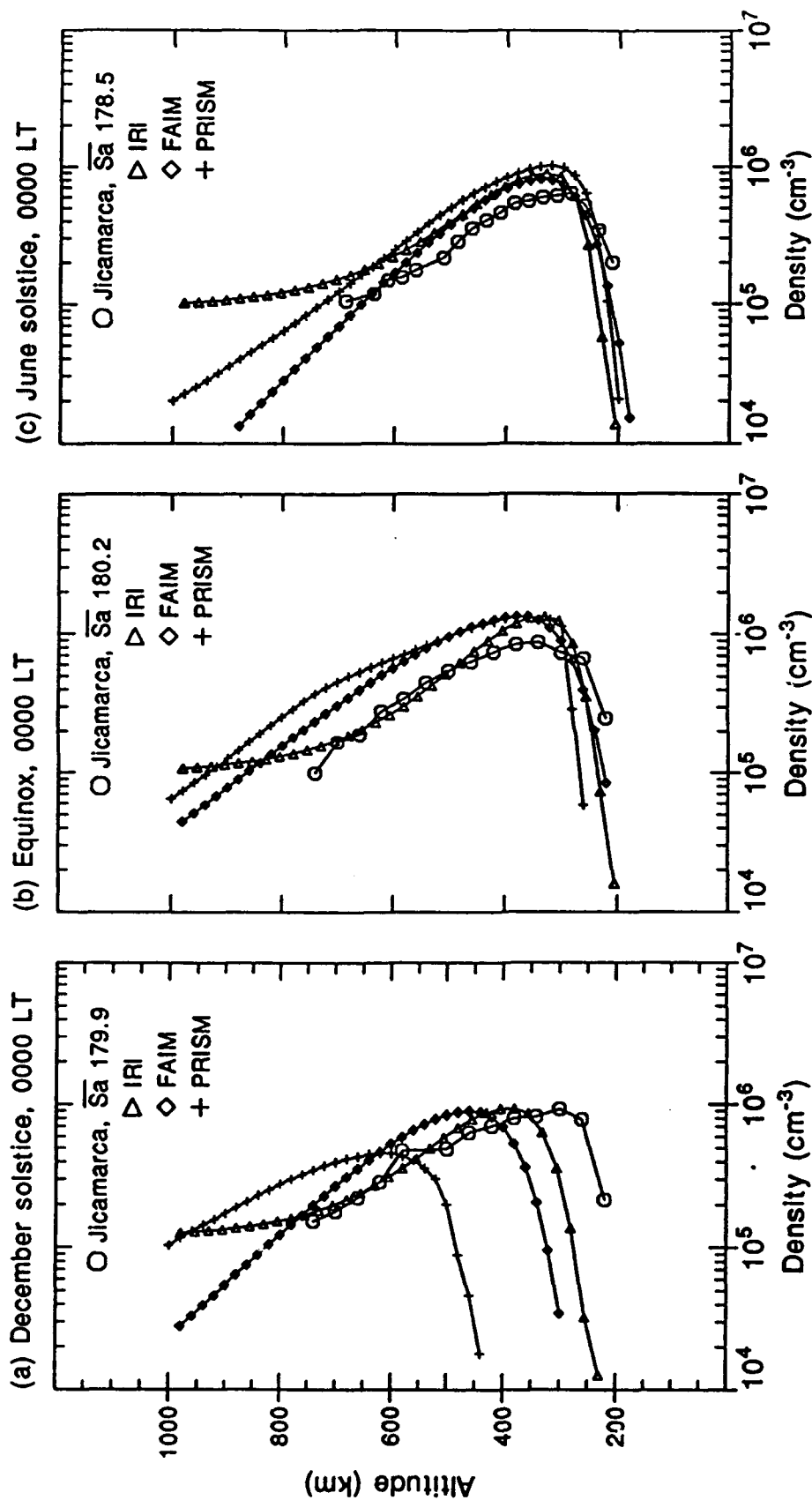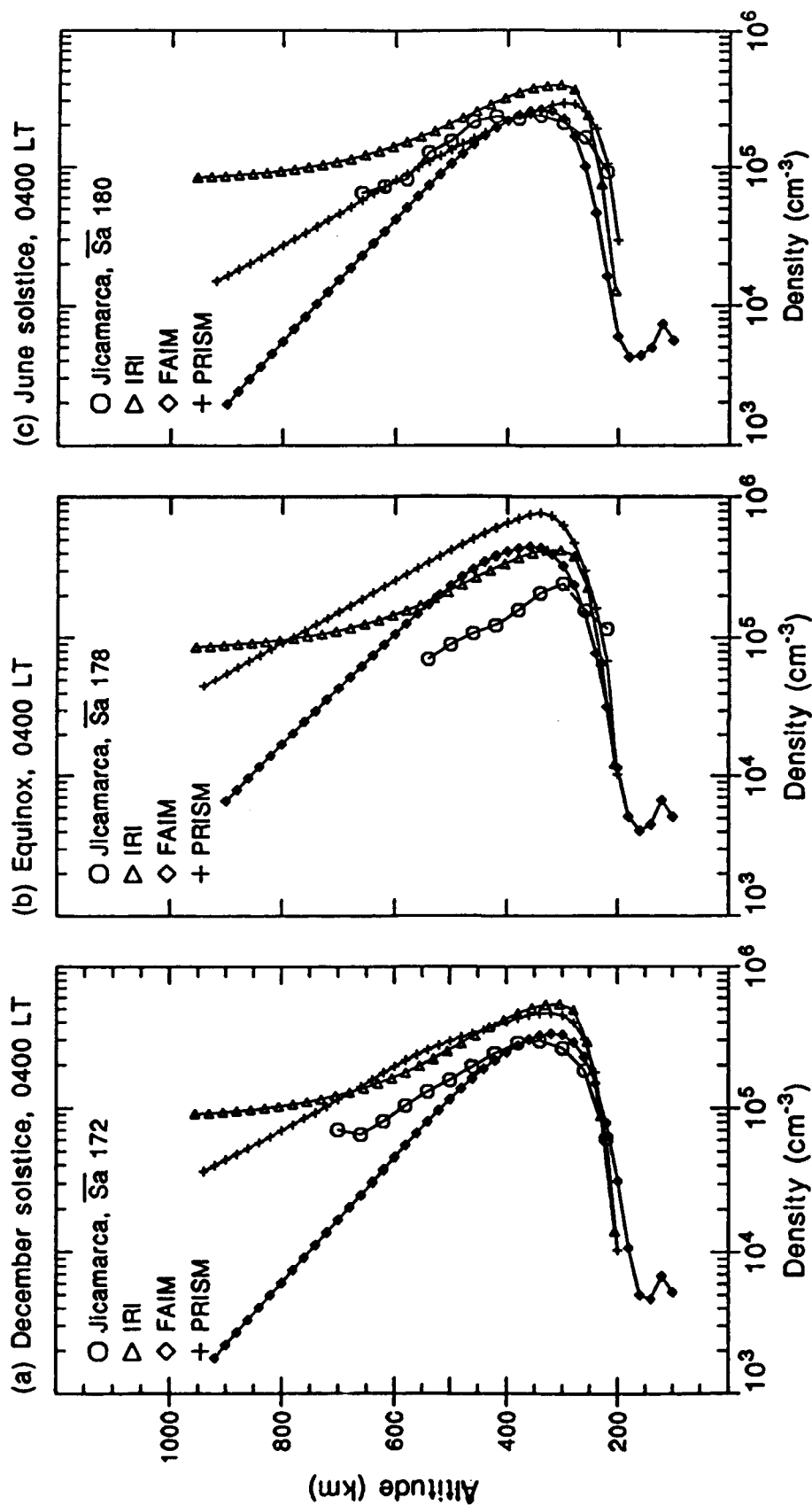
Fig. 59. Seasonal comparison of IRI, FAIM, and PRISM with the Jicamarca average profile for 0400 LT, quite-time solar maximum conditions. The average flux for the data is given in the upper right corner of each panel. The models were run with a flux of 210 units.

TABLE 22. Comparison of Jicamarca (JRO) NmF2 (cm^{-3}), hmF2 (km), and layer thickness (km) with IRI, FAIM, and PRISM calculations at 0400 LT, solar maximum conditions.

		Summer	Equinox	Winter
JRO	NmF2	3.43×10^5	3.80×10^5	3.20×10^5
	hmF2	330	343	316
	ΔH	279	194	303
IRI	NmF2	5.42×10^5	4.24×10^5	3.92×10^5
	hmF2	305	305	305
	ΔH	266	249	211
FAIM	NmF2	3.3×10^5	4.60×10^5	2.56×10^5
	hmF2	320	360	340
	ΔH	226	249	211
PRISM	NmF2	4.69×10^5	7.77×10^5	2.88×10^5
	hmF2	324	341	315
	ΔH	234	216	258

topside layers. The layer thickness calculations are poor for all seasons.

3. The PRISM layers show higher peak densities than the data in summer and equinox. The layer heights calculated by PRISM give the better fit of the three models to the data for all seasons. The PRISM bottomsides fit the solstitial data well. The topside PRISM layer gives the better fit in winter. The layer thickness is less than the data for solstices, and the model comes the closest to the data thickness at equinox.

The 0400 LT comparisons seem to be better for each model for parameters where they were weak at other hours. For example, FAIM gives an excellent fit to the peak density in summer. The comparisons with the equinoctial data are very

weak because of the limited Jicamarca data for this season and time. It is difficult to determine the equinoctial bottomside fit.

There is no single parameter at any season or hour for solar maximum that any of the models excels at reproducing. With few exceptions, the IRI did not give a good estimate of the layer thickness of the experimental data. The IRI fit to the density is good in the evening in winter. FAIM gives the better fit to all parameters at midnight in summer and 2000 LT at equinox. PRISM gives a good representation of all parameters in the evening for summer and equinox. It gives the better fit to all parameters at noon and prior to sunrise in winter. Of the 54 parameters (3 seasons x 6 hours x 3 parameters) FAIM comes closest to the data 20 times, PRISM 19 times, and IRI 15 times. This does not imply that in coming closest to the experimental data parameter the model gives a good fit.

5.4. Parameter Variations With Flux

In this section we describe the variation of peak density (NmF2), peak height (hmF2), and layer thickness (ΔH) with flux of the experimental data compared with the model results.

5.4.1. Midday Comparisons

The scatter plots of flux versus peak density, flux versus peak height, and flux versus layer thickness are

presented in Figures 60, 61, and 62, respectively, for 1200 LT. The heavy line is a least squares fit to the quiet time data. The models were run for every ten flux units and a least squares fit was applied to the peak densities, heights, and layer thickness. Each panel illustrates the variability of the parameters the models must match.

The models are able to reproduce the increase in density with flux for all seasons at 1200 LT. The better fit to the data occurs at equinox for all models. IRI provides the better fit to NmF2 during the solstices. FAIM is clearly lower than the average during solstices, but compares well with the equinox data, especially at higher flux. The PRISM peak densities are lower than the data peaks in summer, equinox, and the lower flux levels of winter. Above 100 flux units the predicted peaks by PRISM are higher than the data average.

The data peak heights at 1200 LT increase with approximately the same rate for all seasons, as seen in Figure 61. The IRI hmF2 fit is better at equinox. The IRI layer is higher than the data layer during the solstices for all flux. The FAIM layer is lower than the data in summer, and higher in winter and equinox. The fit of PRISM to the data is good in summer and equinox, but the PRISM layer is substantially higher than the data in winter. This parameter is the most variable in the data and with more samples the model performance might improve.

Fig. 60. Seasonal comparisons of Jicamarca and modeled NmF2 at 1200 LT. The lines represent least squares fits to the data and models. The open circles are quiet-time observations, the stars denote data obtained under disturbed conditions.

Fig. 61. Seasonal comparisons of Jicamarca and modeled hmF2 at 1200 LT. The lines represent a least squares fit to the data and models. The open circles are quiet-time observations, the stars denote data obtained under disturbed conditions.

Fig. 62. Seasonal comparisons of Jicamarca and modeled ΔH at 1200 LT. The lines represent a least squares fit to the data and models. Data obtained under disturbed conditions were not used.

The layer thickness of the data shows the largest increase at noon during June solstice. Figure 62 illustrates the models' comparisons of layer thickness with the data layer. Each modeled layer thickness is substantially higher than the data. The IRI layer is the only one that actually decreases in equinox and winter. Of the three panels, the December solstice comparison is the most realistic for the models.

5.4.2. Evening Comparisons

The equinoctial peak densities predicted by the models have a good fit to the data at 1700 LT and 1800 LT, equinox. Figure 63 illustrates the 1800 LT seasonal peak density variation with flux. The IRI fit is the better to this parameter for all seasons and all flux levels. FAIM underestimates the peak density for during summer. The PRISM fit is good at equinox; it predicts the peak density too low/high at December/June solstice.

The IRI hmF2 is consistently lower than the data hmF2 for all seasons at 1700 LT and 1800 LT. The better fit is in winter (see Figure 64). FAIM fits the peak height well in summer, but overestimates it at higher flux levels in winter and overestimates it for all flux levels at equinox. PRISM underestimates the peak heights in summer and equinox and gives an excellent fit to the data for all flux.

The 1800 LT layer thickness comparisons provide the better illustration of model performance for this parameter
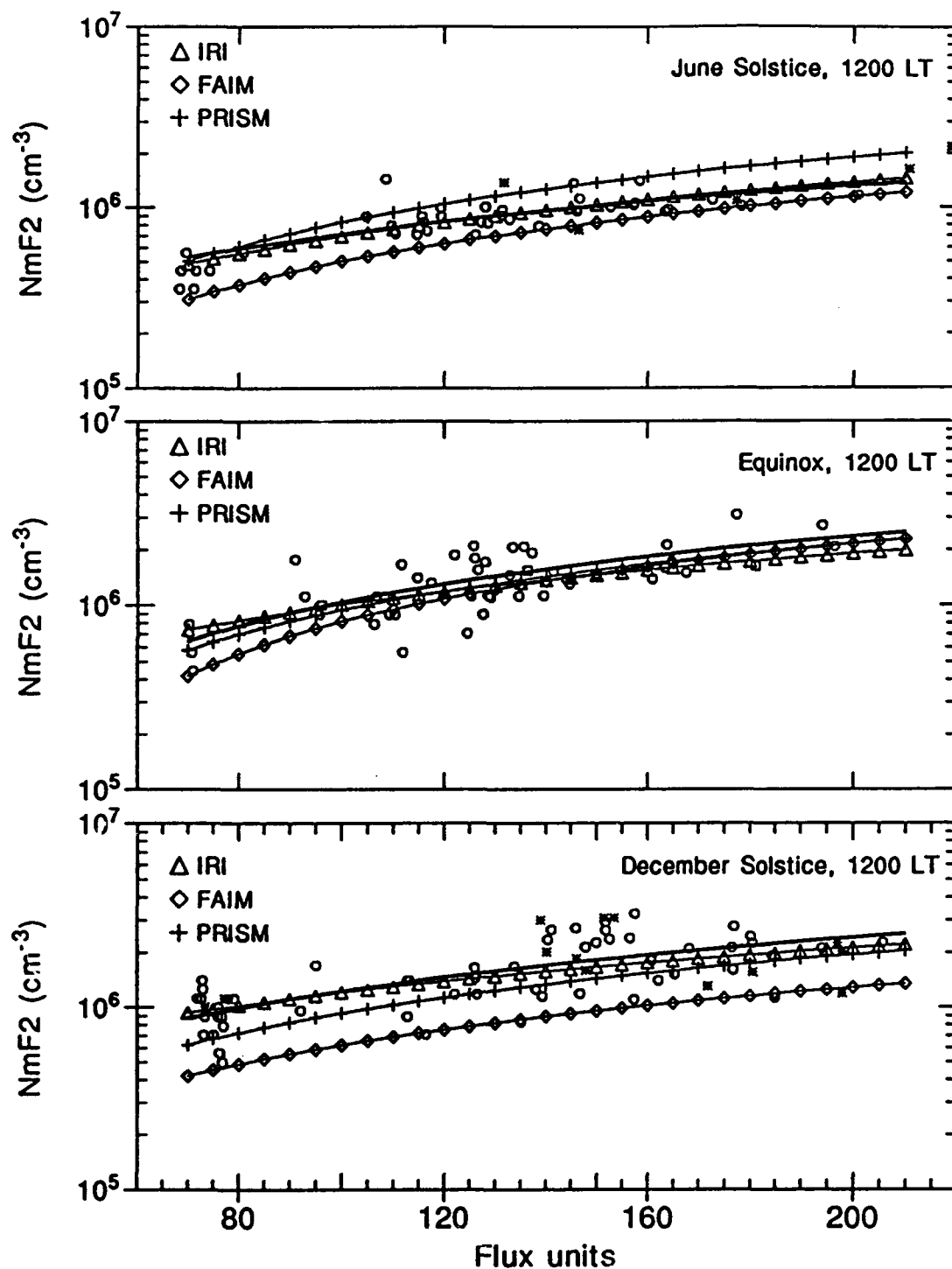
Fig. 63. Seasonal comparisons of Jicamarca and modeled NmF2 at 1800 LT. The lines represent a least squares fits to the data and models. The open circles are quiet-time observations, the stars denote data obtained under disturbed conditions.
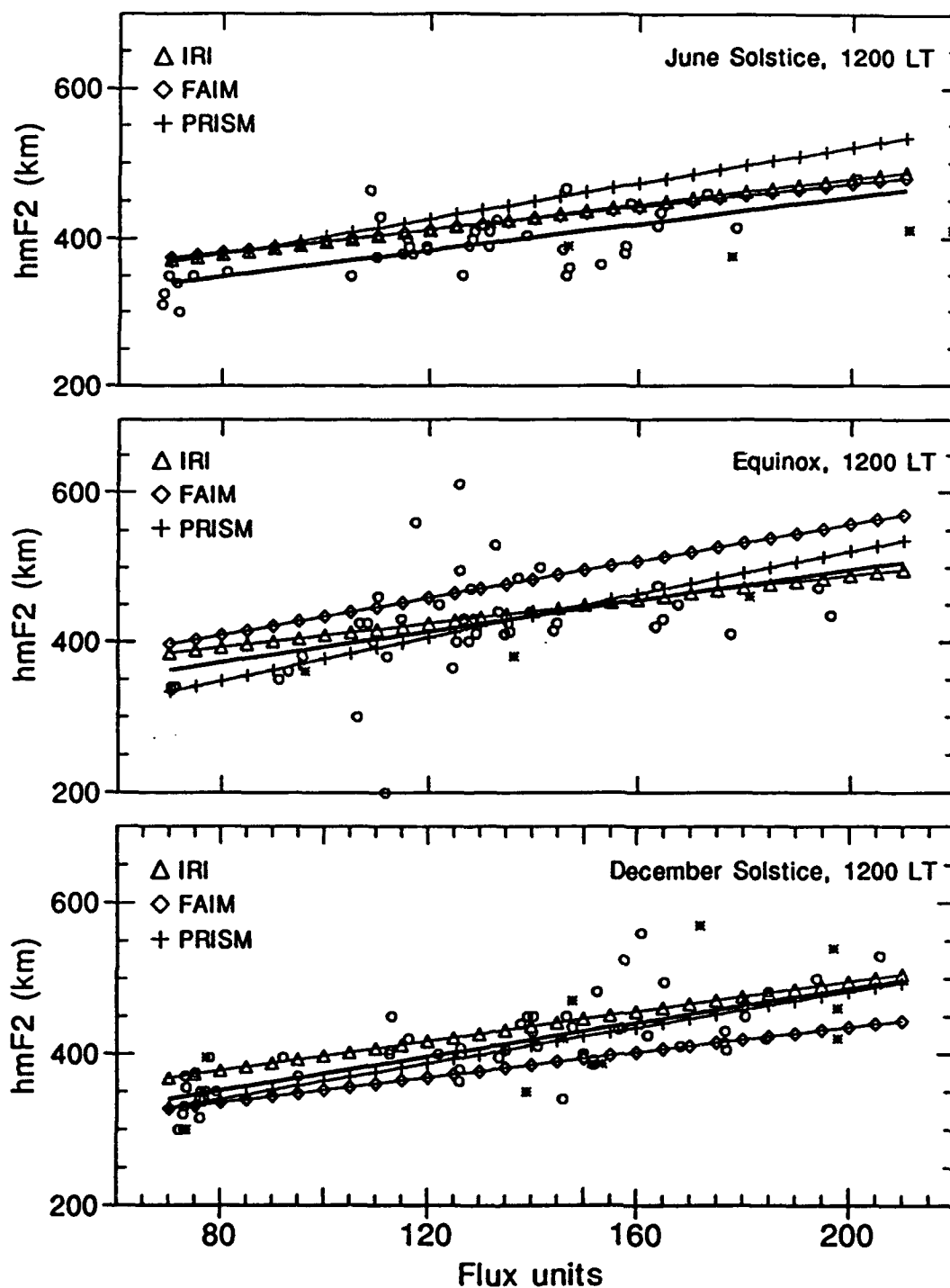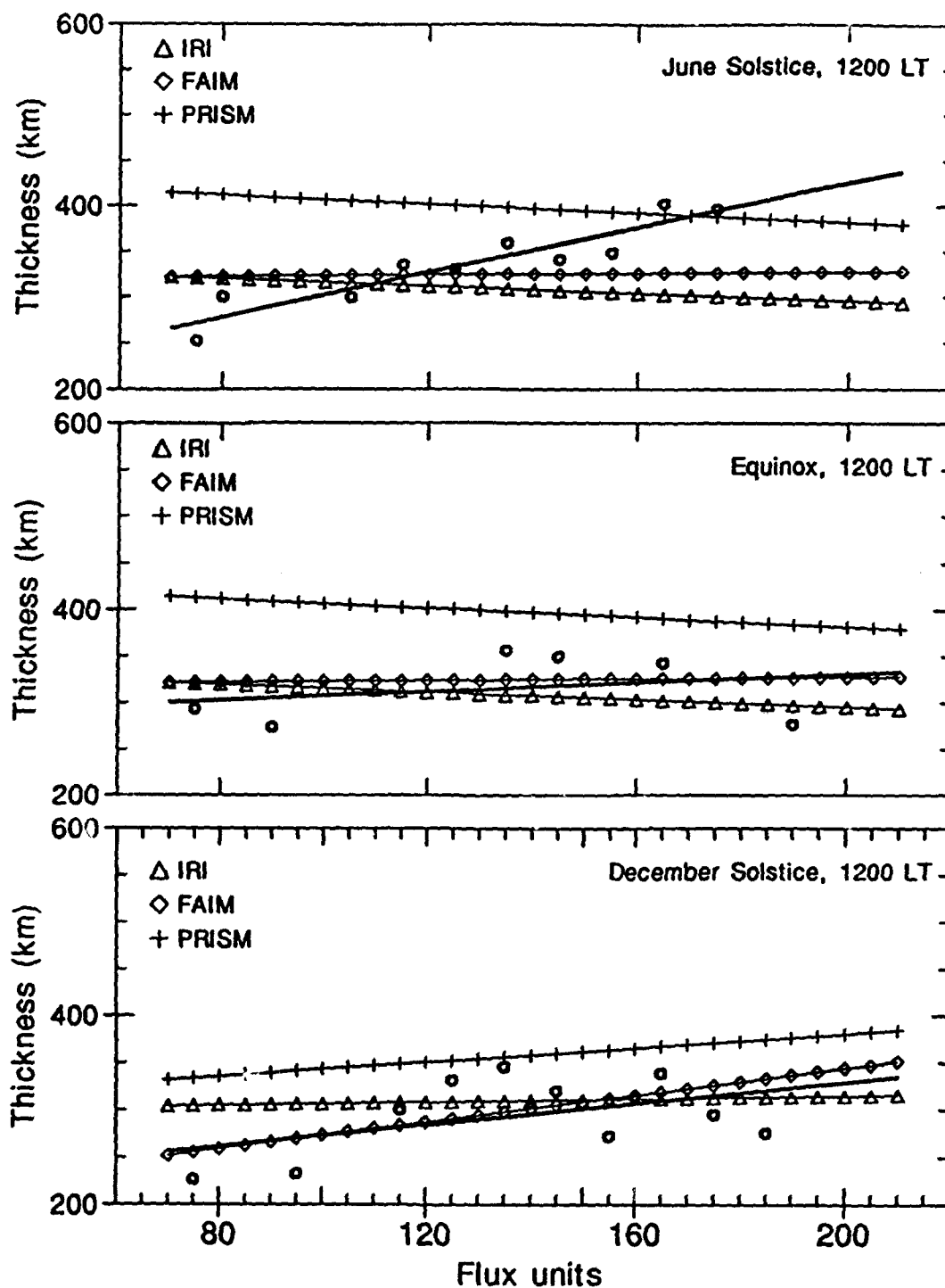
Fig. 64. Seasonal comparisons of Jicamarca and modeled hmF2 at 1800 LT. The lines represent a least squares fits to the data and models. The open circles are quiet-time observations, the stars denote data obtained under disturbed conditions.

in Figure 65. The models give a good estimate to the thickness for lower flux levels, but deviate substantially from the data curve for higher flux. The FAIM fit to the data is the better in winter, but is consistently lower than the data. The IRI fit is significantly lower than the data at higher flux levels. The PRISM layers are thicker than the data layers at all flux levels, but the model correctly predicts the increase in layer thickness with flux.

5.4.3. Post-sunset Comparisons

At 2000 LT the equinoctial fit of the models to the data peak density is the better fit of the three seasons (see Figure 66). The models overestimate the peak density in winter and underestimate it in summer. The IRI gives the better fit to this parameter for all seasons. The PRISM peaks are significantly higher than the data peaks in winter while the FAIM peaks are substantially lower than the data peaks in summer.

The peak layer height predicted by IRI is markedly lower than the data in summer and equinox. For lower flux levels in winter the IRI gives a good fit to the data hmF2, but above 100 units it significantly underestimates this parameter, as shown in Figure 67. FAIM fits the data well in winter, but is approximately 50 km too low at every flux level in summer. The PRISM hmF2 fits are the best of the three models in summer, and match the data almost exactly for all flux levels. PRISM also performs well for lower flux in

Fig. 65. Seasonal comparisons of Jicamarca and modeled ΔH at 1800 LT. The lines represent a least squares fit to the data and models. Data obtained under disturbed conditions were not used.
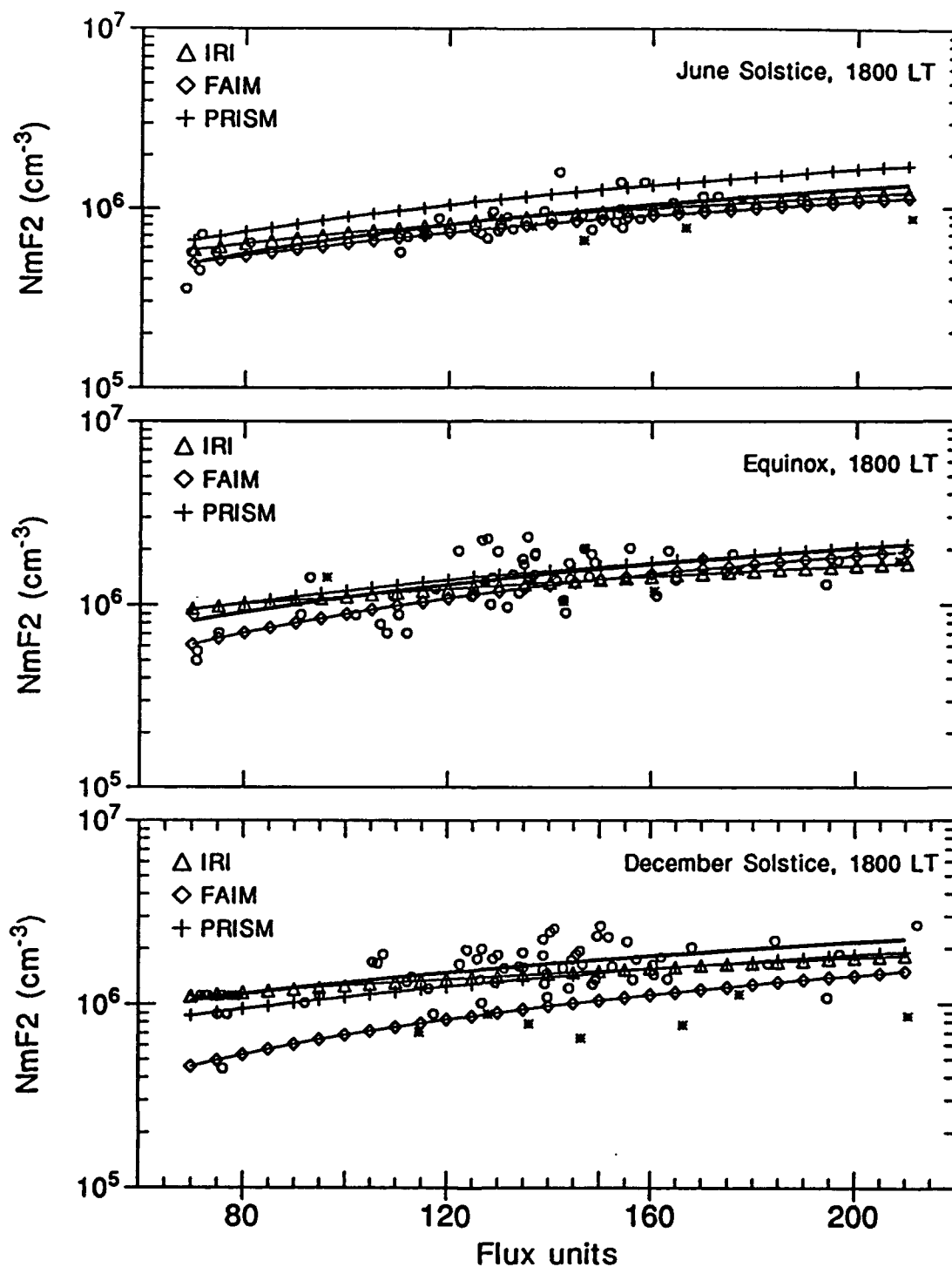
Fig. 66. Seasonal comparison of Jicamarca and modeled NmF2 at 2000 LT. The lines represent a least squares fit to the data and models. The open circles are quiet-time observations, the stars denote data obtained under disturbed conditions.
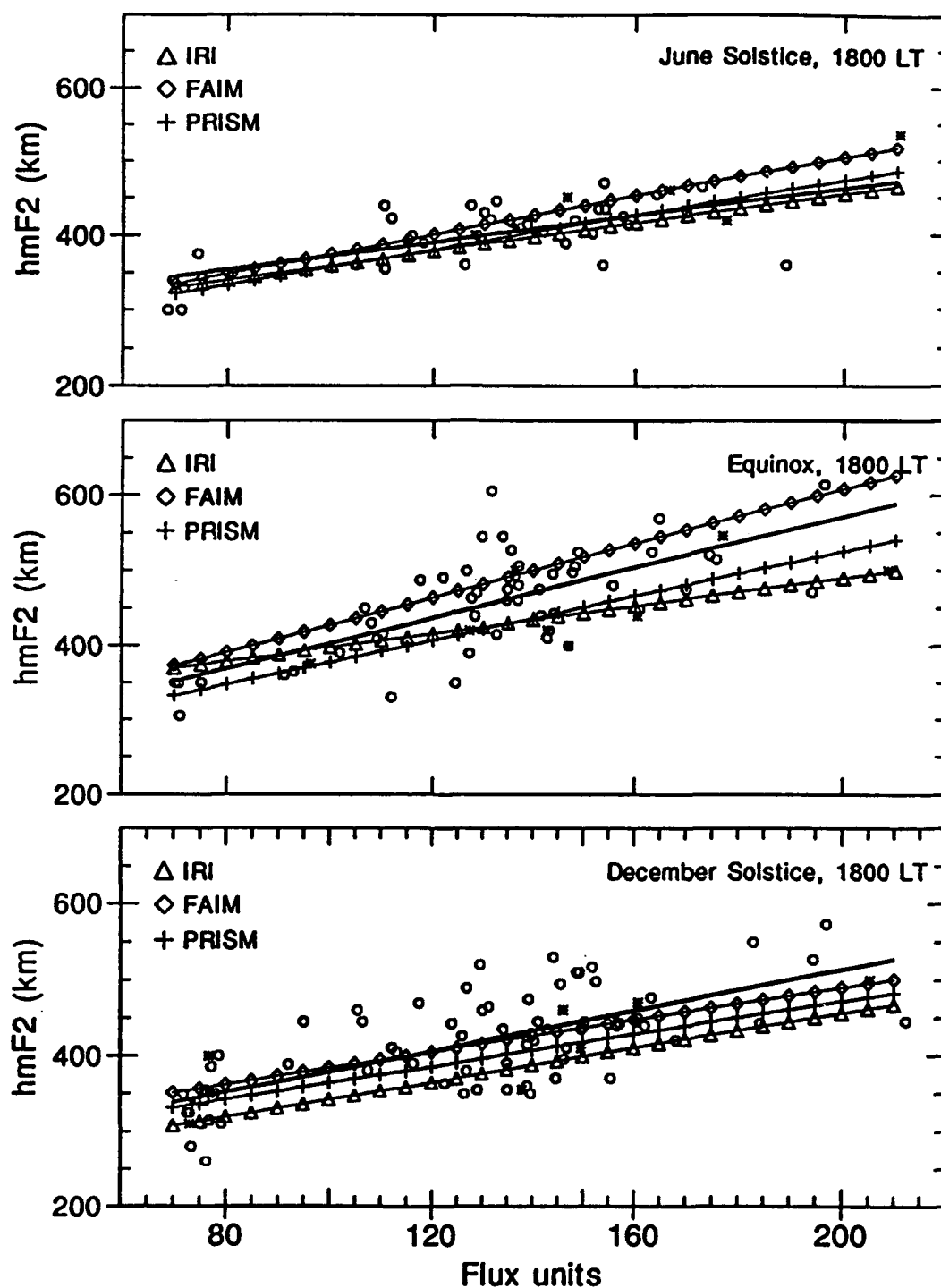
Fig. 67. Seasonal comparisons of Jicamarca and modeled hmF2 at 2000 LT. The lines represent a least squares fit to the data and models. The open circles are quiet-time observations, the stars denote data obtained under disturbed conditions.

winter, but becomes too low at higher flux. During equinox both PRISM and FAIM underestimate the layer height for low flux, and overestimate it for high flux.

The models give a good fit to the data layer thickness at 2000 LT for all flux levels during December solstice (see Figure 68). Each modeled layer thickness does not increase with the data layer thickness during equinox and shows a decrease in winter, in poor comparison with the data.

5.4.4. Midnight Comparisons

The IRI performs well in predicting the peak density at 0000 LT for the solstices, particularly at higher flux in winter. It overestimates the peak density in equinox. FAIM has a similar comparison of good fits at the higher flux levels during solstice with overestimated peaks during equinox. The PRISM layer provides a good fit in winter and equinox, but substantially underestimates the peak density in summer. These comparisons are illustrated in Figure 69.

The modeled winter peak heights fit the data better at 0000 LT for all flux levels. FAIM gives the better fit to the data during equinox. IRI and PRISM underestimate the layer peak height at equinox. The model performance in summer is poor, but the summer data are also the most variable of the set, as shown in Figure 70.

The IRI gives a good fit to the 0000 LT data thickness at higher flux in winter and lower flux in summer. The FAIM fits are good for lower flux in winter and for all flux in
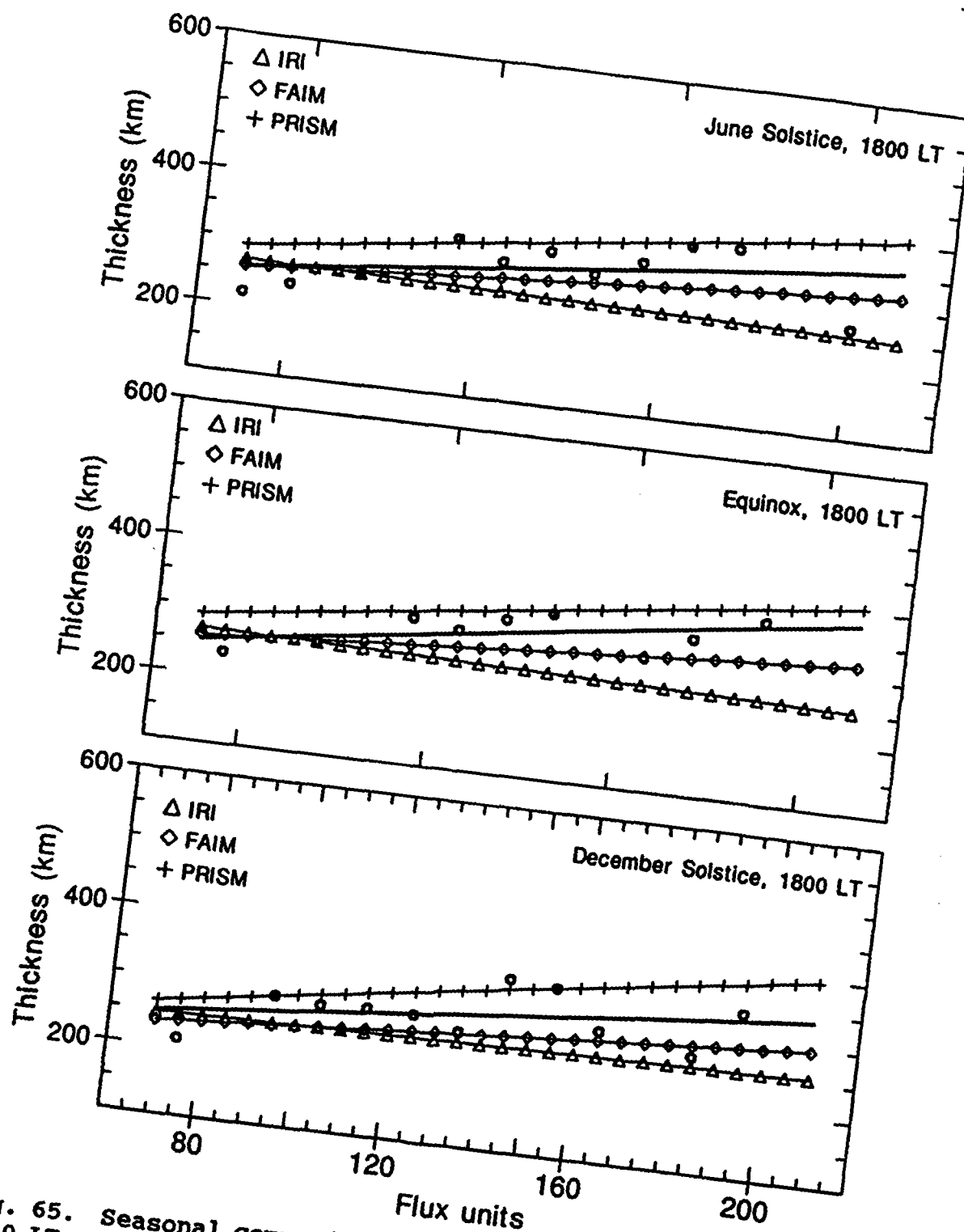
Fig. 68. Seasonal comparison of Jicamarca and modeled ΔH at
2000 LT. The lines represent a least squares fit to the data
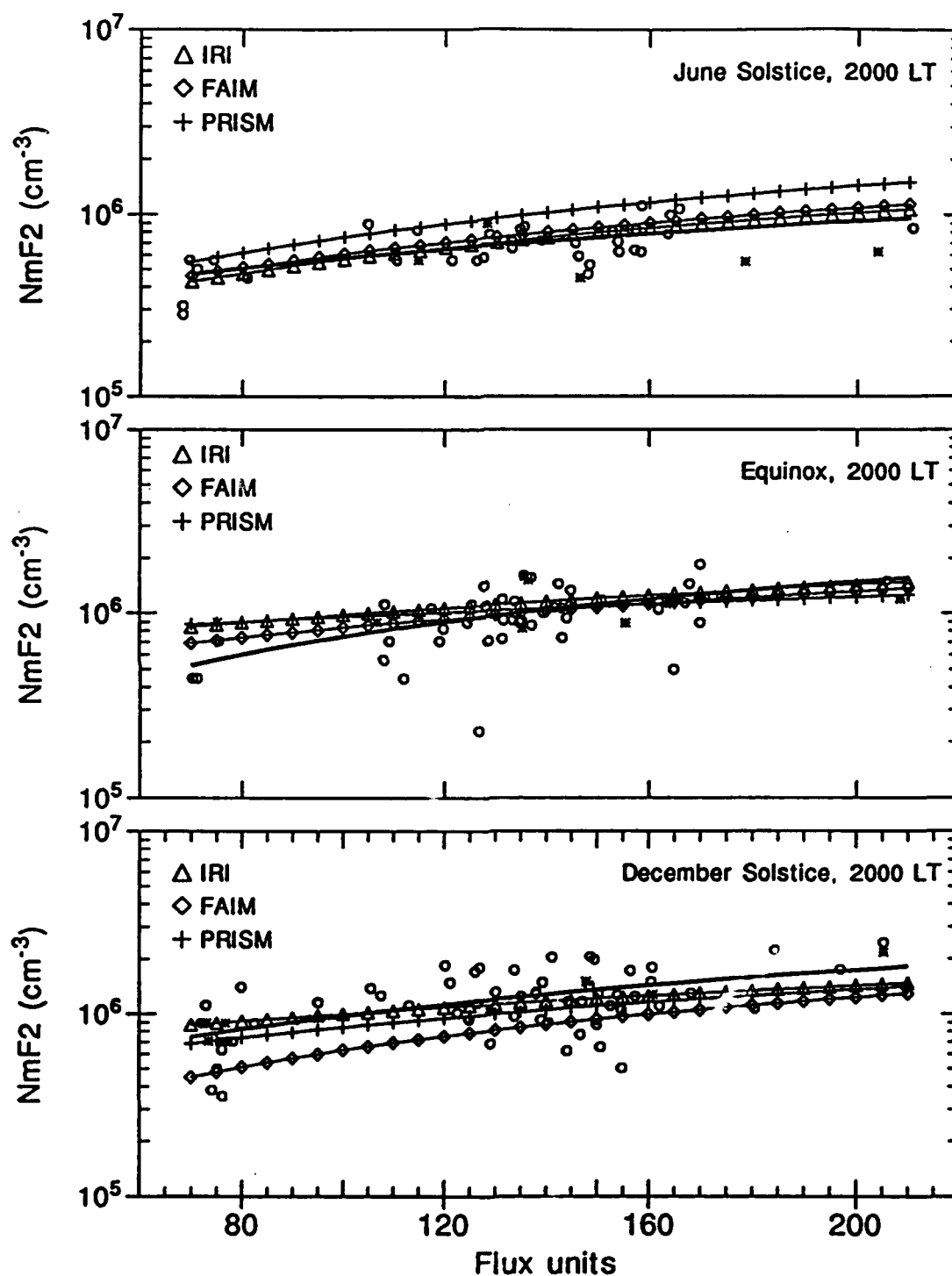and models. Data obtained under disturbed conditions were
not used.

Fig. 69. Seasonal comparisons of Jicamarca and modeled NmF2 at 0000 LT. The lines represent a least squares fit to the data and models. The open circles are quiet-time observations, the stars denote data obtained under disturbed conditions.
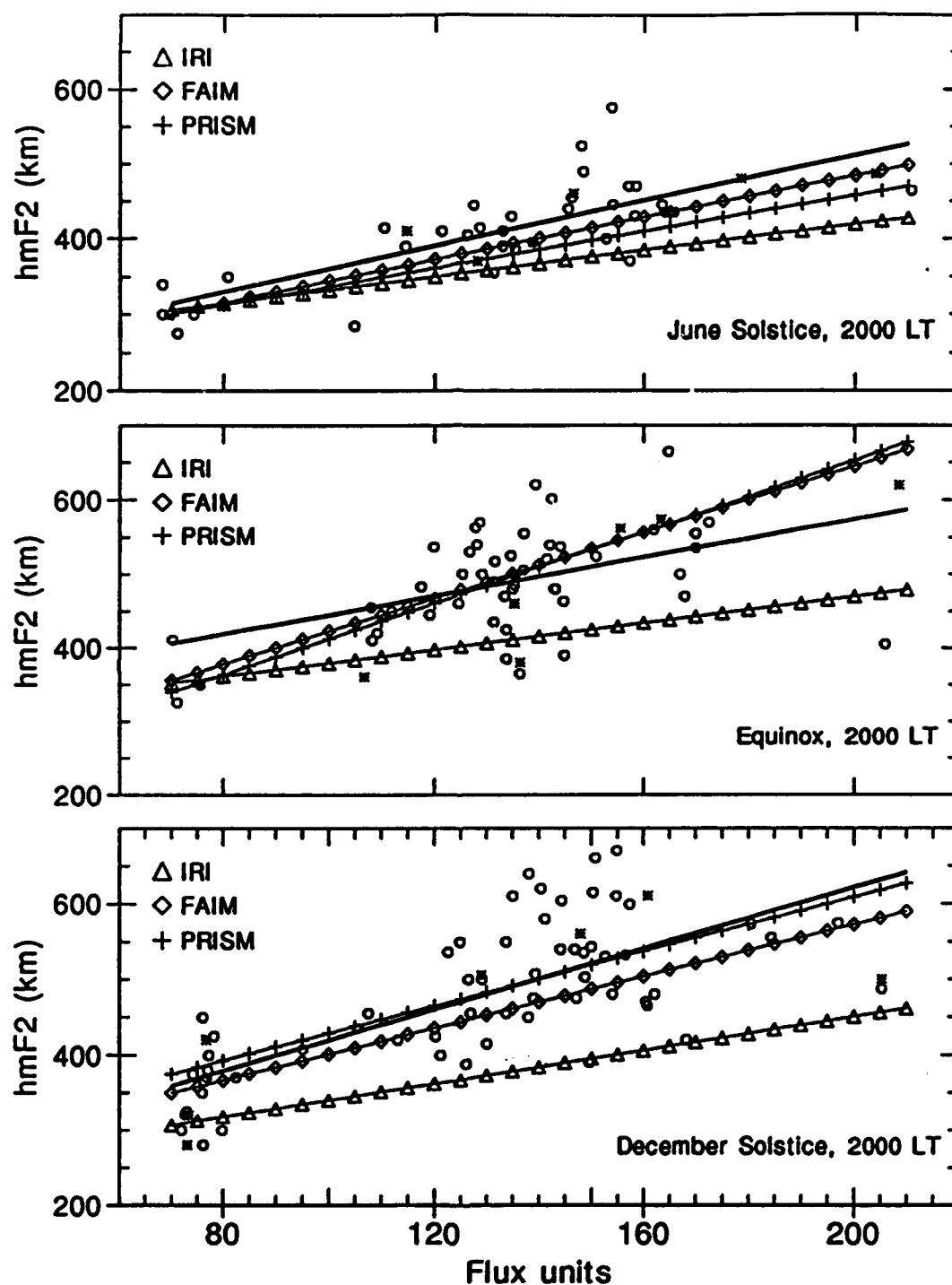
Fig. 70. Seasonal comparisons of Jicamarca and modeled hmF2 at 0000 LT. The lines represent a least squares fit to the data and models. The open circles are quiet-time observations, the stars denote data obtained under disturbed conditions.

equinox. The PRISM layers are thicker than the data for all flux in equinox and winter. The Jicamarca layer in summer is decreasing, so comparisons are both unfair and unreliable. These comparisons are provided in Figure 71.

5.4.5. Pre-sunrise Comparisons

At 0400 LT the better model fits to the data occur in summer, as shown in Figure 72. FAIM accurately reproduces the increase in density with flux in summer and for middle flux levels in equinox. The IRI performs well for low flux in summer, but overestimates the peak density for higher summer flux. Conversely, the IRI fits the data better at higher flux for equinox and winter. PRISM fits the data well for higher flux in summer, but overestimates the peak densities in equinox and underestimates the peak densities in winter.

The IRI fits the winter Jicamarca peak height data well for higher flux levels, Figure 73. It performs well for lower flux levels in equinox and middle flux levels in summer. FAIM gives the same results as the IRI in summer. It overestimates the equinox layer height and performs poorly in winter. PRISM gives a good fit to the data at mid and high flux levels for all seasons.

Based on the data for 0400 LT, the layer thickness (see Figure 74) decreases with increasing flux in summer and equinox. Because this result is unrealistic, the comparisons with the models are meaningless. The models perform well for
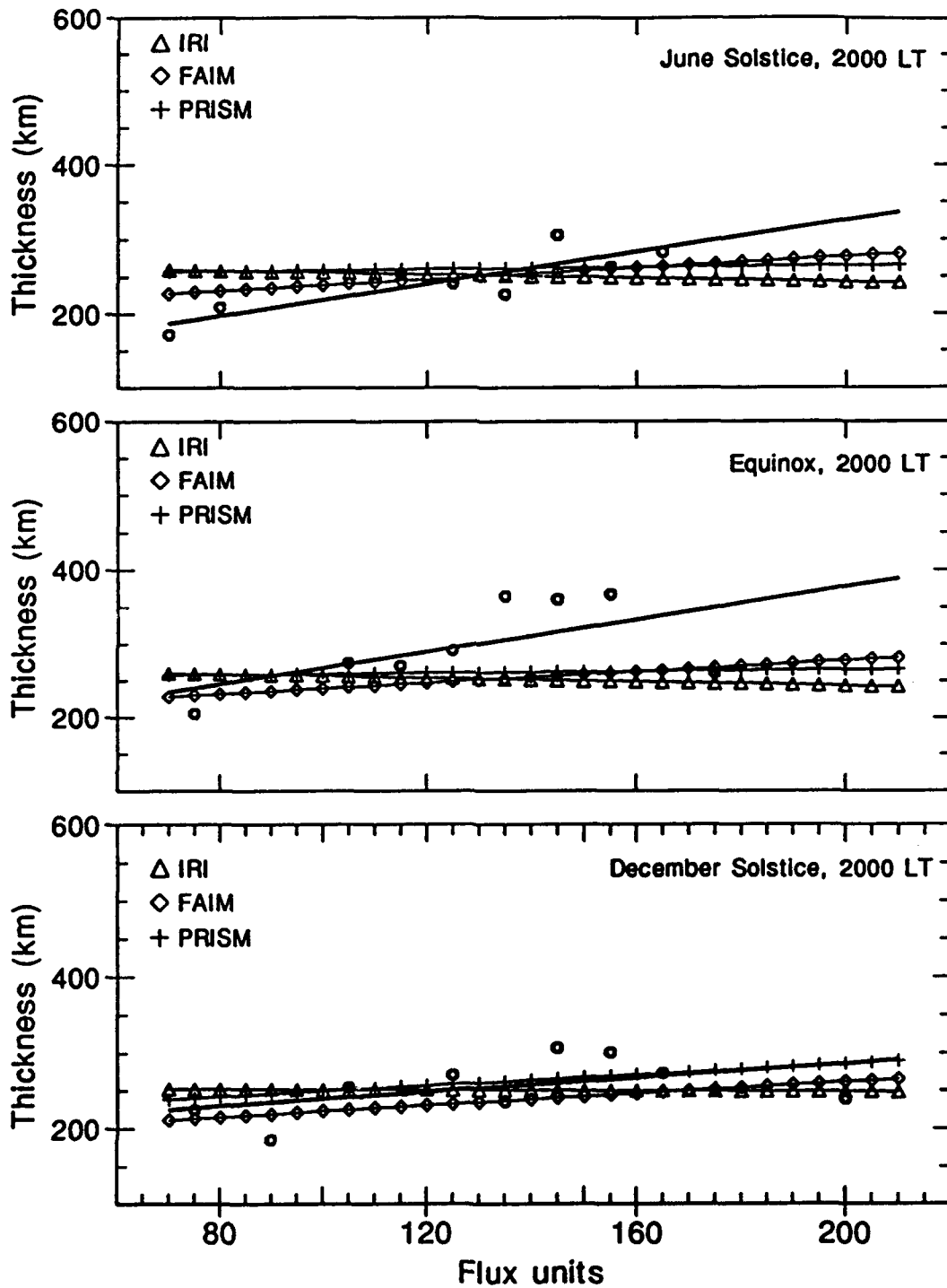
Fig. 71. Seasonal comparisons of Jicamarca and modeled ΔH at
0000 LT. The lines represent a least squares fit to the data
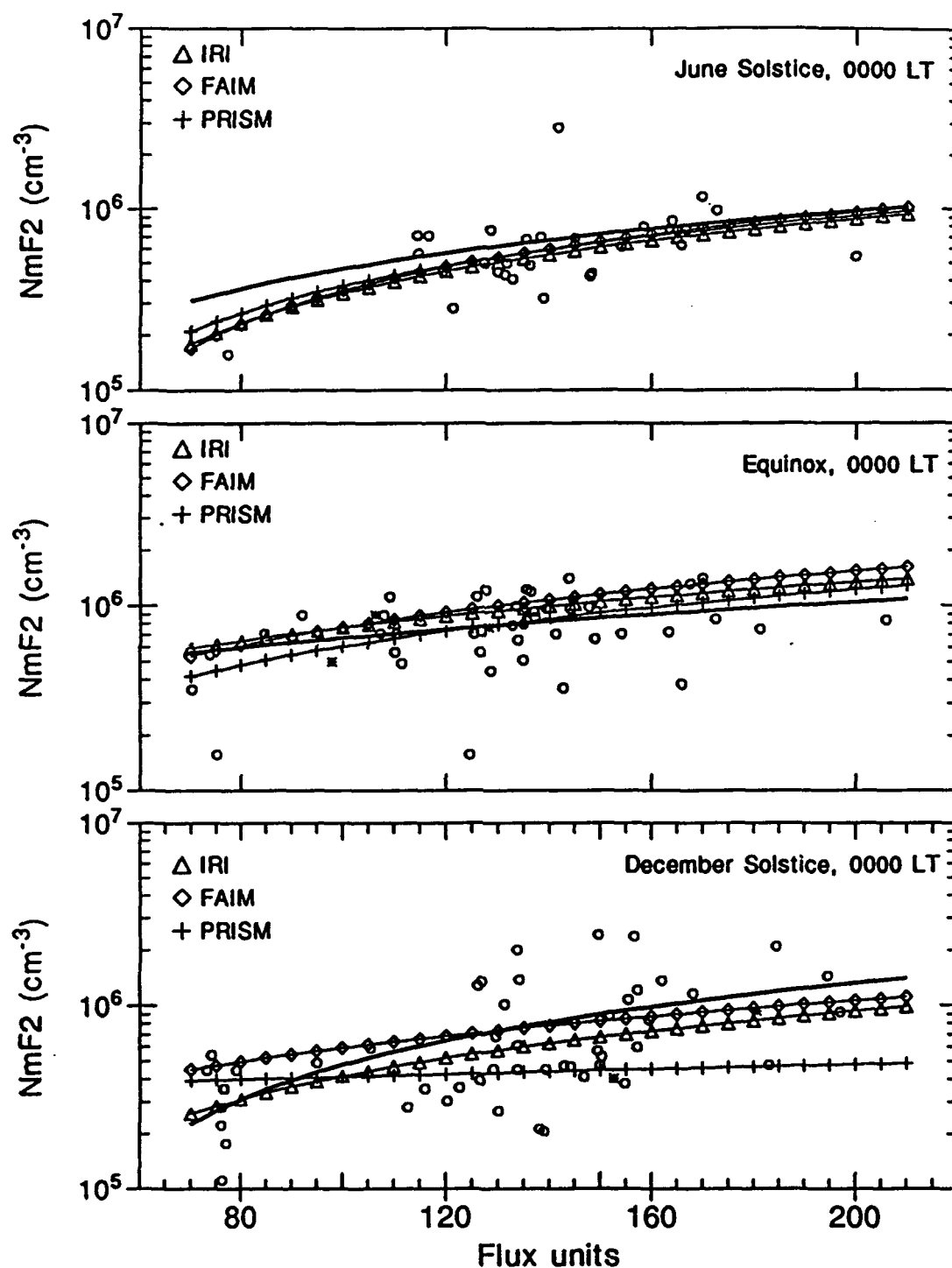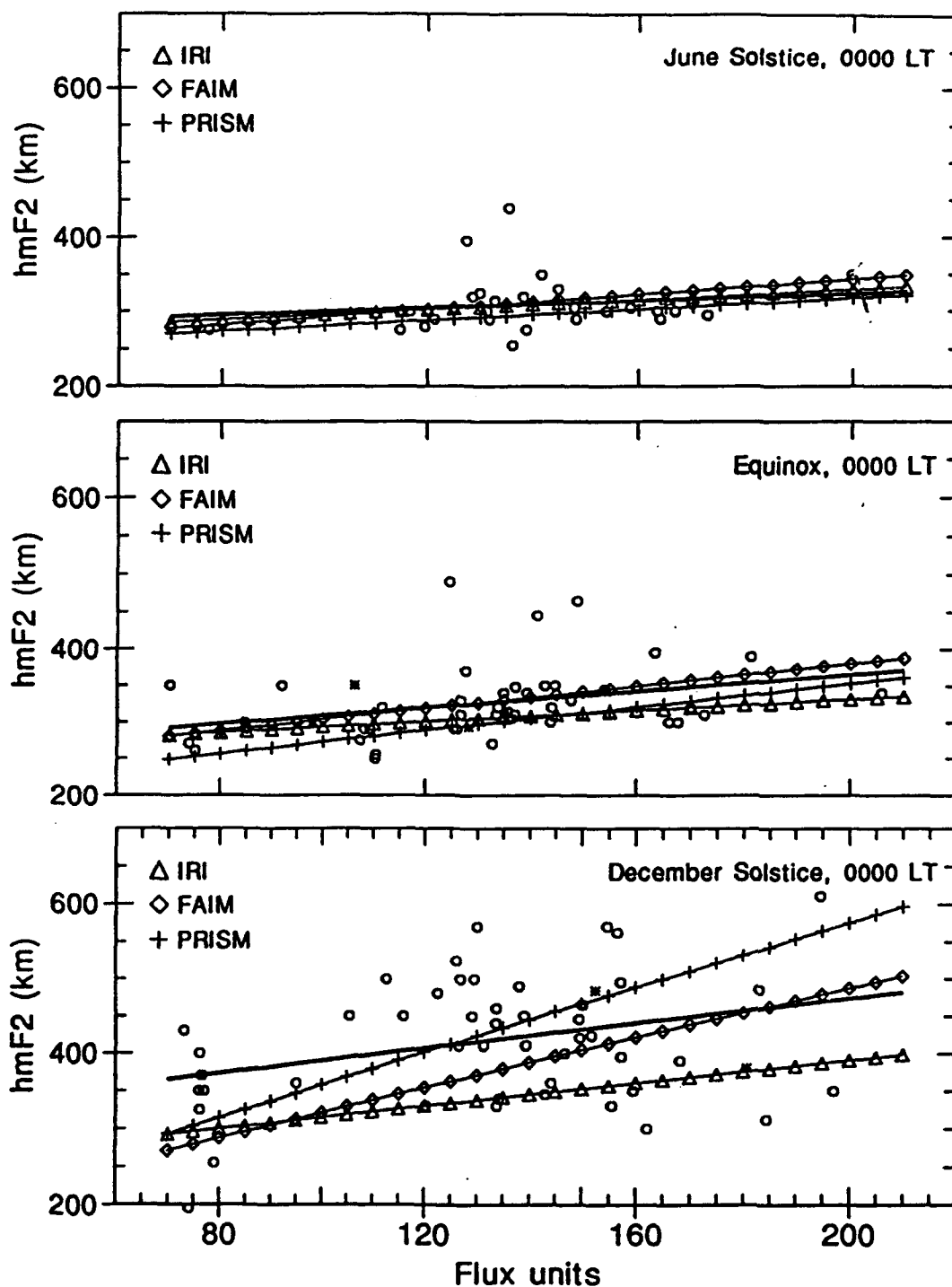and models. Data obtained under disturbed conditions were
not used.

Fig. 72. Seasonal comparisons of Jicamarca and modeled NmF2
at 0400 LT. The lines represent a least squares fit to the
data and models. The open circles are quiet-time
observations, data obtained under disturbed conditions were
not used.

Fig. 73. Seasonal comparisons of Jicamarca and modeled hmF2 at 0400 LT. The lines represent a least squares fit to the data and models. The open circles are quiet-time observations, data obtained under disturbed conditions were not used.
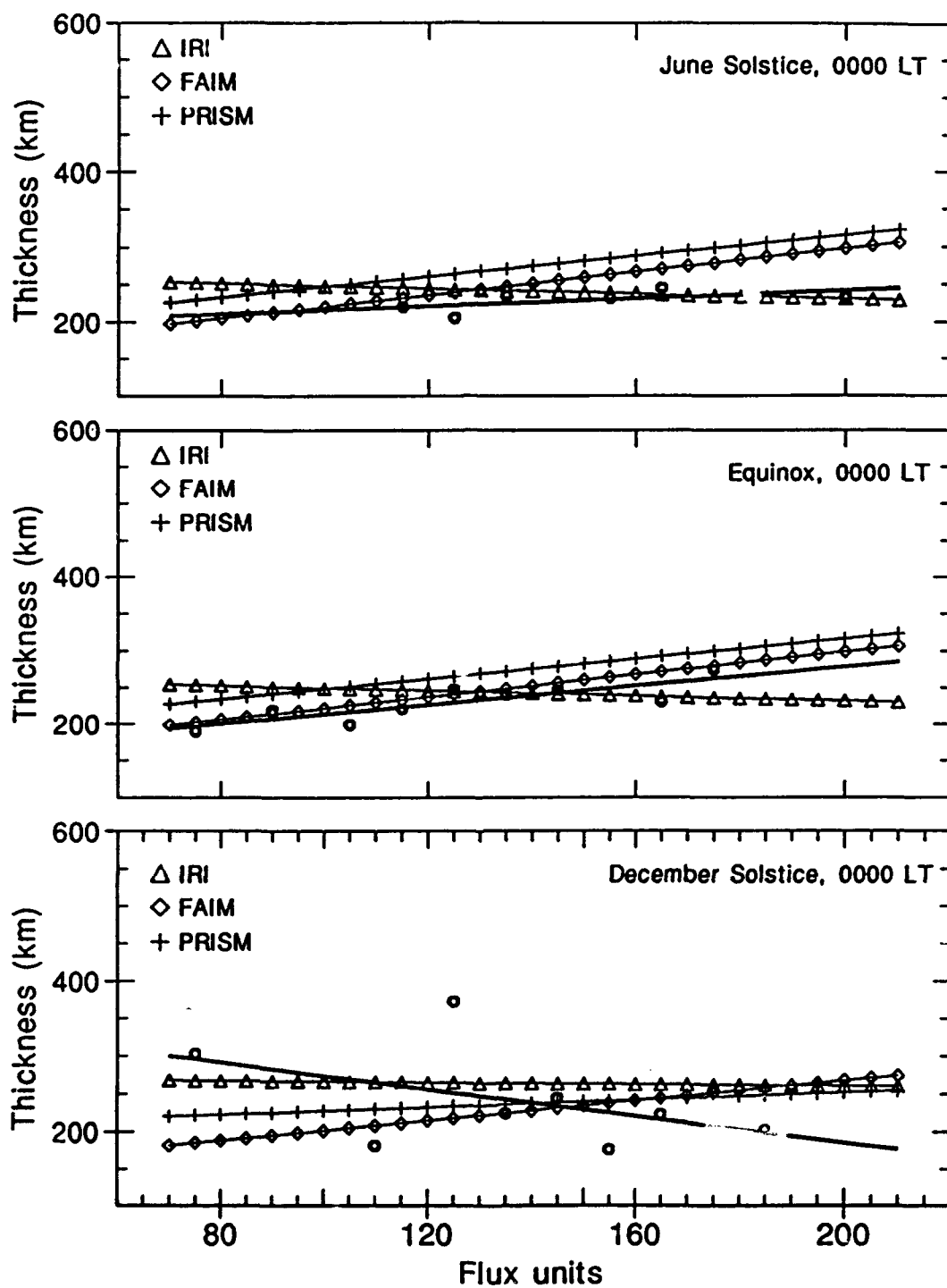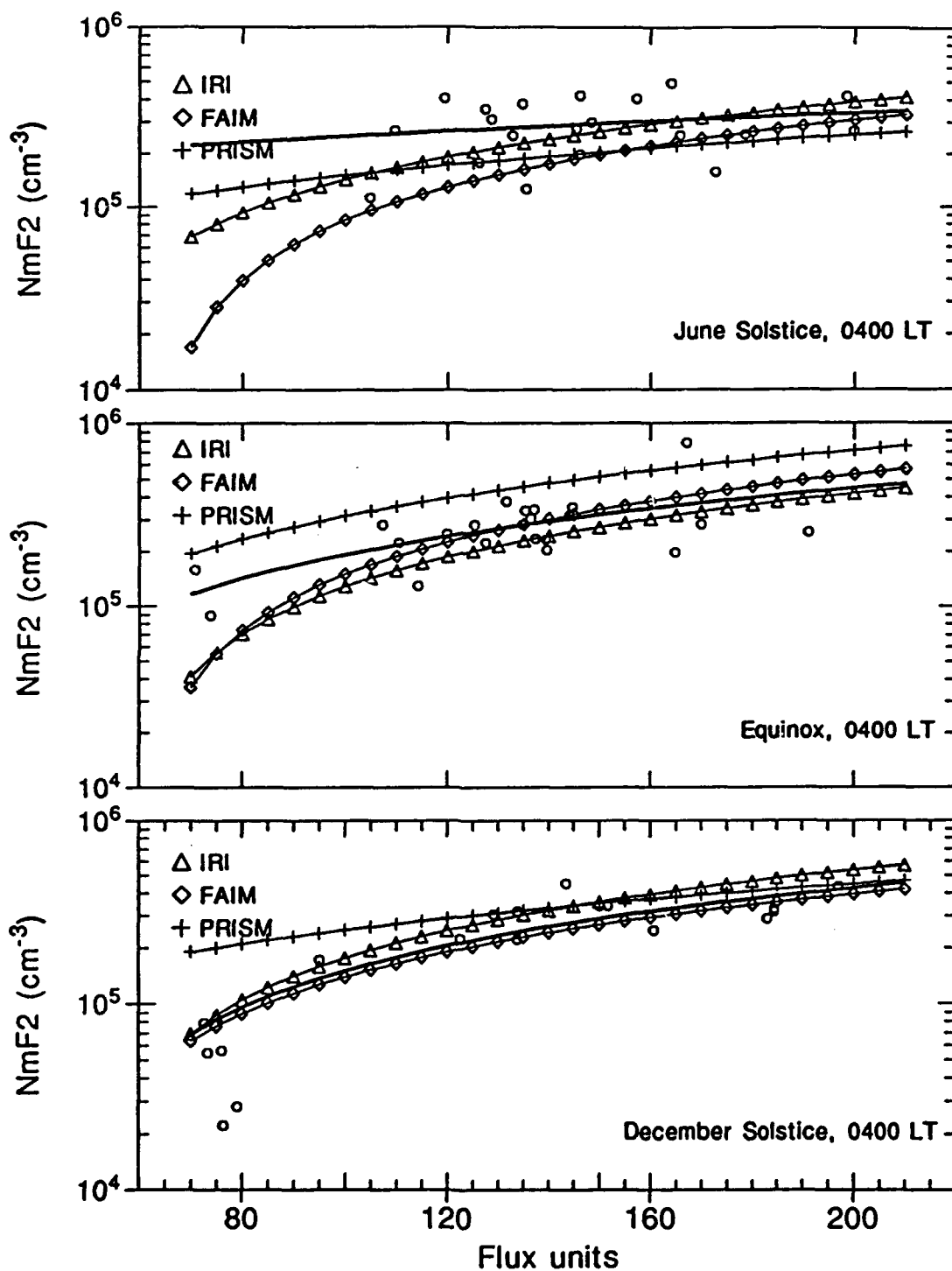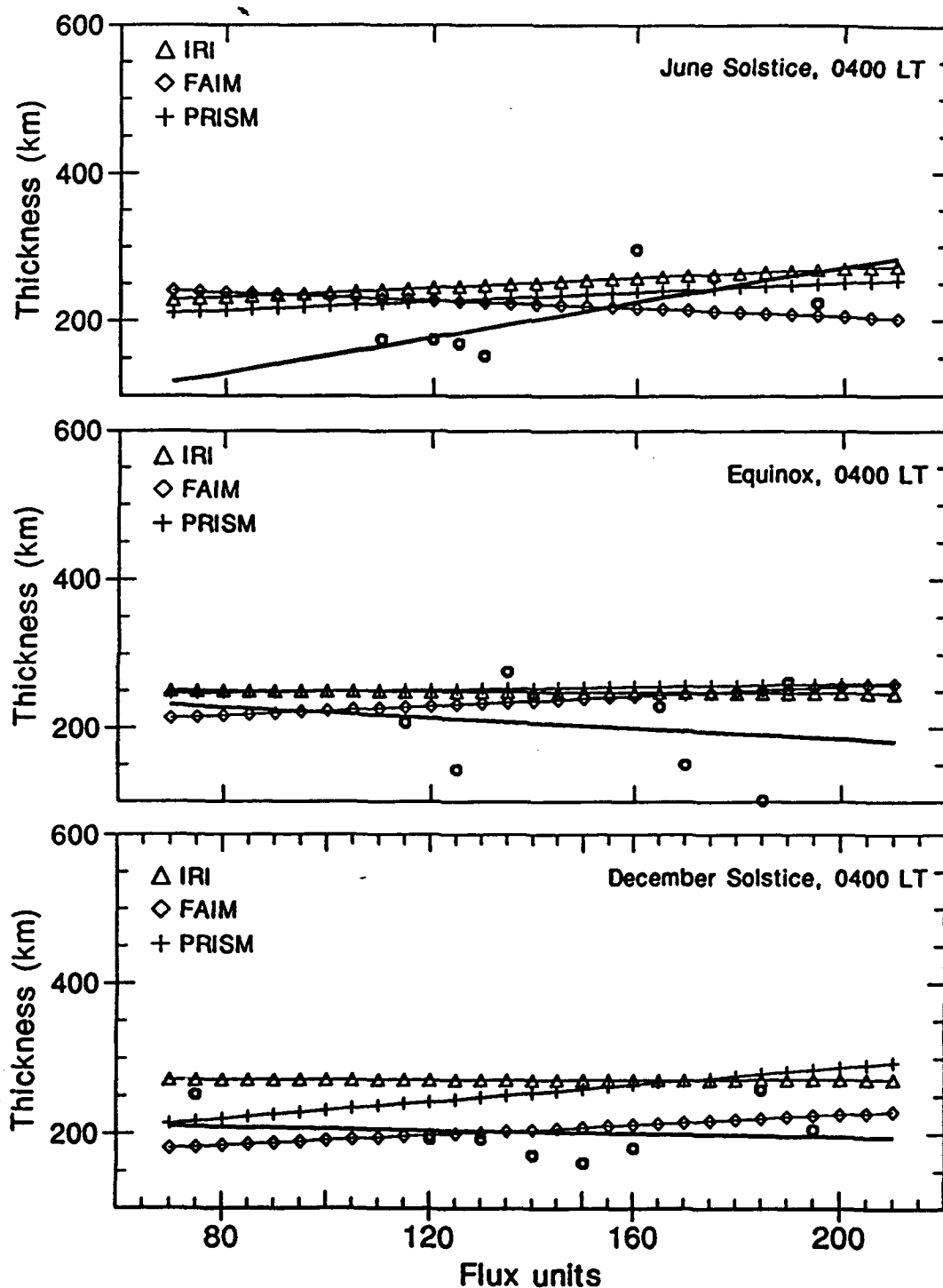
Fig. 74. Seasonal comparisons of Jicamarca and modeled ΔH at 0400 LT. The lines represent a least squares fit to the data and models. The open circles are quiet-time observations, data obtained under disturbed conditions were not used.
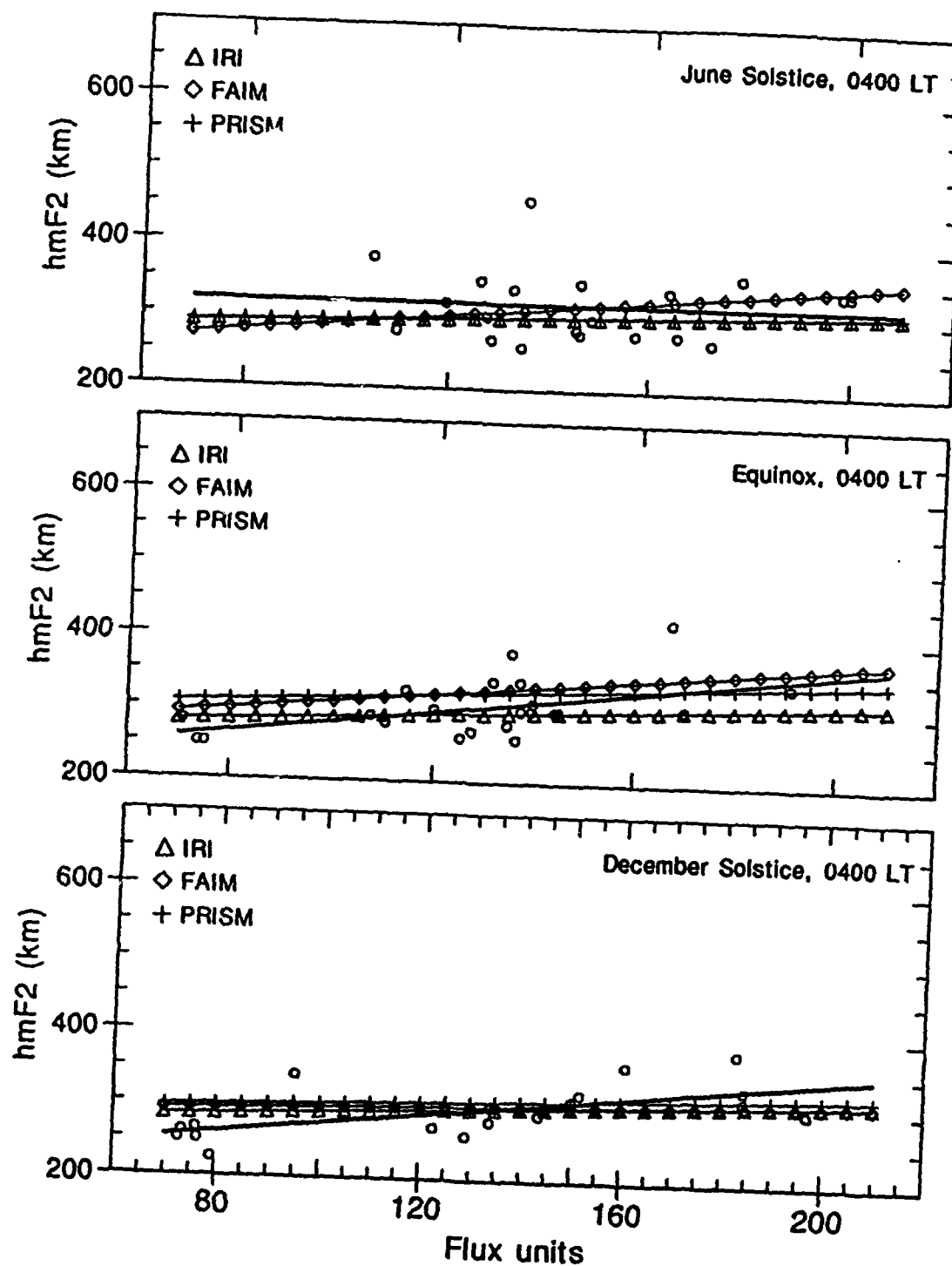
high flux in June solstice, but overestimate the thickness at low flux. Each model fits the data at low flux for equinox, but overestimates the thickness at high flux. FAIM gives the better summer fit.

We find that typically the IRI gives the better fit to peak density over a solar cycle for all seasons. There are exceptions, notably at 1800 and 2000 LT under equinoctial conditions and late at night. This finding is in good agreement with the knowledge that the URSI-89 parameters used in IRI-90 are derived in part from Huancayo, Peru, ionosonde data. FAIM gives a good estimate of peak density in winter and equinox, but significantly underestimates the summer NmF2. PRISM displays a tendency to overestimate the June solstice peak densities. All three models perform well during equinox for the hours considered.

Based on a comparison of the variation of hmF2 with flux, PRISM gives the better fit for all seasons and all flux levels, with some exceptions. The post-sunset layer has the worst comparison of the three models for all seasons except at December solstice (2000 LT) where the PRISM hmF2 is in excellent agreement with the data for all flux. There is no significant trend in FAIM or IRI performance.

FAIM gives the better representation of the midday December solstice and equinoctial layer thickness. The IRI decreases the thickness with flux; PRISM overestimates the midday ΔH. The evening modeled layer thickness shows better agreement with the models for low flux levels. IRI gives a

good fit to the layer thickness at lower flux levels, but consistently underestimates this parameter at moderate and high flux levels for all seasons. FAIM is in good agreement for lower flux levels, but underestimates the layer thickness at high flux in the evening and overestimates it during the day and late at night. PRISM generally overestimates the layer thickness for all flux levels, but shows a similar increase in thickness as the data. An increase in samples would improve this comparison.

Brown et al. [1991] gave a description of TEC comparisons between measurements at various stations with several models, among them the IRI and FAIM. Their results are similar to our comparisons of layer thickness with the models, keeping in mind the two parameters are proportional to one another. They found the model accuracy is worse for solar maximum comparisons than for solar minimum, which is in good agreement with our results. We find, however, that the IRI is consistently narrower than the data for high Φ, an effect we attribute to the altitude range of our calculations, typically 200 to 800 km, which eliminate a portion of the high density IRI topside profile. Brown and colleagues also state that an improved calculation of foF2 would improve the TEC calculations, which we do not dispute. We will add that in cases where the modeled layer thickness was substantially different from the data even though the peak density calculation was accurate, the topside and

bottomside density profiles may have a greater effect on the calculations than NmF2/foF2.

Though most of our findings in these comparisons point to FAIM as the best model, PRISM has the most potential to give a consistently good representation of the ionosphere. The IRI performs well with NmF2 and hmF2 calculations, but the layer shape falls short of representing a "typical" equatorial profile and the layer thickness agreement is good only for low solar activity conditions. In addition, the IRI may not be able to give as good a performance in regions where there is not an ionosonde contributing to the database. The comparisons were made with the initial runs of the physical models for PRISM. Similar comparisons made with the model after it has been in operational use and updated with real-time data will give a true indication of the model's ability to forecast ionospheric conditions.

CHAPTER VI

CONCLUSIONS

The daily and seasonal dynamic behavior of the ionospheric plasma density parameters over Jicamarca, Peru, has been studied using incoherent scatter radar observations from 1964 to the present. The seasonal average Jicamarca profiles were compared with modeled profiles from the IRI, FAIM, and PRISM models for similar season and solar activity. The models were evaluated on their ability to reproduce the ionospheric plasma density features present in the average Jicamarca profiles.

The analysis of the seasonal and solar cycle variations on the Jicamarca data yields the following results:

1. The peak densities show considerable variation from day to day, and with season and level of solar activity. The daytime and evening plasma densities are largest during December solstice (local summer) and smallest during June solstice (local winter) for all levels of solar activity. The nighttime profiles tend to be most dense during equinox.

2. The variation of the peak height with time, season, and solar cycle is highly variable. Typically the peak height increases with flux for all seasons and the heights are highest in local summer and lowest in winter. There is considerable variability even during magnetically quiet times, particularly during evening and nighttime.

3. The shape of the bottomside of the F layer is dependent on the seasonal changes of the vertical drift. The electron densities typically show small variability below about 300 km, but large variability at higher altitudes. The variability of the topside layers is strongly dependent on the vertical drift. In general, the higher the layer the more variable the corresponding density. The topside electron density gradient is generally most negative during December solstice.

5. The layer thickness increases with flux for all seasons. The greatest increase is during June solstice.

6. The effect of magnetic disturbance on the peak plasma density is minimal. There is no significant increase or decrease of plasma density or plasma layer height. However, the topside layer density is typically larger during magnetically disturbed periods.

7. The four-month seasonal averages do not always provide an appropriate representation of the equatorial electron density profiles. We found profiles with a typical equinoctial shape among the summer observations and both summer-type and winter-type profiles among the equinoctial observations, especially for moderate and high solar activity.

The comparison of the results from IRI, FAIM, and PRISM with the Jicamarca data shows:

1. The IRI gives a good fit to the average peak density for all flux and all seasons. There is little seasonal and

solar cycle variation in modeled peak layer height, in contrast to the changes seen for the data. The IRI fit to the bottomside density is good during solar minimum, but the bottomside layer is significantly higher than the data during moderate and high solar activity conditions. The IRI overestimates the topside layer densities for low solar activity and underestimates them for high solar activity. The modeled layer thickness follows a similar trend; the fits at solar minimum are good, but the thickness for moderate and high activity are substantially narrower than those of the data.

2. FAIM gives a good fit to the Jicamarca NmF2 during equinox and June solstice, but the profile density is typically lower than the data by as much as a factor of two in December solstice. The modeled layer peak heights are well within the variability of the data. The modeled bottomside electron density gradients are too steep during midday for low and moderate solar conditions and too gradual for high solar activity. However, the overall bottomside representations are better than those of the IRI. FAIM gives good fits to the topside layer densities and gradients for all seasons and all flux. The layer thickness agreements with the average data are better for low and moderate solar activity.

3. PRISM gives a good fit to the data peak density in summer and equinox, but is frequently denser than the data during winter. There is good agreement with the peak layer

heights for all seasons and solar flux levels. The modeled bottomside layer fits the data well with some exceptions: the PRISM evening bottomside density gradients tend to be shallower than the data, especially during equinox. The modeled topside layers are significantly denser and higher than the data during the day and evening for all seasons. This is primarily due to a secondary peak present in the daytime and evening model topside layers. The fits of PRISM to the topside data are good at night. PRISM gives a better representation of the layer thickness than IRI or FAIM. The model layer tends to be broader than the data layer, but within the variation of the data thickness.

We have shown that each model is capable of calculating a profile that falls within the day-to-day variability of the Jicamarca observations regardless of whether it matches the average data profile. The difference in model performance is greatest for profile shapes. Both PRISM and FAIM are able to reproduce the broadness of the equatorial ionospheric plasma density layers. The IRI layer shape is typically a mid-latitude solar minimum layer that shows little change in layer thickness over the solar cycle.

A significant amount of work has been done to research the seasonal and solar cycle variations of the plasma density profile at Jicamarca. Further research into equinoctial variations of the plasma density profiles near the solstitial months will yield useful information about these transition periods. This database should be expanded to include all

hours. The comparisons with IRI should be repeated after the next update to the model. As PRISM is tested and updated, a similar study should be conducted to chart improvements of the new model performance.

REFERENCES

Abdu, M.A., B.M. Reddy, G.O. Walker, R. Hanbaba, J.H.A. Sobral, B.G. Fejer, R.F. Woodman, R.W. Schunk, and E.P. Szuszczewicz, Processes in the quiet and disturbed equatorial-low latitude ionosphere: SUNDIAL campaign 1984. Ann. Geophysicae, 6, 69, 1988.

Anderson, D.N., Daily Variation of the Ionospheric F2 Equatorial Anomaly in the American and Asian Sectors, Ph.D. dissertation, University of Colorado, 1971.

Anderson, D.N., A theoretical study of the ionospheric F-region equatorial anomaly, I, Theory. Planet. Space Sci., 21, 409, 1973a.

Anderson, D.N., A theoretical study of the ionospheric F-region equatorial anomaly, II, Results in the American and Asian sectors. Planet. Space Sci., 21, 421, 1973b.

Anderson, D.N., Modeling the ambient, low latitude F-region ionosphere -- a review, J. Atmos. Terr. Phys., 43, 8, 753, 1981.

Anderson, D.N., M. Mendillo, and B. Herniter, A semi-empirical low-latitude ionospheric model. Radio Science, 22, 292, 1987.

Anderson, D.N., J.M. Forbes, and M. Codrescu, A Fully Analytic, Low-and Middle-Latitude Ionospheric Model. J. Geophys. Res., 94, 1520, 1989.

Anderson, D.N., R.E. Daniell, L.D. Brown, W.G. Whartenby, R.W. Simon, D.T. Decker, P.H. Doherty, and M.W. Fox, A Parameterized Real-time Ionospheric Specification Model (PRISM), Draft Technical Report for the Geophysics Directorate, Phillips Laboratory, Hanscom AFB, MA 01731, 1991.

Appleton, E.V., Two anomalies in the ionosphere, Nature, 157, 691, 1946.

Bailey, G.J., The Effect of a Meridional E x B Drift on the Thermal E x B Plasma at L = 1.4. Planet. Space Sci., 31, 389, 1983.

Bailey, G.J. and R. Sellek, A mathematical model of the Earth's plasmasphere and its application in a study of He+ at L = 3. Ann. Geophysicae., 8, (3), 171, 1990.

Bilitza, D., The worldwide Ionospheric Data Base, National Space Science Data Center/World Data Center A for Rockets and Satellites publication, 1989.

Brace, L.H., and R.F. Theis, Global empirical models of ionospheric electron temperature in the upper F-region and plasmasphere based on in situ measurements from the Atmosphere Explorer-D, ISIS 1, and ISIS 2 satellites, J. Atmos. Terr. Phys., 43, 1317, 1981.

Brown, L.D., R.E. Daniell, M.W. Fox, J.A. Klobuchar, and P.H. Doherty, Evaluation of six ionospheric models as predictors of total electron content, Radio Sci., 26, 1007, 1991.

Ching, B.K. and Y.T. Chiu, A phenomenological model of global ionospheric electron density in the E-, F1- and F2-regions. J. Atmos. Terr. Phys., 35, 1625, 1973.

Chiu, Y.T., An improved phenomenological model of ionospheric density. J. Atmos. Terr. Phys., 37, 1563, 1975.

Farley, D.T., Early incoherent scatter observations at Jicamarca, J. Atmos. Terr. Phys., 53, 665, 1991.

Fejer, B.G., The equatorial ionospheric electric fields, A review, J. Atmos. Terr. Phys., 43, 377, 1981.

Fejer, B.G., Low latitude electrodynamic plasma drifts: a review, J. Atmos. Terr. Phys., 53, 677, 1991.

Fejer, B.G, and M.C. Kelley, Ionospheric irregularities, Rev. Geophys., 18, 401, 1980.

Fejer, B.G., D.T. Farley, R.F. Woodman, and C. Calderon, Dependence of Equatorial F Region Vertical Drifts on Season and Solar Cycle, J. Geophys. Res., 84, 5792, 1979.

Fejer, B.G., E. Kudeki, and D.T. Farley, Equatorial F Region Plasma Drifts, J. Geophys. Res., 90, 12,249, 1985.

Fejer, B.G., E.R. de Paula, I.S. Batista, E. Bonelli, and R.F. Woodman, Equatorial F Region Vertical Plasma Drifts During Solar Maxima. J. Geophys. Res., 94, 12,049, 1989.

Fejer, B.G., E.R. de Paula, S.A. Gonzalez, and R.F. Woodman, Average Vertical and Zonal F Region Plasma Drifts Over Jicamarca, J. Geophys. Res., 96, 13,901, 1991.

Forbes, J.M., Atmospheric Tides 1. Model Description and Results for the Solar Diurnal Component. J. Geophys. Res., 87, 5222, 1982a.

Forbes, J.M., Atmospheric Tides 2. The Solar and Lunar Semidiurnal Components J. Geophys. Res., 87, 5241, 1982b.

Hedin, A.E., A revised thermospheric model based on mass spectrometer and incoherent scatter data, MSIS-83. J. Geophys. Res., 88, 10,170, 1983.

Hedin, A.E., MSIS-86 Thermospheric Model, J. Geophys. Res., 92, 4649, 1987.

Hedin, A.E. Empirical global model of upper thermosphere winds based on Atmospheric and Dynamics Explorer satellite data, J. Geophys. Res., 93, 9959, 1988.

Kelley, M.C., The Earth's Ionosphere, Plasma Physics and Electrodynamics, Academic Press, Inc., San Diego, Ca, 1989.

Kendall, P.C. and W.M. Pickering, Magnetoplasma diffusion at F2-region altitudes, Planet. Space. Sci., 15, 825, 1967.

Klobuchar, J.A., D.N. Anderson, and P.H. Doherty, Model studies of the latitudinal extent of the equatorial anomaly during equinoctial conditions. Radio Science, 26, 1025, 1991.

Lyon, A.J., and L. Thomas, the F2-region equatorial anomaly in the African, American and East Asian sectors during sunspot maximum, J. Atmos. Terr. Phys., 25, 373, 1963.

Mead, G.D., International geomagnetic reference field 1965.0 in dipole coordinates, J. Geophys. Res., 75, 4372, 1970.

McClure, J.P., D.T. Farley, and R. Cohen, Ionospheric Electron Concentration Measurements at the Magnetic Equator, 1964, ESSA Technical Report ERL 186-AL4, Boulder, Colorado, U.S.A., 1970.

Raghavarao, R., R. Sridharan, J.H. Sastri, V.V. Agashe, B.C.N. Rao, P.B. Rao, and V.V. Somayajulu, The Equatorial Ionosphere, WITS Handbook, Vol.1, 48-93, Edited by C.H. Liu and B. Edwards, University of Illinois, Urbana, IL, 1988.

Rajaram, G., Structure of the equatorial F-region, topside and bottomside -- a review, J. Atmos. Terr. Phys., 39, 1125, 1977.

Rajaram, G. and R.G. Rastogi, Equatorial electron densities -- seasonal and solar cycle changes, J. Atmos. Terr. Phys., 39, 1175, 1977.

Rawer, K., Modelling of Neutral and Ionized Atmospheres, in Encyclopedia of Physics, 49/7, Springer-Verlag, 1984.

Richards, P.G., An improved algorithm for determining neutral winds from the height of the F2 peak electron density, _J. Geophys. Res., 96_, 17,839, 1991.

Richards, P.G., and D.G. Torr, Ratio of photoelectron to EUV ionization rates for aeronomic studies, _J. Geophys. Res., 93_, 4060, 1988.

Richmond, A.D., M. Blanc, B.A. Emery, R.H. Wand, B.G. Fejer, R.F. Woodman, S. Ganguly, P. Amayenc, R.A. Behnke, C. Calderon, and J.V. Evans, An empirical model of quiet-day ionospheric electric fields at middle and low latitudes, _J. Geophys. Res., 85_, 4658, 1980.

Rishbeth, H., Day-to-Day Ionospheric Variations in a Period of High Solar Activity, Unpublished manuscript, 1991.

Rishbeth, H., and O.K. Garriott, _Introduction to Ionospheric Physics_, Academic Press, New York, 1969.

Roble, R.G., R.E. Dickinson, and E.C. Ridley, Seasonal and Solar Cycle Variations of the Zonal Mean Circulation in the Thermosphere. _J. Geophys Res., 82_, 5493, 1977.

Rush, C.M., M. PoKempner, D.N. Anderson, J. Perry, F.G. Stewart, and R.K. Reasoner, Global Maps of fof2 Derived From Observations and Theoretical Values, U.S. Department of Commerce, National Telecommunications and Information Administration Report 84, 1984.

Schunk, R.W., The terrestrial ionosphere, in _Solar-Terrestrial Physics_, edited by R.L. Carovillano and J.M. Forbes, p. 609, D. Reidel Publishing Company, Dordrecht, Holland, 1983.

Schunk, R.W., and W.J. Raitt, Atomic nitrogen and oxygen ions in the daytime high-latitude F-region. _J. Geophys. Res., 85_, 1255, 1980.

Schunk, R.W., and J.J. Sojka, Ion temperature variations in the daytime high-latitude F region, _J. Geophys. Res., 80_, 3121, 1975.

Schunk, R.W., and J.J. Sojka, Ionospheric hot spot at high latitudes, _Geophys. Res. Lett., 9_, 1045, 1982.

Schunk, R.W., and E.P. Szuszczewicz, First principle and empirical modeling of the global-scale ionosphere, _Ann. Geophysicae_, 6, 19, 1988.

Schunk, R.W., and J.C.G. Walker, Theoretical ion densities in the lower ionosphere. _Planet. Space Sci., 21_, 1875, 1973.

Schunk, R.W., W.J. Raitt, and P.M. Banks, Effect of electric fields and other processes upon the nighttime high-latitude F layer, J. Geophys. Res., 81, 3271, 1976.

Sharma, R.P., and E.J. Hewens, A study of the equatorial anomaly at American longitudes during sunspot minimum, J. Atmos. Terr. Phys., 38, 475, 1976.

Sojka, J.J, and R.W. Schunk, A theoretical study of the global F-region for June solstice, solar maximum, and low magnetic activity. J. Geophys. Res., 90, 5285, 1985.

Sojka, J.J., W.J. Raitt, and R.W. Schunk, Effect of displaced geographic and geomagneitc poles on high-latitude plasma convection and ionospheric depletions, J. Geophys. Res., 84, 5943, 1979.

Sojka, J.J., W.J. Raitt, and R.W. Schunk, A comparison of model predictions for plasma convection in the northern and southern polar regions, J. Geophys. Res., 85, 1762, 1980.

Spiro, R.W., P.H., Reiff, and L.J. Maher, Precipitating electron energy flux and auroral zone conductances: An empirical model, J. Geophys. Res., 87, 8215, 1982.

Sterling, D.L., W.B. Hanson, R.J. Moffett, and R.G. Baxter, Influence of electromagnetic drifts and neutral air winds on some features of the F2 region, Radio Science, 4, 1005, 1969.

Szuszczewicz, E.P., B.G. Fejer, E. Roelof, R.W. Schunk, R. Wolf, R. Leitinger, M. Abdu, B.M. Reddy, J. Joselyn, P. Wilkinson, and R. Woodman, SUNDIAL: a world-wide study of interactive ionospheric processes and their roles in the transfer of energy and mass in the Sun-Earth system. Ann. Geophysicae, 6, 3, 1988.

Szuszczewicz, E.P., P. Wilkinson, M.A. Abdu, E. Roelof, R. Hanbaba, M. Sands, T. Kikuchi, R. Burnside, J. Joselyn, M. Lester, R. Leitinger, G.O. Walker, B.M. Reddy, and J. Sobral, Solar-Terrestrial conditions during SUNDIAL-86 and Empirical Modelling of the Global-Scale Ionospheric Response. Ann. Geophysicae, 8, 387, 1990.

Szuszczewicz, E.P., B. Fejer, E. Roelof, R. Schunk, R. Wolf, M. Abdu, T. Bateman, P. Blanchard, B.A. Emery, A. Feldstein, R. Hanbaba, J. Joselyn, T. Kikuchi, R. Leitinger, M. Lester, J. Sobral, B.M. Reddy, A.D. Richmond, R. Sica, G.O. Walker, and P. Wilkinson, Modelling and Measurements of Global-Scale Ionospheric Behavior under Solar Minimum, Equinoctial Conditions, Adv. Space Res., 12, 105, 1992.

Thomas, L., The F2-region equatorial anomaly during solstice periods at sunspot maximum, *J. Atmos. Terr. Phys., 30*, 1631, 1968.

Torr, D.G., and M.R. Torr, Chemistry of the thermosphere and ionosphere, *J. Atmos. Terr. Phys., 41*, 797, 1979.

Torr, M.R., D.G. Torr, P.G. Richards, and S.P. Yung, Mid- and low-latitude model of thermospheric emissions 1. $O^+(^2P)$ 7320 Å and $N_2(2P)$ 3371 Å, *J. Geophys. Res., 95*, 21,147, 1990.

Woodman, R.F., Vertical drift velocities and east-west electric fields at the magnetic equator, *J. Geophys. Res., 75*, 6249, 1970.

Woodman, R.F., R.G. Rastogi, and C. Calderon, Solar cycle effects on the electric fields in the equatorial ionosphere, *J. Geophys. Res., 82*, 5257, 1977.